PREPARATION OF ACTIVATED KAOLIN FOR BLEACHING RICE BRAN OIL AND SYNTHETIC KAOLINITE TO ASSESS SORPTION PROPERTIES OF THESE PARTICLES IN RELATION TO THEIR MORPHOLOGY

MISS LEI LEI AUNG

A THESIS SUBMITTED IN PARTIAL FULFILLMENT
OF THE REQUIREMENT FOR
THE DEGREE OF DOCTOR OF PHILOSOPHY (BIOTECHNOLOGY)
SCHOOL OF BIORESOURCES AND TECHNOLOGY
KING MONGKUT'S UNIVERSITY OF TECHNOLOGY THONBURI
2014

THESE

Pour l’obtention du Grade de

DOCTEUR DE L’UNIVERSITE DE POITIERS

(Faculté des Sciences Fondamentales et Appliquées)
(Diplôme National - Arrêté du 7 août 2006)

Ecole Doctorale : Sciences pour l’Environnement Gay Lussac
Secteur de Recherche : Terre solide et enveloppe superficielle

Présentée par :

Lei Lei AUNG

Maître ès Sciences

****

PREPARATION OF ACTIVATED KAOLIN FOR BLEACHING RICE BRAN OIL AND SYNTHETIC KAOLINITES TO ASSESS SORPTION PROPERTIES OF THESE PARTICLES IN RELATION TO THEIR MORPHOLOGY

****

Directeurs de Thèse : Sabine Petit/ Paitip Thiravetyan

Co-directeur de thèse : Emmanuel Tertre/ Niramon Worasith/ Parinda Suksabye

****

Soutenue prévue le 02 mai 2014 devant la Commission d’Examen

****

JURY

Dr. Krisnangkura Kanit	KMUTT University (Thailande)	Member
Dr. Thiravetyan Paitip	KMUTT University (Thailande)	Member
Dr. Petit Sabine	Université de Poitiers (France)	Member
Dr. Tertre Emmanuel	Université de Poitiers (France)	Member
Pr. Suddhiprakarn Anchalee	Kasetsart University (Thailande)	Member
Dr. Aryusuk Kornkanok	KMUTT University (Thailande)	Invited
Dr. Worasith Niramon	RMUTK University (Thailande)	Invited
Dr. Suksabye Parinda	Suan Dusit Rajabhat University (Thailande)	Invited

Preparation of Activated Kaolin for Bleaching Rice Bran Oil and Synthetic Kaolinite to Assess Sorption Properties of These Particles in Relation to Their Morphology

Miss Lei Lei Aung M.Sc (Industrial Chemistry)

A Thesis Submitted in Partial Fulfillment of the Requirements for
Doctor of Philosophy (Biotechnology)
School of Bioresources and Technology
King Mongkut's University of Technology Thonburi
2014

THESE
Pour l'obtention du Grade de
DOCTEUR DE L'UNIVERSITE DE POITIERS
(ECOLE SUPERIEURE d'INGENIEURS de POITIERS)
(Diplôme National - Arrêté du 7 août 2006)
Ecole Doctorale : Gay-Lussac
Secteur de Recherche : Terre solide et enveloppes superficielles
Présentée par :
Lei Lei AUNG.

Thesis Committee

………………………………………………… Chairman of Thesis Committee
(Assoc. Prof. Dr. Kanit Krisnangkura, Ph.D.)

Paitip T
………………………………………………… Member and Thesis Advisor
(Assoc. Prof. Dr. Paitip Thiravetyan, Ph.D.) for KMUTT

………………………………………………… Member and Thesis Advisor
(DR. Sabine Petit, Ph.D.) for University of Poitiers

E. Tertre
………………………………………………… Member and Thesis Co-Advisor
(Dr. Emmanuel Tertre, Ph.D.) for University of Poitiers

Thesis Committee (Cont.)

N. Worasith
……………………………………………… Member and Thesis Co-Advisor
(Asst. Prof. Dr. Niramon Worasith, Ph.D.) for KMUTT

Parinda Suksabye
……………………………………………… Member and Thesis Co-Advisor
(Lect. Dr. Parinda Suksabye, Ph.D.) for KMUTT

K. Aryusuk
……………………………………………… Member for KMUTT
(Assoc. Prof. Dr. Kornkanok Aryusuk, Ph.D.)

A. Suddhiprakarn
……………………………………………… External Examiner for KMUTT
(Prof. Dr. Anchalee Suddhiprakarn, Ph.D.)

J Brendlé
……………………………………………… Referee for University of Poitiers
(Pr. Jocelyne Brendlé)
(Institut de Science des Matériaux de Mulhouse
(IS2M), France)

Thesis Title	Preparation of Activated Kaolin for Bleaching Rice Bran Oil and Synthetic Kaolinites to Assess Sorption Properties of these Particles in Relation to their Morphology
Thesis Credits	36
Candidate	Miss Lei Lei Aung
Thesis Advisors	Assoc. Prof. Dr. Paitip Thiravetyan Dr. Sabine Petit
Thesis Co-advisors	Dr. Emmanuel Tertre Asst. Prof. Dr. Niramon Worasith Lect. Dr. Parinda Suksabye
Program	Doctor of Philosophy (double badged degree)
Field of Study	Biotechnology/ Terre solide et enveloppes superficielles
Division	Biotechnology/ Gay-Lussac
Faculty	School of Bioresources and Technology (KMUTT)/ Sciences Fondamentales et Appliquées, Institut de Chimie des Milieux et Matériaux de Poitiers (Université de Poitiers)
Academic Year	2014

Abstract

The dissertation consists of two main parts; the first part is devoted to the effect of physical/thermal and chemical activation of kaolin on bleaching of rice bran oil. In this study, samples were prepared from natural Ranong kaolin. This study focused on the effects of both thermal treatment (from 100 to 900°C) and chemical activation (sulfuric acid, hydrochloric acid, citric acid and oxalic acid using different acid concentrations or different clay/acid ratio) on the capacity of kaolins to bleach rice bran oil. When kaolin was treated with high temperature (>100°C) prior to reflux and with a high acid concentration during reflux, the kaolinite structure was partially or completely destroyed associated to a dramatic leaching of alumina, and amorphous silica dominated the samples. The measured maximum bleaching capacity obtained was not consistent with the highest specific surface area and pore volume; rather, it depended on the alumina contents in the samples. Thus, the partial preservation of the kaolinite structure is crucial to obtain an appropriate bleaching capacity of kaolin. This is directly related to the preservation of the aluminol sites present at the kaolinite surface. XRF analysis showed that the alumina contents of 28-34% were values to reach in order to obtain optimum bleaching capacities of kaolin, independently of the different acid used. Finally, optimum bleaching of ~83%, ~82% and ~81% were achieved by grinding the kaolin prior to reflux with low acid concentration of hydrochloric acid (0.5 M), sulfuric acid (0.3 M) and citric acid (0.5 M), respectively with clay/acid ratio of 1:50.

The second part of the thesis aims to elucidate the influence of morphology of kaolinites on their sorption properties. For that, Na^+/H^+ sorption isotherms in water saturated conditions of synthetic kaolinites and natural well crystallized kaolinite, called KGa--1b commercialized by the Clay Mineral Society, were performed and interpreted. Kaolinites used in this study were hydrothermally synthesized from partially crystallized kaolinite as a function of different final pH (pH_F) ranging from 0.8 to 8.3. Results obtained for KGa--1b were compared with data obtained in literature for this mineral, in order to fully validate this approach. This study found that cation exchange capacity, due to both isomorphic substitutions in the crystals (permanent charge), and silanol and aluminol edge sites were highly variable. Typically, CEC at pH=9 varied from ~0.8 $cmol_c$/kg for well crystallized kaolinite (pH_F 0.8) to ~33 $cmol_c$/kg for disordered lath-shaped kaolinite (pH_F 8.3). Na^+/H^+ sorption isotherms were obtained for all synthetic kaolinites as a function of pH ranging from pH 3 to 11. Results showed that sorption of Na^+ increases dramatically with pH. Typically for all kaolinite samples except for the one synthesized at pH_F=8.3, Na^+ sorption is rigorously equal to zero when pH<7, indicating no permanent charge in the samples (in contrast to natural KGa--1b kaolinite), and increases when pH>7 due to sorption on edge sites. The amount of dissolved silica measured during Na^+/H^+ isotherm is higher for experiments performed with kaolinites synthesized in basic conditions (for pH_F 7.4 and pH_F 8.3) than for kaolinites synthesized in acid conditions (for pH_F 0.8 and pH_F 3.3). These latter results lead to conclude that sorption site density can be considered constant when pH is between 4 and 10, independently of the morphologies of particles. In this context, a thermodynamic modeling procedure using a complexation model was applied to interpret the data obtained with hexagonal- and lath-shaped particles. During this procedure, selectivity coefficient between Na^+ and H^+ cations were obtained considering the total edge site densities calculated from lateral specific surfaces estimated for synthetic kaolinites and crystallography data. Results showed that the Na^+/H^+ selectivity coefficient depends on the kaolinite's size/morphology since for hexagonal-shaped particles a log $Kc(Na^+/H^+)$ equal to -5.5 was required to interpret experimental data, *versus* log $Kc(Na^+/H^+)$ of -4.7 for lath-shaped particles.

Keywords: Alumina/ Bleaching/ Kaolin/ Kaolinite/ Morphology/ pH/ Rice Bran Oil/ Selectivity Coefficient/ Sorption Isotherm

Résumé

Cette étude a fait l'objet de deux parties. L'une porte sur l'effet de différents types d'activation (chimique, thermique, mécanique) de kaolins (géo-matériaux riches en kaolinite) sur leurs propriétés de décoloration vis-à-vis de l'huile de riz. L'autre traite de l'effet de la taille et de la morphologie de kaolinites de synthèse sur leurs propriétés d'adsorption.

Cette étude a montré que lorsque le kaolin était chauffé à plus de 100°C avant de subir une activation acide en milieu sulfurique, citrique ou oxalique, la capacité de décoloration vis-à-vis de l'huile de riz était fortement réduite. Cet effet a été directement mis en relation avec la destruction partielle ou totale de la structure de la kaolinite, associée à une forte lixiviation de l'aluminium de l'échantillon et à la précipitation de silice amorphe. Il s'est donc avéré que la préservation des sites aluminols présents sur les surfaces externes des particules de kaolinites semblait être un critère primordial à conserver en vue d'obtenir de bonne capacité de décoloration. Dans ce contexte, les meilleures capacités de décoloration (82% environ) ont été obtenues en utilisant conjointement un traitement thermique modéré (<100°C), un broyage mécanique de l'échantillon avant l'étape d'activation acide, une concentration en acide de l'ordre de 0.3 à 0.5 mol/L et un rapport (argile)/(solution acide) de l'ordre de 1/50. Notons que les plus fortes valeurs de surfaces spécifiques n'ont pas forcément été associées aux échantillons présentant les meilleures capacités de décoloration en raison de la présence de silice amorphe et de la non-préservation des sites aluminols de la kaolinite ; sites responsables de l'adsorption des pigments de molécules de chlorophylle-a.

Par ailleurs, aucune étude à notre connaissance ne reliait directement les morphologies de particules de phyllosilicates à leurs propriétés d'adsorption vis-à-vis de deux cations inorganiques. Dans le cas des kaolinites naturelles, une charge permanente souvent significative et attribuable à des impuretés minéralogiques empêche toute tentative de relier directement la forme des particules à un coefficient de sélectivité entre deux cations pour des sites latéraux donnés. Des kaolinites ont donc été synthétisées par voie hydrothermale en considérant différentes conditions physico-chimiques, afin d'obtenir des morphologies variées (hexagones plus ou moins anisotropes). Pour ces échantillons synthétiques pour lesquels aucune impureté minéralogique et charge permanente n'a été détectée, des isothermes expérimentales d'adsorption entre Na^+ et H^+ ont été mesurées. Ces cations ont été choisis étant donné leur présence ubiquiste dans les eaux naturelles et leur fort pouvoir compétiteur par rapport aux cations traces métalliques. Grâce aux surfaces spécifiques des sites latéraux et des densités de site issues de la cristallographie des différentes faces présentes dans nos échantillons ((010), (110), (1-10)), un coefficient de sélectivité entre Na^+ et H^+ sur l'ensemble des sites latéraux d'une morphologie donnée a pu être estimé à l'aide d'un modèle de complexation de surface. Les résultats ont montré que le coefficient de sélectivité Na^+/H^+ dépendait très fortement de la morphologie de la particule, et que par conséquent les propriétés d'adsorption des kaolinites ne pouvaient pas être obtenues avec précision sans une connaissance fine de la morphologie des particules.

Mots clés: kaolin / huile de riz / décoloration / kaolinite / synthèse hydrothermale / morphologie / isotherme d'adsorption / coefficient de sélectivité.

ACKNOWLEDGEMENTS

First of all, I would like to express my deepest gratitude and special thanks to my advisor, Assoc. Prof. Dr. Paitip Thiravetyan, King Mongkut's University of Technology Thonburi, Thailand for her immense support, tireless guidance and kind permission to utilize the facilities of the laboratory throughout the entire course of this dissertation research. I would also like to thank my co-thesis advisors, Asst. Prof. Dr. Niramon Worasith and Dr. Parinda Suksabye profoundly for their willingness to be members of the supervisory committee and their valuable comments on some aspects of the work.

I am also sincerely grateful and deeply indebted to my advisor, Dr. Sabine Petit, Director of IC2MP Laboratory, University of Poitiers, France for kindly allowing me to do research there, and also for rendering valuable suggestions and firm support for my research project. I owe my heartfelt thanks to my esteemed co-advisor, Dr. Emmanuel Tertre for his thorough guidance of my research work at the University of Poitiers and for in-depth discussion of some results of my research work done in Thailand. I have learnt a lot from him and enjoyed the educative discussion with him relative to the clay mineral processing and surface charge.

Sincere thanks are also due to the Committee members Assoc. Prof. Dr. Kanit Krisnangkura and Assoc. Prof. Dr. Kornkanok Arysusuk for kindly attending my seminars and defense, and giving invaluable suggestions wherein. I am also profoundly grateful to the referees Prof. Dr. Anchalee Suddhiprakarn, Kasetsart University, Thailand and Pr. Jocelyne Brendlé, Institut de Science des Matériaux de Mulhouse (IS2M), France for their thorough and comprehensive assessment of my thesis.

These acknowledgements could not be deemed complete unless I mention the blessing of my benefactors Thailand Research Fund (TRF), Thailand International Co-operation Agency (TICA) and the French Embassy in Indonesia whose commendable joint sponsorship (RGJ program) had made possible my participation in the Ph.D. program. I appreciate very much the assistance of Had Som Pan Co., Ltd. and Thai Edible Oil Co., Ltd. for providing me with a sufficient quantity of the kaolin and rice bran oil, respectively required for my research work.

Furthermore, I wish to acknowledge my genuine gratitude and sincere thanks to all the staffs and colleagues of the King Mongkut's University of Technology Thonburi, Thailand and the University of Poitiers, France respectively for their unstinting help and spontaneous cooperation throughout my study at both Universities.

Finally, I most humbly thank the Ministry of Education, Government of the Union of Myanmar, the Department of Higher Education (Lower Myanmar) and University of Yangon for selecting and nominating me for the award of the scholarship.

In Conclusion, my acknowledgement will be never completed without special mention to my parents. I find no words to express how grateful I am to my parents for their love and support throughout my life. They always encourage me to do my best in everything I do and give moral support to me to demonstrate the "Yes, I can" attitude in this particular scholastic endeavour. I also dedicate this thesis to my elder brothers, sisters, nieces, nephews and friends who have always provided me love and care.

CONTENTS

PAGE

CHAPTER

CONTENTS (Cont.)

LIST OF TABLES

LIST OF TABLES (Cont.)

TABLES **PAGE**

LIST OF FIGURES

FIGURES **PAGE**

LIST OF FIGURES (Cont.)

LIST OF FIGURES (Cont.)

FIGURES **PAGE**

LIST OF FIGURES (Cont.)

LIST OF FIGURES (Cont.)

LIST OF FIGURES (Cont.)

FIGURES **PAGE**

ABBREVIATIONS

$>Al_2OH$ = aluminol
$>AlOH_2^+$ = protonated Al edges
$>SiO^-$ = deprotonated Si edges
AAS = Atomic Absorption Spectroscopy
BC = Bleaching Capacity
BET = Brunauer-Emmet-Teller Method
CEC = Cation Exchange Capacity
CMS = Clay Mineral Society
CSD = Size of the Coherent domain of the synthetic kaolinites
DRIFT = Diffuse Reflectance Infrared Fourier Transform
FUG2 = Unground Kaolins heated at different temperatures before reflux with 2M sulfuric acid
FG2 = Ground Kaolins heated at different temperatures before reflux with 2M sulfuric acid
FTIR = Fourier Transform Infrared Spectroscopy
FWHM = Full Width at Half Maximum
GK = Ground Kaolin
GRC = Samples ground and refluxed with citric acid
GRH = Samples ground, and refluxed with hydrochloric acid
GRO = Samples ground, and refluxed with oxalic acid
GRS = Samples preheated at 100˚C or not, ground, and refluxed with sulfuric acid
HI = Hinckley Index
KGa--1b = a referenced low-defect kaolinite from the Clay Mineral Society
PB = pseudoboehmite
pH_F = kaolinite products obtained as a function of final synthesis pH
R_2 = crystallinity index
SEM = Scanning Electron Microscopy
SM = partially crystallized kaolinites
SSA = Specific Surface Area
TEM = Transmission Electron Microscopy
UGK = Unground Kaolin
V_p = total pore volume
V_{me} = mesopore volume
V_{mi} = micropore volume
XRD = X-Ray Diffraction
XRF = X-Ray Fluorescence

CHAPTER 1 INTRODUCTION

1.1 Rational /Problem statement

Rice bran oil, which is produced from the rice bran and germ of *Oryza sativa* seeds, is primarily consumed as cooking oil in Asian Countries such as Japan, Korea, Thailand (Kahlon, et al., 1992). Rice bran oil is also of interest for its potential health benefits because it contains approximately 80% unsaturated fatty acids, mainly as linoleic acid (Bhattacharyya et al., 1985). Crude rice bran oil, however, has a dark brown, dark greenish brown or greenish yellow color due to the presence of chlorophyll-a. During heating, this molecule decomposes to pheophytin pigment compounds, which results in dull and dark-colored oil, causes an off-flavor, and promotes oil oxidation, consequently reducing the shelf-life of the oil (Diosady, 2005).

Rocks that are rich in kaolinite are known as kaolin or china clay. Kaolin, one of the low-cost adsorbents that is commonly used in wastewater treatments (Bhattacharyya et al., 2008; Nandi, et al., 2009; Shirsath, et al., 2013), is abundantly found in Thailand. Kaolin clay consists of clay minerals such as kaolinite, illite, halloysite, and montmorillonite, and of non-clay minerals as quartz and feldspar, anastase, and gibbsite (Panda et al., 2010). Kaolinite is a 1:1 type aluminosilicate clay mineral, $(Si_4)^{IV}(AL_4)^{VI}O_{10}(OH)_8$ which a variable charge that depends on the pH, on alumina face and on the edges arising from the protonation and deprotonation of exposed hydroxyl groups (White, 1987; James, 1995). It has no swelling and low cation exchange capacity due to the lack of interlayer cations and water molecules in the interlayer sites. Adjacent layers of kaolinite are linked to each other by hydrogen bonds. Generally, kaolin have low adsorption properties towards pigment sorption such as chlorophyll-a. To improve these properties of clays, many researchers have treated those mechanically or chemically, in particular using sulfuric acid (acid activation) (Falaras et al., 1999; Sabah and Çelik, 2005; Salawudeen et al., 2007; James et al., 2008; Nguetnkam et al., 2008; Didi et al., 2009; Worasith et. al., 2011a). However, the effect of heating the kaolins prior to mechanical and/or chemical treatment on their capacity of adsorb organic pigments has not been assessed. There is also no study about the correlation between the structural, mineral and textural properties of hydrochloric or citric acid activated Ranong kaolin and its bleaching performance.

The use of kaolinite for the studies of ion-exchange phenomena is one of the oldest and most perspective for adsorption studies. A number of studies about inorganic cation adsorption on kaolinite have been conducted (Zhabrova and Egorov, 1961; Vesely and Pekárek, 1972; Breeuwsma and Lyklema, 1973; Miranda-Trevino and Coles, 2003; Tertre et al., 2006). This was motivated by the fact that this mineral is ubiquitous in many of natural geological environments (soils, sediments, natural water). The monovalent cation sodium, is one of the major constituents of natural water (1 to 1000 mg/L) and found in ground water and surface water at relative high concentrations in growing urban areas (Buttle and Labadia, 1999; Mason et al., 1999). It comes from the human activities such as effluents from industrial and municipal facilities, leachate from municipal landfills and some agricultural chemicals. The presence of sodium in natural water at irregular levels adversely affects the municipal and private water supplies (Cleary, 1978), soil chemistry and impacting the aquatic environment. Moreover, this major cation is always a strong competitor of trace organic or inorganic elements for sorption sites onto solid surfaces in natural waters. Then, it is crucial to have tools predicting with good confidence the adsorption of this cation on kaolinites.

In literature, the effect of both size and morphology of the particles on the sorption properties on minerals was studied only for oxides and hydroxides (Lloyd and Conley, 1970; Yue-hua et al., 2003). However, the influence of the morphology of kaolinite particles on its sorption properties was not studied up to now. This is due to the fact that generally, in experimental studies, mineralogical impurities are present in kaolinite samples, as well as a permanent charge in the whole material, and the chemistry of the aqueous phase is rarely well controlled. Note that even for the low-defect Georgia kaolinite KGa--1b widely studied in literature, a permanent charge is measured (around 0.6 $\mathrm{cmol_c/kg}$ (Wan and Tokunaga, 2002)) due probably to the presence of few organic matters. By working with synthetic kaolinites, characterized by zero mineralogical impurities as well as no permanent charge, the effect of morphology of kaolinite particles on their sorption properties towards Na^+ and H^+ cations can be assessed.

1.2 Research objectives

1.2.1 To study the effect of mechanical, thermal, chemical treatments on Ranong kaolin's bleaching capacities.
1.2.2 To investigate the effect of morphology of synthetic kaolinite particles on their sorption properties.

1.3 Scopes of the study

1.3.1 Ranong kaolins were activated by thermal, mechanical and chemical treatments. These materials were characterized in term of structure and mineralogy using XRD, XRF, FTIR, BET and SEM analyses.
1.3.2 The bleaching capacities of these activated kaolins were assessed and discussed with the structure, texture and mineralogy results.
1.3.3 The influence of particle size/morphology on synthetic kaolinite's sorption was studied. To do that: (1) synthetic kaolinites with different morphologies and without mineralogical impurities, were prepared, (2) these synthetic products were characterized with XRD, FTIR, TEM, BET and CEC analysis, (3) the approach was validated by comparing the results obtained with KGa--1b and the results from literature and (4) Na^+/H^+ sorption isotherms obtained for different morphology particles were interpreted.

CHAPTER 2 THEORIES

2.1 Clay mineralogy

Clay is a natural, earthy, fine-grained material which becomes plastic and mouldable when mixed with water (Wilson, 1987). Clay minerals are formed by hydrothermal action (Grim, 1968) or exposed to the chemical weathering by the atmosphere. These minerals have been deposited as sediment over extended periods of time at, or near, the Earth's surface (Sposito, 1989; Velde, 1995; Moore and Reynolds, 1997). Clays are hydrous aluminium silicates which consists of the colloid fraction (<2µm) of soils, sediments, rocks and water and may be composed of mixtures of fine grained clay minerals and clay-sized crystals of other minerals such as quartz, feldspar, carbonates and metal oxides (Bhattacharyya and Gupta, 2008). According to Wentworth scale, the upper limit of clay size is less than about 4 microns (µ) but clay can be concentrated in a size smaller than 2 microns when the clay is soaked in water. A large number of analyses have shown that non-clay minerals are not smaller than 1 to 2 microns. Although there is no sharp universal boundary between the particle size of clay and non-clay minerals, the upper limit for the best separation between clay and non-clay minerals is at 2 microns (Grim, 1968). Less than 2 µm fraction is also better size for studying coarser-grained clay minerals such as kaolinite and chlorite (Srodon, 2006).

Clays invariably contain exchangeable cations and anions held to the surface. The prominent cations and anions found on clay surface are Ca^{2+}, Mg^{2+}, H^+, K^+, NH_4^+, Na^+, and SO_4^{2-}, Cl^-, PO_4^{3-}, NO_3^-. These ions can be exchanged with other ions relatively easily without affecting the clay mineral structure. Large specific surface area, chemical and mechanical stability, layered structure, high cation exchange capacity (CEC), etc., have made the clays excellent adsorbent materials (Bhattacharyya and Gupta, 2008).

2.1.1 Clay structure

Clay has a large fraction of layer silicate minerals that has a strong influence on the clay's nature. Clay minerals are composed of silica, alumina or magnesia and water, but iron substitutes for aluminum and magnesium in varying degrees, and appreciable quantities of potassium, sodium, and calcium are frequently present as well. Both the structural and chemical characteristics of the constituent layer silicates are the fundamental features that affect the properties of clay materials. Layer silicate minerals can be classified owing to their characteristics as shown in Tables 2.1 and 2.2. Structural arrangements include the type of silicate layer and chemical compositions consist of both the net layer charge (x) per unit formula and the interlayer material type.

Table 2.1 Classification of planar hydrous phyllosilicate
(Source: Martin et al., 1991)

Layer type	**Interlayer material**	**Group**	**Octahedral character**[a]	**Species**
1:1	None or H_2O only (x ~ 0)	Serpentine-Kaolin	Tri	Lizardite, etc.
			Di	Kaolinite, dickite, nacrite, halloysite,
			Di-tri	Odinite
2:1	None (x ~ 0)	Talc-Pyrophyllite	Tri	Talc, kerolite, etc.
			Di	Pyrophyllite, etc.
	Hydrated exchangeable cations (x ~ 0.2- 0.6)	Smectite	Tri	Saponite, etc.
			Di	Montmorillonite, nontronite, etc.
	Hydrated exchangeable cations (x ~ 0.6- 0.9)	Vermiculite	Tri	Tri octahedral Vermiculite
			Di	Di octahedral Vermiculite
	Non-hydrated monovalent cations (x ~ 0.6- 1.0)	True Mica	Tri	Biotite, etc.
			Di	Muscovite, illite, etc.
	Non-hydrated divalent cations (x ~ 1.8- 2.0)	Brittle Mica	Tri	Clintonite, etc.
			Di	Margarite
	Hydroxide sheet (x =variable)	Chlorite	Tri	Chamosite, etc.
			Di	Donbassite
			Di-tri	Sudoite, etc.
2:1 Regular Interstratified (x=variable)	-	-		Aliettite, etc.
	-	-		Rectorite, etc.

* x = net layer charge per unit formula.
[a] tri = trioctahedral, di=dioctahedral

Table 2.2 Classification of non-planar hydrous phyllosilicate
(Source: Martin et al., 1991)

Layer Type	Modulated component	Unit layer	Group	Species
A. Modulated Structure				
1:1	Tetrahedral sheet	7 Å	Serpentine	Antigorite, pyrosmtalite, etc.
2:1	Tetrahedral sheet	9.5 Å	Talc	Minnesotaite
		12.5 Å	Mica	Ganophyllite, eggletonite
		9.6-12.5 Å	Mica/complex	Zussmanite, lennilenapeite, etc.
		14 Å	Chlorite	Gonyerite
	Octahedral sheet	12.7 Å- 13.4 Å	Pyribole	Sepiolite, palygorskite, etc
B. Rolled and Spheroidal Structures				
1:1	None	-	Serpentine	Chrysotile, pecoraite
		-	Kaolin	Halloysite (nonplanar)

Some clay minerals may be expressed using ideal chemical formulas as the following: $(Si_4)^{IV}(Al_4)^{IV}O_{10}(OH)_8$ (kaolinite), $Mg_6Si_4O_{10}(OH)_8$ (serpentine), $4SiO_2.3MgO.H_2O$ (talc) and $(Si_{7.8}Al_{0.2})^{IV}(Al_{3.4}Mg_{0.6})^{VI}O_{20}(OH)_4$ (montmorillonite). Obviously, structural features are interrelated with chemical characteristics (Wilson, 1987; Bhattacharyya and Gupta, 2008).

Clay minerals composed of octahedral sheets and tetrahedral sheets. One surface of the layer consists entirely of oxygen atoms (Ob) belonging to the tetrahedral sheet, while the other surface is composed of Ooct (mostly OH groups) from the octahedral sheet (Figure 2.1). In the 2:1 or TMT layer the tetrahedral sheets are inverted and two-thirds of the octahedral hydroxyl groups are replaced by tetrahedral apical oxygen atoms.

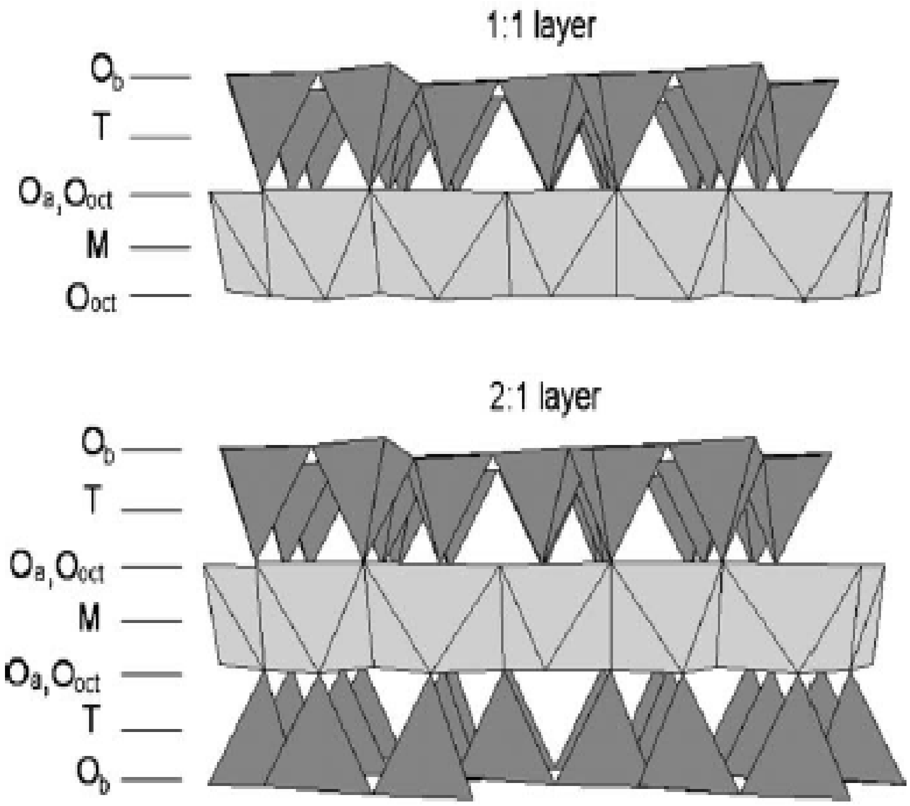

Figure 2.1 Models of a 1:1 and 2:1 layer structure. O_a, O_b, and O_{oct} refer to tetrahedral basal, tetrahedral apical, and octahedral anionic position, respectively. M and T indicate the octahedral and tetrahedral cation, respectively. **(Source:** Brigatti et al., 2006)

The structural unites of clays consist of either alternating tetrahedral and octahedral sheets (OT or 1:1 structure), as in the kaolinite group of clay minerals; a sandwich of one octahedral sheet between two tetrahedral sheets (TOT or 2:1 structure), as in illite and the smectite clay minerals, of which the most common member is montmorillonite; or an arrangement in which the three-layer TOT units alternate with a brucite layer (2:1:1 structure) as in chlorite. The basic structural arrangements of the regularly and randomly interstratified phyllosilicates are illustrated schematically in Figure 2.2. Mixed-layer phyllosilicates or interstratified phyllosilicates can be built up by two or more different components. Structures with more than two components are less common, possibly because it is difficult to recognize all the different layers. Interstratified clay minerals can have (i) ordered or regular mixed-layer structures if different layers alternate along the c* direction in a periodic pattern (e.g., the stacking of generic type A and type B layers can be …ABABAB… or …AABAABAA… or …AAAABAAAABAAAAB…etc.) and (ii) disordered or irregular mixed-layer structures, if the stacking along the c* direction of type A and B layers is random (e.g., …ABBABAA… or …AAABABBAAAAABABA…) (Brigatti et al., 2006).

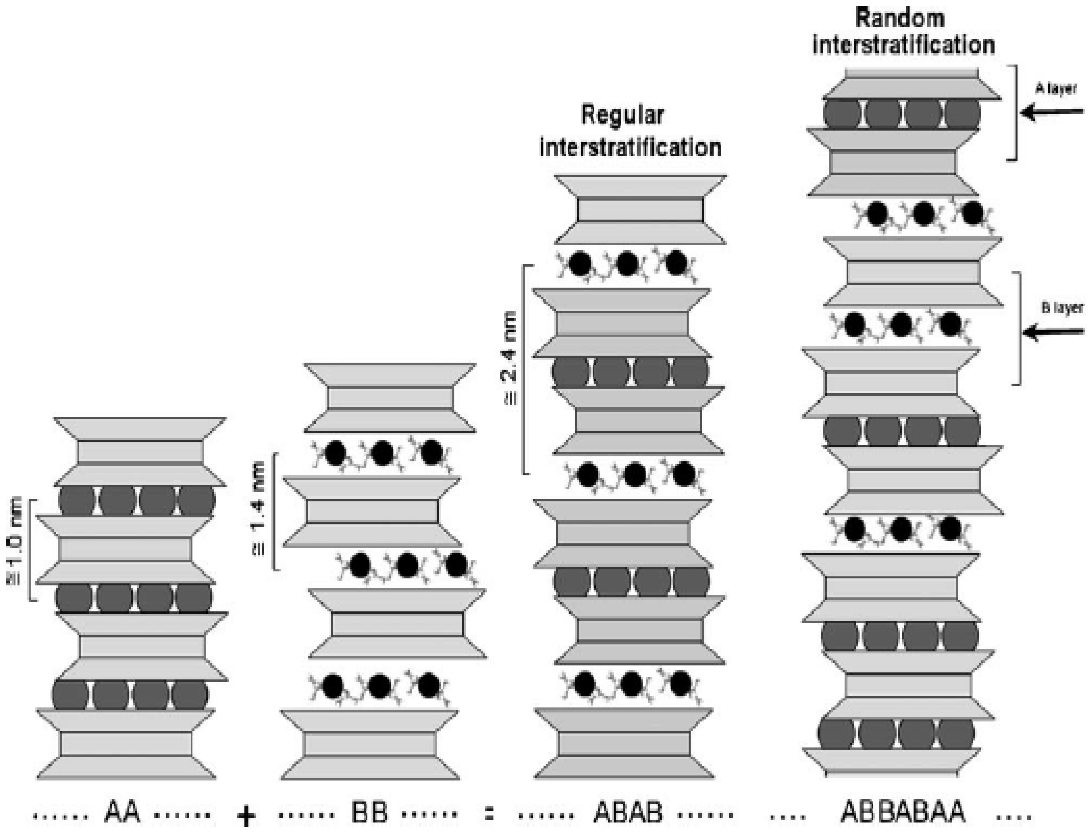

Figure 2.2 Regularly and randomly interstratified phyllosilicates. A and B are layers with different periodicity along the c direction. (**Source**: Brigatti et al., 2006)

2.1.2 Kaolinite

Kaolin forms at relatively low temperatures and pressures mostly from the feldspar and muscovite, both of which consist of alumina and silica. It mainly consists of kaolinite. Kaolinite is a layered silicate clay mineral with the chemical composition $(Si_4)^{IV}(Al_4)^{VI}O_{10}(OH)_8$. It has the theoretical composition expressed in oxides of SiO_2 46.54%, Al_2O_3 39.50%, H_2O 13.96%. The formula indicates that there is no substitution of Si^{4+} with Al^{3+} in the tetrahedral layer and no substitution of Al^{3+} with other ions (e.g., Mg^{2+}, Zn^{2+}, Fe^{2+}, Ca^{2+}, Na^+ or K^+) in the octahedral layer. Thus, the net layer charge of kaolinite is zero as shown in Figure 2.3a, but in nature, kaolinite has a small net negative charge arising from broken edges on the clay crystals. This small negative charge makes the surface not being totally inert (Wilson, 1987; Bhattacharyya and Gupta, 2008). Many researchers, however, reported that the edge surface contributes variable charges which may be positive or negative depending on the pH conditions. The silica tetrahedral face of kaolinite is negatively charged at $pH>4$, whereas the alumina octahedral face of kaolinite is positively charged at $pH<6$, and negatively charged at $pH>8$. Many analyses have also shown that a very small amount of iron and/or titanium is substituted with aluminium in the very poor crystalline kaolinite (Grim, 1968).

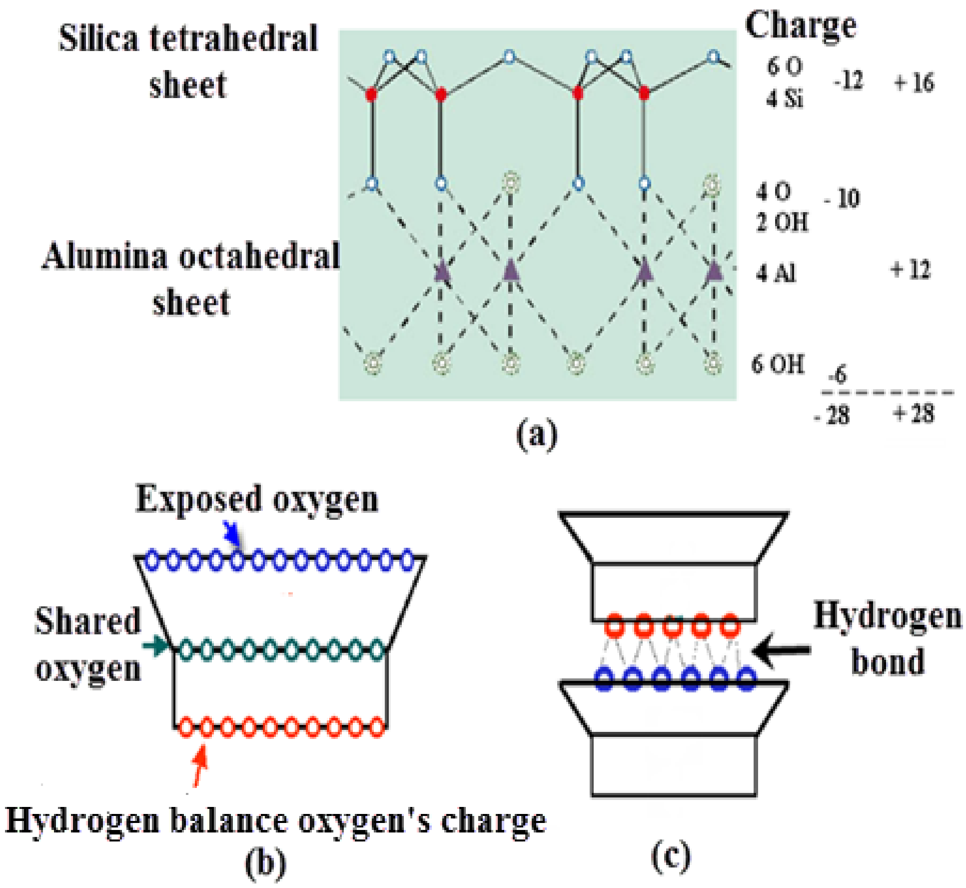

Figure 2.3 Kaolinite structure (a), schematic representation of a unit of kaolinite (b) and two unit of kaolinite (c).

The structure of kaolinite consists of a single sheet of silica tetrahedral and a single alumina octahedral sheet combined to form a common layer and consequently, the tips of the silica tetrahedrons towards the octahedral layer as shown in Figure 2.3b (Grim, 1968). That means the aluminum side of the layer is covered in hydroxyl groups (aluminol) and the silicon side is in oxygen atoms (siloxane surface) (Wypych, 2004). In the layer common to the octahedral and tetrahedral groups, two-thirds of the oxygen atoms are shared by the silicon and aluminum and the remaining one-third is filled for only aluminum in the octahedral sheet (Grim, 1968). A high cohesion between the layers by hydrogen bonding gives the clay a very rigid structure (Figure 2.3c) that cannot be swollen by changing pH or solution ionic strength. There are also no water molecules or metal cations in the interstack space, with the result that kaolinite shows no swelling and has a low exchange capacity. Kaolinite has a low cation exchange capacity of about 5 cmol$_c$/kg compared with other 2:1 type clay minerals such as montmorillonite (100 cmol$_c$/kg) (Olphen, 1963; Lyklema, 1995). However, cation exchange capacity of kaolinite varies in the range of 3.6-10 cmol$_c$/kg depending on the different regions and sources of kaolinite (Ferris and Jepson, 1975; Adams, 1984).

The two surfaces (hydroxyl and siloxane) have very different structures and relative to surface chemistries. Hydroxyl groups, known as terminal OH groups, located at broken edges, steps and related defects of clay minerals and oxides are different. These OH groups are under-coordinated and more reactive than the charge-neutral OH groups on basal surfaces. They carry either a positive or negative charge depending on the pH of the ambient aqueous solution (Figure 2.4). Though kaolinite is the least reactive clay, its high pH dependency enhances or inhibits the adsorption of metals according to the pH of the environment (Bhattacharyya and Gupta, 2008; Wilson, 1987). At pH values higher than the point of zero charge (p.z.c.) of a mineral, the surface will have a net negative charge and will tend to accumulate cationic species. When the ambient pH is lower than the p.z.c, the edge surface will have a net positive charge. Since the terminal OH groups have either a partial positive or partial negative charge groups, they also possibly chemisorb certain types of ions, regardless of the pH value. (Schoonheydt and Johnston, 2006).

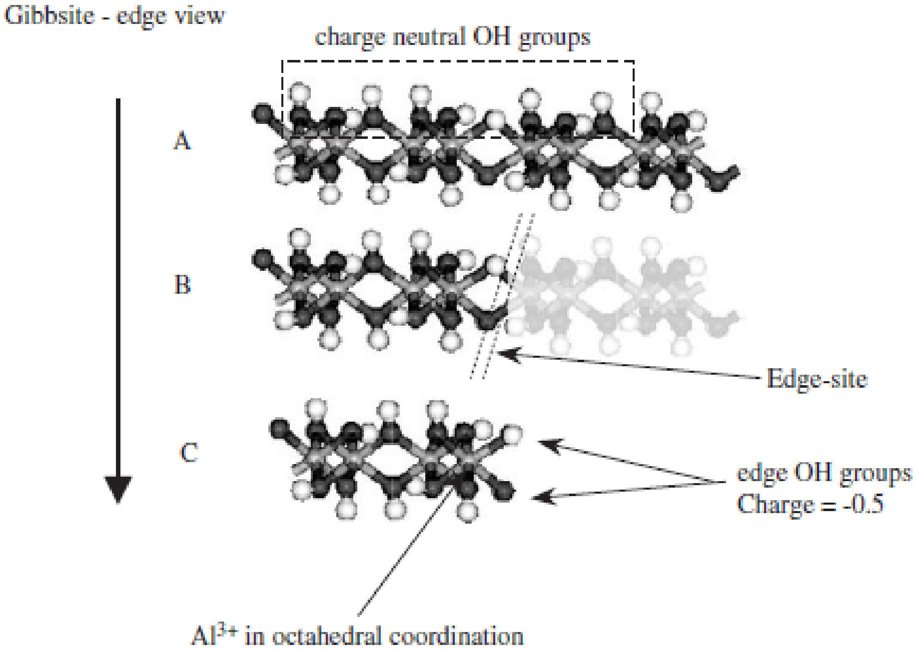

Figure 2.4 Edge sites of kaolinite. (**Source:** Schoonheydt and Johnston, 2006)

2.1.3 Montmorillonite

Montmorillonite is composed of units in which alumina octahedral sheet is sandwiched between two silica tetrahedral sheets. Thus, it is referred to as 2:1 type clay mineral with T-O-T structure (Wypych, 2004). All the tips of the tetrahedrons point toward the hydroxyl layers of the octahedral sheet and then, a common layer is formed as shown in Figure 2.5. Instead of hydroxyl atoms, oxygen atoms become common to both tetrahedral and octahedral layer (Grim, 1968). In the stacking of these units, oxygen layers of each unit are adjacent to oxygen of the neighboring units. The low interaction between the layers causes a very weak bond and consequently, the unit can be easily cleavage (Wypych, 2004).

The formula for montmorillonite is $(Si_{7.8}Al_{0.2})^{IV}$ $(Al_{3.4}Mg_{0.6})^{VI}$ O_{20} $(OH)_4$ and theoretical composition without the interlayer material is SiO_2 66.7%, Al_2O_3 28.3%, H_2O 5%. According to the above formula, Si^{4+} is substituted by Al^{3+} in the tetrahedral layer and Al^{3+} is substituted by Mg^{2+} in the octahedral layer (Grim, 1968). These substitutions cause the montmorillonite has a negative charge; the net layer charge is

[7.8(+4)]+[0.2(+3)]+[3.4+(+3)][0.6(+2)][20(-2)][4(-1)] = -0.8 charge per unit cell (Bhattacharyya and Gupta, 2008). That resulting net negative layer charge is balanced by interlayer exchangeable cations (Francisco and Santos, 2001).

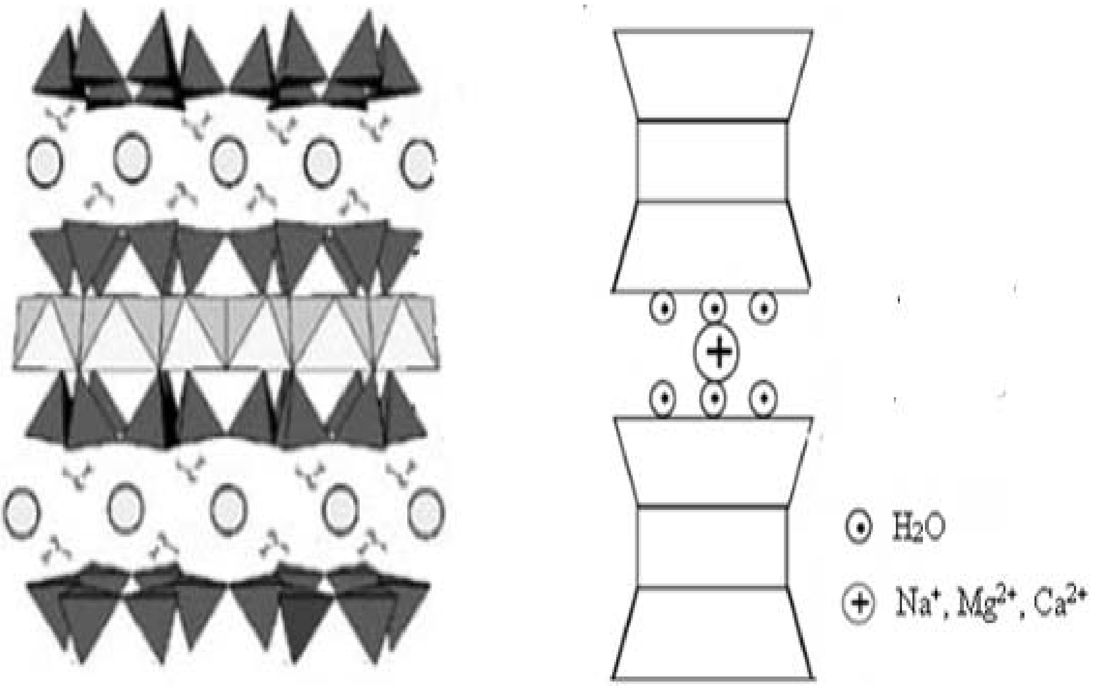

Figure 2.5 Structure of montmorillonite. (**Source**: Brigatti et al., 2006)

In montmorillonite, the adsorption can occur both at the edge sites and planar (internal) sites on the minerals which results in inner-sphere complex and outer-sphere complex, respectively (Bhattacharyya and Gupta, 2008). The Al^{3+} in tetrahedral sheet of the acid-treated montmorillonite reveals their acidic role. It is widely aware that partially removing of the octahedral ions is essential to render the acid activated montmorillonite with maximum bleaching capacity, and the acid activation process results in somewhat destruction of the original montmorillonite (Yang et al., 2006). Physicochemical properties of commercial bleaching clay (montmorillonite) are shown in Table 2.3.

Table 2.3 Physicochemical properties of commercial bleaching clay (montmorillonite) (Taylor, 2005)

Properties	**Natural**	**Acidified**
Free moisture (wt%)	10-15	10-15
pH (2% slurry)	6-8	2.5-5.5
Residual acidity (mg KOH/g)	<1	1-10
Surface area (m^2/g)	50-100	150-350
Pore volume (cc/g)	0.05-0.15	0.3-0.35
Bulk density (kg/m^3)	960-1200	550-800
wt% passing 200 mesh (75μm)	70-100	70-100
wt% passing 325 mesh (45μm)	60-75	60-75
Particle size (Ave. diam., mm)	15-35	15-35
Oil retention (wt%)	25-35	30-40

2.2 Modification of clay's adsorption properties by activation

To activate the adsorption capacities of a natural clay, many industries uses: physical treatment - alteration of particle size (the specific surface area) mechanically; thermal treatment – alteration of chemical composition and/or crystalline structure by the effect of temperature; and chemical treatment- massive destruction of the clay mineral structure (Francisco and Santos, 2001).

2.2.1 Physical activation of clay (Mechanical activation)

The mechanical activation of kaolinite using centrifugal planetary machine give a high efficiency to the clay being activated. Under intensive mechanical activation, the structure of OH group is disordered along with the occurrence of water and hydroxonium ions in activated kaolinite (Dudkin et al., 2005). The unground kaolinite appears needle-shape and after 4 hours of grinding, this shape disappeared completely accompanied by the occurrence of spherical particles. The particle size of the kaolin decreased from 5.4 μm to 4.0 μm. Besides the particles breakage, the aggregates are also formed. Although Al_2O_3 of the unground sample is difficult to leach, mechanical activation enhanced the dissolution of Al_2O_3 (Tang et al., 2010). Tang et al. (2010) showed that the combined mechanical and acid activation was more effective than acid treatment alone.

2.2.2. Thermal activation of clay

Thermal treatment (calcinations) also increases the reactivity of the particles besides removing the physically and chemically combined water and any organic materials in pores. It was also claimed that during the calcinations process, kaolinite can be converted to metakaolinite which makes it possible to extract Al^{3+} with hot acid solution.

In the course of a thermal activation, kaolinite loses the most part of its structural water and passes into a metastable state (Dudkin et al., 2005) resulting in collapsed and disarranged clay structure (Sabir et al., 2001) and hence a decrease in the specific surface area which leads to decreased in color removal (James et al., 2008). The main changes were initially observed at below 200°C where water absorbed in pores and on the surface is released (Ilic et al., 2010). When kaolin is heated to temperature between 100°C and 400°C, predehydration process occurred resulting in weight loss and the octahedral layer reorganized. Most of the dehydration occurs between 400°C and 525°C. At 500°C to 700°C, dehydroxylation process occurred leading to the transformation of kaolin into metakaolin and resulting in collapsed and disarranged clay structure. Above 700°C, a new crystalline phase started to form rendering its resistant to leaching (Kakali et al., 2001; Sabir et al., 2001 and Foo et al., 2011). When the kaolinite is heated to about 800°C, all water molecules and (OH)-ions are evaporated and kaolinite become metakaolinite. Beyond 800°C, kaolinite structure is destroyed and cannot be reconstituted by rehydration.

2.2.3 Chemical activation of clay (Acid activation)

The industrial utilization of kaolin is closely related to its reactivity and surface properties, which depend strongly on surface modification. Acid activation has been widely studied as a chemical treatment method for the improvement of the surface and catalytic properties of kaolin. The method involves leaching of the clays with inorganic acids, causing disaggregation of clay particles, elimination of mineral impurities, and dissolution of the external layers, thus altering the chemical composition and the structure of the clays (Panda et al., 2010).

On acid attack, the crystalline structure of kaolinite is transformed thermally to amorphous metakaolin and the octahedral Al^{3+}ions are preferentially released from the clay structure leading to formation of additional Al-OH and Si-OH bonds, without changing the original mineral structure (Bhattacharyya and Gupta, 2008). The exchanges of interlayer cation by proton improve the bleaching capacity of clays (Nguetnkam et al., 2008). A possible scheme of the structural disordering of kaolinite by protons was studied by the dissolution of kaolinite in $HClO_4$ (perchloric acid) solutions. It was assumed that a hydrated proton penetrates into the octahedral network and, stage-by-stage, polarizes and ruptures bonds between the octahedral and tetrahedral networks of the kaolinite layer. By this way, acid activation leaves a large number of highly active silanol and aluminol groups on the adsorbent sites as shown in Figure 2.6 (Dudkin et al., 2005).

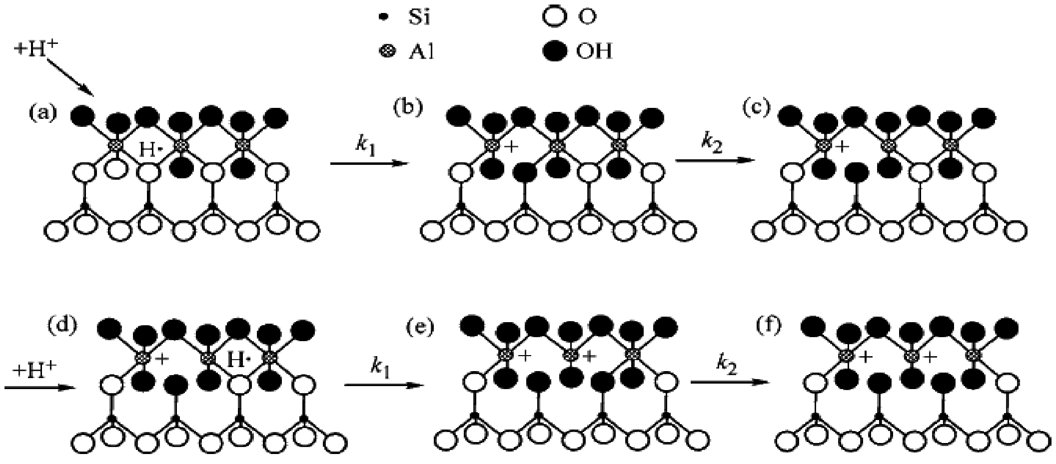

Figure 2.6 Possible scheme of interaction of a proton with the structure of kaolinite. (Dudkin et al., 2005)

The acid treatment also opens the edges of the platelets, eliminate several mineral impurities and partially dissolve the external layer (Bhattacharyya and Gupta, 2008). As a consequence of all these changes, the surface area, pore volume and pore diameter are increased with increasing acid strength (Francisco and Santos, 2001; Bhattacharyya and Gupta, 2008). Upon 1M sulfuric acid treatment, the new surface area of the original kaolin is three times greater and with 10 M acid treatment the surface area increased to 143 m^2/g (Panda et al., 2010). Acid activation drastically reduces the Lewis acid sites but generate Brönsted acid sites on the clay matrix (James et al., 2008). Both Brönsted acid sites and Lewis acid sites also improve the adsorption capacity of clay to a great extent. The Brönsted acidity arises from H^+ ions on the surface, formed by dissociation of water molecules of hydrated exchangeable metal cations on the surface. The Brönsted acidity may also arise if there is a net negative charge on the surface due to the substitution of Si^{4+} by Al^{3+} in some of the tetrahedral positions and the resultant charge is balanced by H_3O^+ cations. The Lewis acidity arises from exposed trivalent cations, mostly Al^{3+} at the edges, or Al^{3+} arising from rupture of Si–O–Al bonds, or through dehydroxylation of some Brönsted acid sites (Bhattacharyya and Gupta, 2008).

Using cold, dilute acid has little effect on metal ion removal efficiency of clay whereas treating with hot, concentrated acid gives much efficiency (Breen et al., 1997). As the strength of the acid increases, the Al_2O_3, MgO, CaO and K_2O contents in the acid treated material decrease progressively. Simultaneously, SiO_2 content increased with increase in the acid strength due to which the Si/Al ratio increased. The decrease in the alumina content in the acid treated sample can be ascribed to the leaching of the Al^{3+} ions from the octahedral layer due to hydrolysis under acidic conditions. Panda et al, (2010) reported that at 10M H_2SO_4 acid treatment on kaolin clay, the Al_2O_3 content decreases from 46.07% to 7.70% whereas the SiO_2 content increases from 43.12% to 87.46%. Increasing the silica to alumina ratio will increase the surface negativity and as a result increases the clay's adsorption capacity (Al-Harahsheh et al., 2009).

2.3 Hydrothermal synthesis of kaolinite

Synthetic clay minerals are prepared to obtain pure products in a short time and at the lowest possible temperature. Minerals or rocks, glasses, and gels can be used as starting materials. The most commonly used starting material is aluminosilicate gel. The Si/Al ratio of gel is important in hydrothermal synthesis. The gels are washed to remove excess ions because contamination of alkali ions inhibits crystallization. At lower Si/Al ratios and higher temperatures, the b-axis ordered kaolinite is formed. Pure kaolinite with spherical morphology was obtained when the system is performed at 150–200˚C, and platy kaolinite at 250˚C in hydrothermal experiments at autogenous pressure. Hydrothermal treatment can induce the formation and crystal growth of clay minerals. The important controlling parameters are temperature (T), synthesis time (t) and solution chemistry, viz., pH. In order to obtain formation of clay minerals, The ion concentrations in solution (Si^{4+}, Al^{3+}, etc.) must be high enough to reach critical oversaturation (S*). This condition is easily reached when the starting materials are gels or glasses because they are highly soluble and have compositions similar to those of the required clay minerals. The clay mineral's growth is strongly dependent on temperature and the syntheses performed at low temperatures often do not succeed. However, at T>500˚C, other silicate or oxide phases become more stable than clay minerals. Most clay mineral syntheses are performed in the temperature range of 100–500˚C. The type of synthetic clay mineral produced depends on the final hydrothermal synthesis pH (pH_F), and kaolinite (1:1 clay mineral) is favorably produced when the treatments consist of Al^{3+} and/or Fe^{3+} at low pH_F (2–6). Fialips et al. (2000) proposed that hydrothermal synthesis of kaolinite from metakaolinite is dependent on the pH and the type of metakaolinite. The less-ordered kaolinite is obtained when the synthesis pH is 4–6 than when the pH is 1. There are two steps in this transformation process; the first process involves dissolution of the metakaolinite followed by crystallization of either thin prismatic or dendritic kaolinite particles that curl due to surface tension, and the second process involves the rapid formation of small, pseudohexagonal kaolinite particles that aggregate and coalesce to form larger particles.

The crystallinity of clay mineral increases with increasing time. Kaolinite's crystallinity is determined by measuring the width of reflections in XRD patterns (mean crystal size coherency obtained using the Scherrer equation), or specific measurements such as the Hinckley index. Kaolinite with spherical morphology is obtained when the gel containing silica and alumina tetrahedral and some alumina octahedral, is precipitated at pH 9.6 whereas the platy morphology with an allophone-like structure is obtained when the gel is precipitated at pH 4.2. During the kaolinite synthesis, the hydroxides or pseudo-hydroxides such as the pseudo-boehmite are observed. These intermediate phases are generally of low crystallinity and/or are non-stoichiometric which are difficult to identify using analytical techniques such as XRD, DTA-TGA, and FTIR. Clay mineral synthesis is a complex heterogeneous reaction. Greater details about in synthesis of kaolinite are in the literature (Carrado et al., 2006).

2.4 Instrumental characterization of clay mineral

2.4.1 X-ray Diffraction

X-ray Diffraction is a versatile, non-destructive technique which is used to identify crystalline phases, determine chemical compositions and crystallographic structure of natural and modified clays. XRD principles in detail (Cullity, 1956) and the interpretation of applied XRD method especially in powder methods (e.g. Moore and Reynolds, 1997) are abundantly found in the literature. X-rays are electromagnetic radiations which lie between Ultraviolet light and Gamma Rays in the electromagnetic spectrum. XRD is obtained when electromagnetic radiation interacts with a periodic structure, whose repeat distance is about the same as the wavelength of the radiation planes. X-ray diffraction occurs when X-rays are scattered by atoms arranged in an orderly array in crystals. The atoms serve as scattering centers reemitting X-rays at the same wavelength as the incident radiation in all directions (coherent scattering) (Moore and Reynolds, 1997). Bragg's law (below equation) was used to explain the interference pattern of X-rays scattered by crystals.

$$n\lambda = 2d\sin\theta$$

where λ is wavelength of X-ray used, θ is an angle between incident X-rays and plane of crystal, d is the distance between planes of particles, n is an integer (1,2,3,…) that represents serial order of diffracted beams. XRD shows the cleavage faces of crystals reflect X-ray beams at certain angles of incidence (theta, θ). By varying the angle theta, the Bragg's Law conditions are satisfied by different d-spacings in polycrystalline materials. Diffraction occurs only when Bragg's Law is satisfied condition for constructive interference (X-rays 1 & 2) from planes with spacing d (Figure 2.7). Plotting the angular positions and intensities of the resultant diffracted peaks of radiation produces a pattern, which is characteristic of the sample. The diffractometer records the intensity of the diffracted beam electronically at precise angles as the specimen is scanned over an angular range. These intensity patterns at specific angles are matched with the intensity of standard samples at precise angular locations. The mineralogical information from the sample is thus obtained. The resulting XRD patterns can be compared with known standards in the JCPDS file which are for random orientations.

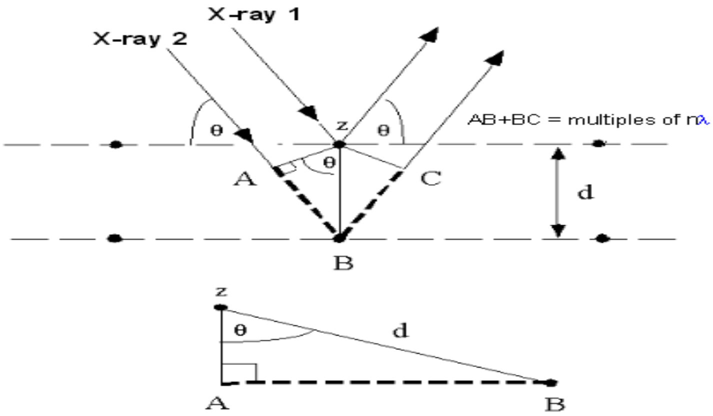

Figure 2.7 Schematic X-ray diffraction interaction of plane of sample.
(Source: Cullity, 1956)

Powder diffraction is mainly used for the characterization and identification of polycrystalline phase of various solid materials. In powder or polycrystalline diffraction, the sample is prepared to have smooth plane surface by grinding the particle into 0.002 mm to 0.005 mm cross section. Then, the randomly oriented sample is pressed into a sample holder. The most commonly used X-ray radiation is that emitted by copper, CuKα radiation λ=1.5418Å, corresponding to an energy of 8,048eV. In normal use, the detector is set to scan over a range of 2θ values at a constant angular velocity. Normally, a θ range of 5 to 70° is sufficient to cover the most useful part of the powder pattern. The scanning speed of the detector is usually 2θ of 2° min^{-1} and, therefore, it takes about 30 minutes to get peaks. The d-spacing value depends only on the shape of the unit cell and it is obtained as a function of 2θ from Bragg's law. Each reflection is fully defined when the d-spacing, the intensity (area under the peak) and the indices h, k, l are known. The poor structural order commonly observed in kaolin minerals is due to the series of stacking faults or defects in the ab plane and along the c-axis. Well-ordered kaolinite shows sharp and narrow peaks, while its disordered counterpart gives less well-defined, broad, and asymmetrical peaks. In extreme cases, peaks lose their identity and merge to form a two-dimensional modulated band of diffracted intensity. Structural order/disorder in kaolinite can be determined by different methods such as the Hinckley index (HI) as shown in Figure 2.8 (Hinckley, 1963), and the Liétard index (R2) (Liétard, 1977) that is sensitive to the presence of arbitrary defects only (Brigatti et al., 2006).

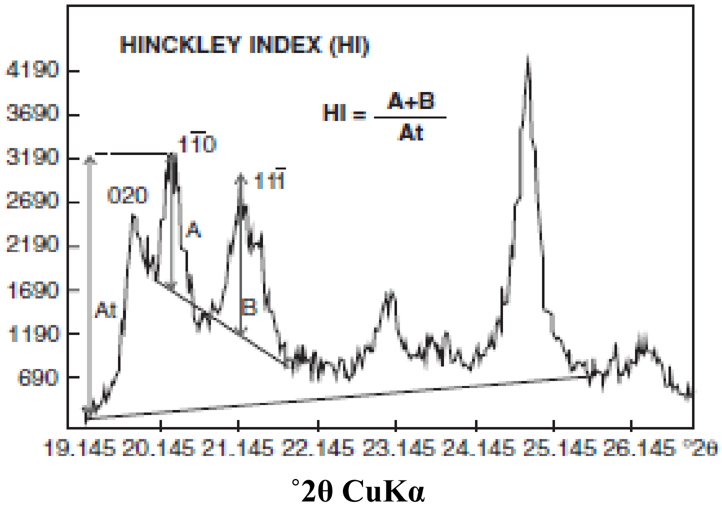

Figure 2.8 Hinckley index method for assessing the degree of structural order in kaolinite.

2.4.2 X-ray fluorescence spectroscopy

X-rays Fluorescence spectroscopy (XRF) is a powerful tool used for qualitative and quantitative elemental analysis. X-rays can be seen as electromagnetic waves with their associated wavelengths, or as beams of photons with associated energies. Figure 2.9 shows that X-rays have wavelengths and energies between γ-rays and ultra violet light. The wavelengths of X-rays are in the range from 0.01 to 10 nm, which corresponds to energies in the range from 0.125 to 125 keV. The wavelength of X-rays is inversely proportional to its energy, according to E*λ=hc. E is the energy in keV and λ the wavelength in nm. The term hc is the product of Planck's constant and the velocity of light and has, using keV and nm as units, a constant value of 1.23985.

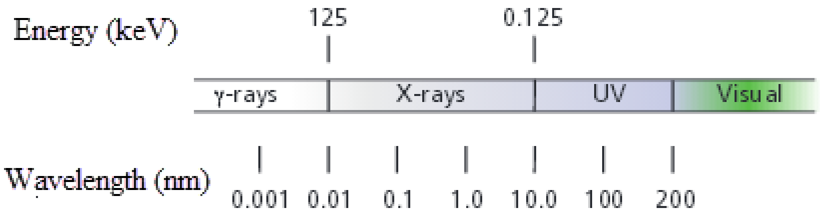

Figure 2.9 X-rays and other electromagnetic radiations.
(Brouwer, 2010)

Many references are available for XRF treatment (Birks, 1969; Tertian and Claisse, 1982; Jenkins, 1999). The various elements in the powder sample are determined by measuring the characteristic secondary radiation emitted from a sample that has been excited with an X-ray source. In XRF spectrometry, high energy X-ray photons are emitted from a source (X-ray tube) and strike the sample. The photons from the X-ray tube have enough energy to knock electrons out of the innermost orbital of atoms in the sample. The classical model of an atom is a nucleus with positively charged protons and non-charged neutrons, surrounded by electrons grouped in shells or orbitals. The innermost shell is called the K-shell, followed by L-shells, M-shells etc. as shown in Figure 2.10 (Brouwer, 2010).

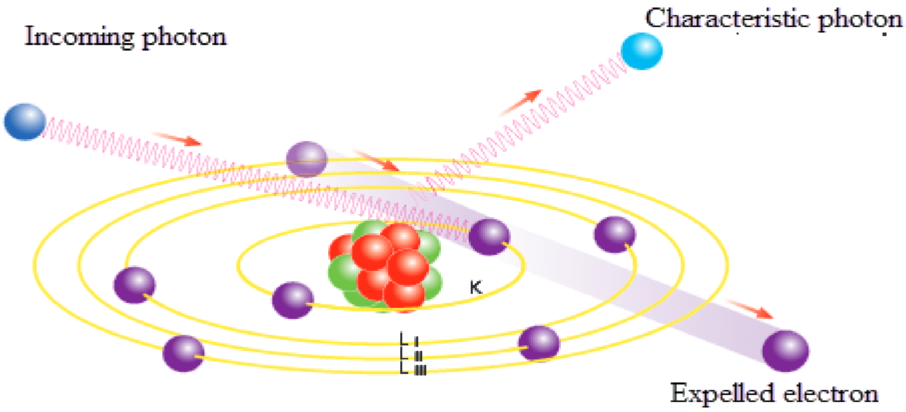

Figure 2.10 Production of characteristic radiation.
(Brouwer, 2010)

When the electrons are knocked out of inner orbitals, the atoms become ions, which are unstable. Electrons seek stability and the lowest possible energy state. Therefore, a more energetic electron from an outer orbital will move into the newly vacant space in the inner orbital. Electrons in outer shells have more energy than electrons in more inner orbitals. They need to release this excess energy as they drop down to fill the vacancy in the inner shell. This released energy is given off as a photon which can be detected by an X-ray detector. This fluorescent light is called the characteristic X-ray of the element. The energy of the emitted photon will be equal to the difference in energies between the two orbitals occupied by the electron making the transition. Because the energy difference between two specific orbital shells, in a given element, is always the same (i.e. characteristic of a particular element), the photon emitted when an electron moves between these two levels, will always have the same energy. Therefore, by determining the energy (wavelength) of the X-ray light (photon) emitted by a particular element, it is possible to determine the identity of that element. The elements with high atomic numbers have better detection limits than the lighter elements. The measurement time depends on the number of elements to be determined and the required accuracy, and varies between seconds and 30 minutes. The analysis time after the measurement is only a few seconds.

The method is fast, accurate and non-destructive, and usually requires only a minimum of sample preparation. Spectrometer systems can be divided into two main groups: energy dispersive systems (EDXRF) and wavelength dispersive systems (WDXRF). The elements that can be analyzed and their detection levels mainly depend on the spectrometer system used. The elemental range for EDXRF goes from sodium to uranium (Na to U). These spectrometers have a detector that is able to measure the different energies of the characteristic radiation coming directly from the sample. The detector can separate the radiation from the sample into the radiation from the elements in the sample. This separation is called dispersion. For WDXRF it is even wider, from beryllium to uranium (Be to U). The concentration range goes from (sub) ppm levels to 100%. These spectrometers use an analyzing crystal to disperse the different energies. All radiation coming from the sample falls on the crystal. The crystal diffracts the different energies in different directions, similar to a prism that disperses different colors in different directions (Brouwer, 2010).

2.4.3 Fourier Transform Infrared Spectroscopy

Infrared spectroscopy is a technique based on the vibrations of the atoms of a molecule. The technique uses the infrared region of electromagnetic spectrum (see Figure 2.11) in which the infrared spectrum can be divided into three main regions: the *far-infrared* (<400 cm^{-1}), the *mid-infrared* (4000–400 cm−1) and the *near-infrared* (11,000–4,000 cm^{-1}) (Petit et al., 1999). The IR spectrum is commonly obtained by passing infrared radiation through a sample and determining what fraction of the incident radiation is absorbed at a particular energy. The energy at which any peak in an absorption spectrum appears corresponds to the frequency of a vibration of a part of a sample molecule (Stuart, 2004). Vibrations can involve either a change in bond length (*stretching*) or bond angle (*bending*). Some bonds can stretch in-phase (*symmetrical* stretching) or out-of-phase (*asymmetric* stretching), as shown in Figure 2.12.

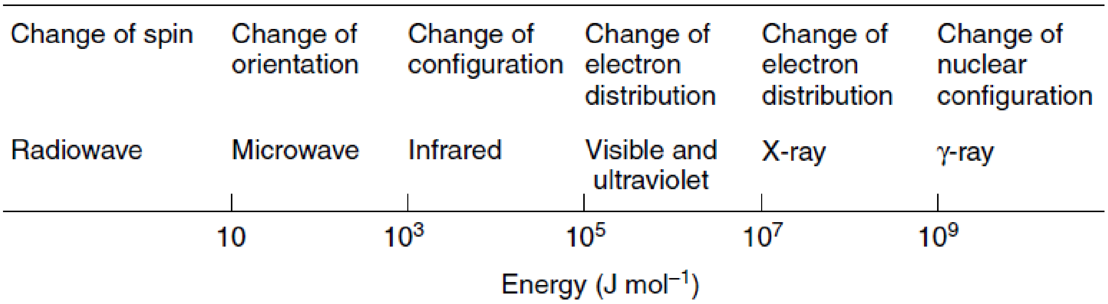

Figure 2.11 Regions of the electromagnetic spectrum.
(Stuart, 2004)

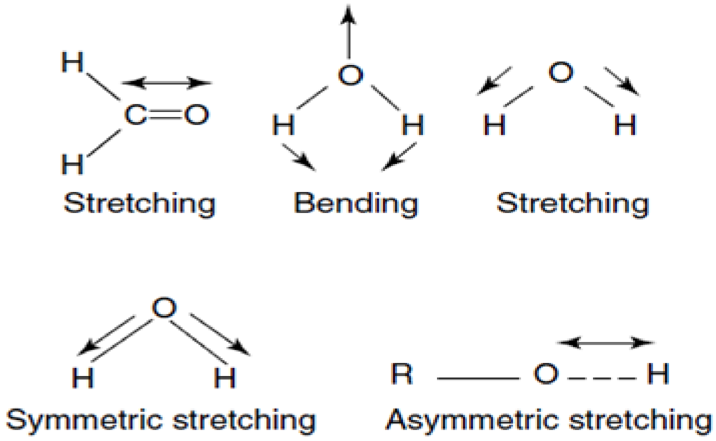

Figure 2.12 Stretching, bending, symmetric stretching and asymmetric stretching vibrations. (Stuart, 2004)

With respect to clay minerals, IR spectroscopy is a well established, useful and relatively economical tool for characterization. The vibrational frequencies obtained from IR spectra can be used to deduce information about the mineral composition and structure (Farmer, 1974, Petit, 2006). IR techniques are also used with XRD to determine the type and group of clay mineral (Madejová and Komadel, 2001). It is also used to study the adsorption mechanism of compounds relative to their frequency shifts. For clay mineral analysis, various techniques such as attenuated total reflectance Fourier transform infrared (ATR-FTIR) spectroscopy, diffuse reflectance infrared Fourier transform spectroscopy (DRIFTS), and transmission IR through self supporting clay films or mineral containing KBr pellets are used (Farmer, 1974).

Transmission spectroscopy is the oldest and most straightforward infrared method. This technique is based upon the absorption of infrared radiation at specific wavelengths as it passes through a sample. The most commonly used alkali halide is potassium bromide (KBr), which is completely transparent in the mid-infrared region. Certain factors need to be considered when preparing alkali halide discs such as the ratio of the sample to alkali halide. Around 2 to 3 mg of sample with about 200 mg of halide is sufficient to make a disc. A disc of about 1 cm diameter made from about 200 mg of material usually results in a good thickness of about 1 mm. The alkali halide should be kept desiccated and warm prior to use in order to minimize this effect of water contribution. In external reflectance, the energy that penetrates one or more particles is reflected in all directions and this component is called *diffuse reflectance*. In the diffuse reflectance (infrared) technique, commonly called DRIFT, a powdered sample is mixed with KBr powder. DRIFT is particularly useful for sampling powders or fibres. The DRIFT cell reflects radiation to the powder and collects the energy reflected back over a large angle. Diffusely scattered light can be collected directly from material in a sampling cup or, alternatively, from material collected by using an abrasive sampling pad (Stuart, 2004).

2.4.4 Brunauer-Emmet-Teller Method

Different methods are used to measure specific surface area and each method can yield different results. Most methods are based on the isothermal adsorption of nitrogen. Either a single point or multipoint method is used to calculate the surface area. The most widely used method for determination of the BET surface area is by gas adsorption. This gas is adsorbed physically on the solid surface and specific surface area of a powder is determined by calculating the amount of adsorbate gas corresponding to a monomolecular layer on the surface. Physical adsorption occurs between the adsorbate gas molecules and the adsorbent surface area of the powder sample by relatively weak van der Waals forces. The determination is usually carried out at temperature of liquid nitrogen. The amount of gas adsorbed can be measured by a volumetric or continuous flow procedure. Adsorption of nitrogen at a temperature of 77.4 K leads to a so-called adsorption isotherm, i.e. BET isotherm. The standard multipoint BET needs a minimum of three points.

The Brunauer, Emmett and Teller (BET), most common method used to describe specific surface area is as follows:

$$\frac{1}{\left[V_a\left(\frac{P_0}{P}-1\right)\right]}=\frac{C-1}{V_mC}\times\frac{P}{P_0}+\frac{1}{V_mC} \qquad (1)$$

where W is weight of gas adsorbed, P is partial vapour pressure of adsorbate gas in equilibrium with the surface at 77.4 K (b.p. of liquid nitrogen), in pascals, P_0 is saturated pressure of adsorbate gas, in pascals, P/P_0 is relative pressure, V_a is volume of gas adsorbed at standard temperature and pressure (STP) [273.15 K and atmospheric pressure (1.013×10^5 Pa)], in millilitres, V_m is volume of gas adsorbed at STP as monolayer on sample surface, in millitres, and C is BET constant.

The value of V_a is measured at each of not less than 3 values of P/Po. Then the BET value

$$\frac{1}{V_a\left(\frac{P_0}{P}-1\right)}$$

is plotted against P/P_o according to equation (1). This plot should yield a straight line usually in the approximate relative pressure range 0.05 to 0.3. The data are considered acceptable if the correlation coefficient, *r*, of the linear regression is not less than 0.9975; that is, r^2 is not less than 0.995. The slope and intercept are used to determine the quantity of nitrogen adsorbed in the monolayer and used to calculate the surface area. From the resulting linear plot, the slope, which is equal to $(C-1)/V_mC$, and the intercept, which is equal to $1/V_mC$, are evaluated by linear regression analysis. From these values, V_m is calculated as 1/(*slope* + *intercept*), while *C* is calculated as (*slope/intercept*) + 1. From the value of V_m so determined, the specific surface area, *S*, in $m^2 \cdot g^{-1}$, is calculated by the equation:

$$S = \frac{V_m N_a}{m \times 22400}$$

where, N is Avogadro constant (6.022×10^{23} mol^{-1}), a is effective cross-sectional area of one adsorbate molecule, in square metres (0.162 nm^2 for nitrogen), m is mass of powder sample, in grams, 22400 is volume occupied by 1 mole of the adsorbate gas at STP allowing for minor departures from the ideal, in millilitres. For a single point method, the intercept is taken as zero or a small positive value, and the slope from the BET plot used to calculate the surface area. The surface area reported will depend upon the method used, as well as the partial pressures at which the data are collected (Leddy, 2010).

2.4.5 Scanning Electron Microscopy (SEM)

Scanning electron microscopy (SEM) is widely used in clay mineralogy because it has a large magnification range and can analyze the solids with almost no magnification to imaging well over 100,000 times. SEM uses a focused electron probe to extract structural and chemical information point-by-point from the surface or near-surface region of a specimen, and gives a three-dimensional large and deep field of SEM images. A scanning electron microscope consists of an electron optical column, a vacuum system, electronics, and software. The electron column of the SEM consists of an electron gun and two or more electromagnetic lenses operating in vacuum as shown in Figure 2.13. The electron gun generates free electrons and accelerates these electrons to energies in the range 1-40 keV in the SEM. The electron lenses create a small, focused electron probe on the specimen. Most SEMs can generate an electron beam at the specimen surface with spot size less than 10 nm in diameter while still carrying sufficient current to form acceptable image. A specimen stage is required at which the specimen is placed relative to the beam. A secondary electron detector collects the electrons and emits a signal that is processed and ultimately displayed on viewing and recording monitors. A vacuum system is necessary to remove air molecules that might impede the passage of the high energy electrons down the column as well as to permit the low energy secondary electrons to travel to the detector. Resolution in a SEM depends on the degree to which the signal, at any instant in time, can be associated with the position of the electron beam; specifically, for a particular beam location, how large is the region within the sample from which the signal originates. This can be affected by a number of factors, including the type of signal, the size of the spot formed by the beam, composition of the sample, the energy of the beam. Generally, at lower voltages, where the beam electrons do not travel far into the sample, the size of the spot is the primary determinant of image resolution. At higher voltages, the volume of interaction, from which the signal originates, may become the primary consideration. Currently, the best SEMs offer resolution below 1 nm to below 1 kV up through the full range of accelerating voltages, allowing the operator to choose beam energy to suit the needs of the analysis; for example, higher energy to provide a wide energy spectrum for X-ray analysis, or lower energy to enhance surface specificity or avoid charging and beam damage. Detailed in SEM principles and operation are available in the literature (Wells, 1974; FEI, 2010)

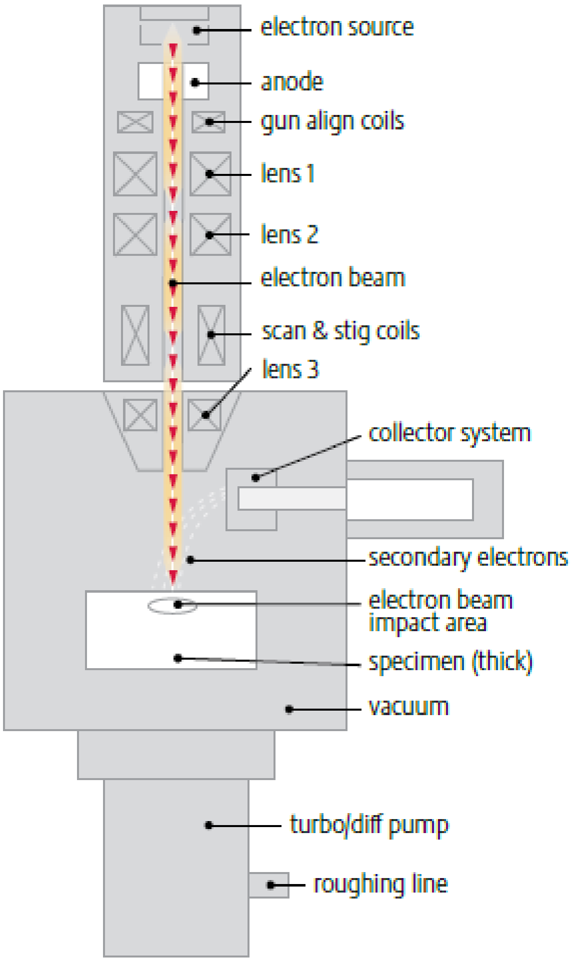

Figure 2.13 Layout of the scanning electron microscope.
(Source: FEI, 2010)

2.4.6 Transmission Electron Microscopy (TEM)

Transmission electron microscopy (TEM) techniques are widely used to determine the morphology in a non-destructive way. It can also be used in conjunction with other techniques to determine the structure, lattice imaging and chemical composition of clay mineral. The transmission electron microscope can be compared with a slide projector. In a slide projector, light from a light source is made into a parallel beam by the condenser lens; this passes through the slide (object) and is then focused as an enlarged image onto the screen by the objective lens. In the electron microscope, the light source is replaced by an electron source, the glass lenses are replaced by magnetic lenses, and the projection screen is replaced by a fluorescent screen, which emits light when struck by electrons, or, more frequently in modern instruments, an electronic imaging device such as a CCD (charge-coupled device) camera (Figure 2.14). The whole trajectory from source to screen is under vacuum and the specimen (object) has to be very thin to allow the electrons to travel through it. The specimen also have to be stable and small enough (some 3 millimeters in diameter) to permit its introduction into the evacuated microscope column and thin enough to permit the transmission of electrons. Different thicknesses are required for different applications (FEI, 2010).

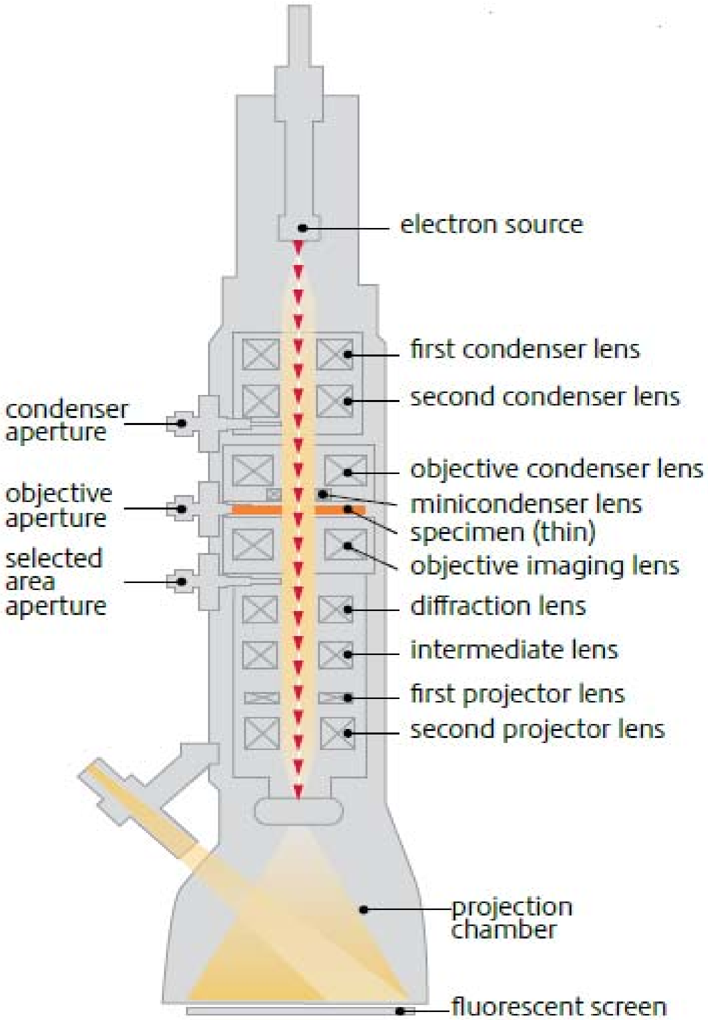

Figure 2.14 Layout of the transmission electron microscope.
(Source: FEI, 2010)

The sampling of data on a microscope grid must be done as for any other sampling method where data on a set of aliquots are acquired. To assess the size of fundamental particles by TEM and XRD, swelling effects must first be eliminated. As these techniques reflect interparticle diffraction by aggregates of fundamental particles, the aggregation of particles and their ability to form mixed-layer clay minerals can be evaluated. Data is recorded at progressive scales including intermediate scales. Several distinct areas (at least 3) have to be checked all over the grid because of the sample heterogeneity or segregation effects. The measured parameters generally qualify the size (diameter, area) of layers, particles or aggregates. Image analysis is also concerned with the organization of the material in the wide sense, such as distances between objects, arrangement of organo-mineral associations, and density of objects, as a function of physical or chemical variables. The measurement of parameters that refer to individual objects may allow objects to be separated into classes (e.g., grain size) or selection criteria (e.g., loose or aggregated). For particles having a regular shape (circle, square, rectangle), size parameters such as length and width are easily measured. The particles of many clay minerals, however, are non-rigid, and hence their linear (size) dimensions can only be roughly characterized. Size measurements give a fair approximation of the clay mineral surface (Elsass, 2006). The transmission electron micrograph of kaolinite crystals is shown in Figure 2.15.

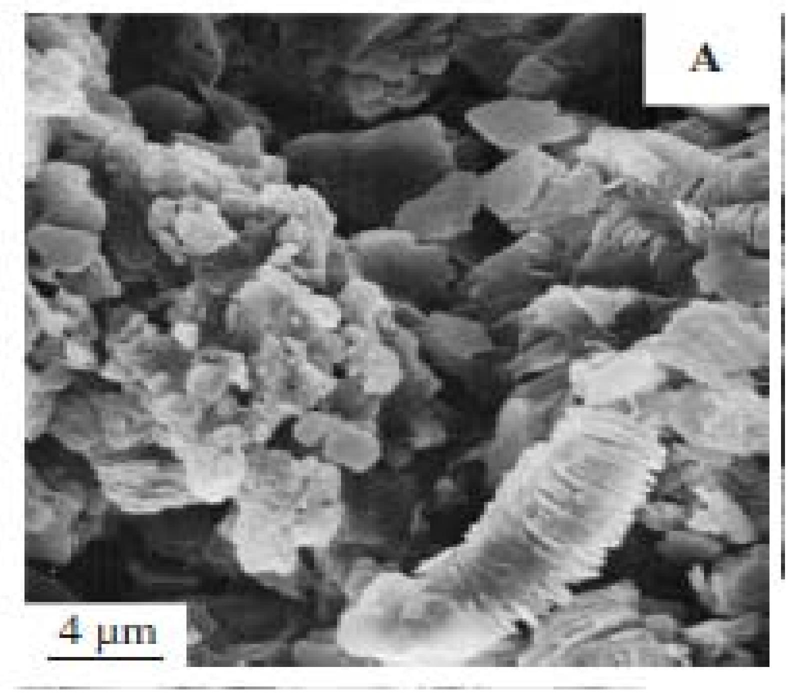

Figure 2.15 Transmission electron micrograph of kaolinite from Sasso (Italy) showing typical books of particles. **(source:** Bergaya and Lagaly, 2006)

2.5 Adsorption of pigments on clay

The potential adsorption sites on kaolinite include the silanol and aluminol groups on the mineral edges and the permanently charged sites on the basal surfaces as shown in Figure 2.16 (Gu and Evans, 2008).

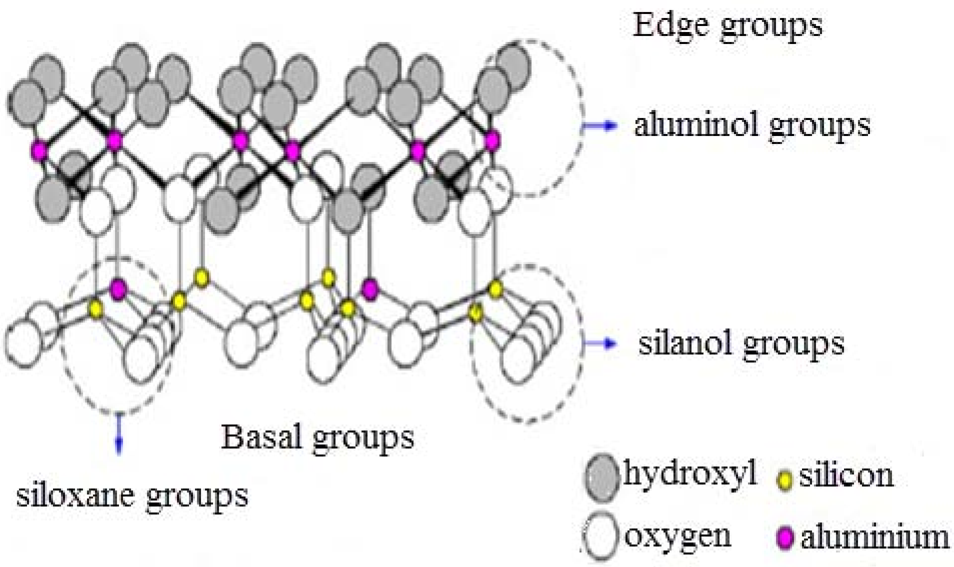

Figure 2.16 Proposed charged sites on kaolinite used in the two site adsorption model. (Gu and Evans, 2008)

Adsorption can be divided into two sub-groups: physisorption and chemisorptions. In physical adsorption (physisorption), there is a relatively weak interaction between the adsorbate and the adsorbent. The interaction depends mostly on van der Waals forces, which are mainly caused by electronic and/or electrostatic interactions between electron-rich or electron-poor regions of the adsorbate and receptive sites on the adsorbent. Such weak forces between the adsorbent and adsorbate can be broken down using various solvent extraction techniques. In contrast, the molecules bound by covalent bonds with the clay surface (chemisorptions) cannot be removed easily (Taylor, 2005). In chemisorptions, electron transfer or sharing of electron takes place between the adsorbate and adsorbents. As a result, chemical bonds are formed between them and new chemical compounds are occurred in the adsorbent during the adsorption process (James et al., 2008).

2.6 Rice bran

Rice is the seed of *Oryza sativa* with the second-highest worldwide production and is mainly consumed by a large part of the world's population especially Asian countries. The relative proportion of major rice components are illustrated in Figure 2.17. The grain consists of the starchy endosperm, caryopsis or brown rice and hull. 5-8 % of the brown rice weight is the bran and 1-2% is the embryo alone. The bran composed of pericarp, seed coat, nucellus and embryo. Rice bran is the byproduct of rice milling industry and the available rice bran from the milling industry throughout the world is about 30 million tons (Dunford, 2005).

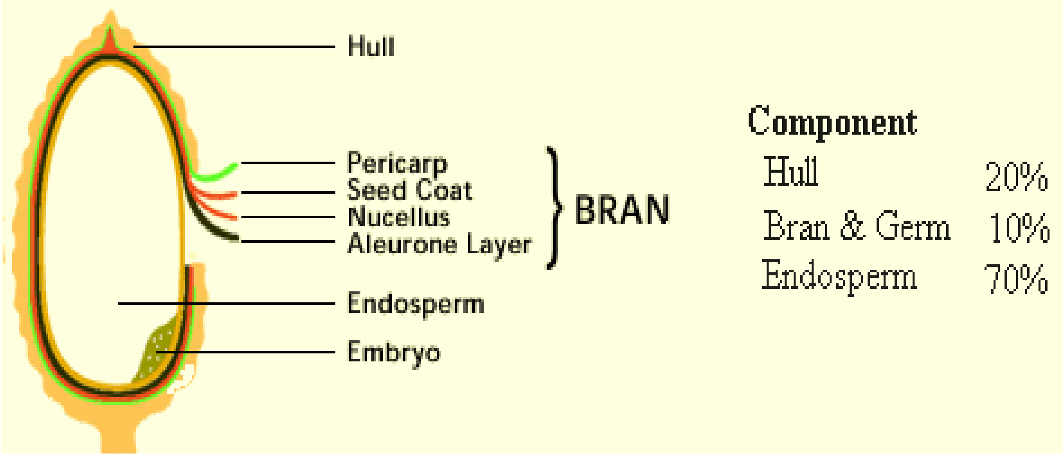

Figure 2.17 The structure of rice grain. (Orthoefer, 2005)

Rice bran is rich in lipids, proteins, minerals, vitamins, phytin, and lipase. By comparing with other cereal grains, rice bran with germ has higher fat content but the nearly same amount of protein, fibre and ash. As a source of low cost nutrients, rice bran is widely used in animal feed (Orthoefer, 2005). Rice bran typically contains 16-32% oil. The lipid of rice bran and germ are quite similar and mainly consist of triacylglycerols (TAG), free fatty acid (FFA), acylsterylglycosides (ASG), Phosphatidylethanolamine (PE), and Phosphatidylcholine (PC) as shown in Table (2.4). The wax content of rice bran oil varies with the species and it can be up to 8%.

Table 2.4 Lipid composition of rice germ, rice bran and rice bran oil
(Dundford, 2005 and Orthoefer, 2005)

Lipid composition %	Germ	Bran	Rice Bran Oil

Neutral lipid	91-92	88-90	88-89
Glycolipid	2-3	4-5	6-7
Phospholipids	6-7	7-8	4-5
Lipid classes (% total)			
Triacylglycerols	77-79	75-76	88-89
Diacylglycerols	-	-	3-4
Monoacylglycerols	-	-	6-7
free fatty acid	4	4-5	2-4
Acylsterylglycosides	1	2	-
Sterylglycosides	<1	<1	-
Phosphatidylethanolamine	3-4	3	-
Phosphatidylcholine	3-4	3-4	-
Lipophosphatidylethanolamine	<1	<1	-
Others	8-9	8-9	-

2.7 Rice bran oil

Rice bran oil is produced by expressing or extracting from the broken hulls of *Oriza Sativa*. Once the hull is removed, the brown kernel is exposed. The bran is removed by a polishing process that breaks up the bran into finely divided particles and exposes the white kernel. Rice bran contains lipase enzyme that breaks down triglyceride into glycerol and free fatty acid. When the bran is removed from the rice, lipase enzyme is activated and increases the free fatty acid content about 3-7% points per day (Hui, 1996). Rice bran oil with low free fatty acid can be produced from extrusion stabilized bran using hexane. Typical characteristics of refined rice bran oil are shown in Table 2.5. These properties are same as those of other oils but it has nutty, earthy flavor unlike peanut oil. The fatty acid composition of rice bran oil is quite similar to that of groundnut oil. More than 90% of the fatty acid in rice bran oil is palmitic acid, oleic acid and linoleic acids as shown in Table 2.6. The major lipid components of triacylglycerols are palmitic-linolenic-oleic, oleic-linoleic-palmitic, palmitic-linoleic-linoleic, linoleic-linoleic-palmitic and trioleic. Rice bran oil is suitable for cooking and frying applications (Orthoefer, 2005).

Table 2.5 Physicochemical properties of refined, bleached and deodorized rice bran oil (Orthoefer, 1996; Dunford, 2005; Firestone, 2006)

Parameter	Range

Specific gravity (25°C)	0.916-0.921
Refractive index (25°C)	1.470-1.473
Iodine value	92-108
Peroxide value (meq/kg)	1.0 max
Free fatty acid (%oleic acid)	0.05 max
Saponification value	181-189
Unsaponifiable matter (%)	3-5
Hydrocarbons	18
Phytosterols	43
Sterol esters	10
Triterpene alcohols	28
Tocopherols	1
Moisture	0.05 max
Smoke point	231°C
Fire point	352°C
Cloud index	17°C
Color (Lovibond 5.25 inches)	2.5-3.5R, 25-35Y

Table 2.6 Fatty acid composition of rice bran oil
(Orthoefer, 1996; Dunford, 2005; Firestone, 2006)

Fatty acid composition (%)	**Range**

Myristic acid (14:0)	0.5-0.7
Palmitic acid (16:0)	16-28
Palmitoleic acid (16:1)	0.5
Stearic acid (18:0)	2-4
Oleic acid, Elaidic acid, Vaccenic acid (18:1)	38-48
Linoleic acid (18:2)	16-36
Linolenic acid (18:3)	0.2-2.2
Arachidic acid (20:0)	0.5-0.8
Eicosenoic acid (20:1)	0.3-0.5
Behenic acid (22:0)	0.1-0.5
Lignoceric acid (24:0)	0-0.5

Rice bran oil is of interest as "heart oil" because it is found to be very delicious and has a high hypocholesterolemic effect (Yin and Wen, 2011). Rice bran oil contains higher amounts of bioactive components such as phytosterols, tocopherols and tocotrinols, which are the nutritious ones. Although it is nutritive oil, rice bran oil has a dark greenish brown color due to the presence of chlorophyll-a ($C_{55}H_{72}MgN_4O_5$) molecules, which thermally decomposes into pheophytin (Figure 2.18).

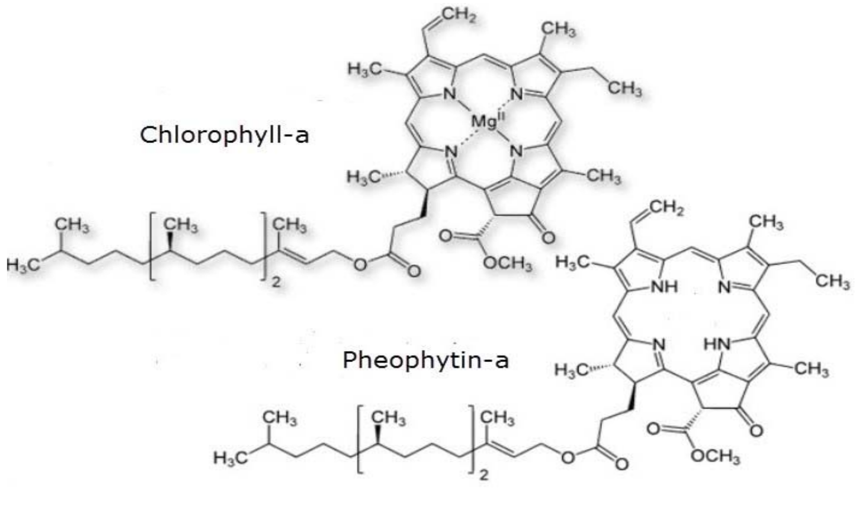

Figure 2.18 Chemical structure of chlorophyll-a, one of the main unsaturated molecules in crude rice bran oil and its derivative pheophytin-a.

2.7.1 Purification of rice bran oil

Fats and oils contain variable amounts of non-glyceride impurities such as phosphatides, protein, free fatty acids together with various colored and odoriferous substances (Tooley, 1971). The presence of phosphatides (gums) makes the refining loss high. They act as emulsifier during neutralization and increase the amount of neutral fat occluded in the soap particles formed during neutralization. They also act a crystal inhibitor during fractionation. As they affect subsequent processing of the oil, it is necessary to remove them before refining/neutralization. About 90% of the phosphatides are removed from the oil by water degumming. The non-hydratable phosphatides are present as calcium and magnesium salts which can be removed from the oil by treating the oil with a small quantity of food grade acid (normally concentrated phosphoric acid).

Alkali refining also known as neutralization removes free fatty acid by treating the oil with strong alkaline solution (normally sodium hydroxide solution 10° to 30° Bé) (Weider Mann, 1981). Free fatty acids react with sodium hydroxide (caustic soda) and convert into water-soluble soap, as represented by the following equation.

$$\begin{array}{ccccccc} \mathrm{RCOOH} & + & \mathrm{NaOH} & \longrightarrow & \mathrm{RCOONa} & + & \mathrm{H_2O} \\ \text{Free fatty acid} & & \text{Caustic soda} & & \text{Soap} & & \text{Water} \end{array}$$

The soap stock is removed from the neutral oil by centrifugation and then, the oil is washed with water several times to remove any residual soap. The water-washed oil is dried under vacuum of 26-28 inHg at about 60-80°C (Schwitzer, 1956). Refining also removes other impurities such as pigments and phospholipids.

Although some pigments such as gossypol are completely removed by neutralization, other pigments, peroxides and traces of metals and soap are removed in bleaching step (Taylor, 2005). Bleaching is normally carried out after neutralization and prior to fractionation/ winterization. Vegetable oils are usually bleached at 80-120°C for 15-30 minutes. Adsorptive bleaching is effective and the amount of adsorbent required depends on the characteristics of the oil as well as the clay. For rice oil bleaching, the bleaching clay dosage ranges from 2-10%.

In addition to wax, rice bran oil also consists of saturated triglycerides causing the oil cloudy even at room temperature. These materials are removed by winterization/fractionation; cooling temperature, residence time and agitation speed affect the crystal formation. Rice bran oil is slowly cooled to 15°C for 12 hour with continuous stirring and then further cooling to 4-5°C without stirring over 24-48 hour period to crystallize the higher melting point trigylcerides. These crystals are removed from the oil by filtration or centrifugation (Orthoefer, 2005).

Deodorization removes rice bran's nutty odors and earthy flavors as well as objectionable odors resulting from degradation of peroxides, ketones and aldehydes (Kirschenbauer, 1960). For this step, rice bran oil is heated to 220-250°C using high pressure steam under vacuum 3-5 mmHg. The oil is then cooled to 60°C, filtered and stored as a high quality refined, bleached and deodorized (RBD) oil (Orthoefer, 2005). The processing flow sheet for purification of rice bran oil is as shown in Figure 2.19.

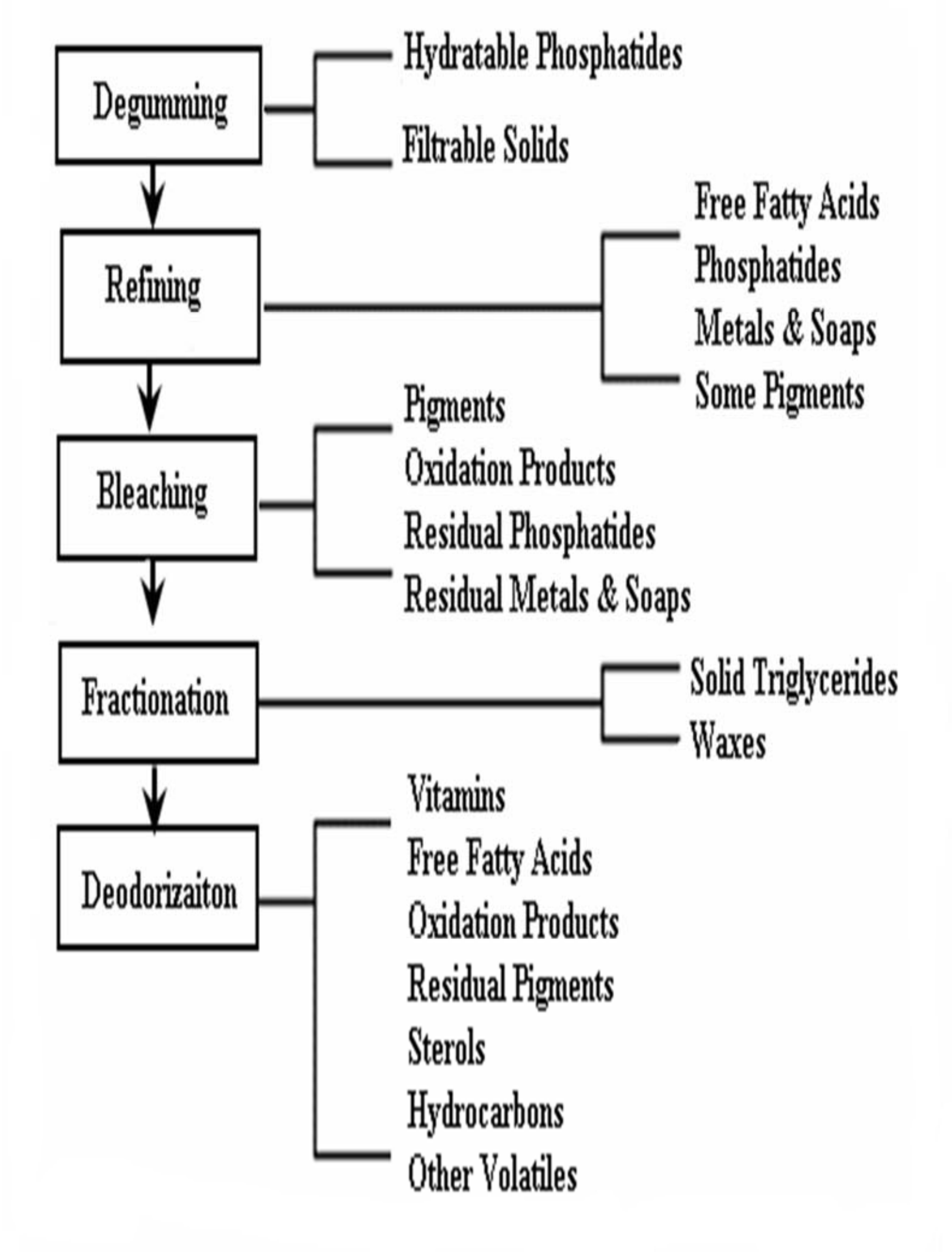

Figure 2.19 Flow sheet of purification of rice bran oil.

2.8 Analysis of oil

2.8.1 Color

Color is one of the most important criterions of vegetable oil processing and quality determination in an edible oil industry. Lovibond tintometer are widely used for color measurement (AOCS, 2004). Color racks consisting of red, yellow, blue, and neutral racks with color readings as follows, and fitted with colorless compensating slides:

Red	0.1 - 0.9, 1.0 - 9.0, 10.0 and 70.0
Yellow	0.1 - 0.9, 1.0 - 9.0, 10.0 - 70.0
Blue	0.1 - 0.9, 1.0 - 9.0, 10.0 - 40.0
Neutral	0.1 - 0.9, 1.0 - 3.0

2.8.2 Free fatty acid

Acid value is the number of milligrams of potassium hydroxide necessary to neutralize the free acids in 1 gram of sample. With samples that contain virtually no free acids other than fatty acids, the acid value may be directly converted by means of a suitable factor to percent free fatty acids as percent oleic, lauric, or palmitic, dividing the acid value by 1.99, 2.81, or 2.19 respectively (AOCS, 2004).

2.8.3 Peroxide value

Peroxide value is a widely used method (AOCS methods) that determines the amount of oxygen chemically bound to an oil or fat as peroxide, particularly hydroxide. It is defined as the weight in milli-equivalents of peroxide per 1000g of sample, which oxidize potassium iodide under the conditions of the test (AOCS, 2004). Apart from the acid value, the analysis of rancidity should include the determination of peroxide value (Palm Oil Research Institute of Malaysia, 1993). However, when these hydroperoxides start breaking down to produce off-flavor compounds, correlation to the quality and stability of the oil will no longer be valid. Peroxide value of freshly deodorized oil should be zero and at the point of use, peroxide value should be less than 0.1 cmol/kg oil (Hui, 1996).

2.9 Literature reviews

2.9.1 Effect of activation on clay's adsorption properties

Smectite-derived clays have high sorption properties due to their high surface area, and these properties are enhanced with acid activation (Odom, 1984; Rupert et al., 1987; Boyd and Jaynes, 1994; James et al., 2008; Didi et al., 2009). Among the activated clays, acid-activated montmorillonite clays have been widely reported and used as adsorbents in edible oil bleaching process due to its higher sorption properties of chlorophyll and other trace pigments from the oil. The acid activation enhances the sorption properties of clays by modifying its structural, mineral and physico-chemical properties with a limited decomposition of its crystal structure (Rupert et al., 1987; Rhodes and Brown, 1992; Tkac et al., 1994). Acid treatments destroy partially or totally the clay's crystal structures, disintegrate the clay particles and decompose the minerals, thereby forming an amorphous and partially protonated silica phase. Upon acid activation, specific surface area, porosity and number of acid centers are also changed in the activated clay due to the leaching of alumina and other mineral impurities (Mills et al., 1950; Grim, 1962; Novak and Gregor, 1969; Fijal et al., 1975; Kolta et al., 1975; Kheok and Lim, 1982; Morgan et al., 1985; Zaki et al., 1986; Rupert et al., 1987; Srasra et al., 1989; Rhodes and Brown, 1992; Kaviratna and Pinnavaia, 1994).

Many studies have been devoted to the decolorization of oil, particularly the use of sorption reactions on clays (Stout et al., 1949; Kheok and Lim, 1982; Boki et al., 1992; Falaras et al., 1999; Hussein et al., 2001; Caglayan and Yigit, 2005; Temuujin et al., 2006; Uğurlu and Kula, 2007; Nguetnkam et al., 2008; Hechi et al., 2009). Most of these studies (Falaras et al., 1999; James et al., 2008; Junamo et al., 2008; Didi et al., 2009) have demonstrated a good correlation between the bleaching capacity and the specific surface area of the activated samples. However, several authors have indicated that this correlation is not systematic (Morgan et al., 1985; Zaki et al., 1986; Nguetnkam et al. 2008; Worasith et al., 2011a) because the pigments attach the adsorbent acidic sites through the combination of electrostatic interactions and chemical bonds (Siddiqui, 1968; Khoo et al., 1979; Morgan et al., 1985; Nguetnkam et al., 2008; Worasith et al., 2011a). For example, Worasith et al. (2011a) demonstrated that a process combining mechanical and chemical treatment dramatically increased the specific surface area, pore volume, and number of mesopores in the 3-4.5 nm range of kaolins. These authors demonstrated that the increase in the number of mesopores in the 3-4.5 nm range was positively correlated with the sorption capacity of the kaolins for chlorophyll molecules present in rice bran oil.

Grinding of the kaolin clays prior to reflux with sulfuric acid induced more extensive leaching of alumina from the samples compared to the procedure without grinding (Tang et al., 2010; Worasith et al., 2011b). They concluded that a combined mechanical and acid treatment was more effective for alumina leaching from kaolin than acid activation alone. Furthermore, previous studies have generally shown that there is an optimal concentration of acid for the reflux step to ensure the best bleaching capacity (James et al., 2008; Junamo et al., 2008; Didi et al., 2009). Beyond this optimum value, the bleaching capacity decreases due to the collapse or the complete disappearance of the crystal structure, which induces a dramatic decrease in the specific surface area.

At high temperatures, an amorphous phase rich in Si dominated the samples and presented a high proportion of functional groups (>SiOH). Nguetnkam et al. (2005) demonstrated that pure silica phases are ineffective for the decolorization of palm oil. Moreover, Molinard et al. (1994) also demonstrated that the surface hydroxyl groups of the broken edge of the alumina sheets in acid-activated montmorillonite form sorption sites. The protonated structure acts as an effective binding site for pigments, such as the chlorophyll-a investigated in the present study. Falaras et al. (1999) demonstrated that the highly hydrophilic protonated montmorillonite structure attracts polar pigments such as chlorophyll-a. Kheok and Lim (1982) observed that sulfuric acid treatment to the non-swelling montmorillonite leached the alumina from the clay and consequently, caused a charge deficiency in the clay lattice and enhanced the clay's pigment sorption properties. Some authors have observed that when high sulfuric acid concentrations (>5 M) are used during the reflux step, the sorption properties of some swelling clays are reduced due to the collapse of the clay structure, causing excessive leaching of alumina from the octahedral sheet. This has been demonstrated for various minerals, including bentonites (James et al., 2008; Didi et al., 2009). Mokaya, et al. (1994) also studied the mechanism of chlorophyll adsorption on acid-activated clays. They observed that increasing acid concentrations decrease the influence of the exchangeable cations on the adsorption process because there was no possible acid site associated with the cations.

2.9.2 Influence of surface charge, cation exchange capacities and crystallinities on kaolinite's sorption properties

Kaolinite has a pH dependent variable charge due to the protonation and deprotonation of exposed hydroxyl groups (silanol, aluminol) present on the gibbsite sheet and on the edges of the particles (Johnston and Tombácz, 2002; Wypych, 2004). Depending on the aqueous pH, the surface charges enhance or inhibit metal sorption. Fialips et al. (2000) prepared kaolinite starting from partially crystallized kaolinite under hydrothermal synthesis as a function of different final pH. Hexagonal particles are obtained when synthesis was performed in acidic condition, whereas the lath morphology appears for synthesis performed with a basic final pH. These authors also proposed that defect density of the synthetic kaolinite was negatively correlated with the increase in sodium adsorbed on the surface. The decrease of the size of the particle tends to increase the global sorption properties towards aqueous species, due to an increase of the specific surface area of the solids. However, the exact contribution of each of the different edge sites located on the mineral is rarely taken into account in the interpretation of the global sorption properties of a particle. This can be predicted simply on the basis of the crystallochemical data and size/morphology of the particle (Bickmore et al., 2001; Liu and Su, 2011; Tertre et al., 2013). Predicted site densities for kaolinite ranged from 0 to 21.8 sites/nm^2 depending on the different methods used to assess these parameters (Koretsky et al., 1998) and the edge faces considered (e.g., (010), (110) and ( ) faces). $0\bar{1}0$

CHAPTER 3 METHODOLOGY

3.1 Part I: Effect of physical/thermal and chemical activation of kaolin on bleaching of rice bran oil

3.1.1 Equipment and apparatus

3.1.1.1 Planetary ball mill
3.1.1.2 Oven
3.1.1.3 Muffle furnace
3.1.1.4 Reflux condenser
3.1.1.5 pH meter
3.1.1.6 Magnetic stirrer
3.1.1.7 Digital balance
3.1.1.8 Centrifuge
3.1.1.9 UV-visible spectrophotometer
3.1.1.10 Lovibond tintometer
3.1.1.11 X-ray diffractometer
3.1.1.12 X-ray fluorescence spectrophotometer
3.1.1.13 Quantachrome autosorb
3.1.1.14 Fourier transform infrared (FTIR) spectroscopy
3.1.1.15 Scanning electron microscope
3.1.1.16 Glassware
3.1.1.17 Mortar and pestle

3.1.2 Chemicals and reagent

Inorganic acids such as sulfuric acid (H_2SO_4), hydrochloric acid (HCl) and organic acids such as citric acid ($C_6H_8O_7$), oxalic acid ($H_2C_2O_4$) used in the acid treatments were AR grade and purchased from Merck, Germany, and Ajax Finechem, Australia, respectively.

3.1.3 Materials

Kaolin from Ranong, Thailand was obtained from Had Som Pan Co., Ltd. The pale yellow-colored kaolin sample was washed with distilled water to remove soluble mineralogical impurities and dried in an oven at 80°C for 24 hours. The sample was then gently crushed using a mortar and pestle and sieved to 200 mesh to obtain a clay powder, referred to as UGK (unground kaolin). Commercial bleaching clay, a reference for bleaching capacity of kaolin, was purchased from Taiko Clay Marketing Sdn. Bhd., Malaysia. Degummed and refined rice bran oil (unbleached oil) was supplied by Thai Edible Oil Co. Ltd., Thailand. The acid value and peroxide value of rice bran oil were 0.28 (% oleic acid) and 16 meq/kg, respectively. This oil has a greenish-brown color due to the presence of chlorophyll-a.

3.1.4 Sample preparation

1. Physical activation of kaolin (Mechanical treatment)

Purified kaolins were ground using a Retsch plantary ball mill (model Retsch S 100) which is made up of stainless steel. A total of 10 g of UGK was ground with the stainless steel balls rotating at 300 rpm for 1 hour; the weight ratio of balls to kaolin was 30:1. This new material was referred to as GK (ground kaolin).

2. Combined thermal and chemical activation of kaolin

Unground kaolin (UGK) was heated for 1 hour in a muffle furnace to temperatures ranging from 100°C to 700°C. Then, 10 g of each heated sample was refluxed with 500 mL of 2 M sulfuric acid (Analar grade) at 90°C for 4 hours under agitation. The resulting clay suspensions were washed with distilled water until reaching pH of 3, at which the sorption properties of acidified kaolin were good (Worasith et al., 2011a). After drying at 80°C for 24 hours, the solid samples were gently crushed using mortar. These samples are referred to as 100UG 2 to 700UG 2, depending on the heating temperature used during preparation.

3. Combined thermal, mechanical and chemical activation of kaolin

Ground kaolin (GK) was subjected to the same treatments as for the UGK samples treatments described above, to test the effect of the presence of small particles on the bleaching results. The purified sieved clays were heated in a muffle furnace to 100°C to 700°C. The heated kaolins were ground with the stainless steel balls rotating at 300 rpm for 1 hour; the weight ratio of balls to kaolin was 30:1. The ground kaolins were then refluxed with 2M H_2SO_4 in the solid-liquid ratio of 1:50 (10g of clay/ 500ml of H_2SO_4) at 90°C for 4 h under mechanical stirring, washed with distilled water adjusted to pH 3 and dried at 80°C for 24 h. These samples were designated as 100GR 2 to 700GR 2.

For other ground samples, a sulfuric acid concentration other than 2 M was used during the activation step (from 0.1 to 2.6 M). These samples, which were obtained using a heating temperature of 100°C prior to reflux with different concentrations of sulfuric acid (0.1 M, 0.3 M, 0.5 M, 1 M, 1.5 M, 1.7 M, 2.6 M), are referred to as 100GR 0.1 to 100GR 2.6, depending on the concentration of sulfuric acid used during the preparation.

4. Combined mechanical and chemical activation of kaolin

The ground kaolins (GK) dried at 80˚C in an oven, were refluxed with different inorganic acids such as sulfuric acid (H_2SO_4), hydrochloric acid (HCl) or organic acids such as citric acid ($C_6H_8O_7$), oxalic acid ($H_2C_2O_4$) at 90°C for 4 h under mechanical stirring. The initial GK were activated using different concentrations of sulfuric acid (0.1 M, 0.3 M, 0.5 M, 0.7 M, 1 M, 1.3 M, 1.5 M and 2 M) with clay/acid ratio of 1:50. Then, the clay suspension was washed with distilled water adjusted to pH 3 and dried in an oven at 80°C for 24 h. Finally, the samples prepared were designated as GRS 0.1, GRS 0.3, GRS 0.5, GRS 0.7, GRS 1, GRS 1.3, GRS 1.5 and GRS 2, respectively. The same experiments were carried out using 0.1M, 0.3M, 0.5M, 0.7M, 1M, 1.3M, 2M hydrochloric acid (for GRH 0.1, GRH 0.3, GRH 0.5, GRH 0.7, GRH 1, GRH 1.3, GRH 2); 0.1M, 0.3M, 0.5M, 0.7M, 1M, 1.3M, 2M citric acid (GRC 0.1, GRC 0.3, GRHC 0.5, GRC 0.7, GRC 1, GRC 1.3, GRC 2) and

0.1M, 0.3M, 0.5M, 0.7M, 1M, 1.3M, 2M oxalic acid (for GRO 0.1, GRO 0.3, GRO 0.5, GRO 0.7, GRO 1, GRO 1.3, GRO 2).

For determining the effect of clay/acid ratio on bleaching capacities of kaolin, the ground kaolin (GK) was refluxed with sulfuric solution using various solid/liquid ratios of 1:2 (10g of clay/ 22ml of 2 M or 4 M H_2SO_4), 1:4 (10g of clay/ 40ml of 2 M or 4 M H_2SO_4), 1:6 (10g of clay/ 60ml of H_2SO_4), 1:8 (10g of clay/ 80ml of H_2SO_4) and 1:50 (10g of clay/ 500ml of H_2SO_4). These samples are regarded as 2GRS 1:2, 4GRS 1:2, 2GRS 1:4, 4GRS 1:4, 2GRS 1:6, 2GRS 1:8 and 2GRS 1:50, respectively according to the different clay/acid used. The same experiments were also done using 0.5 M, 2 M or 4 M hydrochloric acid with various solid/liquid ratios of 1:2, 1:4, 1:40, 1:50 and 1:60 for GRH 0.5 samples; of 1:12 and 1:50 for GRH 2 samples and of 1:2, 1:4, 1:6 and 1:7 for GRH 4 samples. These samples are referred as 0.5GRH 1:2, 0.5GRH 1:4, 0.5GRH 1:40, 0.5GRH 1:50, 0.5GRH 1:60, 2GRH 1:12, 2GRH 1:50, 4GRH 1:2, 4GRH 1:4, 4GRH 1:6 and 4GRH 1:7, respectively. For organic acid treatments, GK was refluxed with 0.1 M oxalic acid with different clay/acid ratio of 1:40, 1:50, 1:80 and 100.

For further studies on the effect of acid concentrations on kaolin's bleaching capacities, activated kaolins (for 0.5GRH 1:50, 2GRH 1:12 and 4GRH 1:6 samples) were also prepared with same hydrochloric acid strength using different acid concentrations and different clay/acid ratios i.e. 0.5GRH 1:50 sample was prepared by treating the GK with 0.5 M hydrochloric acid using clay/acid ratio of 1:50; 2GRH 1:12 by 2 M hydrochloric acid using clay/acid ratio of 1:12; and 4GRH 1:6 by 4 M hydrochloric acid using clay/acid ratio of 1:6. These different acid concentrations with different clay/acid ratios gave the same acid strength for all acid solutions.

3.1.5 Adsorption studies

1. Bleaching of rice bran oil

For the bleaching experiment, degummed and neutralized rice bran oil was preheated to 90°C in an oil bath. When the oil had reached at that temperature, usually in less than 15 minute, 2% (w/w) of initial or activated samples was added to it. The mixture was then agitated at approximately 150 rpm for 30 minutes. The oil was then centrifuged at 3,000 rpm for 15 minutes and filtered through Whatman No.5 filter paper to obtain clear oil. Bleaching experiments were triplicated.

For testing the large-scale bleaching for rice bran oil, some activated kaolins such as GRH 0.5 and GRC 0.5 which gave the optimum bleaching capacities in Laboratory scale experiment were studied for their bleaching capacities according to the same procedure described above. 2% (w/w) of activated kaolin was added to the degummed and neutralized rice bran oil (980 g) which was preheated to 90°C using an oil bath. Bleaching experiments were duplicated.

2. Determination of the bleaching capacity of kaolin

The bleaching capacity of the kaolin was determined by measuring the oil absorbance using UV – visible spectroscopy, a Spectronic 21 spectrophotometer of Banusch & Lomb. The oil samples was diluted with hexane in the proportion of 1 mL of oil for 4 mL of solvent, and determined their absorbance at 410 nm wavelength, which corresponds to the maximum absorption wavelength of chlorophyll-a molecules in the 350-750 nm range. The bleaching capacity was calculated according to the following formula (Foletto et al., 2003):

$$\text{Bleaching capacity (\%)} = [(A_o - A)/ A_o] \times 100$$

where A_o and A are the absorbance of the unbleached and bleached oil, respectively.

3.1.6 Characterization of kaolin

1. X-Ray Diffraction (XRD)

X-Ray Diffraction (XRD) patterns were obtained using a Bruker® D8 advanced diffractometer equipped with a Ni-filtered CuKα radiation generated at 40kV, 40mA. Measurements were done on randomly oriented powder preparation for all samples. Kaolin powder was placed in a flat glass holder, and then the patterns were recorded in the range of $2\theta = 5°$ to 65° with a 0.02 degree step and an acquisition time of 0.4 s per step.

2. X-Ray Fluorescence (XRF)

The elemental chemical compositions of the initial and activated samples were obtained using powder method. The powder samples were put in the cup and analysed in helium atmosphere for 20 minutes using Bruker AXS model S4 spectrometer equipped with a WD-XRF detector. Compositions of samples are expressed as the oxide form in percentages.

3. Fourier Transform Infrared Spectroscopy (FTIR)

For structural analysis of kaolin, Fourier Transform Infrared (FTIR) spectra were recorded using KBr pellets at a resolution of 4 cm^{-1} in the mid-IR range of 4000-400 cm^{-1} with a Nicolet 510 FTIR spectrometer. 16 scans are recorded for each spectrum at 4 cm^{-1} resolution in the mid-IR range (4,000–400 cm^{-1}). KBr pellets were prepared by mixing 1 mg of sample thoroughly with 100 mg of ground potassium bromide (KBr). Then, the mixture was pressed into pellets which were ready to be analyzed by FTIR.

Moreover, Diffuse Reflectance Infrared (DRIFT) spectra of some activated kaolin before and after bleaching were obtained using KBr pellets method with a Perkin Elmer (Spectrum One) Fourier Transform infrared spectrometer. Spectra were recorded by accumulating 16 scans at 4 cm^{-1} resolution in the mid-IR range (4,000–450 cm^{-1}).

4. Brunauer-Emmet-Teller Method (BET)

An Autosorb Automated Gas Sorption instrument was used to determine the surface area and pore volume of the samples. The measurements were performed at a batch temperature of 77.3 K and a relative pressure (P/P_0) ranging up to 0.3; prior to analysis, the samples were degassed with nitrogen gas at 300°C. Isotherms were used to determine the specific surface area by applying the Brunauer-Emmet-Teller method (Brunauer et al., 1938). The total pore volume was obtained by treating the entire isotherm until P/P_0 was equal to ~0.99 according to the Barrett-Joyner-Halenda (BJH) method (Barrett et al., 1951).

5. Scanning Electron Microscopy (SEM)

The microstructure and elemental composition of kaolin samples were evaluated from their micrograph by Scanning Electron Microscope (SEM) along with the Energy Dispersive Spectral analysis (EDS). Before analysis, kaolin samples were coated with gold to increase signal and surface resolution of clay. The analysis was done with energy dispersive X-ray at an accelerating voltage of 20 kV for major and minor elements. The surface morphologies of natural and activated kaolins were investigated by comparing their appearance at magnifications of 50,000 and 100,000 respectively.

3.1.7 Interaction of pigment on kaolin

The spent bleached kaolin was washed with several hexane to remove any rice bran oil retaining in kaolin and dried in an oven at 100°C overnight. The interaction between activated kaolin and oil’s pigment was studied by comparing the color of initial kaolin and hexane-washed spent bleached kaolin.

For further studies to investigate the clay-pigment interaction, the kaolin samples before and after bleaching were studied their diffuse reflectance infrared spectra using the KBr method with a Perkin Elmer (Spectrum One) Fourier Transform Infrared Spectrometer. 1 mg of sample was mixed with 100 mg of KBr, and pressed it into pellets. Then, the spectra were recorded by accumulating 16 scans at 4 cm^{-1} resolution in the mid-IR range (4,000–450 cm^{-1}).

For study desorption of pigments from the clay, the hexane-washed spent bleached kaolin was dried in an oven at 100°C overnight. Then the clay was eluted with ethanol or 0.1 M NaOH until the color doesn’t appear in the elutent. Desorption (%) was calculated according to the following equation:

$$\text{Desorption (\%)} = [\textstyle\sum A_{\text{desorption}} / (A_0 - A)] \times 100$$

where $A_{\text{desorption}}$ is the absorbance of elutent.

A_0 and A are the absorbance of the unbleached and bleached oil, respectively.

3.1.8 Analysis of rice bran oil

1. Color

According to the AOCS official method Cc 13e – 92 (Revised 2002), color changes of oil was measured by Lovibond Tintometer. The method determined the color by matching the color of the light transmitted through a specific depth of liquid fat or oil to the color of the light originating from the same source, transmitted through glass color standards. Red, yellow and blue colors were used for edible oils.

2. Free fatty acid value

According to the AOCS official method Cd 3d – 63 (Revised 2003), 5 ± 0.1grams of sample was weighed into a 300 ml Erlenmeyer flask and dissolved with 125 ml of the neutralized solvent mixture containing equal parts by volume of isopropyl alcohol (AOCS Specification H 18-58) and toluene (AOCS Specificaiton H 19-58). A few drops of phenolphthalein indicator were added and then the solution was shaking vigorously while titrating with 0.1 N standard potassium hydroxide solution to the first permanent pink color of the same intensity as that of the neutralized solvent before the latter was added to the sample. The color must be persisting for 30 seconds.

Calculations

$$\text{Acid value (mg KOH/ g of sample)} = [(A - B) \times N \times 56.1] / W$$

Where, A = ml of standard potassium hydroxide used in the titration
B = ml of standard potassium hydroxide used in titrating the blank
N = normality of standard potassium hydroxide
W = Mass of sample in grams

Free fatty acid as percent oleic acid of rice bran oil was determined by dividing the acid value by 1.99.

3. Peroxide value

According to the AOCS official method Cd 8 – 53 (Revised 2003), 5 ± 0.05 grams of sample was weighed into a 250 ml glass stoppered Erlenmeyer flask and then 30 ml of the 3:2 acetic acid-chloroform solution was added. The flask was swirled until the sample was dissolved in the solution. 0.5 ml of saturated potassium iodide solution was added and the solution was allowed to stand with occasional shaking for exactly 1 minute. Then, 30 ml of distilled water was immediately added and titrated with 0.1 N sodium thiosulfate with constant agitation. 2 ml of starch indicator solution was added when the yellow iodine color had almost just disappeared. The flask was shaken vigorously, especially near to the end point at which the blue color just disappeared, to release iodine from the solvent layer. The blank titration was done to determine the reagents and must not exceed 0.1 ml of 0.1 N sodium thiosulfate.

Calculations

$$\text{Peroxide value (meq/ 1000 g of sample)} = [(S - B) \times N \times 1000] / W$$

Where, S = volume of titrant, (mL of sample)
B = volume of titrant, (mL of blank)
N = normality of sodium thiosulfate solution
W = Mass of sample in grams

3.2 Part II: Correlation between the morphology of synthetic kaolinites on their sorption properties

3.2.1 Equipment and apparatus

3.2.1.1 X-ray Diffractometer (Bruker® D8 advanced diffractometer)
3.2.1.2 Fourier Transform Infrared spectroscopy (Nicolet® 760 FTIR spectrometer)
3.2.1.3 Transmission Electron Microscopy (JEOL® Electron microscope JEM1010)
3.2.1.4 Atomic Absorption Spectroscopy (Varian® AA240FS)
3.2.1.5 Micromeritics® ASAP 2000
3.2.1.6 pH meter (Metrohm® electrode calibrated with 3 NIST pH buffer solutions)
3.2.1.7 UV-visible Spectrophotometer (JENWAY® 6300 spectrophotometer)
3.2.1.8 Centrifuge
3.2.1.9 Oven
3.2.1.10 Digital balance
3.2.1.11 Magnetic stirrer

3.2.2 Materials

Kaolinite was hydrothermally synthesized from amorphous silicoaluminous gel as described in detail in Fialips et al. (2000). Briefly, starting material corresponding to an amorphous gel was obtained by mixing 1 M sodium metasilicate solution (prepared from dissolution of the $SiO_2Na_2O.5H_2O$ salt) with 1 M aluminum nitrate solution (prepared from dissolution of the $Al(NO_3)_3.9H_2O$ salt) and 1 M sodium hydroxide solution (NaOH) according to the stoichiometry of the following reaction:

$$2SiO_2Na_2O + 2Al(NO_3)_3 + 2NaOH \longrightarrow 6NaNO_3 + H_2O + Si_2Al_2O_7 \qquad \text{Reaction 1}$$

The resulting gel ($Si_2Al_2O_7$) was washed with water several times to remove the sodium nitrate salt, dried in an oven at 60°C overnight, and ground to powder in an agate mortar. The amorphous character of the gel was checked by XRD analysis (see Figure 3.1). Then the gel (500 mg) was mixed with 30 ml of distilled water in a Teflon® reactor. The initial pH of this mixture was about 5. The mixture was heated in an oven at 220°C under equilibrium water pressure (23.2 bar), during 14 days. At the end of this step, gel was transformed into partial crystallized kaolinite and regarded as Starting Material (SM).

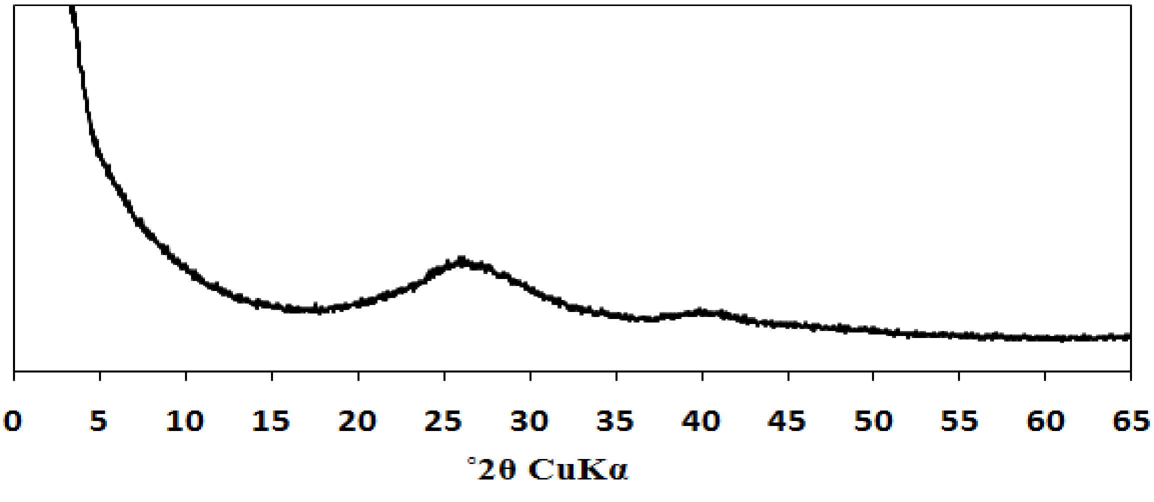

Figure 3.1 XRD pattern (bulk powder) of the amorphous silicoaluminous gel.

3.2.3 Sample preparation

Starting Material, obtained according to the protocol detailed above, was mixed with distilled water using a solid/water ratio equal to ~13 g/L. The hydrothermal aging was conducted for ten different initial pHs (pH_I), equal to around 1.0, 1.2, 5.0, 5.1, 8.1, 8.3, 10.8, 10.9, 11.2 and 11.4, adjusted at room temperature by addition of small quantities of 1M HCl and 1M NaOH solutions. Such initial pHs were chosen according to Fialips et al. (2000) in order to obtain contrasted morphology for final synthetic kaolinites. Hydrothermal syntheses were performed in an oven at 240˚C for 21 days. Final pH (pH_F) of the clay suspension was measured at the end of synthesis. Then, synthesized kaolinites were dried in an oven at 60˚C overnight, grounded to powder and were Na-saturated. This last step was performed to be sure that all sorption sites located on the surfaces of the synthetic particles were fully saturated with only one type of cation (Na^+ in our case). The saturation procedure as well as the steps to remove excess chloride used in this study was described in Tertre et al. (2013). For that, 400 mg of each sample was saturated by washing with 10 ml of 1M NaCl solution under agitation for 3 days. This procedure was repeated two times. Each suspension was carried out dialysis for 2 days to remove chloride ions and each rinsed sample was dried in an oven at 60˚C overnight and gently crushed. The final synthetic products are referred as pH_F 0.8 to pH_F 8.3 according to the final pH of their synthesis.

The natural kaolinite KGa--1b from the Clay Mineral Society (CMS) was used as a reference sample and was chosen due to the huge literature devoted to its sorption properties. KGa-1b is a well-ordered kaolinite with HI of ~1 with trace of anatase, Fe oxides, quartz, and micas. (Pruett and Webb, 1993).

3.2.4 Na^+/H^+ sorption isotherms

Na^+/H^+ sorption isotherms were obtained for each kaolinite which was synthesized and also for KGa--1b mineral which is a kaolinite from the Clay Mineral Society. The reference KGa--1b was also fully Na-saturated using the same method as that used for the synthetic products. In addition, to eliminate possible organic contamination in KGa--1b, Na-saturated KGa--1b was suspended repeatedly in 1 M NaCl/HCl solution at pH 3 according to protocol proposed by Schroth and Sposito (1997) and Wan and Tokunaga (2002). After the pH of supernatant had dropped to pH 3, the sample was suspended again in 1M NaCl solution until its pH was raised to 5. Data of KGa--1b for reference were taken from Ma and Eggleton (1999) and Wan and Tokunaga (2002) in order to compare and validate the experimental data obtained in this study. The Na^+/H^+ sorption isotherms of synthetic kaolinites and KGa--1b kaolinite were performed at different initial pH ranging from 3 to 11. The protocol used is fully detailed in Tertre et al. (2013). Some steps of the procedure are as follows: 40 mg of Na-saturated dried kaolinite was equilibrated for 3 days under agitation with 5 ml of a 0.25 M NaCl solution at different initial pH adjusted by addition of predetermined amounts of NaOH/ HCl solutions and distilled water. After centrifugation, pHs of the supernatants were measured as well as their aqueous Na^+ concentrations at equilibrium. Then, sodium adsorbed on the kaolinite surfaces was desorbed by using a 1 M ammonium acetate solution under a mechanical shaking for 2 days. The mixture was centrifuged again and the concentration of aqueous Na^+ of the supernatant was measured. All aqueous concentrations were obtained using a Varian® AAS. The formula used to determine, from these measurements, the quantity of Na^+ sorbed on the solid sample can be found in Tertre et al. (2011).

3.2.5 Methods for solid characterization

1. X-Ray Diffraction (XRD)

XRD powder patterns were recorded in the 5° to 65° 2θCuKα range with a 0.025 degree step, using an acquisition time of 1.2s per step using a Bruker® D8 advanced diffractometer equipped with a Ni-filtered CuKα radiation generated at 40kV, 40mA. In addition, XRD patterns of oriented slides for samples synthesized at pH_F 7.4, pH_F 7.5 and pH_F 8.3 were registered in order to investigate the possible presence of swelling mineral in the samples. These acquisitions were performed in both air-dried and ethylene glycol conditions. For these oriented samples, XRD patterns were recorded in the 5° to 50° 2θ range with a 0.025 degree step and using an acquisition time of 1s per step.

Defects in kaolinite were characterized by Hinckley Index (HI) corresponding to the ratio between (1) the sum of the heights of the $d_{1\bar{1}0}$ and $d_{11\bar{1}}$ measured from the inter-peak background, and (2) the height of the $d_{1\bar{1}0}$ peak from the background. This index is sensitive to all crystalline defects (i.e., ±nb/3 translations, ±nπ/3 rotations, and random defects). Higher is the index value, lower is the defect density (Hinckley, 1963). Furthermore, the structural order obtained with the R_2 index proposed by Liétard (Cases et al., 1982; Liétard, 1977) was calculated from the intensities of the d_{131} and $d_{\bar{1}31}$ reflections. This parameter is relative to the triclinic character of the crystals with high R_2. Low R_2 values indicate monoclinic character due to the overlapping of these two peaks (Fialips et al., 2000). Using the Scherrer formula (Langford and Wilson, 1978), the mean thickness of coherent scattering domain (CSD) of kaolinite crystals were estimated from the XRD full width half maximum intensity, viz., the d_{001} reflection (CS_{001}) and the d_{060} reflection (CS_{060}) along the c* axis and b axis, respectively. The peak width varies with °2θ (cos θ) and it is inversely proportional to the crystallite size (Drits et al., 1997; Fialips et al., 2000).

2. Fourier-Transform Infrared Spectroscopy (FTIR)

Fourier-Transform Infrared (FTIR) Spectra were obtained by transmission mode at a resolution of $4cm^{-1}$ in the mid-IR range ($4000\text{-}400cm^{-1}$) on a Nicolet® 760 FTIR spectrometer. Samples were prepared using the KBr method. 1 mg of sample was mixed thoroughly with 100 mg of ground potassium bromide (KBr) and then the mixture was pressed into pellets which were heated in an oven at 110°C overnight. The integrated intensity of the absorption bands were measured by using the OMNIC® software.

3. Transmission Electron Microscopy (TEM)

Morphological study of the synthetic particles was carried out by TEM with a JEOL® Electron microscope JEM1010 with 80kV for accelerating voltage. Sample was dispersed in distilled water in the ratio of 1:100 by ultrasonic probe, and a drop of the clay suspension was placed on a Ni-coated microgrid holder and air-dried at room temperature before analysis.

4. Cation Exchange Capacity (CEC)

For each Na-saturated kaolinite obtained, CEC was measured. For that, sorbed Na^+ was displaced with Cs^+ at pH = 9 by mixing 50 mg of Na-saturated kaolinite with 5 ml of a 1 M CsCl solution and pH was adjusted by addition of small quantities of a 10^{-2} M CsOH solution. After a mechanical shaking for 4 days, clear supernatant was obtained from centrifugation of the clay suspension. Then, CEC of the sample was calculated from analysis of the Na^+ concentration measured in the supernatant using Atomic Absorption Spectroscopy (AAS).

5. Brunauer-Emmet-Teller (BET) method

A Micromeritics® ASAP 2000 was used to determine the surface area of the samples. The measurements were performed at a batch temperature of 77.3 K and a relative pressure (P/P0) ranging up to 1; prior to analysis, the samples were degassed with nitrogen gas at 350°C for 4 hours. The specific surface area, corresponding to the specific surfaces of both basal and lateral surfaces, was calculated using the Brunauer-Emmet-Teller method (Brunauer et al., 1938).

6. Method used to assess specific surface of edges

In order to assess the specific surface of the edges (specific lateral surface), TEM images and XRD data were used. From TEM images of 20 particles by sample, an average value of the perimeter of the basal surface of the particles were assessed. Then, we assumed that the averaged thickness of one particle could be assessed considering the Scherrer Equation (Langford and Wilson, 1978; Drits et al., 1997; Fialips et al., 2000), given the size of the coherent domain along c axis with XRD results. With both average perimeter of the basal surface obtained with TEM and average thickness obtained as described above, an average value for the lateral surface (edge surface) was estimated. These data allowed us also to calculate the average volume of the particle. By assuming a grain dry density equal to 2.62 (Rider, 1996), specific lateral surface was assessed (e.g. Bickmore et al. 2001). To validate such an approach, the sum of both specific lateral and basal surfaces obtained by considering these geometric considerations will be compared with measured BET surface.

3.2.6 Methods for aqueous analysis

1. pH

The pH value of the aqueous solutions were measured with a combined Metrohm® electrode calibrated with 3 NIST pH buffer solutions at 25˚C.

2. Aqueous Na^+ concentrations

The concentrations of aqueous Na^+ were measured using an atomic absorption spectrophotometer (Varian® AA240FS). Before the analyses, aqueous samples were prepared in 2% HNO_3 solution, and 1 M ammonium acetate solution were added to Na standards used to measure samples rich in ammonium to account for possible interference during acquisition. The aqueous detection limits were 0.2 mg/L and the total uncertainty in the measured concentration of Na^+ was estimated to be ±2%.

3. Aqueous silica content

The concentrations of aqueous silica were measured in each supernatant for which pH were measured to assess the proportion of the edges which were dissolved all along the Na^+/H^+ isotherms. For that, a colorimetric method using a JENWAY® 6300 spectrophotometer was used (wavelength of 820 nm). From these measurements, percentages of the edge sites involved in dissolution processes were calculated. For that, specific surfaces assessed for lateral sites obtained from morphology particles and theoretical site density of kaolinite equal to 20 sites/nm^2 (Koretsky et al., 1998) were used. For this calculation, a lateral specific surface equal to 11.6 m^2/g was assumed for the reference KGa1b (Wan and Tokunaga, 2002).

CHAPTER 4 RESULTS AND DISCUSSION

4.1 Part I: Effect of physical/thermal and chemical activation of kaolin on bleaching of rice bran oil

4.1.1 Effects of mechanical grinding on kaolin

Bleaching capacities of unground kaolin (UGK) and ground kaolin (GK) are given in Table 4.1. Unground kaolin has the bleaching capacity of about 35% but it increases to about 50% after grinding. This indicates that mechanical activation improves the capacity of kaolin. This may be due to the increase of surface area (see Table 4.4) in ground kaolin.

Table 4.1 Bleaching capacities of unground kaolin (UGK), ground kaolin (GK) and commercial bleaching clay

Sample (2% w/w)	Bleaching capacity (%)
UGK	34.94 ± 0.07
GK	49.77 ± 0.12
Commercial bleaching clay	81.44 ± 0.04

1. X-ray Diffraction (XRD) analysis

The XRD data obtained for unground kaolin (UGK) and ground kaolin (GK) samples are shown in Figure 4.1. The dominant mineral of UGK sample is kaolinite. Other minerals are also found such as illite, quartz and some K-feldspars. The strong peaks of kaolinite are reflected at 7.14, 3.57 and 1.49 Å correspond to the kaolinite d_{001}, d_{002} and d_{060} reflections, and the minor peaks at 4.46, 2.56, 2.49, 2.34, 1.99 and 1.66 Å. In addition, illite is abundantly observed at 9.92, 4.99, 4.46, 2.49, 2.34, 2.13 and 1.66 Å in UGK sample. The common non-clay mineral quartz is found by its sharp peak at 3.34 Å, and minor peaks at 4.26, 2.29, 1.82 and 1.54 Å. Other non-clay mineral K-feldspars is found by small peak at 3.25 Å. These results are in agreement with that of previous studies on Ranong kaolin, Thailand (Worasith et al., 2011b).

For GK sample, XRD data shows that relative intensities of the kaolinite and illite minerals are reduced in compared to that of unground kaolin (UGK). Grinding does not change the chemical composition (see Table 4.2) and the reduction in intensities could be due to the presence of more small clay particles in GK sample than in UGK sample, which in turn produce a coherent scattering domain lower than that of big particles (see Figure 4.1). Grinding caused structural alterations, mainly along the c axis, to the Georgia kaolinites (Sanchez-soto et al., 2000). Sugiyarma et al. (1994) studied the effect of grinding on kaolinite's structure based on the XRD patterns of ground kaolinite using the radial distribution function (RDF) method. They reported that grinding decreased the oxygen coordination number and the corresponding interatomic distance around alumina whereas it did not affect the SiO_4 tetrahedra of kaolinite.

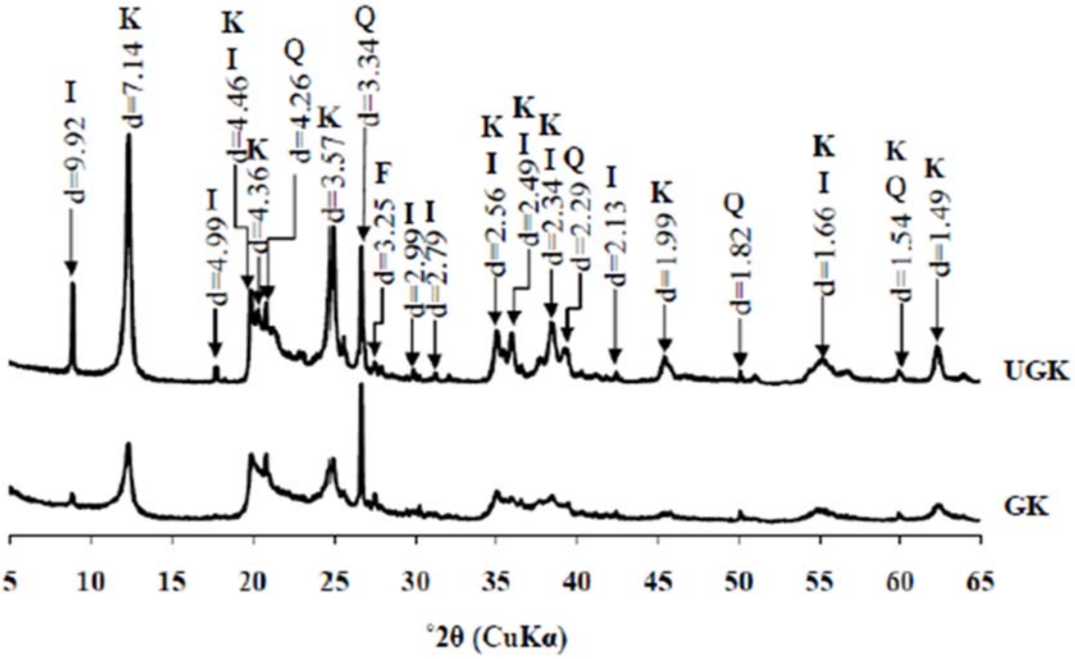

Figure 4.1 Comparison of the XRD patterns obtained from randomly orientated preparations of unground kaolin (UGK) and ground kaolin (GK) samples. K = kaolinite, I = illite, Q = quartz, F = K-feldspars.

2. X-ray Fluorescence Spectra (XRF) analysis

The chemical analysis results for UGK and GK are shown in Table 4.2. Unground kaolin (UGK) sample which mainly consists of silica and alumina, is characterized by an Al/Si value equal to approximately 0.9, corresponding to approximately 54 wt% SiO_2 and 42 wt% Al_2O_3 in the sample (Table 4.2). Other oxides such as potassium oxide, iron oxide, calcium oxide, copper oxide, titanium oxide and magnesium oxide are present in trace amounts. Grinding does not affect the chemical compositions of kaolin in which the Al:Si ratio is about 0.9.

Table 4.2 Chemical compositions of the initial unground kaolin (UGK) and ground kaolin (GK)

	SiO_2 %	Al_2O_3 %	K_2O %	Fe_2O_3 %	CaO %	CuO %	TiO_2 %	MnO %	Al:Si
UGK	53.90	42.40	2.03	1.11	0.03	0.06	0.04	0.07	0.89
GK	54.10	42.00	2.07	1.03	0.04	0.06	0.05	0.07	0.88

3. Fourier Transform Infrared Spectroscopy (FTIR)

The FTIR spectra of the initial UGK and GK are shown in Figure 4.2 and the corresponding band assignments are shown in Table 4.3. The spectrum of UGK exhibit well-resolved peak at 3620 cm^{-1}, corresponding to the inner hydroxyl vibrations (Ledoux and White, 1964; Barrios et al., 1977; Rouxhet et al., 1977), and peaks at 3696, 3669, and 3653 cm^{-1}, which are assigned to the vibrations of the three inner-surface hydroxyl groups. In the 1400–400 cm^{-1} range (Figure 4.2), the Si-O stretching vibrations of kaolinite are clearly observed at 1114, 1031, and 1008 cm^{-1}. The FTIR spectrum of UGK also contain a band at 790 cm^{-1} that is attributed to quartz (Nuntiya and Prasanphan, 2006; Worasith et al., 2011b), which is in agreement with the XRD data. The bands at 753 and 693 cm^{-1} correspond to Si-O-Si stretching (Ekkose, 2005), those at ~537 cm^{-1} correspond to Si-O-Al (octahedral) stretching, and those at 469 and 430 cm^{-1} correspond to Si-O bending vibrations (Farmer, 1974). This diversity of bands could be due to the presence of different aluminosilicates in the sample (kaolinite, illite, and K-feldspars).

The FTIR spectrum of GK is nearly superimposable with that of UGK, suggesting that the grinding step does not significantly change the mineralogy compared to the initial unground sample as indicated by the XRF results (see Table 4.2). However, the bands corresponding to the hydroxyl stretching region of kaolinite (Van der Marel and Krohmer, 1969) in GK are less resolved than those of UGK. The decrease of bonding energy of OH groups is essentially finished after 1 h of grinding (Aglietti et al., 1986). The reduction of Al-Al-OH stretching region (912 cm^{-1} and 938 cm^{-1}) indicates that the breakage of Al-OH linkage (Kristóf et al., 1993).

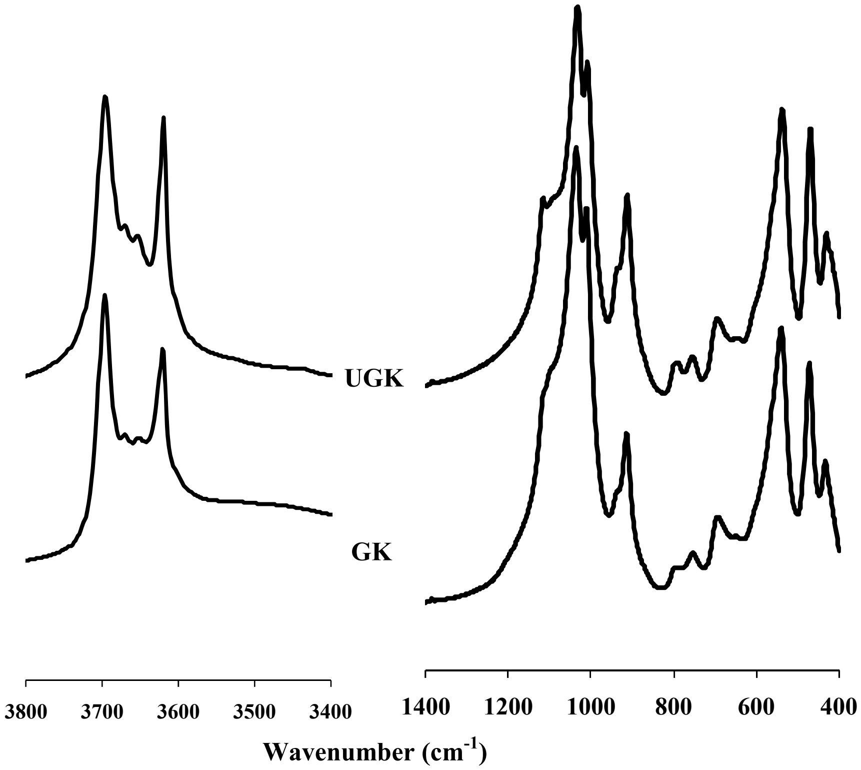

Figure 4.2 Comparison of the FTIR spectra of the initial unground (UGK) and ground (GK) samples.

Table 4.3 Important FTIR bands of initial and activated kaolin clays with their possible assignments

Bands (cm^{-1})	**Assignments**

3696 3620	γOH (structural hydroxyl group) valence linked to Al-OH
3445	γOH (physisorbed water)
1008, 1031, 1114	γSi-O
912	δOH deformation AlOH
790	Quartz
753	γSi-O
693	γSi-O valence characteristic of kaolinite
537	γSi-O-Al
469	δSi-O
430	related Si-O-Si

4. Physical properties of kaolin

The specific surface area (SSA), total pore volume (V_p), mesopore volume (V_{me}), micropore volume (V_{mi}), and average pore diameter (D) of initial unground and ground kaolin are shown in Table 4.4. Surface area, pore volume and mesopore volume of natural kaolin are increased upon grinding i.e., the value of S_{BET} from ~42 m^2/g to ~61 m^2/g and of V_p from 0.2 cc/g to 0.28 cc/g. This is due to the particle size is decreased in ground kaolin as seen in SEM micrograph (see Figure 4.4). The mesopore volume (V_{me}) is increased from 0.05 cc/g to 0.128 cc/g. The pore size distribution curve (Figure 4.3) also shows that there is a higher proportion of pores in UGK at <20 Å which represents micropore. Grinding increases the pores proportion in the ~40 Å range which is mesopores.

Table 4.4 Specific surface area (SSA), total pore volume (Vp), mesopore volume (V_{me}), micropore volume (V_{mi}), and bleaching capacity (BC) of the initial unground and ground samples (UGK and GK samples)

Sample	SSA (m^2/g)	V_p (cc/g)	V_{mi} (cc/g)	V_{me} (cc/g)	BC (%)
UGK	41.89	0.2	0.01	0.05	34.94
GK	60.69	0.28	0.0	0.12	49.77

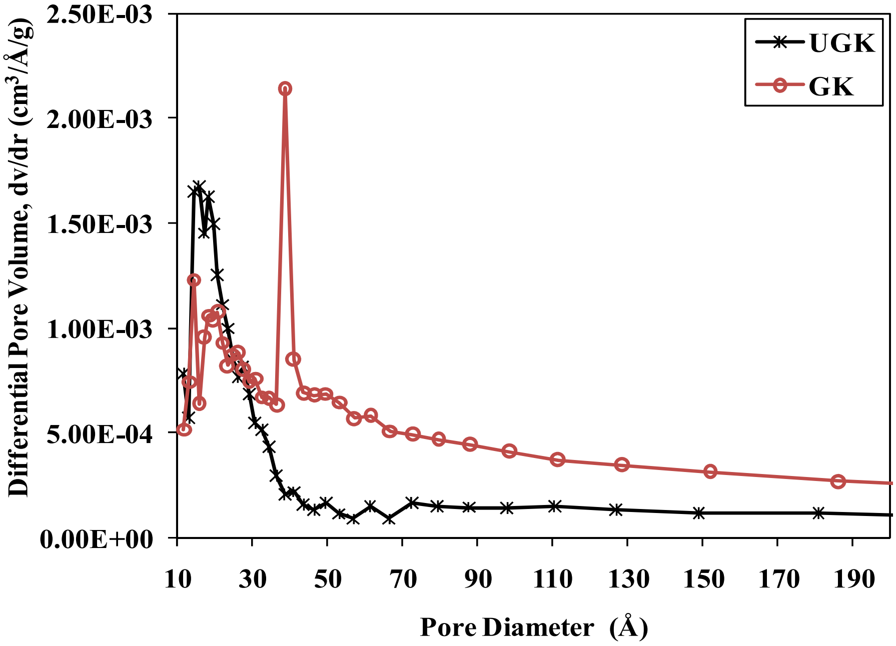

Figure 4.3 Pore size distribution curve of the initial unground (UGK) and ground (GK) samples.

5. Scanning electron microscopy

Scanning electron micrograph (SEM) and representative energy dispersive X-ray spectra (EDS) of unground kaolin (UGK) and ground kaolin (GK) samples are shown in Figure 4.4. The UGK has tubular morphology corresponding to halloysite. Worasith et al. (2011b) also observed the tubular morphology in untreated kaolin indicating the presence of halloysite in it. Grinding decreases the particle size and destroys the tubular-shaped into amorphous globular-shaped. Thereby, specific surface area and pore volume are increased in GK (Table 4.4). The elemental analysis of kaolins was performed using EDX analysis. The spectra show that Si, Al, O are the major elements in both samples and K is minor components. C and Au are appeared from the coating of clay prepared for the SEM analysis.

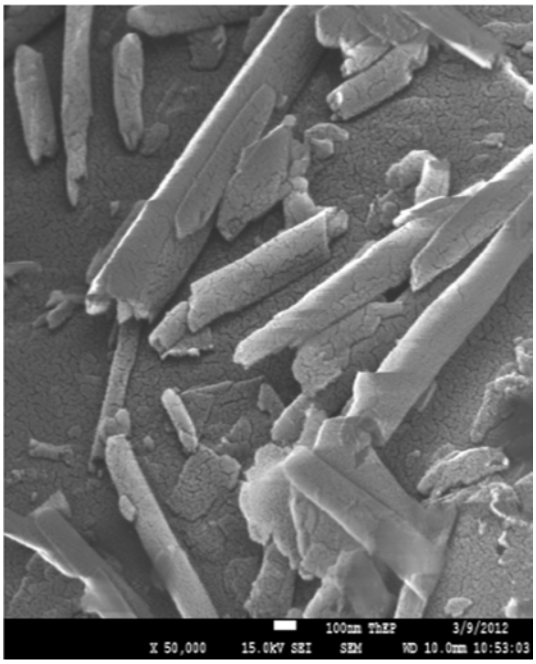
100nm ThEP
3/9/2012
X 50,000
15.0kV SEI
SEM
WD 10.0mm 10:53:03

(A - i)

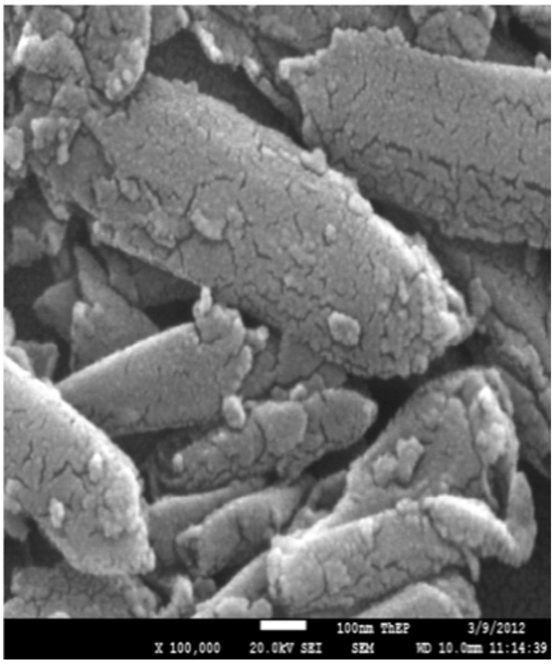
100nm ThEP
3/9/2012
X 100,000
20.0kV SEI
SEM
WD 10.0mm 11:14:39

(A - ii)

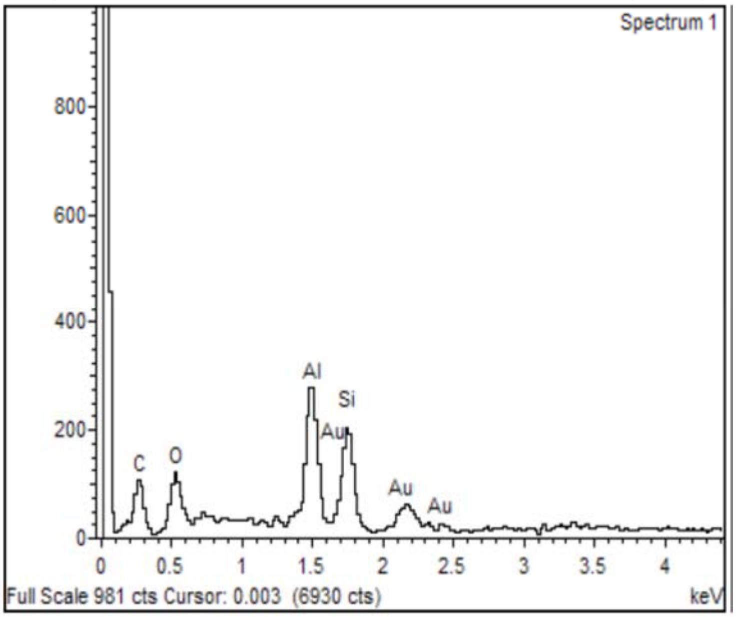
Spectrum 1
800
600
400
200
0
C
O
Al
Au
Si
Au
Au
0
0.5
1
1.5
2
2.5
3
3.5
4
Full Scale 981 cts Cursor: 0.003 (6930 cts)
keV

(A - iii)

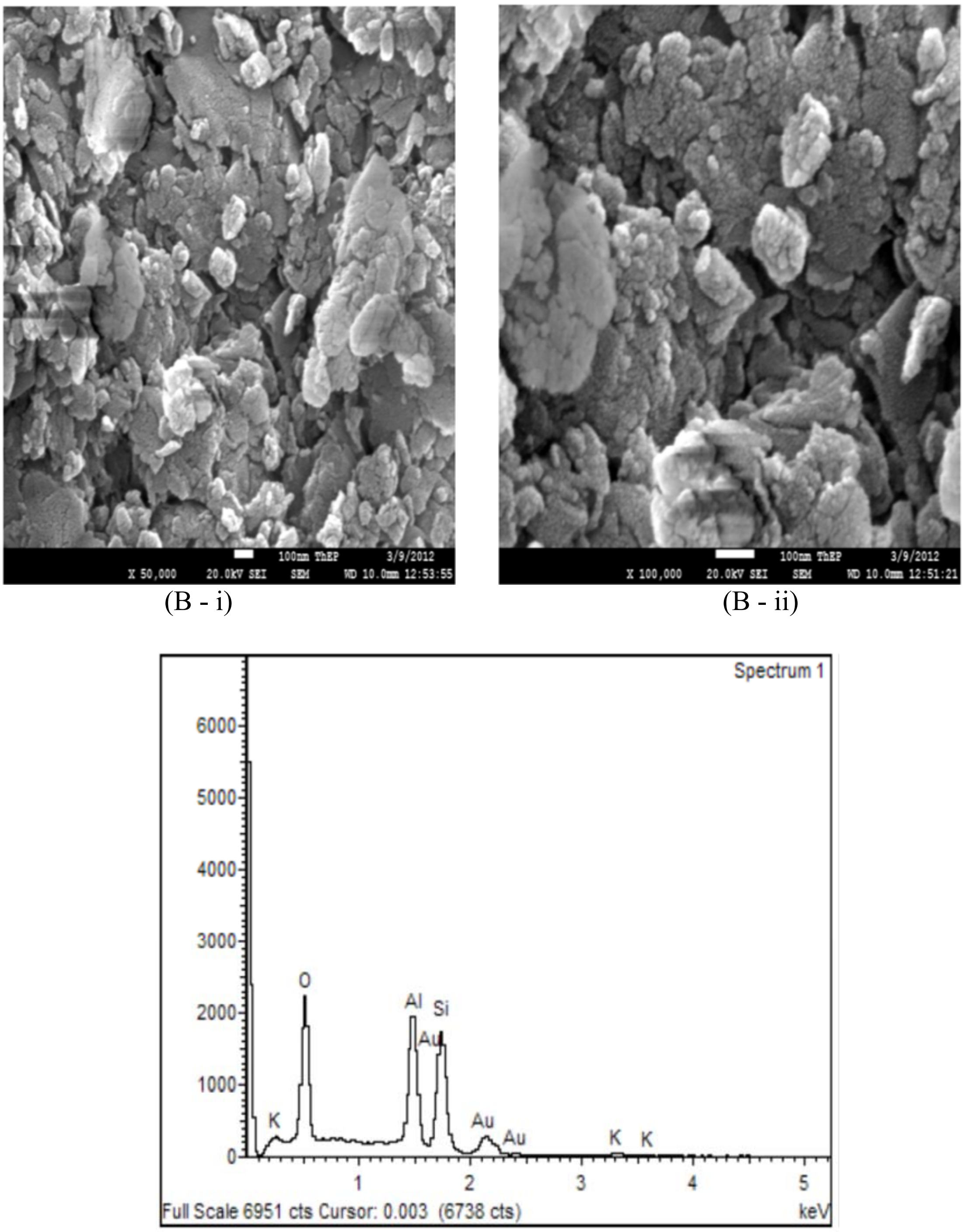

(B - i)

(B - ii)

(B - iii)

Figure 4.4 Scanning electron microscope micrographs of kaolins (A) UGK and (B) GK; samples magnified x 50,000 (i), magnified x 100,000 (ii) and representative energy dispersive X-ray analysis spectra (iii) from small areas on the surface of samples. Scale bars = 100 nm.

4.1.2 Effects of thermal and chemical treatments on kaolin

Table 4.5 shows the bleaching capacities of initial unground kaolin (UGK) and activated kaolins which are heated at different temperatures and refluxed with 2M sulphuric acid with the clay/acid ratio of 1:50 (FUG 2 samples). The initial UGK sample has a bleaching capacity of ~35%. For the FUG 2 samples, as the temperature increases, the bleaching capacity increases slightly to ~39% at 100˚C, decreases to ~16% at 600˚C, and then shows little changes at ~14% at 900˚C. It is found that the higher the temperature, the lower the bleaching capacity of kaolin. This is due to the extensive leaching of alumina and simultaneously formation of amorphous silica phase due to high temperature treatment prior to reflux. Among them, the 100UG 2 sample gives the maximum value but it is quite lower than that of commercial bleaching clay.

Table 4.5 Bleaching capacities of initial kaolin (UGK), activated samples (FUG 2) and commercial bleaching clay

Sample (2% w/w)	Bleaching capacity (%)
[a]UGK	34.94 ± 0.07
[b]100UG 2	38.5 ± 0.03
[b]200UG 2	37.61 ± 0.04
[b]300UG 2	33.95 ± 0.03
[b]400UG 2	32.01 ± 0.03
[b]500UG 2	28.74 ± 0.05
[b]600UG 2	16 ± 0.07
[b]700UG 2	15.08 ± 0.05
[b]900UG 2	13.69 ± 0.06
Commercial bleaching clay	81.75 ± 0.05

[a]UGK= unground kaolin (no thermic and reflux treatment); [b]FUG 2 = samples heated at temperatures equal to 100˚C, 200˚C, 300˚C, 400˚C 500˚C, 600˚C, 700˚C, 900˚C before reflux with 2M sulfuric acid (100UG 2 to 900UG 2).

1. X-ray Diffraction (XRD) analysis

The XRD patterns of initial and activated UGK are shown in Figure 4.5. Preheating UGK at 100˚C prior to reflux with 2 M sulfuric acid does not affect the global structure of the sample. The intensities of kaolinite are slightly reduced when it is heated up to 300˚C. By contrast, for 500UG 2, the reflections due to kaolinite disappear, while those of other minerals such as illite, K-feldspar, and quartz are preserved.

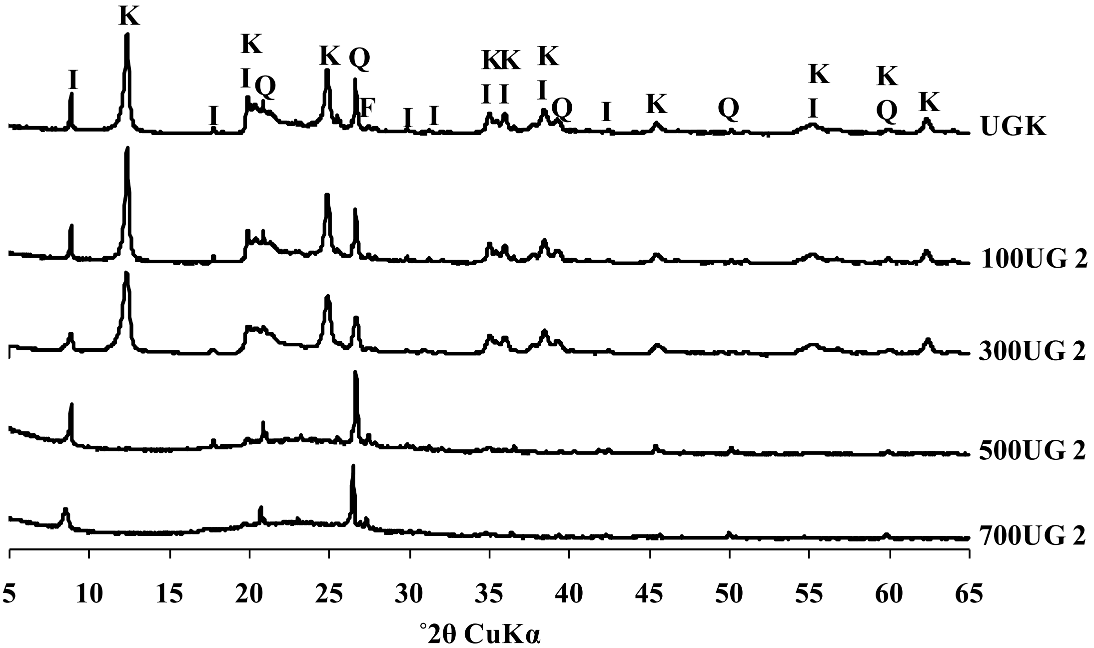

Figure 4.5 Comparison of the XRD patterns obtained from randomly orientated preparations of the initial (UGK) and activated samples (FUG 2) heated at different temperatures from 100°C to 700°C prior to refluxing with 2 M sulfuric acid (100UG 2 to 700UG 2).

The relative proportion of kaolinite present in these samples is calculated based on the intensity values recorded for the d_{001} reflection of kaolinite in the XRD data and assuming 100% kaolinite for the UGK sample. The kaolinite proportion slightly decreases at 300°C (300UG 2 sample) and sharply decreases to approximately 3% when the kaolin is preheated at higher temperatures (500UG 2 and 700UG 2) (see Figure 4.6). Such behavior is in agreement with the dehydroxylation temperature (~500°C) of kaolinite. It also consistents with the work of Panda et al. (2010) who reported that the coordinated and structural water was lost when the kaolin was heated to high temperature as well as the results of others authors (Fernandez et al., 2011; Foo et al., 2011) who demonstrated that the amorphous phases were formed when dehydroxylation temperature was reached.

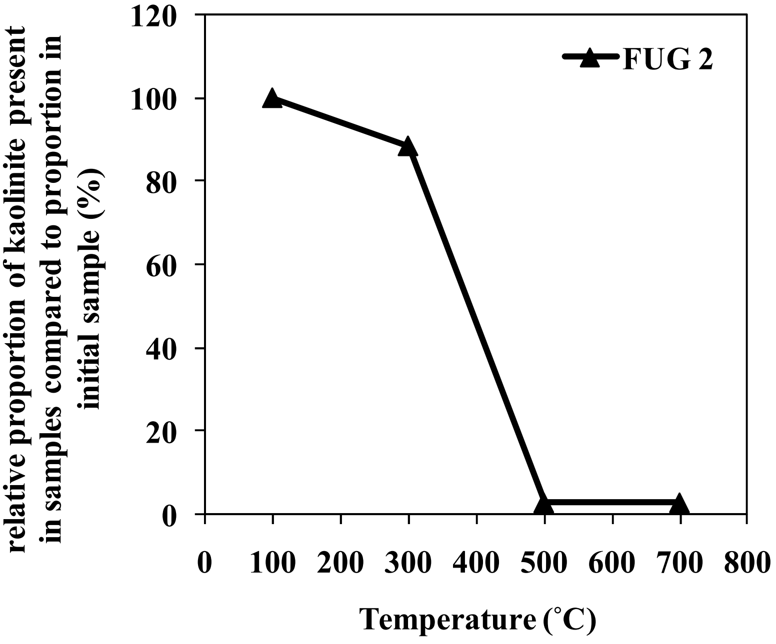

Figure 4.6 Relative proportion of kaolinite present in the activated kaolins (FUG 2) as a function of the temperature used for heating prior to refluxing in 2 M sulfuric acid. FUG 2 = samples heated at different temperatures and refluxed with 2 M sulfuric acid (100UG 2 to 700UG 2).

2. X-ray Fluorescence Spectra (XRF) analysis

The UGK sample has an Al/Si value equal to approximately 0.9, corresponding to approximately 54 wt% SiO_2 and 42 wt% Al_2O_3 in the sample (Table 4.6). Furthermore, activated samples preheated up to 700°C prior to reflux with sulfuric acid are characterized by a higher silica and lower alumina content than that of the initial sample (i.e., UGK). For example, the SiO_2 content progressively increases from ~54 to ~93 wt%, while the Al_2O_3 content dramatically decreases from ~42% in UGK to ~5 wt% in the sample preheated at 700°C prior to reflux (700UG 2). These chemical results are in agreement with the structural data (XRD and FTIR) (see Figures 4.5 and 4.8), which indicates the disappearance of kaolinite and the presence of an amorphous phase rich in Si in samples prepared with a high temperature step. These results are also comparable with that of Okada, et al. (1998) who prepared the metakaolinite by calcining the kaolinite at 600˚C for 24 h and then treating it with 20% sulfuric acid at 90˚C for 0.5-5 h. They reported that alumina decreased dramatically after leaching with 20% sulfuric acid, whereas the silica increased to more than 90% after 1.5 h leaching. Extensive leaching of alumina from the unground kaolin causes a largely decreased in the relative proportions of kaolinite in the activated samples for 500UG 2 and 700UG 2 samples (see Figure 4.7).

Table 4.6 Chemical compositions of the initial kaolin (UGK) and activated kaolins (FUG 2)

	SiO_2 %	Al_2O_3 %	K_2O %	Fe_2O_3 %	CaO %	CuO %	TiO_2 %	MnO %	Al:Si
[a]UGK	53.90	42.40	2.03	1.11	0.03	0.06	0.04	0.07	0.89
[b]100UG 2	60.50	35.80	1.95	0.69	0.19	0.05	0.07	0.04	0.67
[b]300UG 2	61.50	35.20	2.22	0.72	0.10	0.05	0.04	0.05	0.65
[b]500UG 2	89.20	7.31	2.31	0.63	0.07	0.05	0.05	0.05	0.09
[b]700UG 2	92.70	4.90	1.44	0.47	0.04	0.05	0.04	0.03	0.06

[a]UGK = unground kaolin;
[b]FUG 2 = samples heated at different temperatures and refluxed with 2 M sulfuric acid (100UG 2 to 700UG 2).

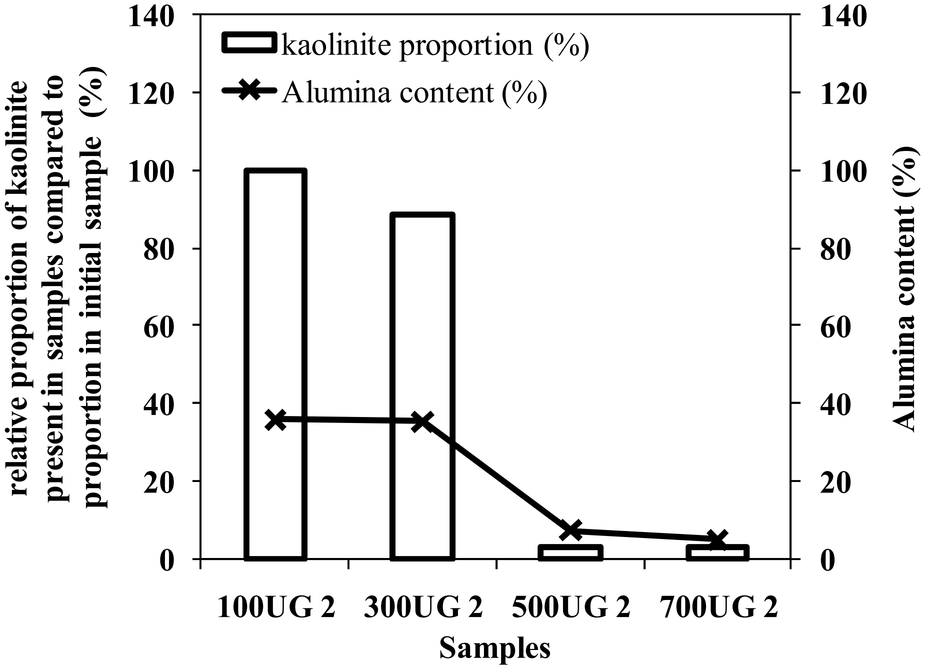

Figure 4.7 Comparison of relative proportions of kaolinite and alumina content present in the activated kaolins (FUG 2) as a function of the temperature used for heating prior to refluxing in 2 M sulfuric acid. FUG 2 = samples heated at different temperatures and refluxed with 2 M sulfuric acid (100UG 2 to 700UG 2).

3. Fourier Transform Infrared Spectroscopy (FTIR)

No difference is observed between the FTIR spectra obtained for the 100UG 2, 300UG 2, and initial UGK samples (Figure 4.8). These results indicate that the kaolinite is resistant to thermal treatment until 300˚C. However, preheating of the UGK above the hydroxylation temperature of 500°C destroys the kaolin's structure (see the FTIR spectra of 500UG 2). Indeed, the four bands characteristic of kaolinite in the stretching region (3696, 3669, 3653, and 3620 cm^{-1}) have completely disappeared. The bands at 1114, 1031, and 1008 cm^{-1} for Si-O stretching, those at 753 cm^{-1} for Si-O-Si stretching, and those at 537 cm^{-1} for Si-O-Al stretching also disappear. The intensities of the bands at 938 and 912 cm^{-1} from the Al-Al-OH groups decrease and merge into a single band at 950 cm^{-1}. The increase in the band intensity at 1092 cm^{-1} suggests that a three-dimensional network of amorphous Si-O-Si units is formed. These observations are in agreement with the XRD results (see Figure 4.5), which demonstrate that the kaolinite structure is completely destroyed and replaced by an amorphous Si phase when the initial UGK is preheated at 500°C or higher prior to the reflux step.

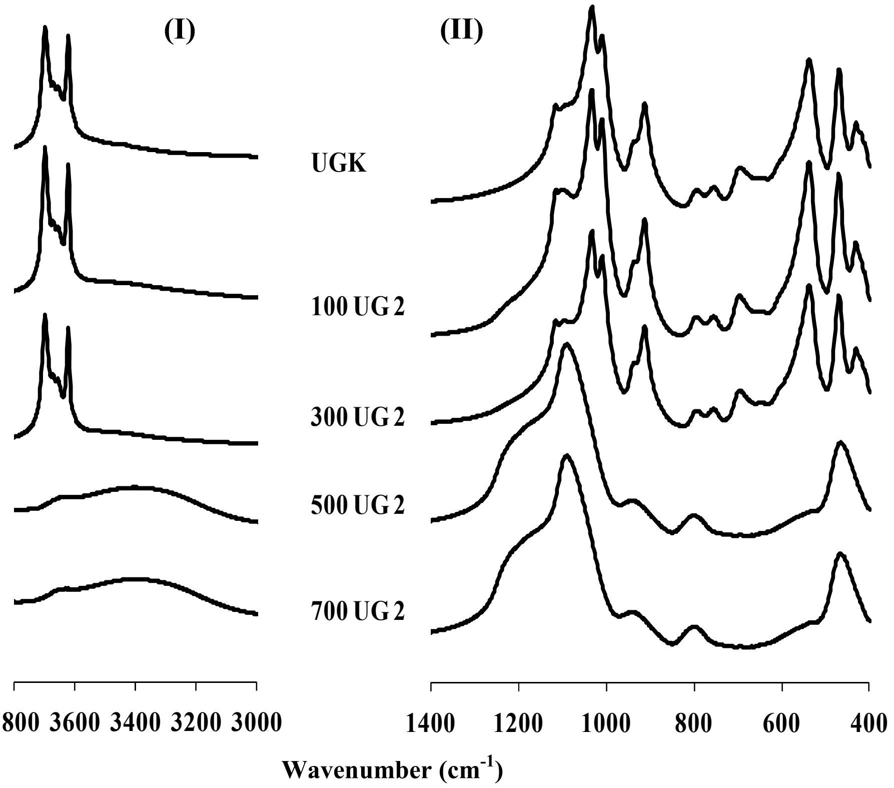

Figure 4.8 Comparison of the FTIR spectra of the initial unground (UGK) and activated (FUG 2) samples.

4. Physical properties of kaolin

The specific surface area (SSA), total pore volume (V_p), mesopore volume (V_{me}) and micropore volume (V_{mi}) of initial unground (UGK) and activated kaolins (FUG 2) are shown in Table 4.7. The specific surface area and pore volume are increased with increasing preheating temperature under the same acid concentration. The specific surface area and total pore volume of the activated samples are generally higher than those of UGK. For example, UGK has a specific surface area and a pore volume of 42 m^2/g and 0.2 cc/g, respectively, whereas 700UG 2 is characterized by a specific surface area and a total pore volume of approximately 456 m^2/g and 0.4 cc/g, respectively. The micropore volume (V_{mi}) and mesopore volume (V_{me}) are increased from 0.01 cc/g to 0.2 cc/g and from 0.05 cc/g to 0.1 cc/g, respectively. Okada, et al. (1998) also reported that the surface area and micropore volumes were increased to ~340 m^2/g and ~0.2 cc/g, respectively by calcining the kaolinite at 600˚C for 24 h prior to chemical treatment. They also mentioned that these micro- and mesopores occurred in the interlayer regions between silica tetrahedron layers.

Table 4.7 Specific surface area (SSA), total pore volume (Vp), mesopore volume (V_{me}), micropore volume (V_{mi}) and bleaching capacity (BC) of the initial unground and activated samples (UGK and FUG 2)

Sample	SSA (m^2/g)	V_p (cc/g)	V_{mi} (cc/g)	V_{me} (cc/g)	BC (%)
[a]UGK	41.90	0.2	0.01	0.09	34.9
[b]100UG 2	81.30	0.3	0.01	0.30	38.5
[b]300UG 2	74.13	0.2	0.10	0.10	33.9
[b]500UG 2	304.50	0.3	0.10	0.20	28.7
[b]700UG 2	456.20	0.4	0.20	0.20	15.1

[a]UGK = unground kaolin;
[b]FUG 2 = samples heated at different temperatures and refluxed with 2 M sulfuric acid (100UG 2 to 700UG 2).

The pore size distribution curve (Figure 4.9) also shows that the peaks of the samples at ~ 40 Å increase when the unground kaolin is preheated at higher temperature before reflux with sulfuric acid. The sample 100UG 2, however, has a higher proportion of mesopores in the 45-130 Å where as the samples 500UG 2 and 700UG 2 have a higher micropore content > 20 Å. This means treating the kaolin at higher temperatures cause destruction in the structure of activated kaolins.

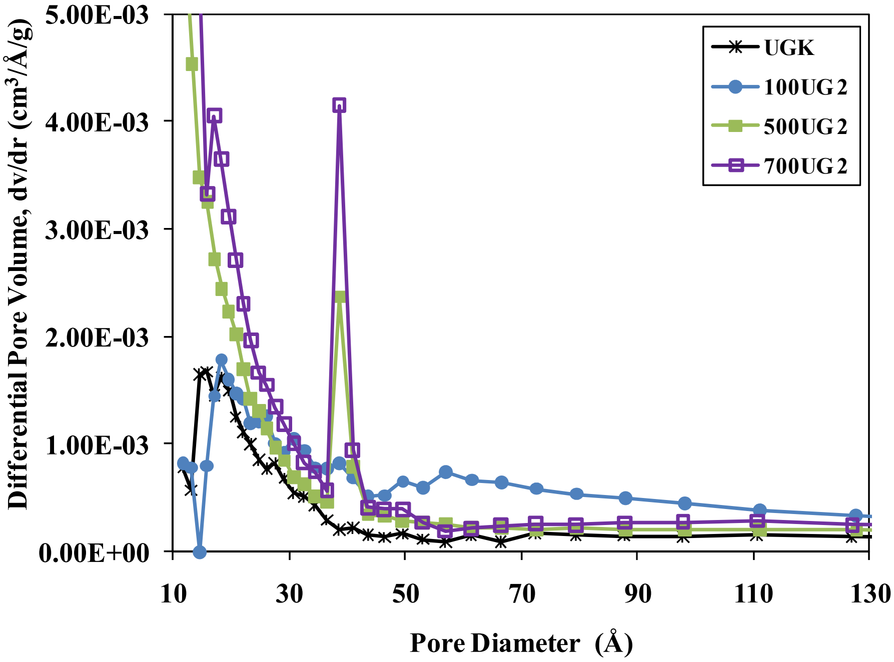

Figure 4.9 Pore size distribution curve of the initial unground (UGK) and activated (FUG 2) samples. UGK = unground kaolin; FUG 2 = samples heated at different temperatures and refluxed with 2 M sulfuric acid (100UG 2 to 700UG 2).

4.1.3 Effects of thermal, mechanical and chemical treatments on kaolin

Table 4.8 shows the bleaching capacities of initial ground kaolin (GK) and activated kaolins which are heated at different temperatures, ground and refluxed with 2M sulphuric acid with the clay/acid ratio of 1:50 (FG 2 samples). The GK sample has a bleaching capacity of ~50%. Sample 100 GR 2 gives the maximum bleaching capacity of about 67% which is lower than that of commercial clay (~82%). Preheating the kaolin at 100˚C prior to ground and reflux with 2 M sulfuric acid slightly increases its bleaching capacity. After that the capacities, however, are decreased with increasing preheating temperature. For example, as the temperature increases, the bleaching capacity decreases from ~67% at 100˚C to ~15% at 600˚C, and then slightly reduces to ~12% at 900˚C. The same pattern is observed for both FUG 2 and FG 2 samples (see Tables 4.5 and 4.8). The bleaching capacities of activated samples with or without grinding are decreased when the samples are preheated to higher temperatures. This means heating the kaolin to high temperatures is not good for its sorption properties.

The effect of acid concentration on kaolins is tested by treating the ground kaolin preheated at 100˚C with different sulfuric acid concentrations equal to 0.1 to 2.6 M. Table 4.9 shows the bleaching capacities of ground kaolin (GK) and activated kaolins (100GRS samples). The bleaching capacities are increased with increasing sulfuric acid concentration up to 0.5 M. Sample 100GR 0.5 gives the optimum bleaching capacity of about 80% which is slightly lower than that of commercial bleaching clay (~82%). Beyond this optimum condition, the capacities of kaolins are continuously decreased to ~67% in 100GR 2.6. This is probably due to the excessive replacement of the alumina by the hydrogen ions releasing from the acid solution (James et. al., 2008).

Table 4.8 Bleaching capacities of initial sample (GK), activated samples (FG 2) and commercial bleaching clay

Sample (2% w/w)	Bleaching capacity (%)
[a]GK	49.77 ± 0.12
[b]100GR 2	67.12 ± 0.03
[b]200GR 2	43.26 ± 0.05
[b]300GR 2	34.55 ± 0.05
[b]400GR 2	26.55 ± 0.04
[b]500GR 2	20.36 ± 0.05
[b]600GR 2	14.68 ± 0.06
[b]700GR 2	13.34 ± 0.04
[b]900GR 2	12.32 ± 0.03
Commercial bleaching clay	81.60 ± 0.07

[a]GK= ground kaolin (no thermic and reflux treatment); [b]FG 2 = samples heated at temperatures equal to 100˚C, 200˚C, 300˚C, 400˚C 500˚C, 600˚C, 700˚C, 900˚C prior to ground and reflux with 2M sulfuric acid (100GR 2 to 900GR 2).

Table 4.9 Bleaching capacities of ground kaolin (GK), activated kaolins (100GRS) and commercial bleaching clay

Sample (2% w/w)	Bleaching capacity (%)
[a]GK	49.77 ± 0.12
[b]100GR 0.1	70.20 ± 0.02
[b]100GR 0.3	78.96 ± 0.07
[b]100GR 0.5	79.79 ± 0.03
[b]100GR 1	77.74 ± 0.04
[b]100GR 1.5	74.86 ± 0.05
[b]100GR 1.7	75.26 ± 0.45
[b]100GR 2	67.12 ± 0.05
[b]100GR 2.6	66.88 ± 0.16
Commercial bleaching clay	81.51 ± 0.04

[a]GK= ground kaolin (no thermic and reflux treatment); [b]100GRS = samples preheated at 100˚C prior to ground and reflux with different concentrations of sulfuric acid (100GR 0.1 to 100GR 2.6).

1. X-ray Diffraction (XRD) analysis

The XRD patterns of initial and activated GK are shown in Figure 4.10A. The intensities of kaolinite are slightly reduced when it is heated up to 300˚C. Beyond 500˚C (500GR 2 and 700 GR 2), the relative intensity of the reflections characterizing kaolinite completely disappear compared with those of the initial GK sample and 100GR 2 and 300GR 2 (see the XRD data in Figure 4.10A). It is found that other minerals such as illite, K-feldspar, and quartz are resisted to above dehydroxylation temperature. The relative proportion of kaolinite present in these samples is calculated based on the intensity values recorded for the d_{001} reflection of kaolinite in the XRD data (Figure 4.10A) and assuming 100% kaolinite for the GK sample. The relative proportions of kaolinite are decreased to about 60% in 100GR 2 and about 50% in 300GR 2 due to the structural changes of kaolinite (see Figure 4.11A). For 500GR 2 and 700GR 2, the kaolinite proportions decrease dramatically to 6%, in agreement with the dehydroxylation temperature of kaolinite (500°C) and the transformation of the material to amorphous metakaolin (Suraj et al., 1998; Sánchez et al., 1999; Cheng et al., 2010).

The XRD patterns of the initial GK and activated kaolin samples (100GRS) are shown in Figures 4.10B. There are no significant structural changes when the GK sample is heated at 100˚C prior to reflux with a 0.1 M sulfuric acid solution. After treatment with 0.5 or 2 M sulfuric acid, the relative intensities of the kaolinite reflections for samples preheated at 100°C (100GR 0.5 and 2) decrease slightly, while those of quartz, illite, and K-feldspar are preserved. The nonclay minerals quartz, illite, and K-feldspar are resistant to acid treatment, whereas the kaolinite structure is only partially preserved when sulfuric acid concentrations of 2 M are used. The relative proportion of kaolinite in 100GR 0.1 is approximately the same as that of the GK sample (~100%; see Figure 4.11B). When the acid concentration used is increased to 0.5 M (100GR 0.5), the relative proportions of kaolinite decrease dramatically to 66%. Further acid treatment to kaolin with 2 M sulfuric has a small effect on the kaolinite proportion which is 62% in 100GR 2 sample.

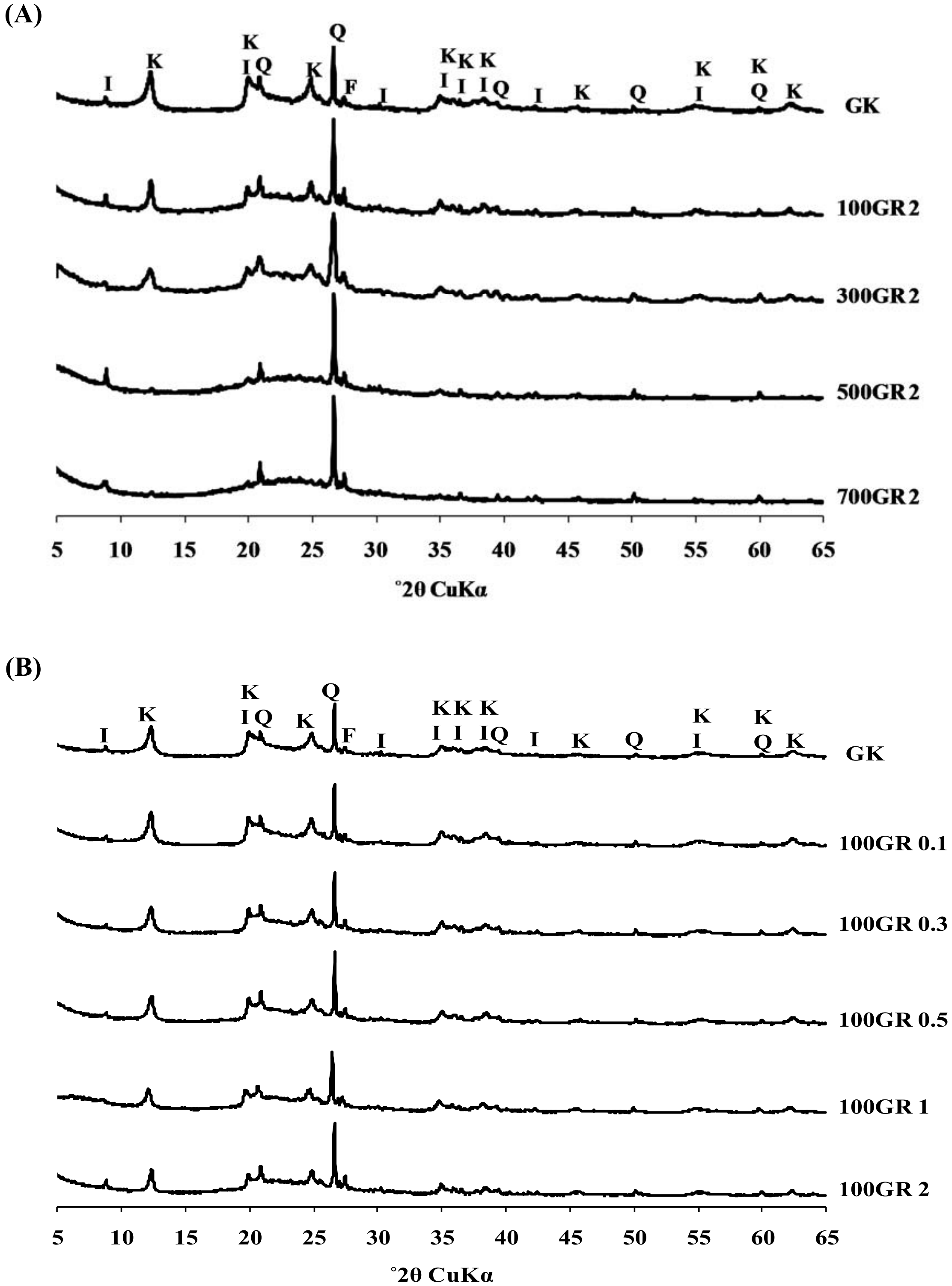

Figure 4.10 Comparison of the XRD patterns obtained from randomly orientated preparations of the GK and activated samples (FG 2) heated at different temperatures from 100°C to 700°C prior to ground and reflux with 2 M sulfuric acid (100GR 2 to 700GR 2) (A), and initial ground kaolin (GK) and samples (100GRS) heated at 100°C, ground, and refluxed with different concentrations of sulfuric acid equal to 0.1, 0.3, 0.5, 1 and 2 M (100GR 0.1 to 100GR 2) (B).

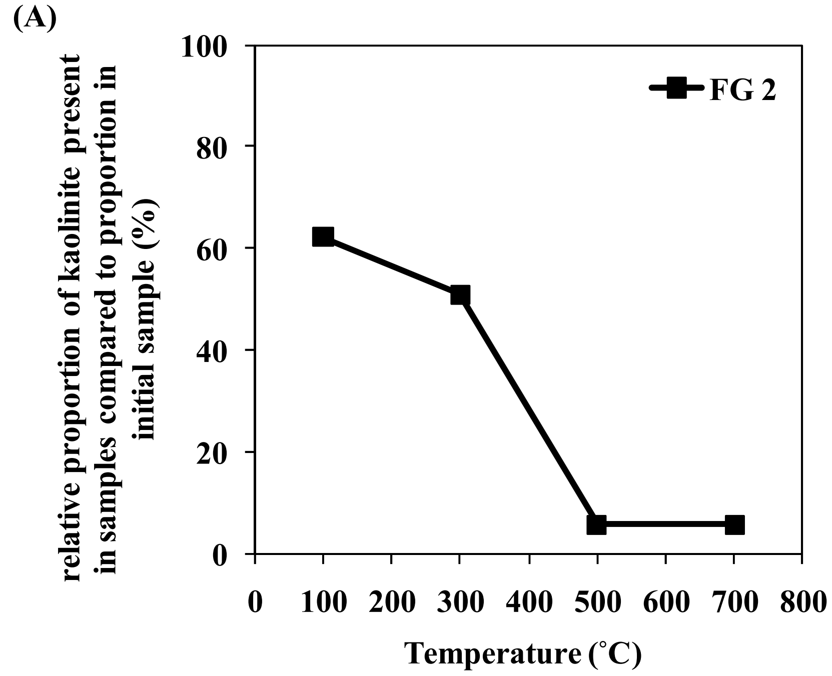

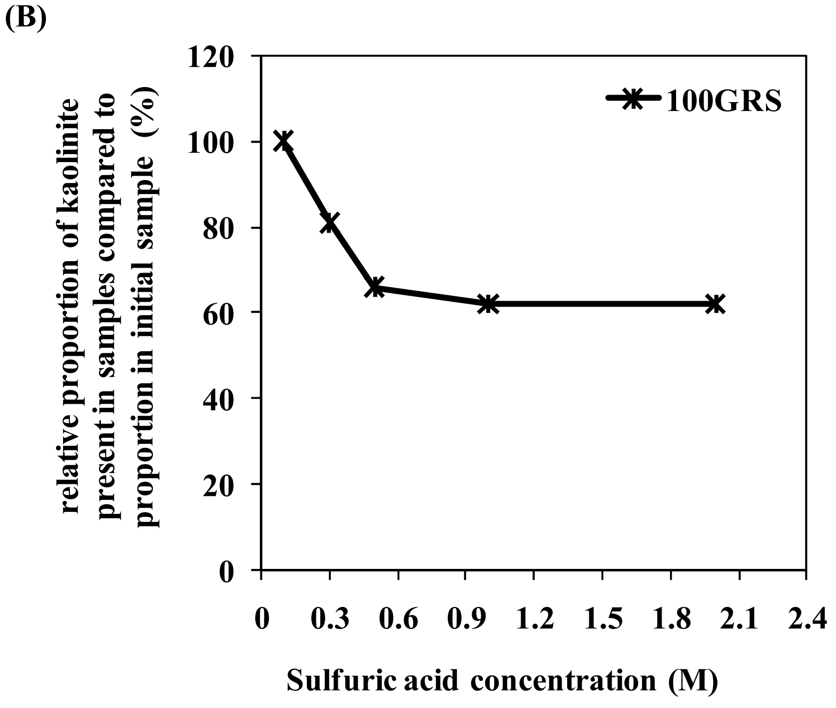

Figure 4.11 Relative proportion of kaolinite present in the activated kaolins (FG 2) as a function of the temperature used for heating prior to ground and refluxing in 2 M sulfuric acid (100GR 2 to 700GR 2) (A), and in the samples (100GRS) heated at 100˚C, ground, and refluxed with different concentrations of sulfuric acid equal to 0.1, 0.3, 0.5, 1 and 2 M (100GR 0.1 to 100GR 2) (B).

2. X-ray Fluorescence Spectra (XRF) analysis

The GK sample has an Al/Si value equal to approximately 0.9, corresponding to approximately 54 wt% SiO_2 and 42 wt% Al_2O_3 in the sample (see Table 4.10). For activated samples (FG 2 samples), the SiO_2 contents increase while the Al_2O_3 contents decrease dramatically compared to the GK sample as the preheating temperature used prior to reflux increases. For example, 700GR 2 has an Al/Si value equal to 0.04, in contrast to the value of 0.88 for GK. This Al/Si value of 700GR 2 is in agreement with the complete disappearance of kaolinite and the presence of an amorphous phase rich in Si indicated by both XRD and FTIR for this sample (see Figures 4.10A, 4.11A and 4.13A). Relative proportions of kaolinite in 500GR 2 and 700GR 2 samples also dramatically decrease due to extensively leaching of alumina from the samples (see Figure 4.12A). The chemical compositions of the 100GRS samples are also reported in Table 4.10. The SiO_2 content increases with increasing acid concentration. When the GK sample is treated with a 2 M sulfuric acid solution (100GR 2), the SiO_2 content increases dramatically from ~54% to ~80%, in agreement with the increase in the proportion of an amorphous phase rich in Si detected by FTIR for these samples (see Figure 4.13B). In parallel, the Al_2O_3 content decreases from ~42 to ~16%, while other metal oxides, expressed as K_2O, Fe_2O, CuO, and MnO, are leached from the samples. The Al/Si ratio of ~0.4 in 100GR 0.3 decreases to ~0.2 in 100GR 2. For 100GRS samples, the relative proportions of kaolinite gradually decrease from 80% to ~60% along with the reduced of alumina from ~25% to ~17% when the ground kaolin is treated with 0.3 M to 2 M sulfuric acid concentration (see Figure 4.12B).

Table 4.10 Chemical compositions of the ground kaolin (GK) and activated kaolins (FG 2 and 100GRS)

	SiO_2 %	Al_2O_3 %	K_2O %	Fe_2O_3 %	CaO %	CuO %	TiO_2 %	MnO %	Al:Si
GK	54.10	42.00	2.07	1.03	0.04	0.06	0.05	0.07	0.88
Samples heated at different temperatures from 100˚C to 700˚C prior to ground and reflux with 2 M sulfuric acid (FG 2 samples)									
100GR 2	80.20	16.60	1.97	0.55	0.10	0.05	0.03	0.04	0.23
300GR 2	84.40	12.70	2.02	0.44	0.06	0.05	0.04	0.03	0.17
500GR 2	91.40	5.68	1.91	0.42	0.06	0.05	0.06	0.03	0.07
700GR 2	94.40	3.48	1.27	0.31	0.06	0.05	0.04	0.00	0.04
Samples heated at 100˚C, ground, and refluxed with different concentrations of sulfuric acid equal to 0.3 to 2 M (100GRS samples)									
100GR 0.3	71.12	24.87	1.45	0.57	0.10	0.01	0.03	0.04	0.40
100GR 0.5	73.69	23.10	1.40	0.55	0.11	0.01	0.04	0.04	0.36
100GR 1	79.14	17.79	1.42	0.42	0.11	0.00	0.03	0.03	0.26
100GR 2	80.20	16.60	1.97	0.55	0.10	0.05	0.03	0.04	0.23

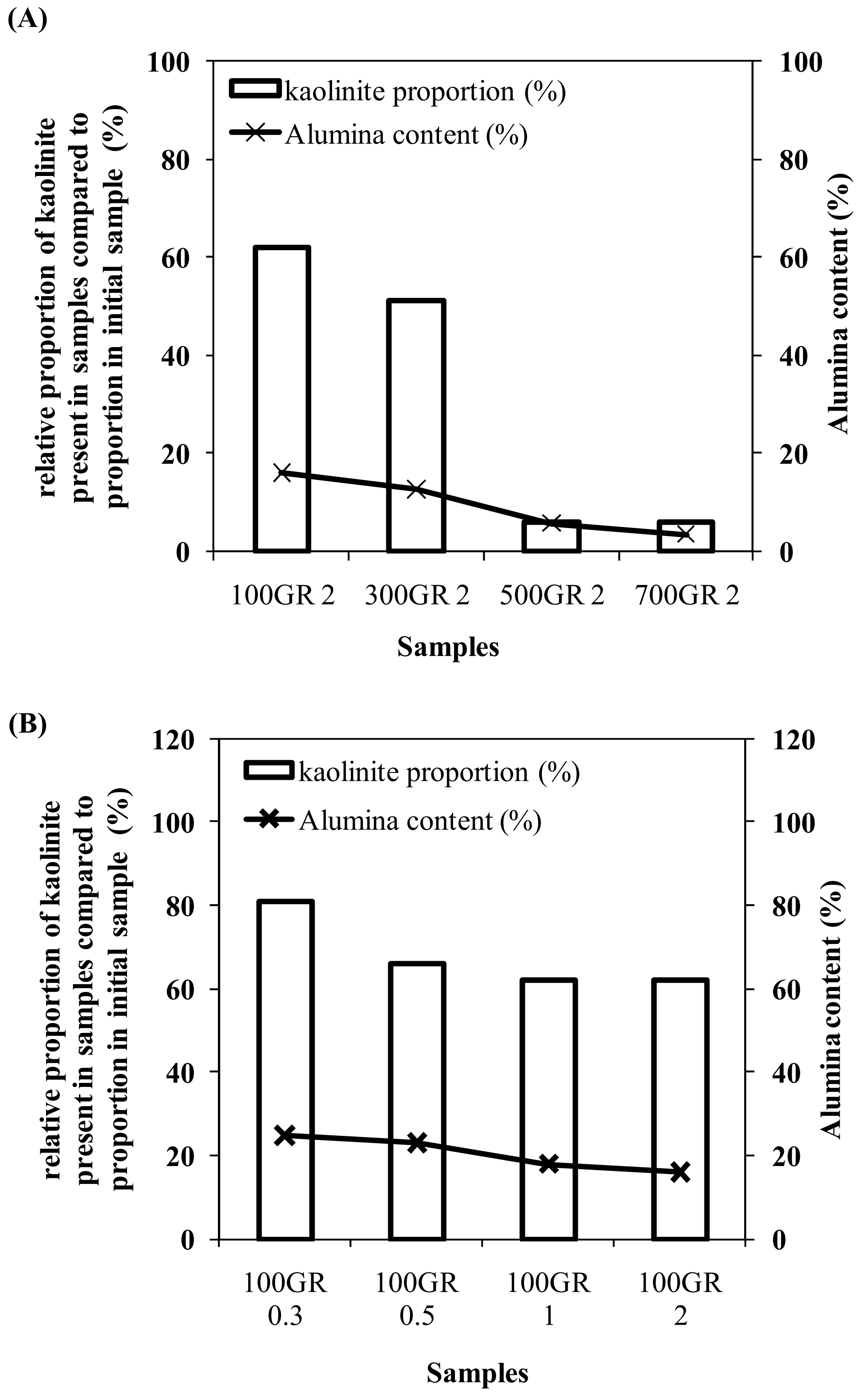

Figure 4.12 Comparison of relative proportions of kaolinite and alumina present in the activated kaolins (FG 2) as a function of the temperature used for heating prior to ground and refluxing in 2 M sulfuric acid (100GR 2 to 700GR 2) (A), and in the samples (100GRS) heated at 100°C, ground, and refluxed with different concentrations of sulfuric acid equal to 0.3, 0.5, 1 and 2 M (100GR 0.3 to 100GR 2) (B).

3. Fourier Transform Infrared Spectroscopy (FTIR)

The FTIR spectra of the GK and activated kaolin (FG 2) samples are compared in Figure 4.13A. The four typical hydroxyl bands of kaolinite (3696, 3669, 3653, and 3620 cm^{-1}) are well resolved in GK, 100GR 2, and 300GR 2 but nearly absent in 500GR 2. The shoulder at 1092 cm^{-1} corresponding to the Si-O band increases in intensity as the preheating temperature increases and become the most intense band for all FG 2 samples. This behavior suggests the presence of an amorphous phase rich in Si, the contribution of which increases as the temperature used during the preparation of the sample is increased. The Si-O stretching vibrations of kaolinite at 1031 and 1008 cm^{-1} remain present in 100GR 2 and 300GR 2, indicating that the kaolinite structure is partially preserved in these samples at these low temperatures; in contrast, kaolinite is nearly absent in the sample prepared with a heating step at 500°C (500GR 2).

Figure 4.13B shows the FTIR spectra of the GK and 100GRS samples. The intensities of the kaolinite hydroxyl bands at 3696, 3669, 3653, and 3620 cm^{-1} are better resolved at an acid concentration of 0.1 M (100GR 0.1). As the acid concentration is increased, the intensity of the 3696 cm^{-1} band decreases relative to the 3620 cm^{-1} band, indicating that there are some modification of the inner hydroxyl groups of 100GR 0.5 and 100GR 2 compared to the GK sample. The bands at 1031 and 1008 cm^{-1}, which correspond to Si-O stretching vibrations of kaolinite in 100GR 0.1, are more intense than those of 100GR 0.5 and 100GR 2, indicating that the kaolinite structure is only partially preserved in 100GR 0.5 and 100GR 2, in agreement with the XRD results. The shoulder at 1090 cm^{-1} dramatically increases when the acid concentration increases, and the most intense peak is obtained for 100GR 2. This result suggests that the presence of a significant proportion of an Si-rich amorphous phase in this sample. The Al-Al-OH bending vibrations at 938 and 912 cm^{-1} are also reduced after acid treatment.

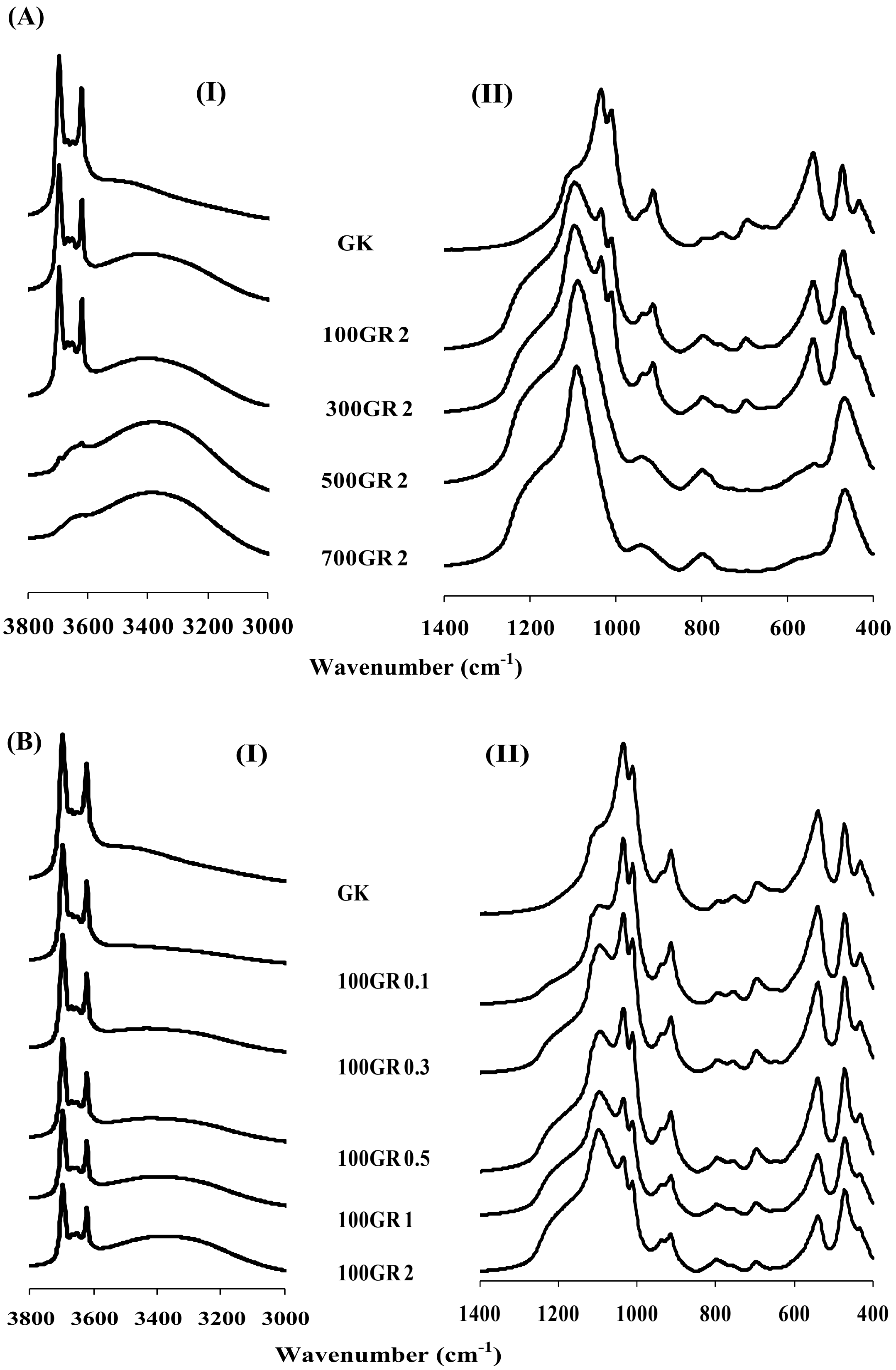

Figure 4.13 Comparison of the FTIR spectra of the GK and activated samples (FG 2) heated at different temperatures from 100°C to 700°C prior to ground and reflux with 2 M sulfuric acid (100GR 2 to 700GR 2) (A), and ground kaolin GK and samples (100GRS) heated at 100°C, ground, and refluxed with different concentrations of sulfuric acid equal to 0.1, 0.3, 0.5, 1 and 2 M (100GR 0.1 to 100GR 2) (B).

4. Physical properties of kaolin

The specific surface area (SSA), total pore volume (V_p), mesopore volume (V_{me}), and micropore volume (V_{mi}) of ground (GK) and activated kaolins (FG 2 and 100GRS) are shown in Table 4.11. The specific surface area and total pore volume of the activated samples are generally higher than those of GK. With thermal treatment at 100˚C (100GR 2), an approximately six-fold increased in the surface area to ~372 m^2/g and a three-fold increased in the total pore volume to ~0.9 cc/g are observed. The specific surface area and pore volume are decreased beyond 100˚C under the same acid concentration. Preheating of the GK sample to 700˚C causes a decrease in both the surface area and total pore volume to ~304 m^2/g and ~0.3 cc/g, respectively. With increasing preheating temperature from 100 to 700˚C, the micropore volumes (V_{mi}) are increased from 0.01 cc/g to 0.1 cc/g while mesopore volumes (V_{me}) are decreased from 0.9 cc/g to 0.2 cc/g. This means heating the ground kaolin to above dehydroxylation temperatures enhances the formation of micropore in the activated samples. Some researchers prepared microporous silica by calcinating the kaolinite at above dehydroxylation temperature prior to acid treatment (Okada, et al., 1998).

Increasing acid concentrations also enhanced the surface area and pore volume in the activated samples (100GRS samples) as shown in Table 4.11. Ground sample preheated at 100˚C followed by refluxing with 0.1 M sulfuric acid (100GR 0.1 sample) has the specific surface area of ~172 m^2/g and pore volume of 0.3 cc/g. Sample 100GR 0.1 shows about 3-fold increased in specific surface area as compared to GK sample. After treating the preheated GK with 2 M sulfuric acid concentration, activated sample (100GR 2) has 6-fold increased in specific surface area and 3-fold increased in pore volume along with 3-fold increased in mesopore volumes.

Table 4.11 Specific surface area (SSA), total pore volume (Vp), mesopore volume (V_{me}), micropore volume (V_{mi}) and bleaching capacity (BC) of the ground and activated samples (GK, FG 2 and 100GRS)

Sample	SSA (m^2/g)	V_p (cc/g)	V_{mi} (cc/g)	V_{me} (cc/g)	BC (%)
GK	60.7	0.3	0.00	0.3	49.8
Samples heated at different temperatures from 100˚C to 700˚C prior to ground and reflux with 2 M sulfuric acid (FG 2 samples)					
100GR 2	372.1	0.9	0.01	0.9	67.1
300GR 2	369.4	0.9	0.03	0.9	34.6
500GR 2	294.9	0.5	0.10	0.4	20.4
700GR 2	304.8	0.3	0.10	0.2	13.3
Samples heated at 100˚C, ground, and refluxed with different concentrations of sulfuric acid equal to 0.1 to 2 M (100GRS samples)					
100GR 0.1	172.1	0.3	0.025	0.3	70.2
100GR 0.3	244.8	0.4	0.047	0.4	78.9
100GR 0.5	257.2	0.5	0.048	0.4	79.8
100GR 1	299.6	0.8	0.030	0.8	77.7
100GR 2	372.1	0.9	0.010	0.9	67.1

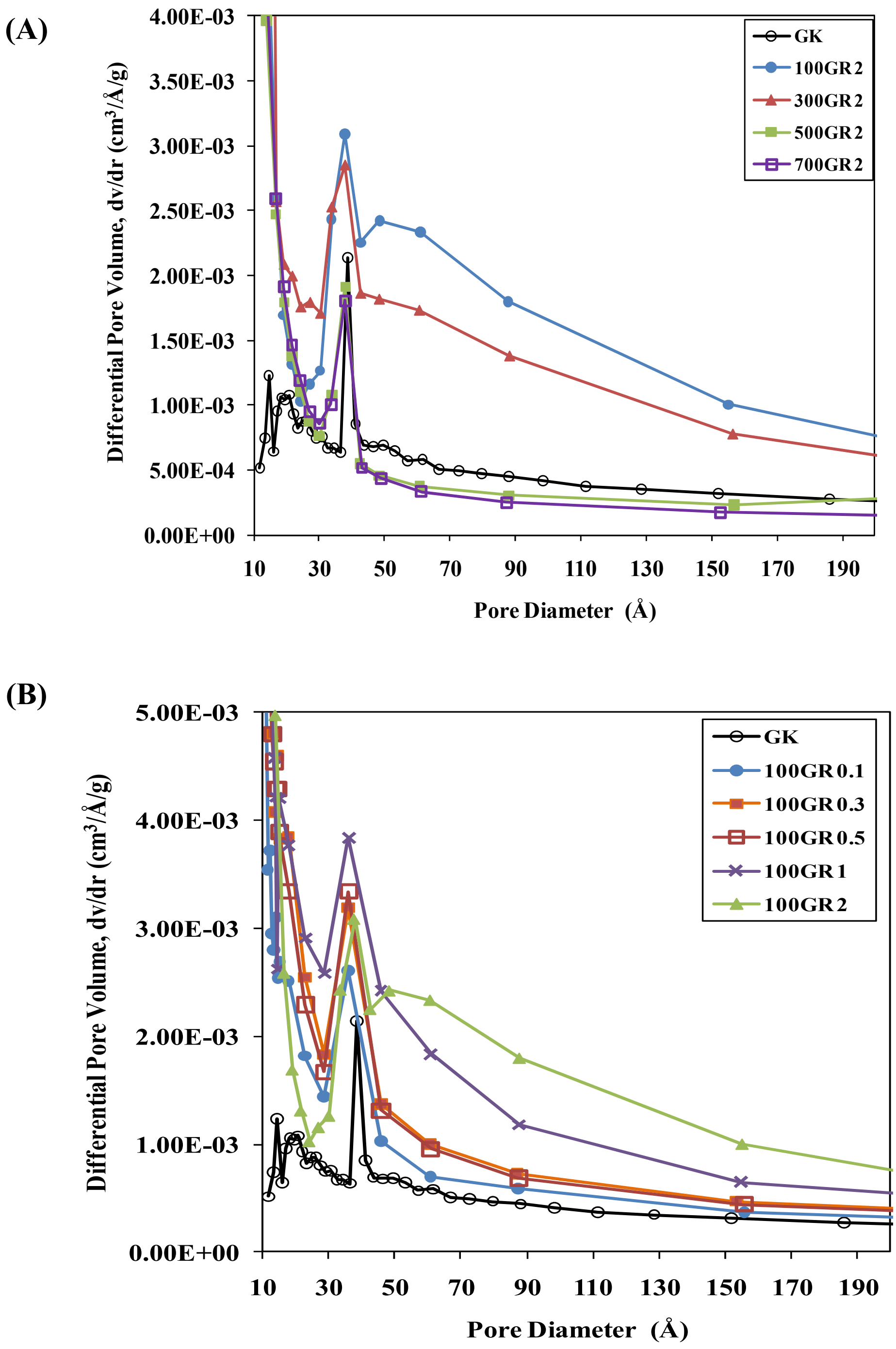

Figure 4.14 Pore size distribution curve of the GK and activated samples (FG 2) heated at different temperatures from 100˚C to 700˚C prior to ground and reflux with 2 M sulfuric acid (100GR 2 to 700GR 2) (A), and ground kaolin (GK) and samples (100GRS) heated at 100˚C, ground, and refluxed with different concentrations of sulfuric acid equal to 0.1, 0.3, 0.5, 1 and 2 M (100GR 0.1 to 100GR 2) (B).

The pore size distribution curve (Figure 4.14A) also shows that preheating the GK at 100˚C and 300˚C enhance the mesopore volumes in the activated samples. 100GR 2 sample contains the highest differential pore volume in the > 40 Å range. Beyond the dehydroxylation temperatures (above 500˚C), the mesopore volumes are lower than that of GK sample. Among FG 2 samples, it is seen that the peaks of the activated samples at 40 Å continuously decrease with the increasing temperatures. The samples 500GR 2 and 700GR2, have a lower differential pore volume at > 40 Å than that of GK sample. The effects of acid concentrations on the pore size of activated kaolins are shown in Figure 4.14B. The pore size distribution curve indicated that increasing the acid concentration up to 1 M sulfuric acid promoted the formation of more differential pore volume at 40 Å. After that the peak intensity was decreased in 100GR 2. Using 2 M sulfuric acid, sample 100GR 2 had the highest mesopore volume in the range >40 Å.

4.1.4 Effects of mechanical and chemical treatments on kaolin

The effects of grinding and acid treatment on kaolin's adsorption properties are studied by using different acid such as sulfuric acid, hydrochloric acid, citric acid and oxalic acid. The bleaching capacities of initial and activated kaolins such as GRS, GRH, GRC and GRO are shown in Table 4.12, Table 4.13, Table 4.14 and Table 4.15, respectively. When GK is treated with 0.1M sulfuric acid, the capacity is dramatically increased from ~ 50 to 79% (see Table 4.12). Among GRS samples, GRS 0.3 gives the optimum bleaching value of 81.41% which is same as that of commercial clay (81.62%). After that, the capacities decrease with increasing acid concentration and reach ~ 67% at 2 M sulfuric acid concentration for GRS 2. Acid-activated ground kaolins which are treated using hydrochloric acid, citric acid and oxalic acid also give the same results as sulfuric acid-treated samples. Kaolin's sorption properties are dramatically increased at low acid concentration. At their optimum conditions, 0.5GRH 1:50 gives ~ 83%, 0.5GRC 1:50 gives ~ 81% and 0.1GRO 1:80 gives ~ 79% as shown in Table 4.13, Table 4.14 and Table 4.15, respectively. Beyond the optimum condition, the capacities gradually decrease with increasing acid concentrations. The bleaching capacity of 0.5GRH 1:50 sample is superior to that of commercial clay while those of 0.5GRC 1:50 and 0.1GRO 1:80 are inferior to that of commercial clay.

When kaolin is treated with high acid concentration, low clay/acid ratio gives the better results. For kaolin activating with 2 M or 4 M sulfuric acid as a function of different clay/acid, % color removal initially increases with increasing clay/acid ratio. It goes through a maximum of ~73% for 2GRS 1:4 and ~74% for 4GRS 1:2; after which the bleaching performance gradually decreases with increasing clay/acid ratio. GRH samples treated with different clay/acid ratio also show the same trends as that of GRS samples treated using different clay/acid ratio (see Tables 4.12 and 4.13); the bleaching capacities of GRH samples (2GRH 1:12 and 4GRH 1:4) give the optimum conditions of ~80% and ~75%, respectively. This means that the sorption property of kaolin is optimized with low acid strength. Among GRO samples which are treated with 0.1 M oxalic acid using different clay/acid ratio (see Table 4.15), 0.1GRO 1:80 gives the best bleaching value of ~79%. This indicates that the kaolin has to be treated with high clay/acid ratio when it is activated using very low acid concentration.

Although activated samples (for 0.5GRH 1:50, 2GRH 1:12 and 4GRH 1:6) which are treated with same acid strength, these samples have different bleaching capacities (see Table 4.13). For example, 0.5GRH 1:50 gives the value of ~83%, 2GRH 1:12 gives about ~80% and 2GRH 1:12 gives ~74%. It means that the lower the acid concentration with high clay/acid ratio gives the better results than the higher the acid concentration with low clay/acid ratio.

Salawudeen et al., (2007) reported that acid treatment increased the bleaching capacity of clay up to 94.28% in HCl activated clay and 89.46% in H_2SO_4 activated clay. The results indicated that HCl activated clays are more effective in removing color from oil than H_2SO_4. This is due to the fact that HCl is a strong acid and it can degrade water into H^+ and Cl^- ions. The metal chlorides produced are soluble in water, and can be removed by the pretreatment process (Christidis et al., 1997).

Table 4.12 Bleaching capacities of ground kaolin (GK), activated samples (GRS samples) and commercial bleaching clay

Sample (2% w/w)	Bleaching capacity (%)
GK	49.77 ± 0.12
Commercial bleaching clay	81.62 ± 0.07
Samples heated at 80˚C, ground, and refluxed with different concentrations of sulfuric acid using clay/acid ratio of 1:50	
GRS 0.1	79.00 ± 0.07
GRS 0.3	81.41 ± 0.03
GRS 0.5	79.07 ± 0.06
GRS 0.7	78.56 ± 0.08
GRS 1	78.00 ± 0.12
GRS 1.3	73.00 ± 0.05
GRS 1.5	72.96 ± 0.04
GRS 2	66.86 ± 0.05
Samples heated at 80˚C, ground, and refluxed with 2 M sulfuric acid using different clay/acid ratio	
2GRS 1:2	66.97 ± 0.14
2GRS 1:4	73.43 ± 0.26
2GRS 1:6	71.78 ± 0.26
2GRS 1:8	71.68 ± 0.39
2GRS 1:50	66.86 ± 0.05
Samples heated at 80˚C, ground, and refluxed with 4 M sulfuric acid using different clay/acid ratio	
4GRS 1:2	74.24 ± 0.07
4GRS 1:4	61.07 ± 0.07

Table 4.13 Bleaching capacities of ground kaolin (GK sample), activated samples (GRH samples) and commercial bleaching clay

Sample (2% w/w)	Bleaching capacity (%)
GK	49.77 ± 0.12
Commercial bleaching clay	81.82 ± 0.02
Samples heated at 80˚C, ground, and refluxed with different concentrations of hydrochloric acid using clay/acid ratio of 1:50	
GRH 0.1	70.57 ± 0.06
GRH 0.3	78.71 ± 0.05
GRH 0.5	83.26 ± 0.14
GRH 0.7	82.64 ± 0.05
GRH 1	81.74 ± 0.01
GRH 1.3	78.67 ± 0.07
GRH 2	77.72 ± 0.02
Samples heated at 80˚C, ground, and refluxed with 0.5 M hydrochloric acid using different clay/acid ratio	
0.5GRH 1:2	45.02 ± 0.05
0.5GRH 1:4	51.55 ± 0.05
0.5GRH 1:40	75.70 ± 0.05
0.5GRH 1:50	83.26 ± 0.05
0.5GRH 1:60	80.54 ± 0.03
Samples heated at 80˚C, ground, and refluxed with 2 M hydrochloric acid using different clay/acid ratio	
2GRH 1:12	79.56 ± 0.17
2GRH 1:50	77.72 ± 0.02
Samples heated at 80˚C, ground, and refluxed with 4 M hydrochloric acid using different clay/acid ratio	
4GRH 1:2	74.27 ± 0.17
4GRH 1:4	74.60 ± 0.03
4GRH 1:6	74.45 ± 0.07
4GRH 1:7	70.16 ± 0.05
Samples heated at 80˚C, ground, and refluxed with different hydrochloric acid using different clay/acid ratio	
0.5GRH 1:50	83.26 ± 0.05
2GRH 1:12	79.56 ± 0.17
4GRH 1:6	74.45 ± 0.07

[*] 0.5GRH 1:50 = Samples ground and heated at 80˚C prior to reflux with 0.5M hydrochloric acid with clay/acid ratio of 1:50; 2GRH 1:12 = Samples ground and heated at 80˚C prior to reflux with 2 M hydrochloric acid with clay/acid ratio of 1:12; 4GRH 1:6 = Samples ground and heated at 80˚C prior to reflux with 4M hydrochloric acid with clay/acid ratio of 1:6.

Table 4.14 Bleaching capacities of ground kaolin (GK), activated samples (GRC samples) and commercial bleaching clay

Sample (2% w/w)	Bleaching capacity (%)
GK	49.77 ± 0.12
Commercial bleaching clay	82.37 ± 0.05
Samples heated at 80˚C, ground, and refluxed with different concentrations of citric acid using clay/acid ratio of 1:50	
GRC 0.1	70.65 ± 0.06
GRC 0.3	80.39 ± 0.02
GRC 0.5	81.11 ± 0.01
GRC 0.7	80.61 ± 0.04
GRC 1	80.41 ± 0.05
GRC 1.3	77.08 ± 0.22
GRC 2	75.00 ± 0.05

Table 4.15 Bleaching capacities of ground kaolin (GK), activated samples (GRO samples) and commercial bleaching clay

Sample (2% w/w)	Bleaching capacity (%)
GK	49.77 ± 0.12
Commercial bleaching clay	84.09 ± 0.01
Samples heated at 80˚C, ground, and refluxed with different concentrations of oxalic acid using clay/acid ratio of 1:50	
GRO 0.01	63.17 ± 0.13
GRO 0.03	69.77 ± 0.02
GRO 0.05	75.42 ± 0.06
GRO 0.1	75.50 ± 0.03
GRO 0.3	72.76 ± 0.09
GRO 0.5	45.37 ± 0.09
GRO 1	43.08 ± 0.03
Samples heated at 80˚C, ground, and refluxed with 0.1 M oxalic acid using different clay/acid ratio	
0.1GRO 1:40	75.44 ± 0.07
0.1GRO 1:50	75.50 ± 0.03
0.1GRO 1:60	78.87 ± 0.1
0.1GRO 1:80	79.06 ± 0.1
0.1GRO 1:100	77.40 ± 0.2

1. X-ray Diffraction (XRD) analysis

Activated kaolins which are ground and reflux with different acid such as sulphuric acid, hydrochloric acid, citric acid and oxalic acid are studied their crystrallinites by XRD analysis. Figure 4.15A shows the effect of different sulfuric acid concentration such as 0.3 M, 1 M and 2 M with the clay to acid ratio of 1:50 on Kaolin. There are no significant structural changes when the GK sample is dried at 80˚C prior to reflux with a 0.3 M sulfuric acid solution. The non-clay mineral quartz is resistant to acid treatment whereas the kaolinite structure is only partially preserved when sulfuric acid concentrations of 1 or 2 M are used. These results are same as the report of Noyan et.al, 2007 who found that sulphuric acid treatment has the effect on smectite groups but not on non-clay minerals. The relative proportions of kaolinite in GRS samples dried at 80˚C prior to reflux with different sulfuric acid concentrations also exhibit the same trend as the 100GRS samples (see Figures 4.16A and 4.11B). The relative proportions of kaolinite decrease to 83% and 60% when 0.3 and 2 M sulfuric acid are used, respectively (for GRS 0.3 and GRS 2). The relative proportions of kaolinite are calculated based on 100% kaolinite in the ground sample prior to any thermal or acidic treatment. The proportions are calculated based on the intensity values recorded using XRD for the d_{001} reflection of kaolinite. The 100GR 0.3 and 100GR 2 samples have approximately the same relative proportions of kaolinite as the GRS 0.3 and GRS 2 samples, respectively. Thus, the preheating of GK at 100˚C does not affect the relative proportion of kaolinite in the samples. The crystal structures of ground kaolins refluxed with 2M sulphuric acid; different clay/acid ratio such as 1:4 (10g of clay/40ml of acid), 1:8 (10g of clay/80ml of acid) and 1:50 (10g of clay/ 500ml of acid) are illustrated in Figure 4.15B. The crystallinities of these samples are quite similar and different clay/acid ratio has little effect on kaolinite structure. The relative proportions of kaolinites in 2GRS 1:4 samples decrease from 65% to 60% in 2GRS 1:50 sample.

These results are supported by the XRD patterns of activated kaolin treated with hydrochloric acid, citric acid and oxalic acid as shown in Figure 4.17, Figure 4.19 and Figure 4.21, respectively. The intensities of kaolinite in activated kaolins slightly reduce when the samples are treated up to 0.7 M hydrochloric acid (clay/acid ratio of 1:50) whereas those of GRC 0.5 and GRO 0.1 are similar as that of GK when the initial GK are treated with 0.5 M citric acid and 0.1 M oxalic acid, respectively (see Figures 4.17A, 4.19 and 4.21A). The relative proportions of kaolinites are ~90%, ~96% and ~95% for GRH 0.7, GRC 0.5 and GRO 0.1, respectively as seen in Figure 4.18A, Figure 4.20 and Figure 4.22A, respectively. The intensities of kaolinite are decreased to 71% when the GK is treated with 2 M hydrochloric acid. Kaolinite intensities are slightly decreased when the GK is treated with high acid concentration of 1.3 M or 2 M citric acid. The kaolinite proportions decrease to ~94% in GRC 2. Oxalic acid (0.5 M), however, largely decreases the kaolinite intensity and the kaolinite proportion is ~53% for GRO 0.5 as compared with that of GK. Under using the same acid concentration of 2 M different acid such as sulfuric acid, hydrochloric acid and citric acid, the activated sample treated with citric acid (GRC 2) preserves the kaolinite's structure. Citric acid is weak acid and hence is far less effective at activation of the clays compared to HCl of the same concentration (Foo, et al., 2011).

Figure 4.17B shows the XRD patterns of GRH samples which are activated with 0.5 M hydrochloric acid using different clay/acid ratio. The crystallinities of kaolinites are slightly reduced with increasing clay/acid ratio. The relative proportions of kaolinite decrease to 90% in 0.5GRH 1:4 and 0.5GRH 1:50 samples while those decreased to ~84%

in 0.5GRH 1:60 (see Figure 4.18B). There are no significant changes in the activated samples (GRO samples) treated with 0.1 M oxalic acid using various clay/acid ratio up to 1:100 (see XRD patterns in Figure 4.21B). The relative proportions of kaolinite slightly decrease to ~96% in 0.1GRO 1:100 (Figure 4.22B).

For further studies of the effects of hydrochloric acid volume used on the kaolin's structural and sorption properties, ground kaolin GK is treated with same hydrochloric acid strength using different acid concentrations with different clay to acid ratios (2 M hydrochloric acid with clay to acid ratio of 1:12; 4 M hydrochloric acid with clay to acid ratio of 1:6). The XRD patterns of these samples called 2GRH 1:12, 4GRH 1:6 and 0.5GRH 1:50 are shown in Figure 4.17C. Although these samples are treated with the same acid concentration of the solutions, the intensities of kaolinite decrease with increasing acid concentration from 0.5 M to 4 M hydrochloric acid. The relative proportions of kaolinite decrease from ~90% to ~86% when the acid concentration used is increased from 0.5 M to 4 M hydrochloric acid (Figure 4.18C).

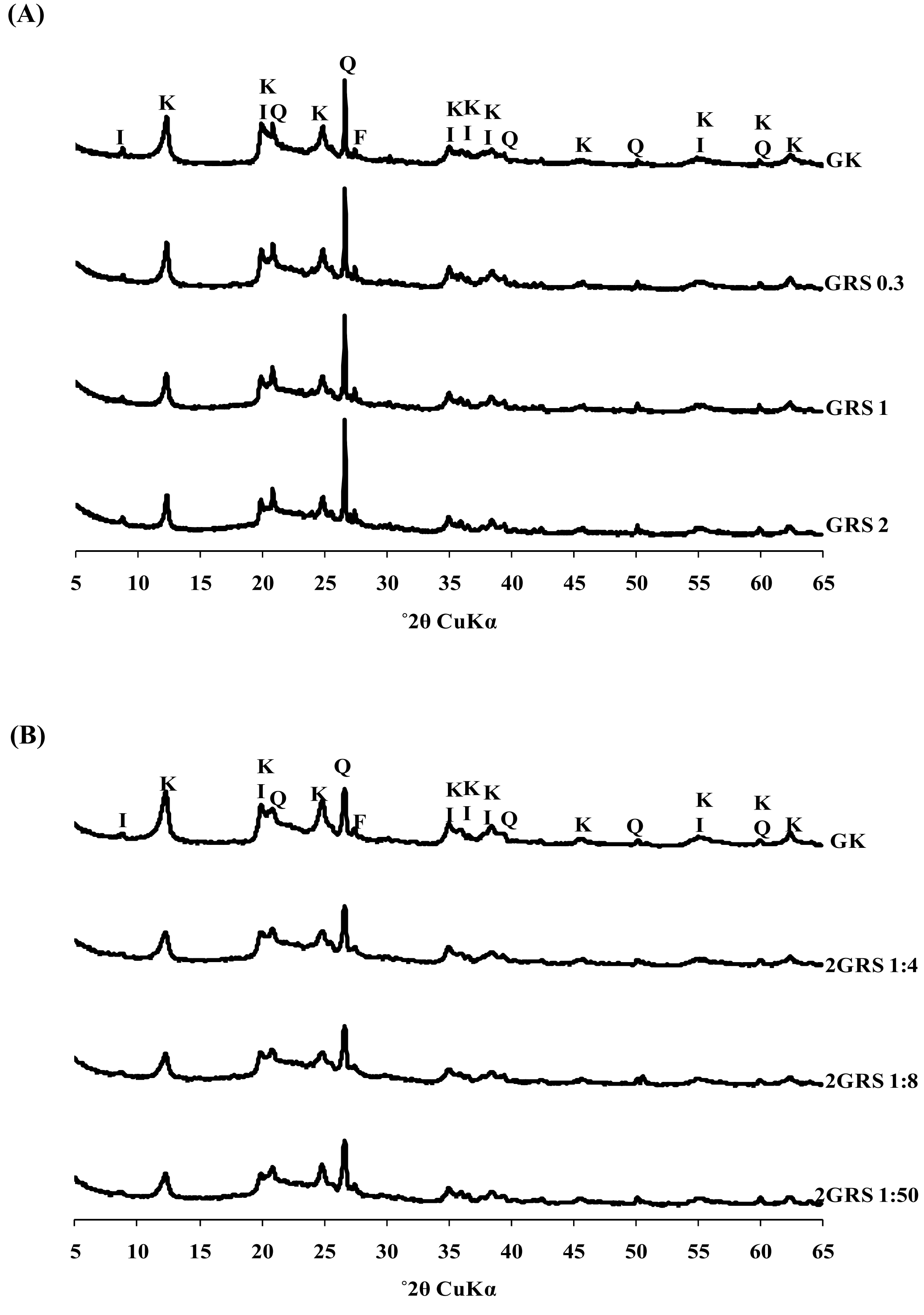

Figure 4.15 Comparison of the XRD patterns obtained from randomly orientated preparations of the GK and activated samples (GRS) dried at 80°C prior to reflux with different sulfuric acid concentration with clay/acid ratio of 1:50 (GRS 0.3 to GRS 2) (A), and ground kaolin (GK) and samples (GRS) dried at 80°C prior to reflux with 2 M sulfuric acid using different clay/acid ratio (2GRS 1:4 to 2GRS 1:50) (B).

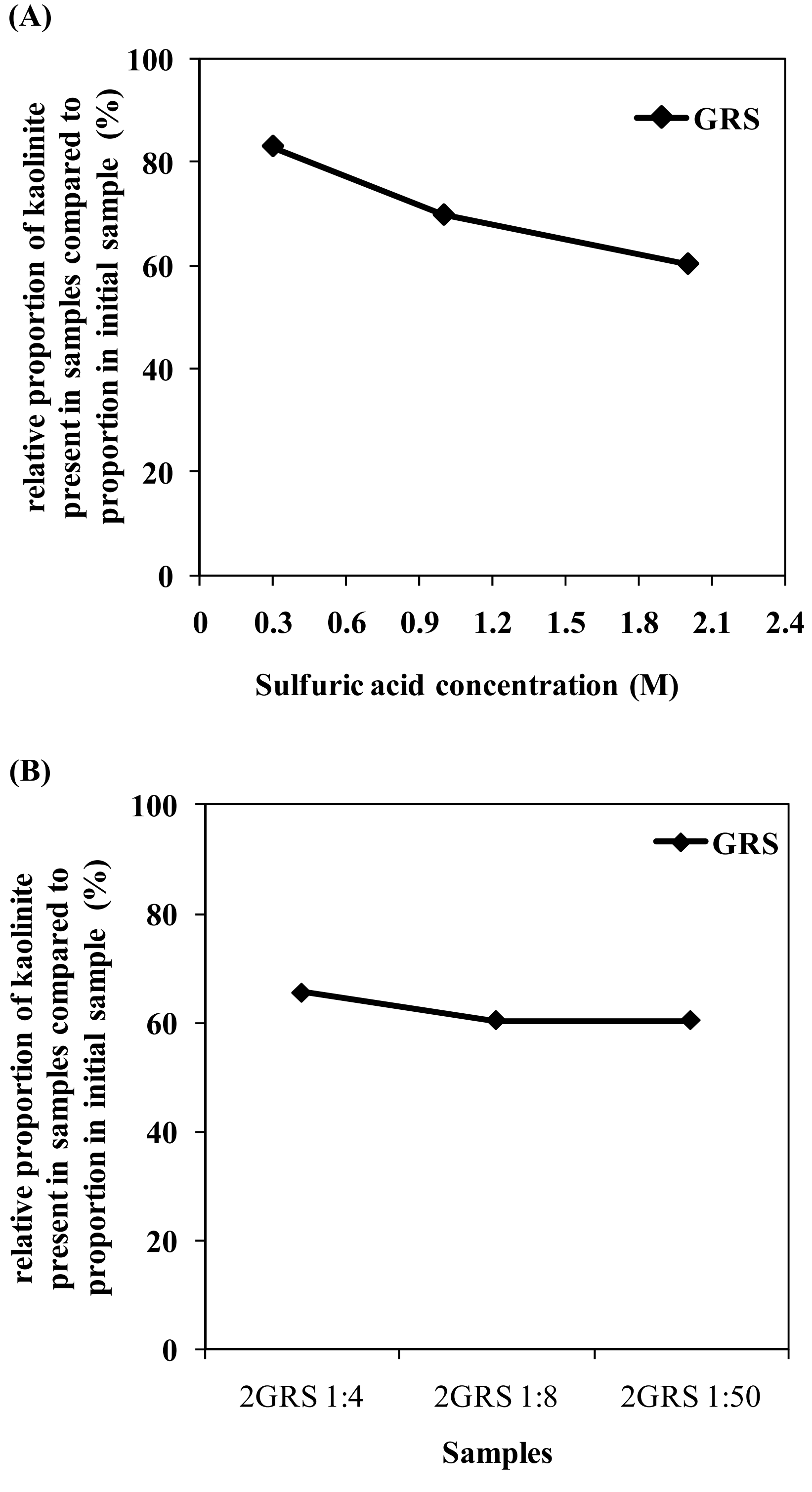

Figure 4.16 Relative proportion of kaolinite present in the activated kaolins (GRS) dried at 80˚C prior to reflux with different concentrations of sulfuric acid as a function of acid concentations equal to 0.3, 1, and 2 M (GRS 0.3 to GRS 2) (A), and in the samples dried at 80˚C prior to reflux with 2 M sulfuric acid as a function of the different clay to acid such as 1:4, 1:8 and 1:50 (2GRS 1:4 to 2GRS 1:50) (B).

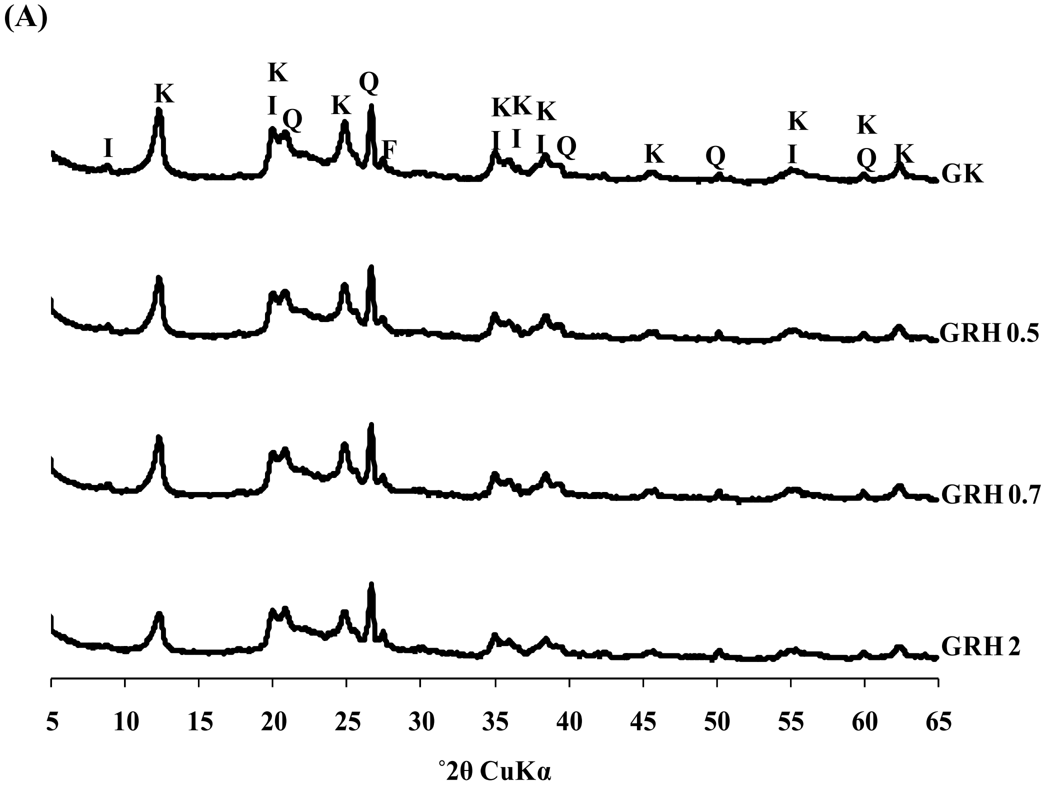
(A)
I
K
K
I
Q
K
Q
F
K
K
K
I
I
I
Q
K
Q
K
I
K
Q
K
GK
GRH 0.5
GRH 0.7
GRH 2
5
10
15
20
25
30
35
40
45
50
55
60
65
°2θ CuKα

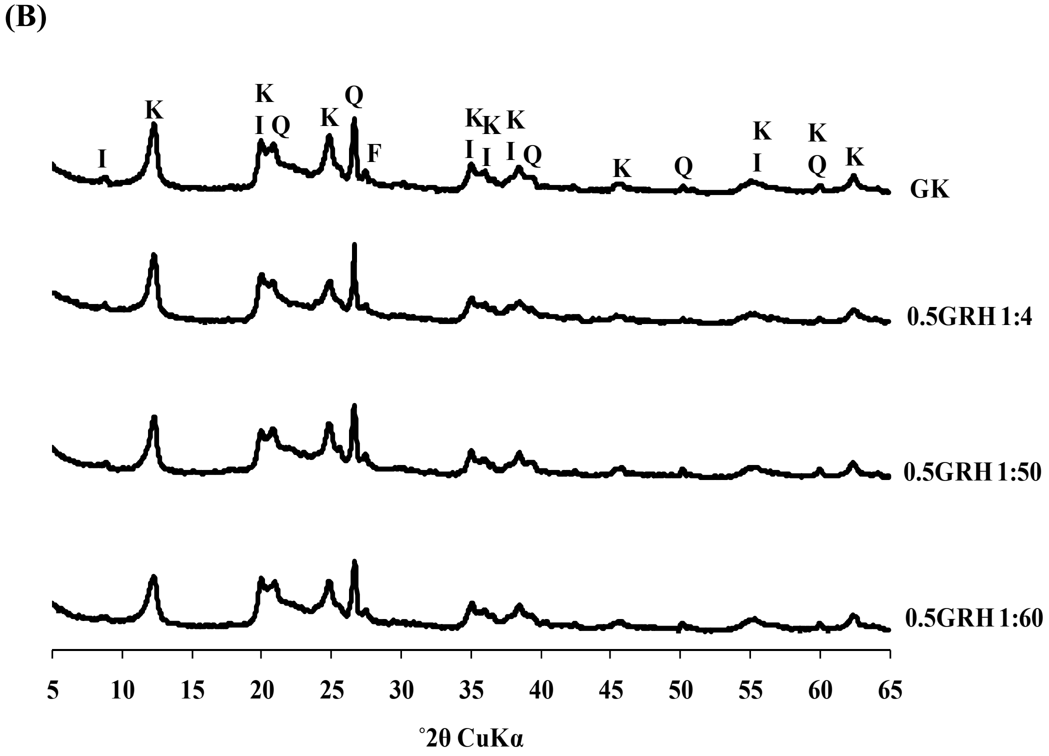
(B)
I
K
K
I
Q
K
Q
F
K
K
K
I
I
I
Q
K
Q
K
I
K
Q
K
GK
0.5GRH 1:4
0.5GRH 1:50
0.5GRH 1:60
5
10
15
20
25
30
35
40
45
50
55
60
65
°2θ CuKα

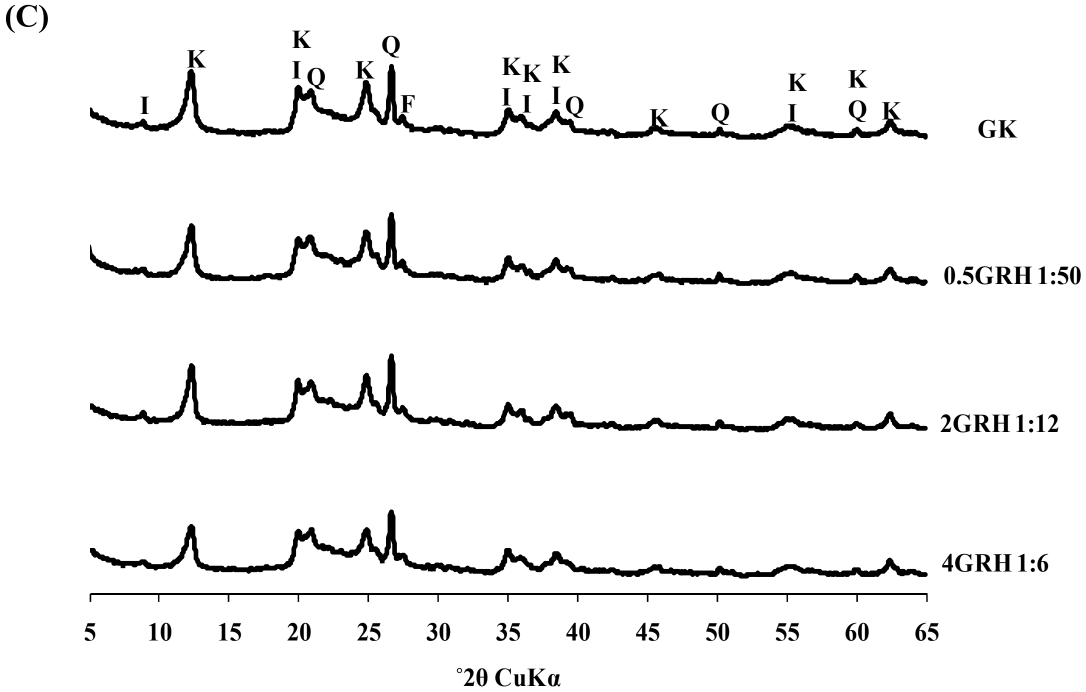

Figure 4.17 Comparison of the XRD patterns obtained from randomly orientated preparations of the GK and activated samples (GRH) dried at 80°C prior to reflux with different hydrochloric acid concentration with clay/acid ratio of 1:50 (GRH 0.5 to GRH 2) (A); ground kaolin (GK) and samples (GRH) dried at 80°C prior to reflux with 0.5 M hydrochloric acid using different clay/acid ratio (0.5GRH 1:4 to 0.5GRH 1:60) (B), and ground kaolin (GK) and samples (GRH) dried at 80°C prior to reflux with different hydrochloric acid concentration using different clay/acid ratio (0.5GRH 1:50, 2GRH 1:12 and 4GRH 1:6) (C).

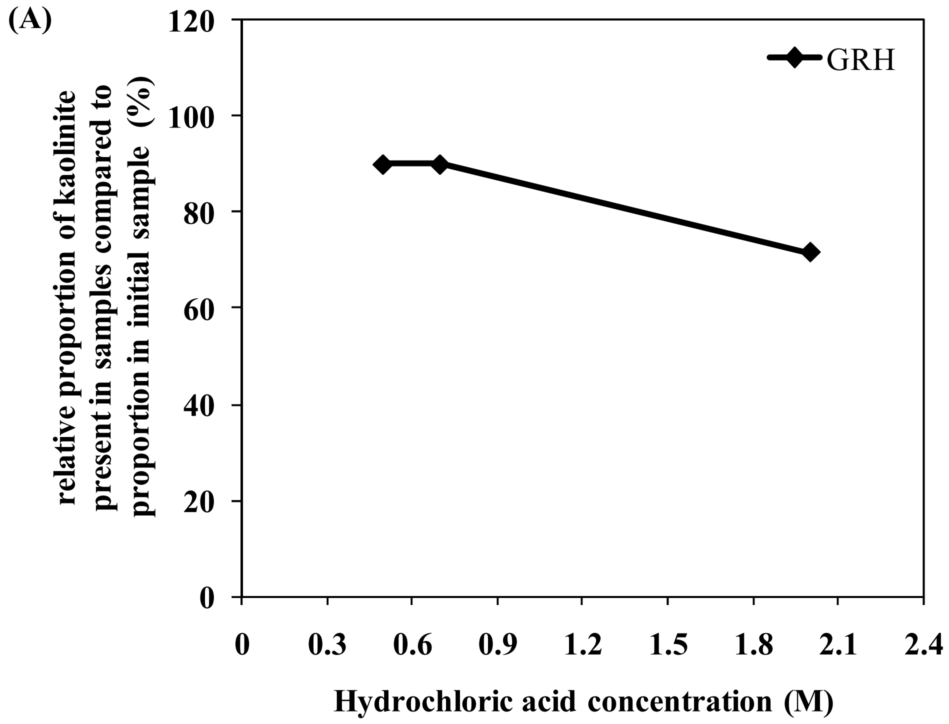
(A)
GRH
relative proportion of kaolinite present in samples compared to proportion in initial sample (%)
120
100
80
60
40
20
0
0
0.3
0.6
0.9
1.2
1.5
1.8
2.1
2.4
Hydrochloric acid concentration (M)

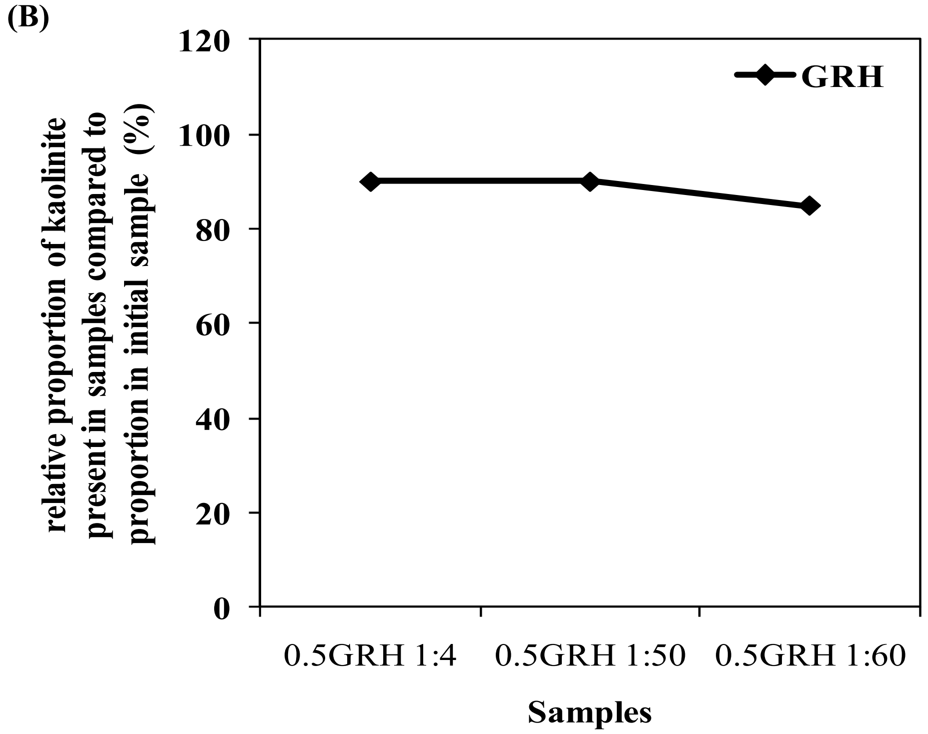
(B)
GRH
relative proportion of kaolinite present in samples compared to proportion in initial sample (%)
120
100
80
60
40
20
0
0.5GRH 1:4
0.5GRH 1:50
0.5GRH 1:60
Samples

(C)

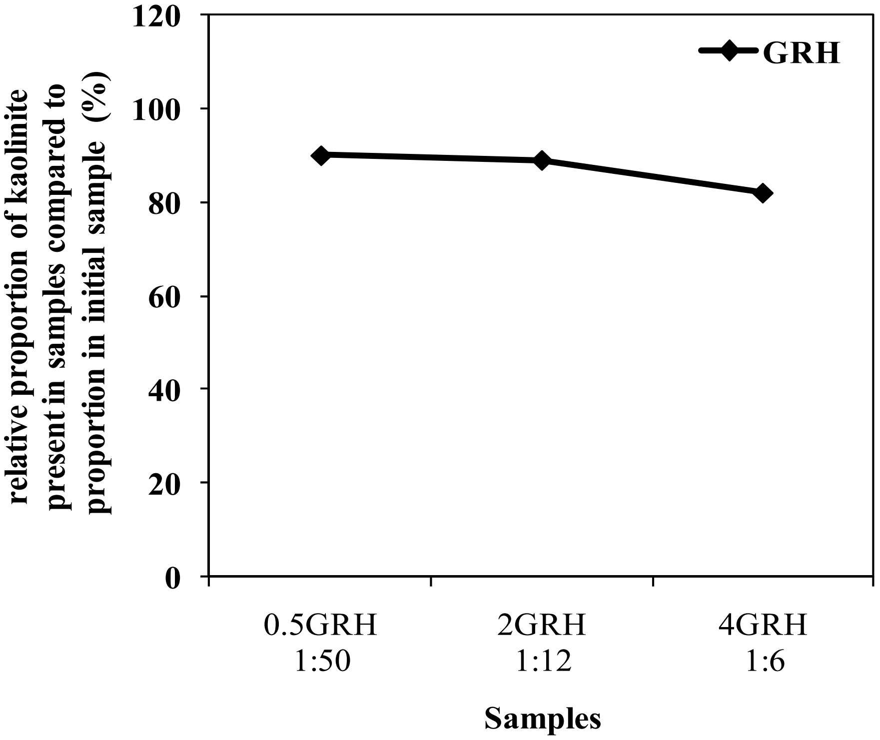

Figure 4.18 Relative proportion of kaolinite present in the activated kaolins (GRH) dried at 80˚C prior to reflux with different concentrations of hydrochloric acid as a function of acid concentations equal to 0.5, 0.7, and 2 M (GRH 0.5 to GRH 2) (A); in the samples dried at 80˚C prior to reflux with 0.5 M hydrochloric acid as a function of the different clay to acid such as 1:4, 1:50 and 1:60 (0.5GRH 1:4 to 0.5GRH 1:60) (B); and in the samples (GRH) dried at 80˚C prior to reflux with different hydrochloric acid concentration using different clay/acid ratio (0.5GRH 1:50, 2GRH 1:12 and 4GRH 1:6) (C).

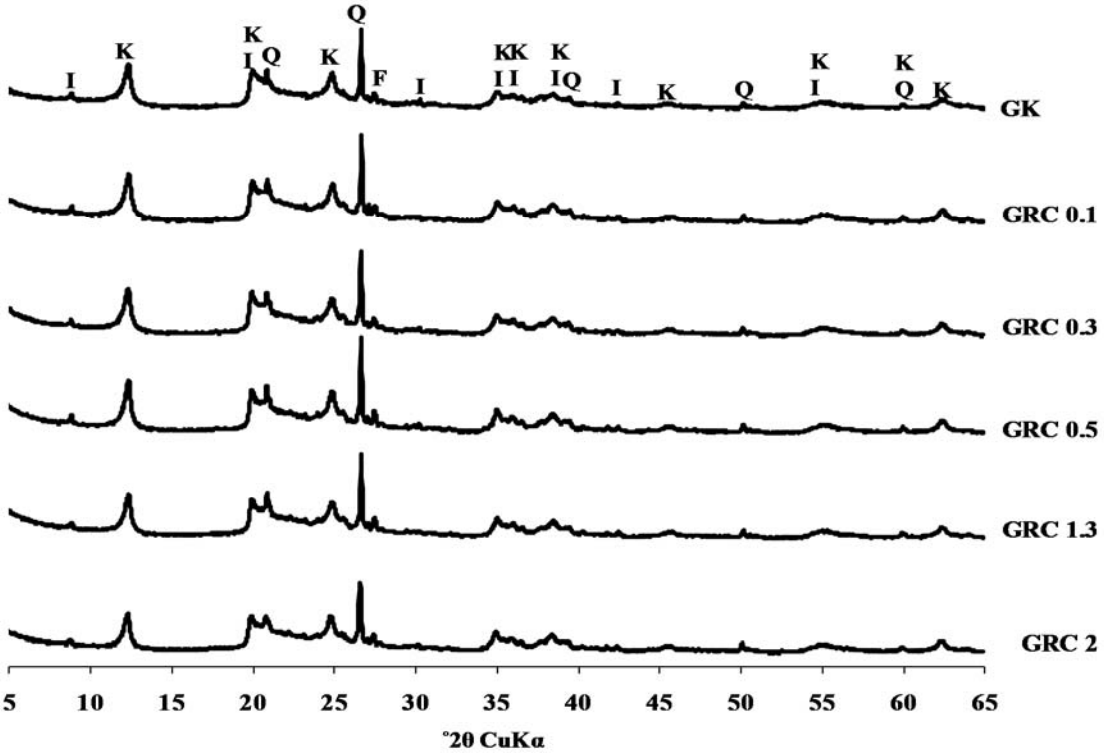

Figure 4.19 Comparison of the XRD patterns obtained from randomly orientated preparations of the GK and activated samples (GRC) dried at 80°C prior to reflux with different citric acid concentration with clay/acid ratio of 1:50 (GRC 0.1 to GRC 2)

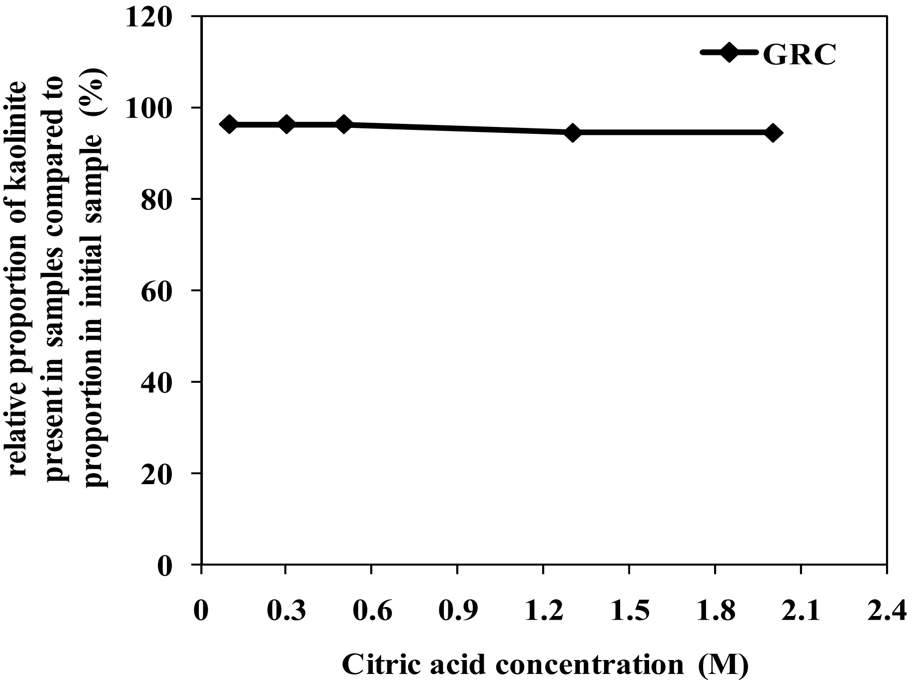

Figure 4.20 Relative proportion of kaolinite present in the activated kaolins (GRC) dried at 80°C prior to reflux with different concentrations of citric acid as a function of acid concentations equal to 0.1, 0.3, 0.5, 1.3, and 2 M (GRC 0.1 to GRC 2).

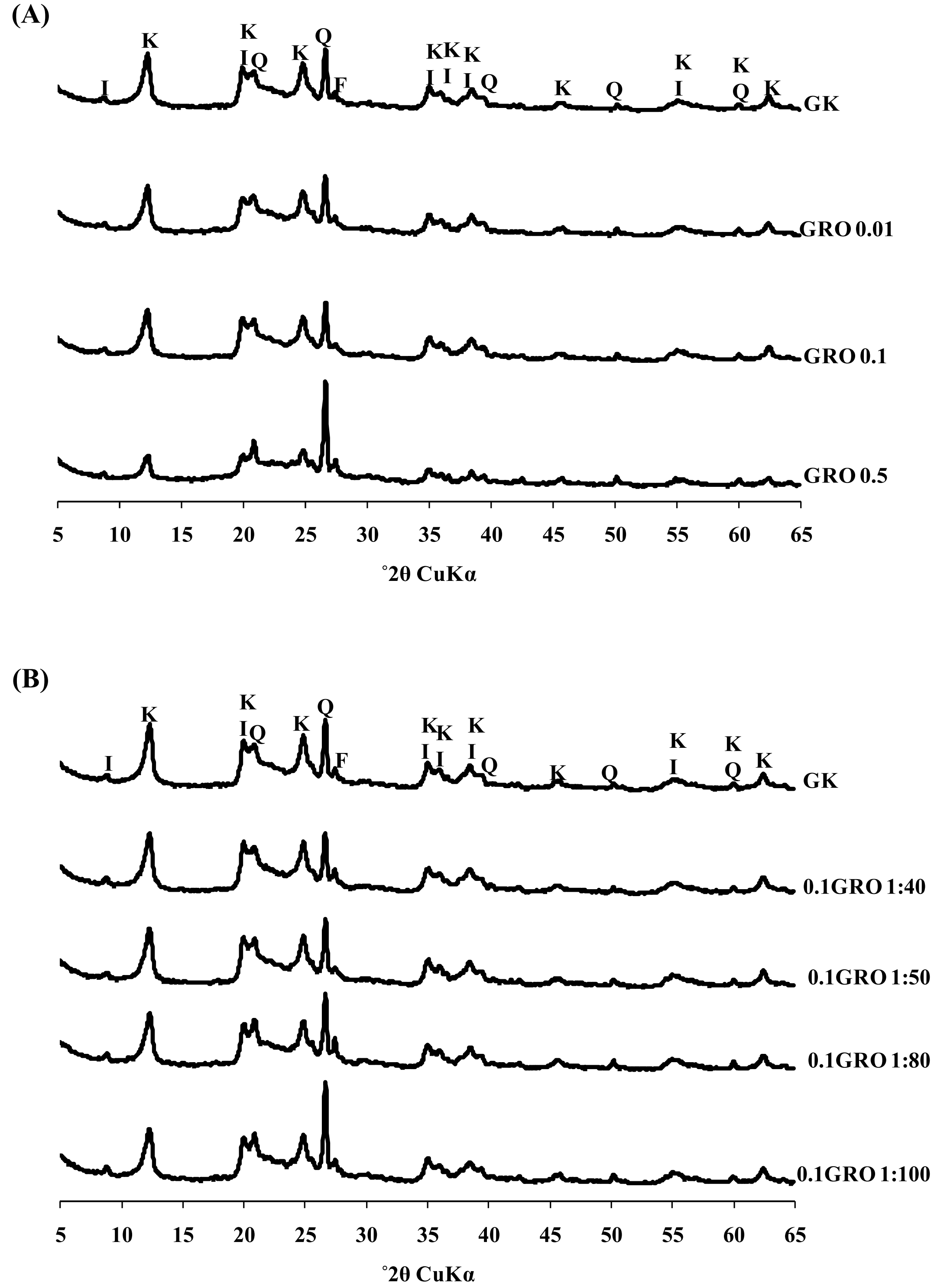

Figure 4.21 Comparison of the XRD patterns obtained from randomly orientated preparations of the GK and activated samples (GRO) dried at 80°C prior to reflux with different oxalic acid concentration with clay/acid ratio of 1:50 (GRO 0.01 to GRO 0.5) (A), and ground kaolin (GK) and samples (GRO) dried at 80°C prior to reflux with 0.1 M oxalic acid using different clay/acid ratio (0.1GRO 1:40 to 0.1GRO 1:100) (B).

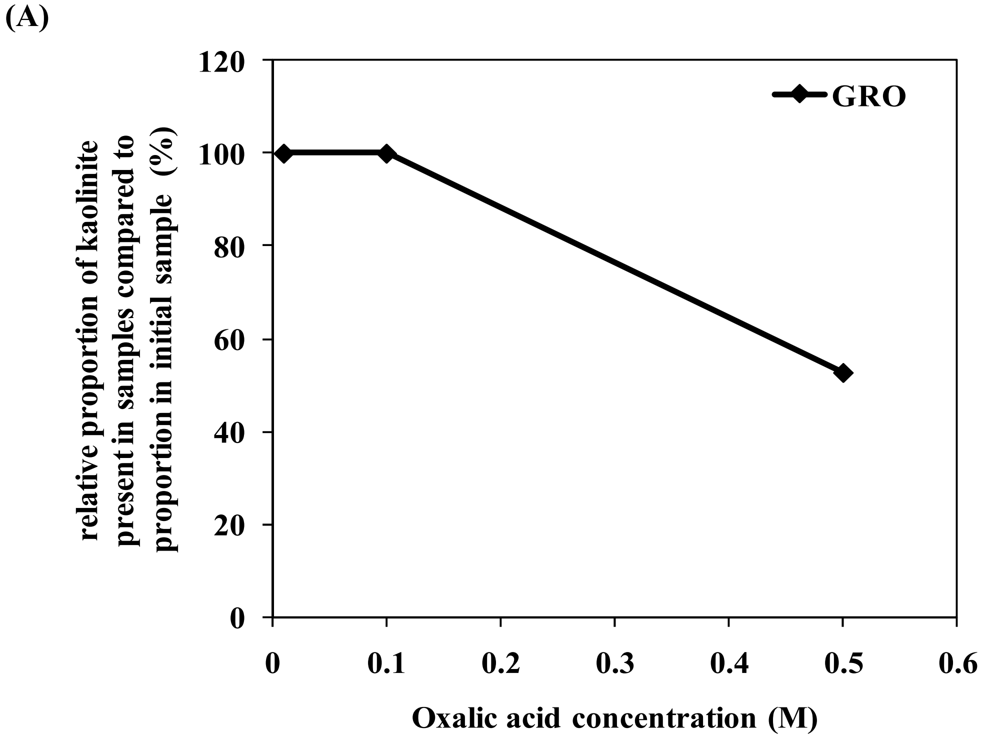

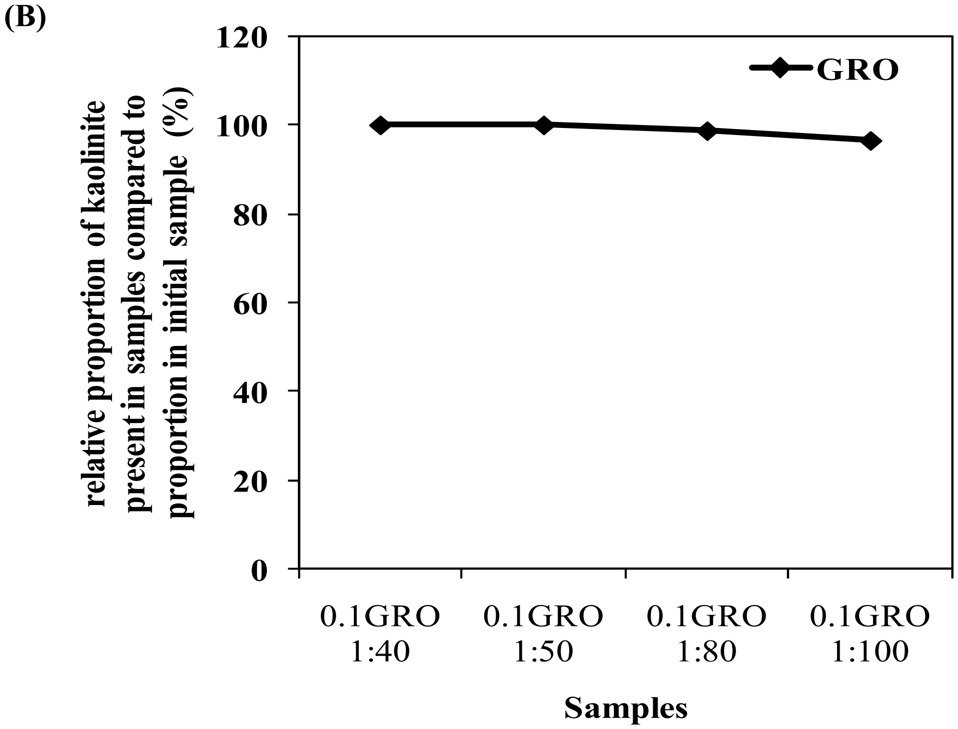

Figure 4.22 Relative proportion of kaolinite present in the activated kaolins (GRO) dried at 80˚C prior to reflux with different concentrations of oxalic acid as a function of acid concentations equal to 0.01, 0.1, and 0.5 M (GRO 0.01 to GRO 0.5) (A), and in the samples dried at 80˚C prior to reflux with 0.1 M oxalic acid as a function of the different clay to acid such as 1:4, 1:50, 1:80 and 1:100 (0.1GRO 1:4 to 0.1GRO 1:100) (B).

2. X-ray Fluorescence Spectra (XRF) analysis

The chemical compositions of the activated samples (GRS, GRH, GRC and GRO) are reported in Table 4.16. The SiO_2 content increased with increasing acid concentration or increasing clay/acid ratio. When the GK sample is treated with a 2 M sulfuric acid, using clay/acid ratio of 1:50 (GRS 2)), the SiO_2 contents increase dramatically from ~54% to ~81%. in agreement with the increased in the proportion of an amorphous phase rich in Si detected by FTIR for these samples (Figure 4.27A). In parallel, the Al_2O_3 contents decrease from ~42 to ~16% for GRS 2. while other metal oxides, expressed as K_2O, Fe_2O, CuO, and MnO, are leached from the samples. When the GK sample is treated with a 0.5 M hydrochloric acid, the SiO_2 contents increase from ~54% to ~64%. Further increasing the acid concentration to 2 M hydrochloric acid increases the silica contents to ~73% in the GRH 2 sample. In parallel, the Al_2O_3 contents decrease from ~42% to ~32% for GRH 0.5 and ~24% for GRH 2. Citric acid treatment also shows the same trend as using hydrochloric acid. The SiO_2 contents slightly increase to ~58% in GRC 0.1 and dramatically increases to ~70% in GRC 2, indicating there is a formation of an amorphous silica phase that is detected by FTIR for these samples (see Figure 4.27C). The Al_2O_3 contents decrease to ~37% in GRC 0.1 and ~27% in GRC 2. After acid treatment on GK, the Al:Si ratio decreases from ~0.9 to ~0.4 in GRS 0.3, ~0.6 in both GRH 0.5 and GRC 0.5 samples whereas further increased in acid concentrations decreases to ~0.2, ~0.4 and ~0.4 in GRS 2, GRH 2 and GRC 2, respectively. Low concentration of oxalic acid extensively leaches alumina from the activated kaolin as compared with other acids such as sulfuric acid, hydrochloric acid and citric acid. GK sample activated with 0.5 M oxalic extensively leaches alumina from ~41% to ~18% and consequently, enhances silica formation (~79%) in GRO 0.5. The Al/Si ratio is decreased from ~0.9 to ~0.3 in GRO 0.5. In accordance with the other authors (Worasith et al., 2011b; Tang et al., 2010), acid leaching of ground kaolin enhances the alumina dissolution from the activated samples. This study also found that leaching the alumina content from the kaolin affects the kaolin's structure and, consequently, decreases the relative proportions of kaolinite in the activated samples (see Table 4.16, and Figures 4.23 to Figure 4.26).

Increasing the clay/acid ratio also has the effects on the formation of silica in activated products. For GRS samples, the silica contents of 2GRS 1:50 are slightly increased from 75% to 81% as compared with that of 2GRS 1:4. Other activated samples (GRH and GRO samples) treated with different clay/acid ratio also show the same trend as GRS samples. For example, the silica is increased from ~54% to ~65% in 0.5GRH 1:60 when the clay/acid ratio is increased from 1:4 to 1:60. The silica content of 0.1GRO 1:40 is ~62 while that of 0.1GRO 1:100 is ~66. Consequently, Al/Si ratios of activated samples are a little decreased upon the effect of different clay/acid ratio. The Al/Si ratios of ~0.3 in 2GRS 1:4, ~0.8 in 0.5GRH 1:4 and ~0.6 in 0.1GRO 1:40 decrease to ~0.2, ~0.5 and ~0.5 in 2GRS 1:50, 0.5GRH 1:60 and 2GRO 1:100 samples, respectively. The results of activated samples treated with same acid concentrations (for 0.5GRH 1:50, 2GRH 1:12 and 4GRH 1:6) shows that GK activated with 4 M hydrochloric acid concentration (for 4GRH 1:6) enhances the alumina leaching from sample than the GK activated with 0.5 M acid concentration (for 0.5GRH 1:50) i.e., Al/Si ratio of 4GRH 1:6 was ~3 while that of 0.5GRH 1:50 was 0.6. When the GK is treated with high acid concentrations or high clay/acid ratios, large amount of alumina is leached from the samples resulting in the decreased in relative proportions of kaolinite in the activated samples (see Figure 4.23 to Figure 4.26).

Table 4.16 Chemical compositions of the ground kaolin (GK) and activated kaolins (GRS, GRH, GRC and GRO samples)

	SiO_2 %	Al_2O_3 %	K_2O %	Fe_2O_3 %	CaO %	CuO %	TiO_2 %	MnO %	Al:Si
GK	54.10	42.00	2.07	1.03	0.04	0.06	0.05	0.07	0.88
Samples ground and heated at 80˚C prior to reflux with different concentrations of sulfuric acid equal to 0.3, 1, and 2 M using clay/acid ratio of 1:50									
GRS 0. 3	68.00	28.30	2.04	0.72	0.06	0.05	0.05	0.05	0.47
GRS 1	74.50	22.20	2.00	0.55	0.00	0.05	0.00	0.04	0.34
GRS 2	80.70	16.20	1.84	0.54	0.09	0.05	0.05	0.04	0.23
Samples ground and heated at 80˚C prior to reflux with 2M sulphuric acid with different clay/acid ratio of 1:4, 1:8 and 1:50									
2GRS 1:4	75.20	21.30	2.07	0.65	0.00	0.05	0.00	0.05	0.32
2GRS 1:8	77.33	19.30	1.98	0.62	0.00	0.05	0.07	0.04	0.28
2GRS 1:50	80.70	16.20	1.84	0.54	0.09	0.05	0.06	0.04	0.23
Samples ground and heated at 80˚C prior to reflux with different concentrations of hydrochloric acid equal to 0.5, 0.7, and 2 M using clay/acid ratio of 1:50									
GRH 0.5	64.40	32.10	2.02	0.78	0.00	0.05	0.05	0.05	0.57
GRH 0.7	65.10	31.20	2.07	0.76	0.02	0.05	0.07	0.05	0.54
GRH 2	72.70	24.40	1.94	0.52	0.00	0.01	0.04	0.04	0.38
Samples ground and heated at 80˚C prior to reflux with 0.5M hydrochloric acid with different clay/acid ratio of 1:4, 1:50 and 1:60									
0.5GRH 1:4	54.80	39.60	1.94	0.89	0.01	0.01	0.03	0.05	0.82
0.5GRH 1:50	64.40	32.10	2.02	0.78	0.00	0.05	0.05	0.05	0.57
0.5GRH 1:60	65.00	31.70	2.00	0.69	0.00	0.01	0.05	0.05	0.55
Samples ground and heated at 80˚C prior to reflux with different hydrochloric acid concentrations with different clay/acid ratio									
*0.5GRH 1:50	64.40	32.10	2.02	0.78	0.00	0.05	0.05	0.05	0.57
*2GRH 1:12	72.20	24.80	1.98	0.53	0.00	0.05	0.06	0.04	0.39
*4GRH 1:6	76.30	20.90	1.85	0.49	0.00	0.04	0.05	0.04	0.31
Samples ground and heated at 80˚C prior to reflux with different concentrations of citric acid equal to 0.1, 0.3, 0.5, 1.3 and 2 M using clay/acid ratio of 1:50									
GRC 0.1	58.27	37.30	1.81	0.82	0.16	0.00	0.05	0.05	0.73
GRC 0.3	62.30	34.20	2.05	0.85	0.00	0.05	0.05	0.06	0.62
GRC 0.5	62.40	34.20	2.07	0.86	0.00	0.05	0.05	0.05	0.62
GRC 1.3	67.40	29.50	1.92	0.77	0.00	0.05	0.05	0.05	0.50
GRC 2	69.93	26.77	1.49	0.67	0.12	0.01	0.03	0.04	0.43

Table 4.16 Cont.

	SiO_2 %	Al_2O_3 %	K_2O %	Fe_2O_3 %	CaO %	CuO %	TiO_2 %	MnO %	Al:Si
Samples ground and heated at 80˚C prior to reflux with different concentrations of oxalic acid equal to 0.01, 0.1, and 0.5 M using clay/acid ratio of 1:50									
GRO 0.01	53.90	41.40	1.88	0.89	0.04	0.01	0.04	0.05	0.87
GRO 0.1	64.50	32.30	2.11	0.65	0.01	0.01	0.04	0.05	0.57
GRO 0.5	79.00	17.70	2.44	0.54	0.01	0.01	0.04	0.04	0.25
Samples ground and heated at 80˚C prior to reflux with 0.1M oxalic acid with different clay/acid ratio of 1:40, 1:50, 1:80 and 1:100									
0.1GRO 1:40	62.20	34.60	2.04	0.74	0.02	0.01	0.04	0.05	0.63
0.1GRO 1:50	64.50	32.30	2.11	0.65	0.01	0.01	0.04	0.05	0.57
0.1GRO 1:80	66.20	30.20	2.38	0.63	0.14	0.01	0.04	0.05	0.52
0.1GRO 1:100	67.40	29.40	2.25	0.60	0.04	0.01	0.05	0.05	0.49

[*] 0.5GRH 1:50 = Samples ground and heated at 80˚C prior to reflux with 0.5M hydrochloric acid with clay/acid ratio of 1:50; 2GRH 1:12 = Samples ground and heated at 80˚C prior to reflux with 2 M hydrochloric acid with clay/acid ratio of 1:12; 4GRH 1:6 = Samples ground and heated at 80˚C prior to reflux with 4M hydrochloric acid with clay/acid ratio of 1:6.

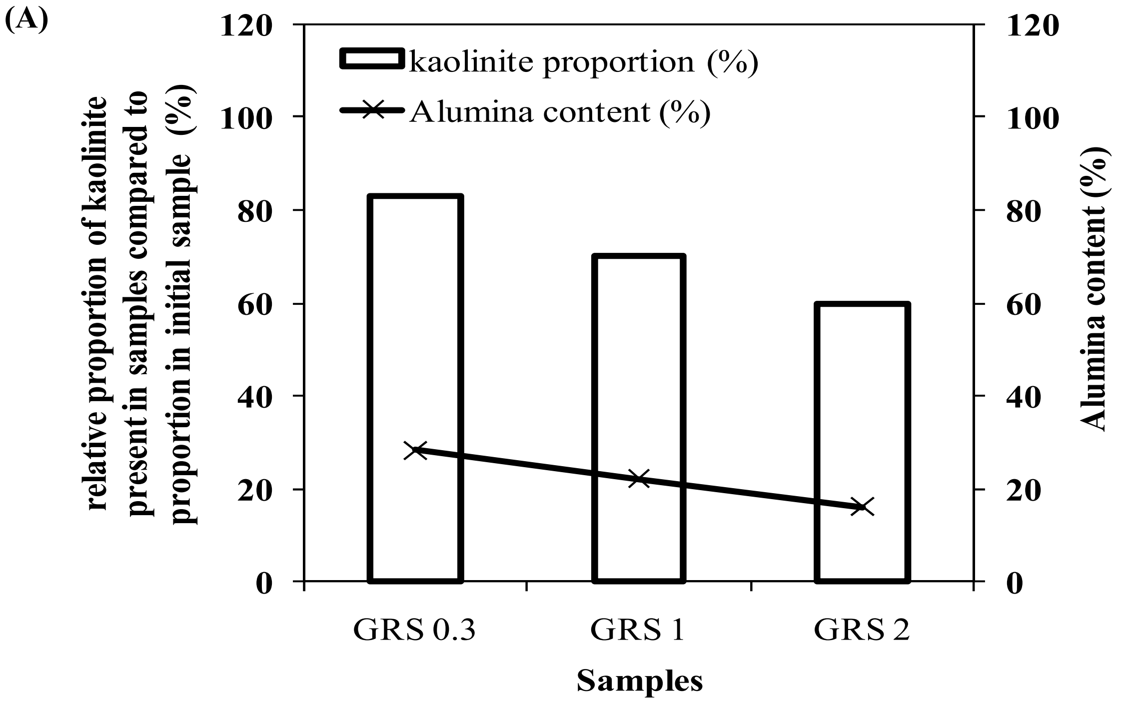

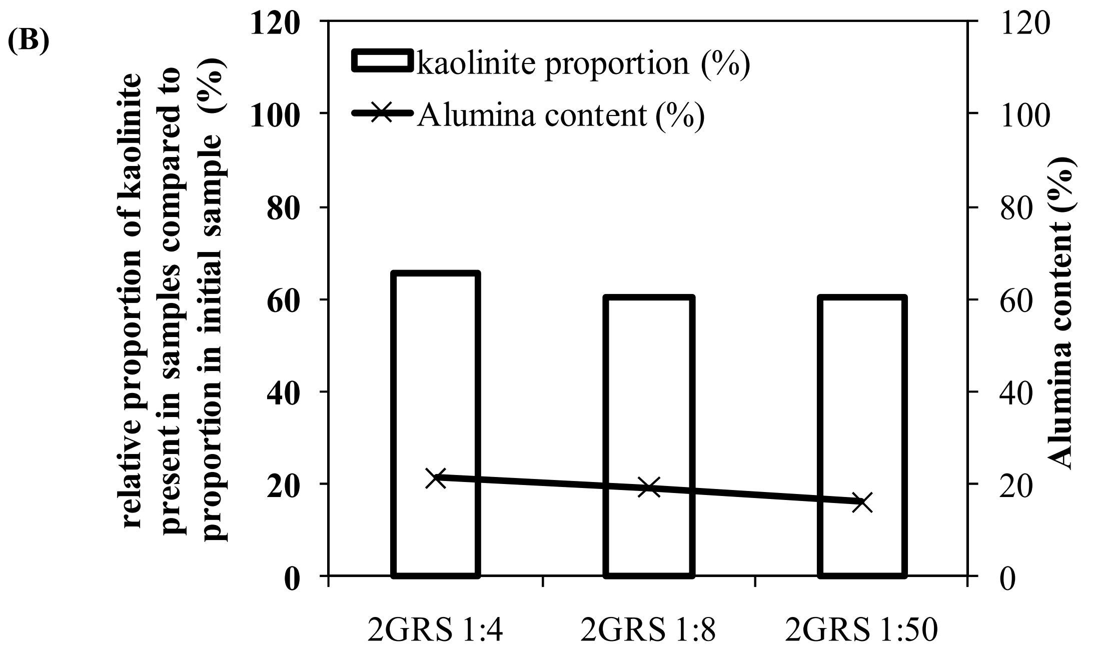

Figure 4.23 Comparison of relative proportion of kaolinite and alumina contents present in the activated kaolins (GRS) dried at 80˚C prior to reflux with different concentrations of sulfuric acid as a function of acid concentations equal to 0.3, 1, and 2 M (GRS 0.3 to GRS 2) (A), and in the samples dried at 80˚C prior to reflux with 2 M sulfuric acid as a function of the different clay to acid such as 1:4, 1:8 and 1:50 (2GRS 1:4 to 2GRS 1:50) (B).

(A)

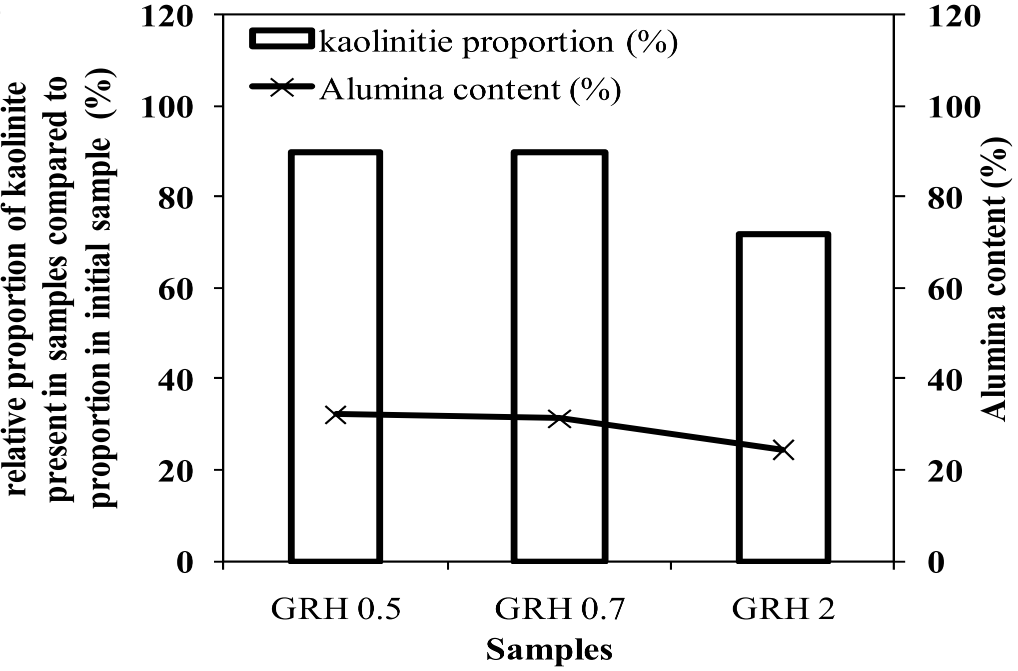
120
100
80
60
40
20
0
relative proportion of kaolinite present in samples compared to proportion in initial sample (%)
kaolinitie proportion (%)
Alumina content (%)
Alumina content (%)
GRH 0.5
GRH 0.7
GRH 2
Samples

(B)

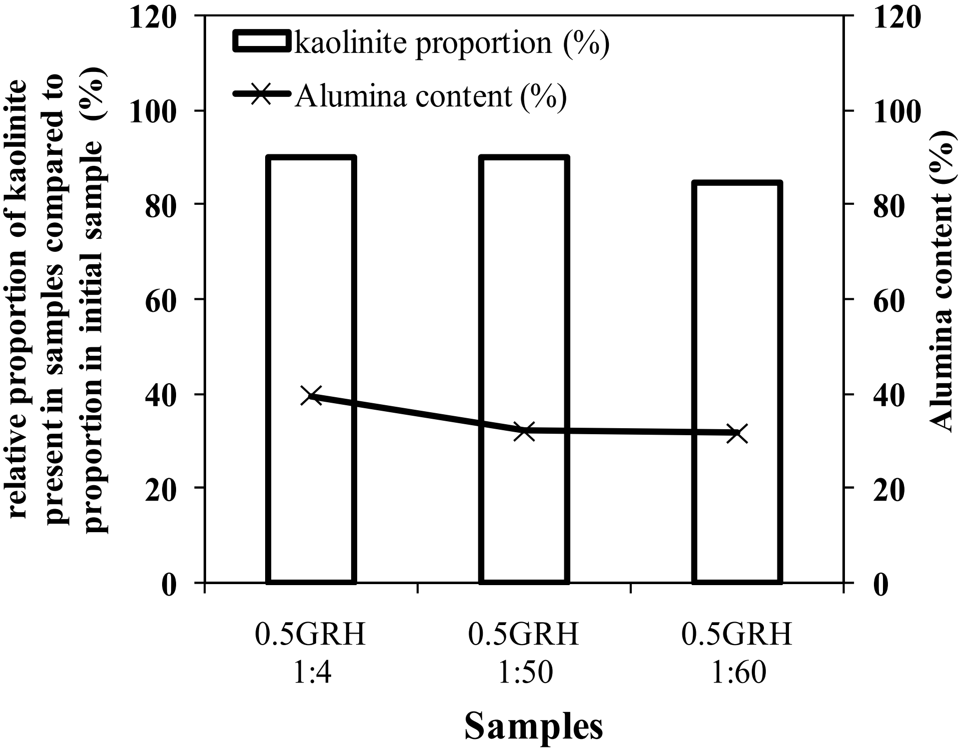
120
100
80
60
40
20
0
relative proportion of kaolinite present in samples compared to proportion in initial sample (%)
kaolinite proportion (%)
Alumina content (%)
Alumina content (%)
0.5GRH 1:4
0.5GRH 1:50
0.5GRH 1:60
Samples

(C)

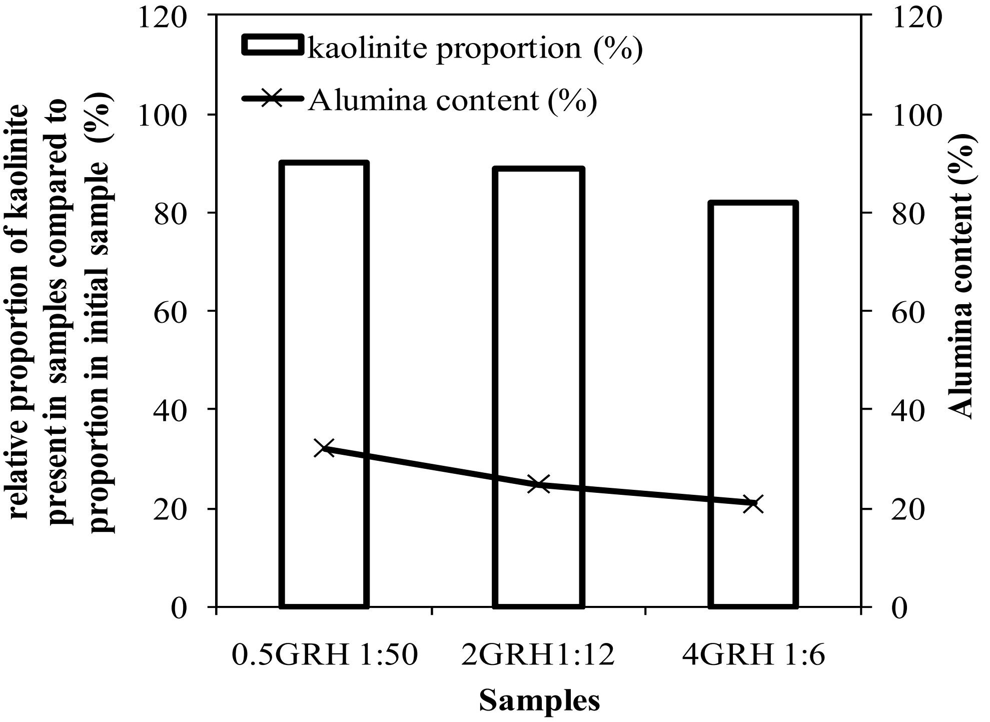

Figure 4.24 Comparison of relative proportion of kaolinite and alumina contents present in the activated kaolins (GRH) dried at 80˚C prior to reflux with different concentrations of hydrochloric acid as a function of acid concentations equal to 0.5, 0.7, and 2 M (GRH 0.5 to GRH 2) (A); in the samples dried at 80˚C prior to reflux with 0.5 M hydrochloric acid as a function of the different clay to acid such as 1:4, 1:50 and 1:60 (0.5GRH 1:4 to 0.5GRH 1:60) (B); and in the samples (GRH) dried at 80˚C prior to reflux with different hydrochloric acid concentration using different clay/acid ratio (0.5GRH 1:50, 2GRH 1:12 and 4GRH 1:6) (C).

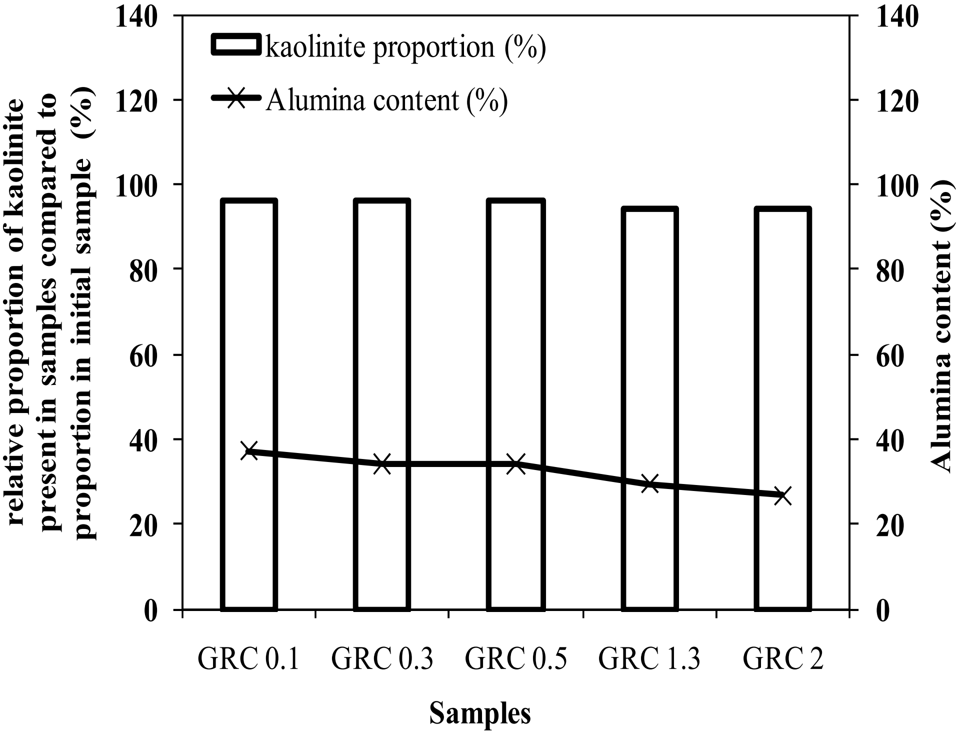

Figure 4.25 Comparison of relative proportion of kaolinite and alumina contents present in the activated kaolins (GRC) dried at 80˚C prior to reflux with different concentrations of citric acid as a function of acid concentations equal to 0.1, 0.3, 0.5, 1.3, and 2 M (GRC 0.1 to GRC 2).

(A)

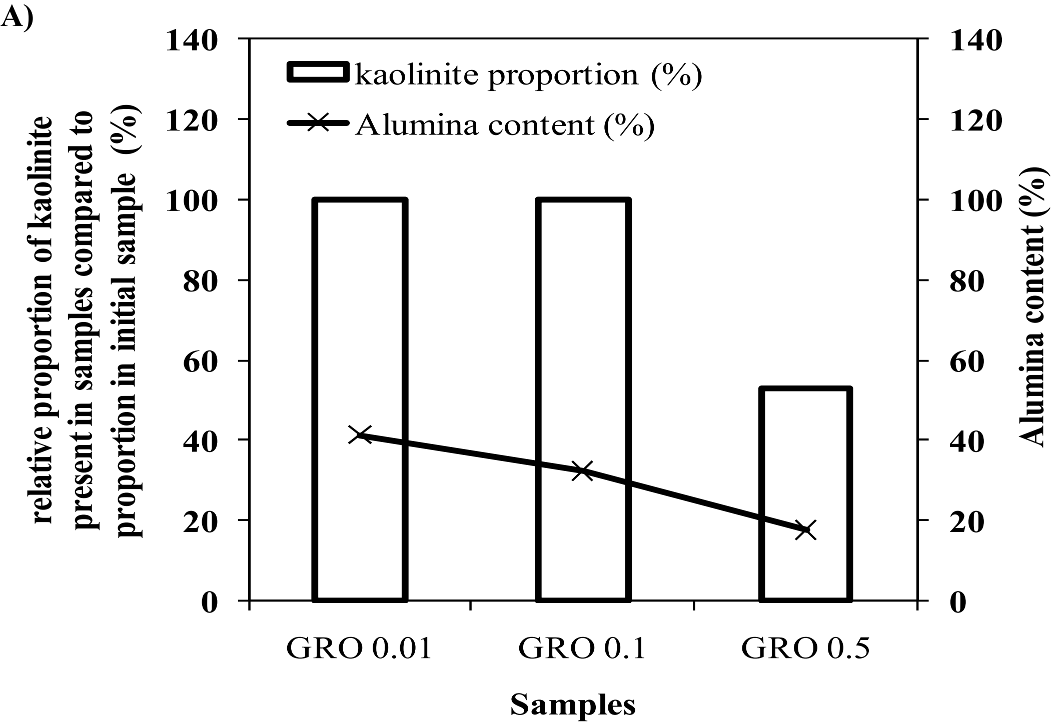

(B)

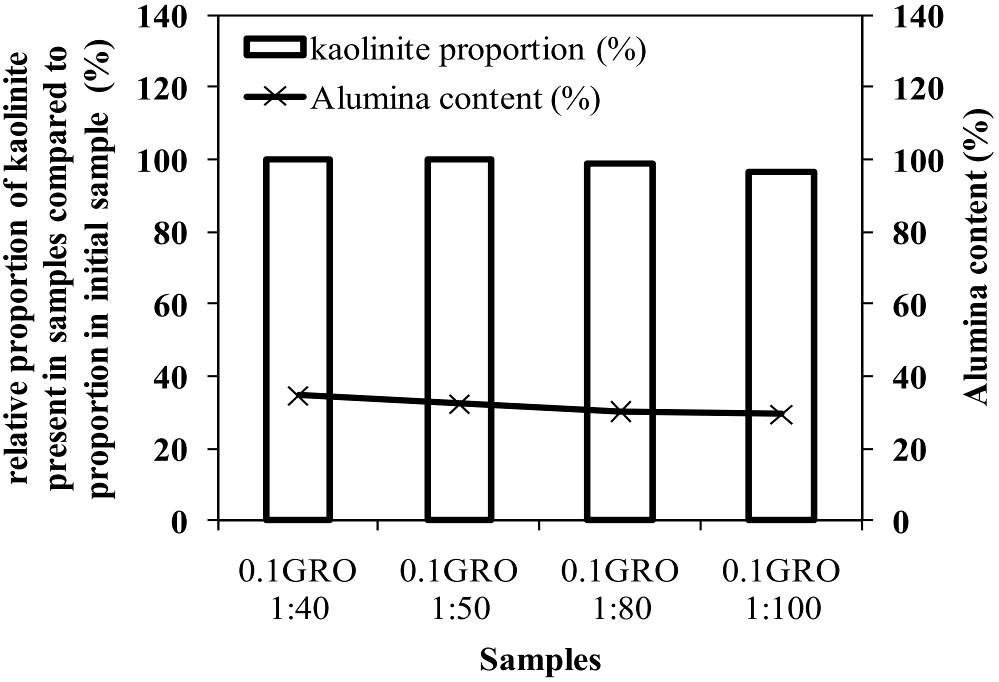

Figure 4.26 Comparison of relative proportion of kaolinite and alumina contents present in the activated kaolins (GRO) dried at 80˚C prior to reflux with different concentrations of oxalic acid as a function of acid concentations equal to 0.01, 0.1, and 0.5 M (GRO 0.01 to GRO 0.5) (A), and in the samples dried at 80˚C prior to reflux with 0.1 M oxalic acid as a function of the different clay to acid such as 1:4, 1:50, 1:80 and 1:100 (0.1GRO 1:4 to 0.1GRO 1:100) (B).

3. Fourier Transform Infrared Spectroscopy (FTIR)

Figure 4.27 shows the FTIR spectra of the GK and activated samples. The intensities of the kaolinite hydroxyl bands at 3696 and 3620 cm^{-1} are better resolved at low acid concentration up to 0.7 M HCl or 1 M H_2SO_4 (GRH 0.7; see Figure 4.27B-I and GRS 1; see Figure 4.27A-I) whereas these bands are less resolved when the GK was treated with 0.5 M oxalic acid (GRO 0.5; see Figure 4.27D-I). This means oxalic acid has strong effect on kaolin's structure. As the acid concentration is increased, the intensity of the 3696 cm^{-1} band in GRS and GRH samples decreased relative to the 3620 cm^{-1} band, indicating that the hydrated protons penetrates into the octahedral network and attacks the structural hydroxyl groups. In this way, dehydroxylation occurs and alumina is leached successively from the octahedral layer of the activated kaolins (Madejova, 2002). The bands at 1031 and 1008 cm^{-1}, which correspond to Si-O stretching vibrations of kaolinite in activated kaolin, diminished when the GK is treated with 2 M sulfuric acid or 2 M hydrochloric acid or 0.5 M oxalic acid (Figure 4.27A-II, Figure 4.27B-II and Figure 4.27D-II) due to structural changes in the tetrahedral cations. The results indicate that the kaolinite structure is only partially preserved in GRS 2, GRH 2 and GRO 0.5 samples, in agreement with the XRD results (see Figure 4.15, Figure 4.17 and Figure 4.21). The shoulder at 1090 cm^{-1} dramatically increases when the acid concentration is increased, and the most intense peak is obtained for GRS 2 among all activated samples. For GRH samples, this shoulder is slightly increased in GRH 0.5 and GRH 0.7 while it is largely increased in GRH 2. This shoulder also becomes intense peak in GRO 0.5 sample. The formation of intense shoulder suggests the presence of a significant proportion of a Si-rich amorphous phase in these samples. The band at 805 cm^{-1} in GRS 2, GRH 2 and GRO 0.5 increases in intensity with increasing acid concentrations. This peak is due to the formation of free amorphous silica. Quartz showed a peak at 790 cm^{-1} (Nuntiya and Prasanphan, 2006; Worasith et al., 2011b) for initial and all acid-treated samples. The band at 753 cm^{-1} is assigned to Si-O-Al stretching vibration of the clay sheet; that at 693 cm^{-1} corresponds to Si-O stretching of kaolinite; that at ~537 cm^{-1} corresponds to Si-O-Al (octahedral) stretching, and those at 469 and 430 cm^{-1} correspond to Si-O bending vibrations (Farmer, 1974), which were also decreased in the activated samples.

There are few structural changes due to citric acid treatments as compared with the structure changes of activated samples due to sulfuric acid or hydrochloric acid or citric acid treatments. The hydroxyl bands at 3696 and 3620 cm^{-1} in GRC samples are well-resolved as those of GK (see Figure 4.27C-I). The shoulder at 1090 cm^{-1} slightly increases with increasing acid concentration. The Al-Al-OH bending vibrations at 938 and 912 cm^{-1} are also reduced after acid treatment (Figure 4.27C-II). This shows that citric acid treatment also attacks the kaolin's structure, leaches the alumina content and enhances the silica phase formation. FTIR results are in agreement with the XRD results indicating that the kaolinite's structure is partially preserved in the acid activated samples (Figure 4.19) and also agree with the XRF results showing that the alumina is leached and the silica phase is formed simultaneously during the acid treatment (Table 4.16).

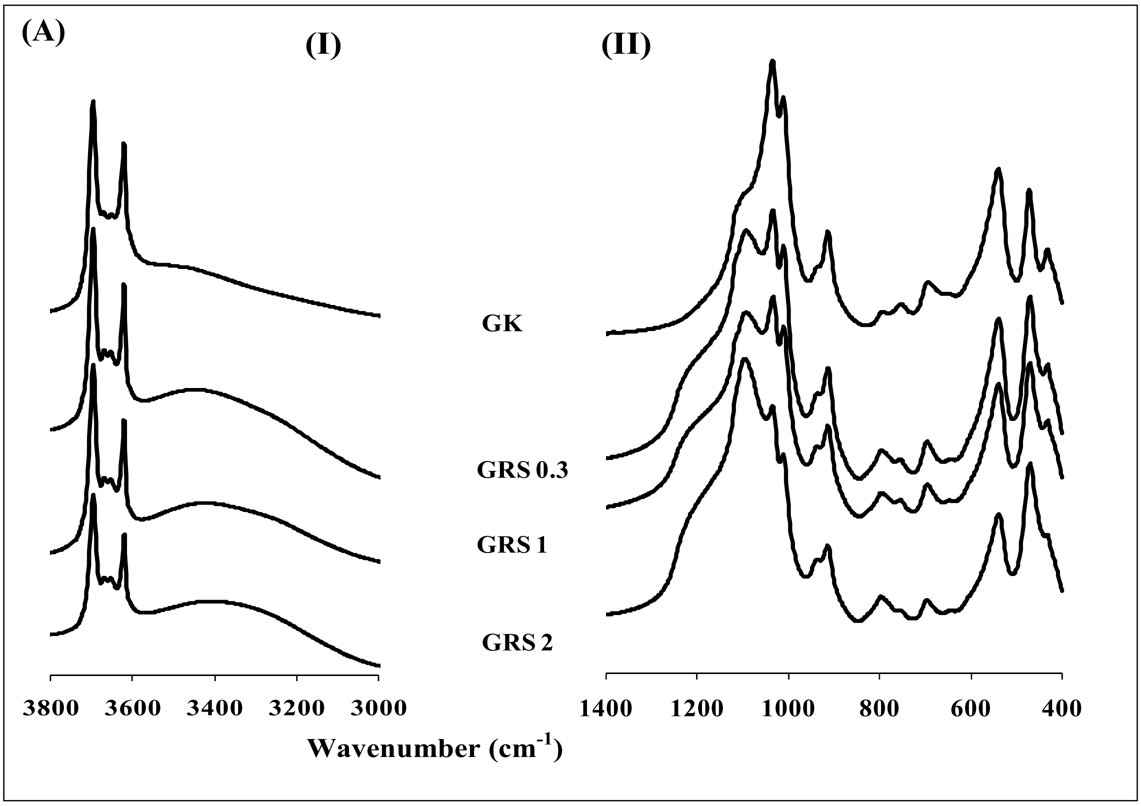
(A)
(I)
(II)
GK
GRS 0.3
GRS 1
GRS 2
3800
3600
3400
3200
3000
1400
1200
1000
800
600
400
Wavenumber (cm^{-1})

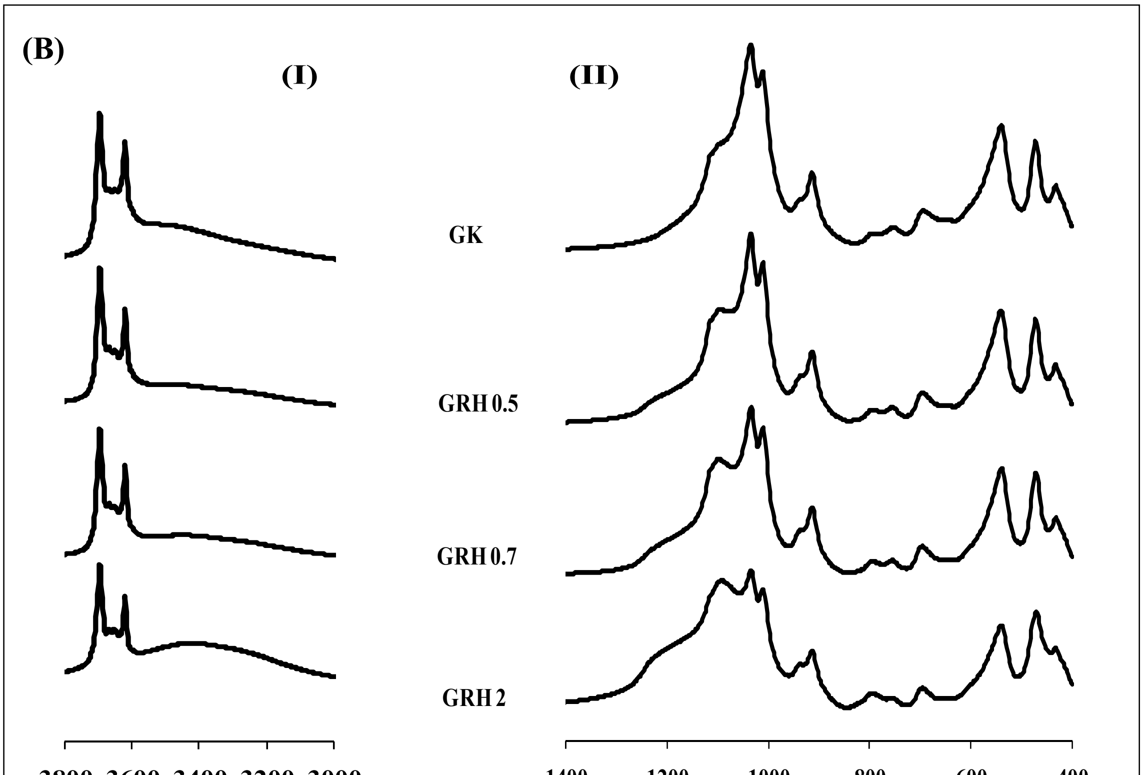
(B)
(I)
(II)
GK
GRH 0.5
GRH 0.7
GRH 2
3800
3600
3400
3200
3000
1400
1200
1000
800
600
400
Wavenumber (cm^{-1})

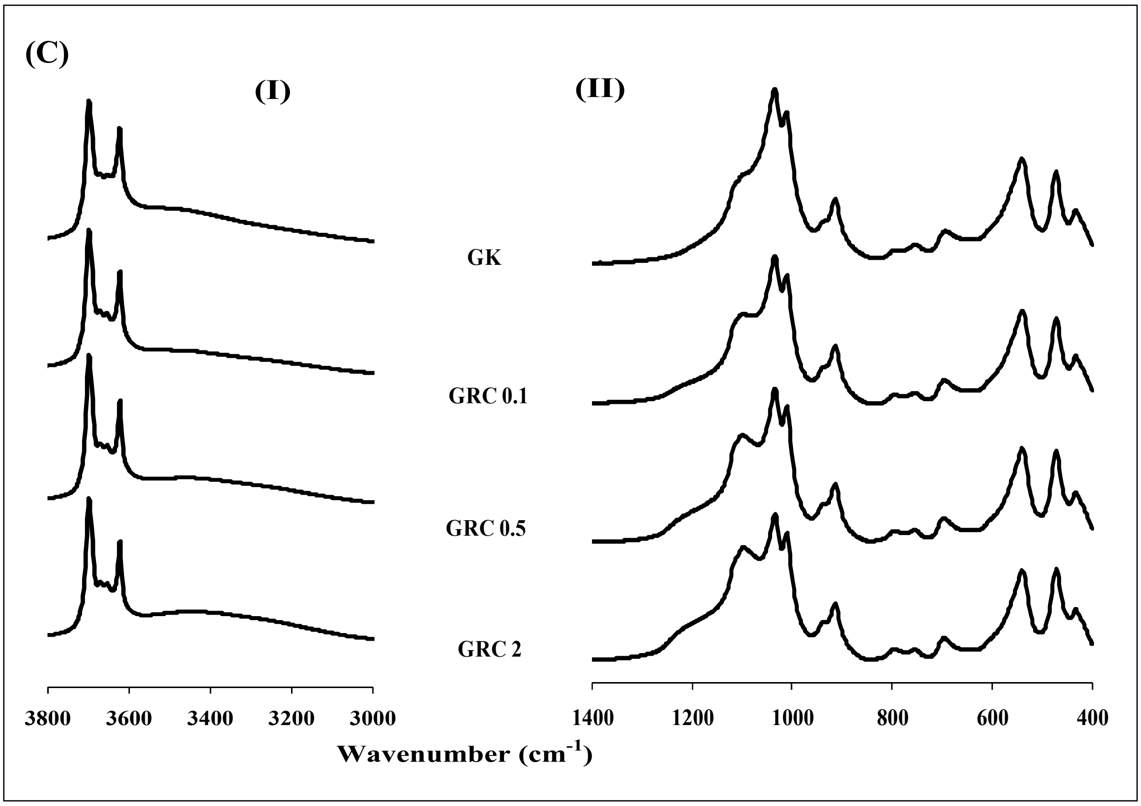

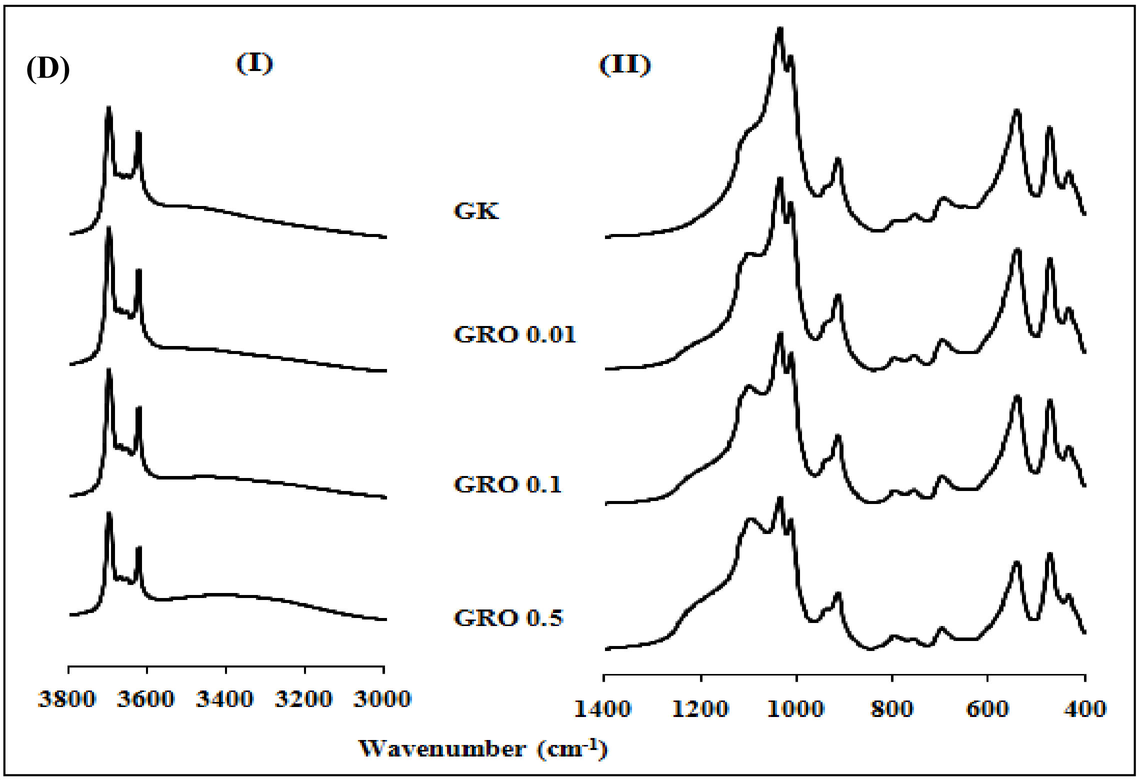

Figure 4.27 Comparison of the FTIR spectra of the initial and activated samples. Ground kaolin (GK) and samples dried at 80˚C prior to reflux with different concentration of sulfuric acid (GRS) (A); Ground kaolin (GK) and samples dried at 80˚C prior to reflux

with different concentration of hydrochloric acid (GRH) (B); Ground kaolin (GK) and samples dried at 80˚C prior to reflux with different concentration of citric acid (GRC) (C) and Ground kaolin (GK) and samples dried at 80˚C prior to reflux with different concentration of oxalic acid (GRO) (D).

4. Physical properties of kaolin

The specific surface area (SSA), total pore volume (V_p), mesopore volume (V_{me}) and micropore volume (V_{mi}) of ground and activated kaolins (GRS, GRH, GRC and GRO samples) are shown in Table 4.17. Increasing sulfuric or oxalic acid concentration to GK continuously increases in specific surface area and pore volume in the activated samples (for GRS and GRO samples). The maximum values of the specific surface area and the total pore volume obtained for GRS 2 are ~294 m^2/g and ~0.8 cc/g and those for GRO 0.5 are ~433 m^2/g and ~0.8 cc/g. When GK is treated with 2 M sulfuric acid, the specific surface area is approximately five-fold increased to ~294 m^2/g and the total pore volume is a three-fold increased to ~0.8 cc/g. However, the specific surface area is about seven-fold increased and the total pore volume is three-fold increased when GK is treated with 0.5 M oxalic acid. The initial ground kaolin (GK) only has 0.3 cc/g mesopore. With increasing acid concentration, the micropore volumes (V_{mi}) and mesopore volumes (V_{me}) are increased to 0.1 cc/g and 0.8 cc/g, respectively in GRS 2 while these micro- and mesopore volumes are increased to 0.07 cc/g and 0.7 cc/g, respectively in GRO 0.5. The pore size distribution curve (Figure 4.28A) also shows that sample GRO 0.01 has the lower micropore and mesopore volume where as samples GRO 0.1 and GRO 0.5 have higher micro-and mesopore volumes than those of initial GK sample. The micropore and mesopore volumes in the activated samples continuously increase with increasing acid concentration from 0.01 to 0.5 M oxalic acid (for GRO 0.01 to GRO 0.5).

Hydrochloric and citric acid leaching of the ground sample also cause an increased in the specific surface area and pore volume in the activated samples (GRH and GRC) as compared with those of GK. The optimum value of the bleaching capacities obtained for both GRH 0.5 and GRH 0.7 are ~83%, although GRH 0.5 has the lowest specific surface area among the HCl-activated ground samples viz., GRH 0.7 and GRH 2. After acid activation on GK, the results of GRH 0.5 show an approximately 3.3-fold increase in specific surface area from ~61 m^2/g to ~204 m^2/g and a 1.3-fold increase in pore volume from 0.3 cc/g to 0.4 cc/g, whereas GRH 0.7 had an approximately 4.4-fold increase in the specific surface area to ~269 m^2/g and a 1.7-fold increase in the total pore volume to 0.5 cc/g. After getting the maximum conditions for the GRH 0.7 sample, the specific surface area decreases to ~260 m^2/g and pore volume increases to ~0.6 cc/g in GRH 2. This result is in agreement with the report of smectite-derived clays that described high acid concentration destroying the clay lamellar structure, leading to decreased in specific surface area (Alther, 1986; Temuujin et al., 2004). Although GRH 2 has the higher specific surface area and pore volume than those of GRH 0.5, it has the lower bleaching value of ~78% as a result of the continuous dissolution of the kaolinite and deposition of amorphous silica (Table 4.17, and Figures 4.17A, 4.18A and 4.27B). Similar results have been reported for citric acid treated clays, where the maximum values of the specific surface area obtained for GRC 1.3 is ~296 m^2/g although its bleaching value is less than that of GRC 0.5, which has the specific surface area of ~246 m^2/g. GRC 0.5 has the optimum bleaching value of ~81%, whereas that of GRC 1.3 is ~77%, indicating that the surface area is not a sole parameter for getting the maximum bleaching performances.

The bleaching capacity is decreased to ~75% following the reduction in specific surface area to ~260 m^2/g in the GRC 2 sample when the GK is treated with 2 M citric acid.

Increasing clay/acid ratios also enhances the surface area and pore volume in the activated samples (GRS, GRH and GRO samples) as shown in Table 4.17. For GRS samples, the surface area and pore volume of 2GRS 1:4 are slightly increased from 269 m^2/g to 294 m^2/g and from 0.4 cc/g to 0.8 cc/g, respectively as compared with those of 2GRS 1:50. GRH samples treated with different clay/acid ratio also show the same trend as GRS samples. For example, the surface area and pore volume are increased from ~117 m^2/g to ~313 m^2/g and from ~0.2cc/g to ~0.7 cc/g, respectively in 0.5GRH 1:60 when the clay/acid ratio is increased from 1:4 to 1:60. The surface area and pore volume increases in the activated samples (for 0.5GRH 1:50, 2GRH 1:12 and 4GRH 1:6) which are treated with same acid strength. These activated samples also have different bleaching capacities (see Table 4.17). For example, 0.5GRH 1:50 gives the value of ~ 83%, 2GRH 1:12 gives about ~ 80% and 4GRH 1:6 gives ~ 74%. This means that treating the ground kaolin using the lower the hydrochloric acid concentration with high clay/acid ratio (eg- 0.5 M HCl with clay to acid ratio of 1:50) gives the better results than using the higher the acid concentration with low clay/acid ratio (eg. 4 M HCl with clay to acid ratio of 1:6). Moreover, low acid concentration with high clay/acid ratio (e.g. 0.5M/1:50 clay/acid ratio treatment for 0.5GRH 1:50) was sufficient to get the optimum bleaching value of the kaolin, although its surface area and pore volumes are the least among the activated samples, viz., 2GRH 1:12 and 4GRH 1:6). Similarly, the sample 4GRH 1:6 has the lowest bleaching capacities although its surface area and pore volumes are the highest among these activated samples, i.e., the surface area and pore volume of 0.5GRH 1:50 are ~204 m^2/g and ~0.4 cc/g, whereas those of 4GRH 1:6 are ~267 m^2/g and ~0.7 cc/g, respectively. This also confirms that the bleaching capacities are not related with the surface area and pore volume in the activated kaolins. The smectite-derived clays also needed to be treated with diluted acid to get the maximum bleaching values, which are not directly related with the highest surface area (Christidis et al., 1997; Morgan et al., 1985; Zaki et al., 1986).

The results of the activated samples which are treated with 0.1 M oxalic acid using different clay/acid ratio show that surface area is increased to a maximum at clay/acid ratio of 1:80 while the pore volume is stable for all 0.1GRO samples. The surface area is increased from ~204 m^2/g to ~267 m^2/g when the clay to acid ratio used is increased from 1:4 to 1:80 (for 0.1GRO 1:4 to 0.1GRO 1:80). After that the specific surface area is decreased to 237m^2/g in 0.1GRO 1:100. Due to the effect of different clay/acid ratio on GK, the maximum surface area and pore volume are around 5-fold and 2-fold increased in both 2GRS 1:50 and 0.5GRH 1:60 samples while surface area is 4-fold increased in 0.1GRO 1:80 samples. Subsequent acid leaching of the ground kaolin promotes the proportions of pore at 40 Å in the activated samples (Figure 4.28B). Among GRO samples, it is seen that the peaks of the activated samples continuously increased with the increasing clay to acid ratio until the GK was treated with 0.1M oxalic acid using clay/acid ratio of 1:80. Beyond this clay/acid ratio, the sample 0.1GRO 1:100 had a lower differential pore volume at > 40 Å than that of 0.1GRO 1:80 sample.

Table 4.17 Specific surface area (SSA), total pore volume (Vp), mesopore volume (V_{me}), micropore volume (V_{mi}) and bleaching capacity (BC) of the initial ground kaolin (GK) and activated samples (GRS, GRH, GRC and GRO).

Sample	SSA (m^2/g)	V_p (cc/g)	V_{mi} (cc/g)	V_{me} (cc/g)	BC (%)
GK	60.70	0.30	0.00	0.30	49.80
Samples ground and heated at 80˚C prior to reflux with different concentrations of sulfuric acid equal to 0.3, 1, and 2 M using clay/acid ratio of 1:50					
GRS 0. 3	223.61	0.37	0.04	0.33	81.40
GRS 1	271.38	0.44	0.04	0.40	78.00
GRS 2	293.92	0.76	0.01	0.75	66.90
Samples ground and heated at 80˚C prior to reflux with 2M sulphuric acid with different clay/acid ratio of 1:4, 1:8 and 1:50					
2GRS 1:4	268.81	0.44	0.05	0.39	73.43
2GRS 1:8	291.84	0.48	0.05	0.43	71.68
2GRS 1:50	293.92	0.76	0.32	0.44	66.90
Samples ground and heated at 80˚C prior to reflux with different concentrations of hydrochloric acid equal to 0.5, 0.7, and 2 M using clay/acid ratio of 1:50					
GRH 0.5	204.12	0.40	0.02	0.38	83.26
GRH 0.7	268.60	0.51	0.02	0.49	82.64
GRH 2	259.20	0.56	0.02	0.54	77.72
Samples ground and heated at 80˚C prior to reflux with 0.5M hydrochloric acid with different clay/acid ratio of 1:4, 1:50 and 1:60					
0.5GRH 1:4	116.50	0.24	0.04	0.20	51.55
0.5GRH 1:50	204.12	0.40	0.02	0.38	83.26
0.5GRH 1:60	312.50	0.69	0.05	0.64	80.54
Samples ground and heated at 80˚C prior to reflux with different hydrochloric acid concentrations with different clay/acid ratio					
*0.5GRH 1:50	204.12	0.40	0.02	0.38	83.26
*2GRH 1:12	213.96	0.45	0.01	0.44	79.56
*4GRH 1:6	266.91	0.69	0.01	0.68	74.45
Samples ground and heated at 80˚C prior to reflux with different concentrations of citric acid equal to 0.1, 0.3, 0.5, 1.3 and 2 M using clay/acid ratio of 1:50					
GRC 0.1	159.60	0.32	0.03	0.29	70.65
GRC 0.3	201.73	0.40	0.21	0.19	80.39
GRC 0.5	245.92	0.54	0.03	0.51	81.11
GRC 1.3	295.52	0.58	0.03	0.55	77.08
GRC 2	260.30	0.62	0.02	0.60	75.00

Table 4.17 Cont.

Sample	SSA (m^2/g)	V_p (cc/g)	V_{mi} (cc/g)	V_{me} (cc/g)	BC (%)
Samples ground and heated at 80˚C prior to reflux with different concentrations of oxalic acid equal to 0.01, 0.1, and 0.5 M using clay/acid ratio of 1:50					
GRO 0.01	77.85	0.27	0.02	0.25	63.17
GRO 0.1	213.40	0.42	0.04	0.38	75.50
GRO 0.5	432.50	0.77	0.07	0.70	45.37
Samples ground and heated at 80˚C prior to reflux with 0.1M oxalic acid with different clay/acid ratio of 1:40, 1:50, 1:80 and 1:100					
0.1GRO 1:40	203.60	0.43	0.04	0.39	75.44
0.1GRO 1:50	213.40	0.42	0.04	0.38	75.50
0.1GRO 1:80	265.80	0.44	0.05	0.39	79.06
0.1GRO 1:100	236.60	0.39	0.04	0.35	77.40

[*] 0.5GRH 1:50 = Samples ground and heated at 80˚C prior to reflux with 0.5M hydrochloric acid with clay/acid ratio of 1:50; 2GRH 1:12 = Samples ground and heated at 80˚C prior to reflux with 2 M hydrochloric acid with clay/acid ratio of 1:12; 4GRH 1:6 = Samples ground and heated at 80˚C prior to reflux with 4M hydrochloric acid with clay/acid ratio of 1:6.

(A)

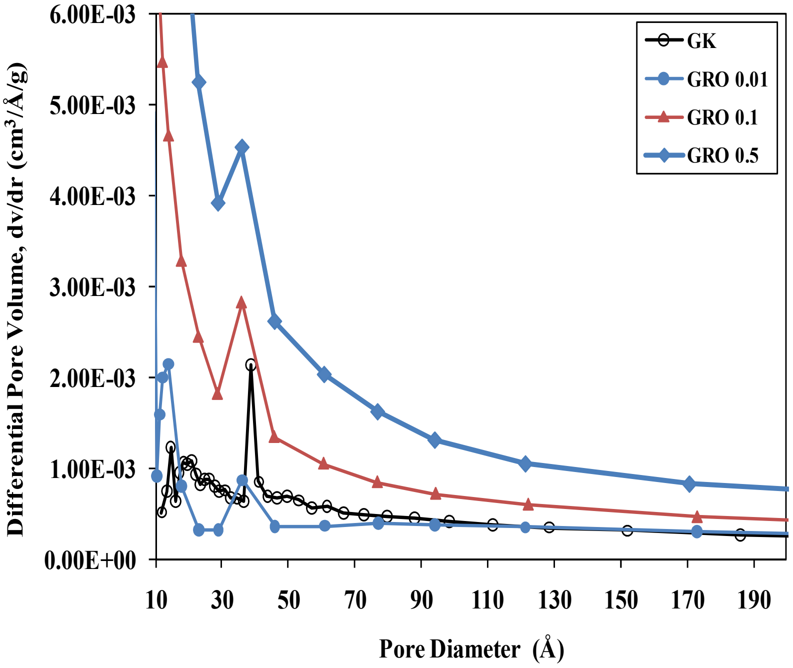

(B)

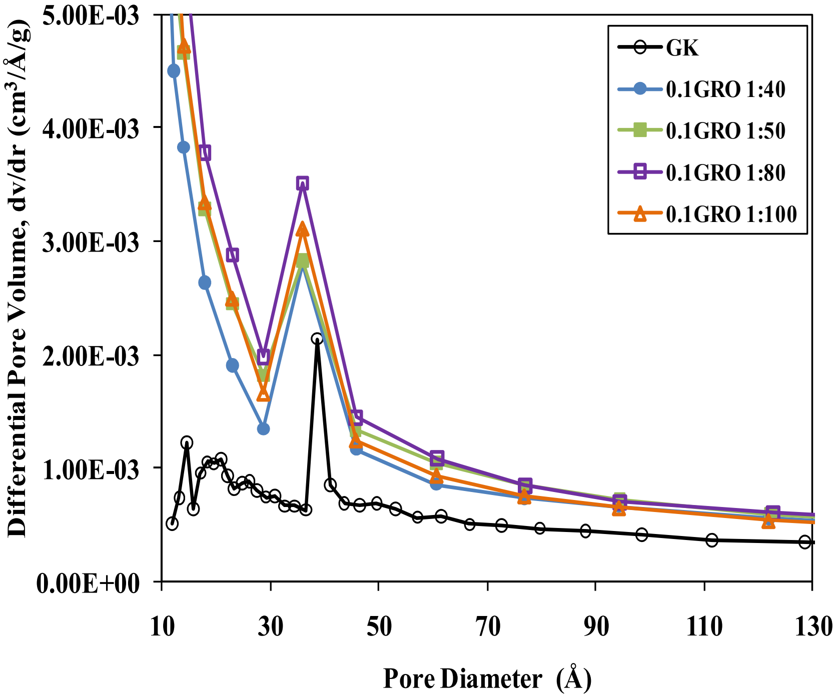

Figure 4.28 Pore size distribution curve of the initial (GK) and activated samples (GRO) dried at 80˚ prior to reflux with different concentration of oxalic acid equal to 0.01, 0.1, and 0.5 M (GRO 0.01 to GRO 0.5) (A), and initial ground kaolin (GK) and samples dried at 80˚C prior to reflux with 0.1 M oxalic acid using different clay to acid ratio (0.1GRO 1:40 to 0.1GRO 1:100) (B).

4.1.5 Relationship between the bleaching capacities of the activated samples and their physico-chemical characteristics

The bleaching capacities of the activated samples (unground and ground) as a function of the temperature used prior to reflux with 2 M sulfuric acid are presented in Figure 4.29A. The initial UGK sample has a bleaching capacity of ~35%. For the FUG 2 samples, as the temperature increases, the bleaching capacity increases slightly to ~39% at 100˚C and decreases continuously to ~14% at 900˚C. Furthermore, the bleaching capacity of the GK sample is higher (~50%) than that of the initial UGK sample (~35%). Heating of the GK sample to 100˚C slightly increases its bleaching capacity to ~67%. Preheating of the ground sample (FG 2 samples) to temperatures of 300˚C and 600 to 900°C result in approximately the same bleaching capacities as those obtained for the unground samples (FUG 2 samples; see Figure 4.29A). UGK has an Al_2O_3 content of ~42%, and this content strongly decreases as the temperature of the pre-heating step increases (Table 4.6 and Figure 4.30A). Among the unground samples, 100UG 2, which has an Al_2O_3 content of ~36%, has the highest bleaching capacity of ~39%, whereas 700UG 2 has an Al_2O_3 content of 5% and a very low bleaching capacity of ~15%. The relative proportion of kaolinite is dramatically decreased from 100% to ~3% in 700UG2. Note that although 700UG 2 has the highest specific surface area and total pore volumes, it also has the lowest bleaching capacity (Table 4.7) among the unground samples. This behavior suggests that a high specific surface area is not the sole parameter governing the bleaching capacity.

The Al_2O_3 of GK is extensively leached when a high temperature is used before acidic reflux (Table 4.10 and Figure 4.30B). Temuujin, et al., 2001 reported that grinding affected the octahedral layers than the tetrahedron layers of kaolinite. The bleaching capacities of the activated samples are decreased due to this extensive leaching of alumina from the samples (Figure 4.30B). For this series, the highest bleaching capacity is obtained for the 100GR 2 sample, whereas the lowest bleaching capacity is obtained for 700GR 2. In contrast to the 100UG 2 sample, the optimum bleaching capacity of ~67% obtained for 100GR 2 is due to the more leaching of alumina content from 42% to ~16% in 100GR 2 than to ~36% in 100UG 2. The bleaching capacities of activated kaolins are not good when the alumina contents are slightly or extensively reduced in the activated samples, i.e. slightly reduced in 100UG 2 to 300UG 2 (see Figure 4.30A) and extensively leached in 500UG 2 to 700UG 2, 300GR 2 to 700GR 2 (see Figure 4.30B). The bleaching capacity of the ground samples cannot be due only to the high specific surface area measured for these activated samples (FG 2). For example, bleaching capacities of 500GR2 and 700GR2 are lower than that of GK although the surface area and pore volume of these activated samples are higher than that of GK sample (see Table 4.11). The relative proportions of kaolinite are dramatically reduced along with the extensively leaching of alumina in the preheated ground or unground kaolin samples prior to reflux with sulfuric acid (see Figures 4.7 and 4.12). The low bleaching capacities of the samples (ground or not) heated at temperatures higher than 100°C prior to acidic reflux can be attributed to the complete disappearance of the kaolinite structure of these samples (see XRD patterns in Figure 4.5 and Figure 4.10A). Indeed, kaolinite is characterized by the presence of aluminol sorption sites on its surface. In contrast to the silanol sites present on the surfaces of quartz and aluminosilicates (kaolinite, illite, and feldspar), which are generally neutral or negatively charged in the pH domain of the clay washing experiments for chemical treatment (pH ~3; see section 3.1.4), the aluminol sites located on the kaolinite surface can be positively charged in this pH domain (Tertre et al., 2006). The sorption of anionic pigments such as chlorophyll-a is favored when the kaolinite structure is preserved.

The bleaching capacities of the ground samples preheating at 100˚C or dried at 80˚C prior to acidic reflux are plotted as a function of the concentration of sulfuric acid used during the reflux step (Figure 4.29B). When a pre-heating step of 100°C is used prior to reflux, the bleaching capacities of the activated samples increase slightly compared to the ground sample when a low concentration of sulfuric acid is used (i.e., 0.1, and 0.5 M). The optimum bleaching capacity (~80%) is obtained for 100GRS 0.5; the bleaching capacity decreases to ~67% for 100GR 2. The Al_2O_3 contents of the 100GR 0.5 and 100GR 2 samples are ~23% and ~16%, respectively (see Figure 4.30B). The slight decrease in the bleaching capacity observed between the 100GR 0.5 and 100GR 2 samples is due to the partial leaching of aluminum during acid activation when a high sulfuric acid concentration is used (2 M). The kaolinite proportion is reduced from ~80% to ~60% in 100GR 2 sample (see Figure 4.12B). This interpretation is in agreement with a more extensive destabilization of the kaolinite structure at 2 M than at 0.5 M. This behavior could result in a decrease in the number of aluminol sites available for the sorption of chlorophyll in samples activated at high sulfuric acid concentrations (e.g., 2 M) and is in agreement with the interpretation proposed above to explain the low bleaching capacity of the samples preheated at temperatures higher than 100°C prior to reflux with a 2 M sulfuric acid solution. Furthermore, for the GRS samples, the optimum bleaching capacity (~82%) is obtained for the sample prepared with a 0.3 M sulfuric acid solution using clay/acid ratio of 1:50 (for GRS 0.3), as illustrated in Figure 4.29B. Further acid treatment reduces the alumina content, and the bleaching capacity tends to decrease due to a lack of positive sorption sites at the surfaces of the mineral constituents of the activated samples. For example, as shown in Figure 4.30B, the Al_2O_3 content is equal to ~28% for samples prepared at low sulfuric acid concentration (GRS 0.3), whereas this content decreases significantly to ~16% for the sample prepared with a higher sulfuric acid concentration (GRS 2). The maximum bleaching capacities of activated kaolins are ~80% and ~82% when the alumina contents in 100GR 0.5 and GRS 0.3 samples are ~23 % and ~28%, respectively.

The effects of grinding and acid treatment on kaolin's adsorption properties are studied as a function of the different acid concentrations with clay/acid ratio of 1:50 using sulfuric acid, hydrochloric acid, citric acid and oxalic acid with clay/acid ratio of 1:50 are illustrated in Figure 4.29C. The initial GK sample has a bleaching capacity of ~50%. When GK is treated with 0.5 M hydrochloric acid, the capacity is dramatically increased from ~50 to ~83%. Among GRH samples, GRH 0.5 gives the optimum bleaching value of ~83%, which is superior to that of commercial clay (~82%). Beyond this optimum condition, the capacities decrease with increasing acid concentrations and reach ~78% at 2 M hydrochloric acid concentration used for GRH 2. Acid-activated ground kaolins that are treated using citric acid also give the same results as hydrochloric acid-treated samples. The bleaching capacities of GRC samples slightly increase with increasing acid concentrations. Kaolin's sorption property is increased to ~71% at 0.1 M citric acid concentration (for GRC 0.1). The bleaching capacities continuously increase with increasing acid concentrations. At the optimum condition, GRC 0.5 sample has a bleaching capacity of ~81%, which is inferior to that of commercial clay (see Table 4.17). After that, the capacities slightly decrease to ~75% when the citric acid concentration is further increased to 2 M. although the surface area, pore volume and mesopore volumes are increased with increasing acid concentrations (see Table 4.17). The maximum bleaching capacities are obtained in both GRH 0.5 and GRC 0.5 when the alumina contents are ~32% in GRH 0.5 and ~34% in GRC 0.5 (see Figure 4.30 D to 4.30 F). The results indicate that hydrochloric acid is more effective in removing color from oil than citric acid. Christidis et al., 1997 studied the effects of hydrochloric acid leaching of smectites and reported that hydrochloric acid is a strong acid and is degraded into H^+ and Cl^- ions in the presence of water. The clay is protonated and the metal chlorides produced are soluble in water and can be removed in the clay washing step. Activating the kaolin with oxalic acid gives the lower bleaching capacities as compared with the value of other acid treatments. The bleaching capacity is continuously increased from ~64% to ~76% along with the leaching of alumina from ~41% to ~32% when the oxalic acid concentration is increased from 0.01 M to 0.1 M with clay/acid ratio of 1:50 (for GRO 0.01 to GRO 0.1 samples) (see Figure 4.30G). Beyond this optimum condition, the capacities are dramatically decreased to ~45% in GRO 0.5 and then slightly decreased to ~43% in GRO 1 which capacities are lower than that of initial GK sample. The alumina contents are also largely decreased to ~17% corresponding to the decrease in kaolinite proportions from 100% to ~50% in GRO 0.5 sample. These results found that bleaching capacities are largely depend on the alumina content in the activated kaolins. The range of alumina content was 28 to 34% for getting the optimum bleaching capacities (<80%) of kaolin depending on the different acid used.

Alumina content is decreased while surface area and pore volume in the acid treated GK are increased with increasing clay/acid ratio (see Table 4.16, Table 4.17). Among the GRS samples treated with different clay/acid ratios (2GRS 1:4 to 2GRS 1:50), 2GRS 1:4 which contained ~21% Al_2O_3 content, has the highest bleaching capacity of ~73% while 2GRS 1;50 sample has ~17% Al_2O_3 and ~66% bleaching capacity (Figure 4.30H). Among the GRH samples treated with 0.5 M hydrochloric acid using various clay to acid ratio of 1:4, 1: 50 or 1:60 (for 0.5GRH 1:4, 0.5GRH 1:50 and 0.5GRH 1:60), the sample 0.5GRH 1:50 has the maximum bleaching capacity (~83%) with alumina content of ~32%. Other samples, 0.5 GRH 1:4 and 0.5GRH 1:60 have the lower bleaching capacities of ~52% and ~80%, respectively which composes of ~40% and ~31% alumina in 0.5 GRH 1:4 and 0.5GRH 1:60, respectively (Figure 4.30I**)**. Activated kaolin treated with 0.1 M oxalic acid using clay/acid ratio of 1:80 which gives the maximum bleaching value among the GRO samples, also has ~30% alumina and its bleaching capacity is ~79% (Figure 4.30J**)**.

Activating the kaolin with same hydrochloric acid strength using different acid concentrations with different clay/acid ratio also shows that the bleaching capacities are not related with the surface area, pore volume and mesopore volume in the activated kaolins (see Table 4.17). Although 0.5GRH 1:50 has the lowest surface area, it has ~32% Al_2O_3 content, which gives the maximum bleaching value of ~83%. When the acid concentration is increased to 4 M with clay/acid ratio of 1:6, the alumina content continuously decreases to ~21% along with steadily decreasing bleaching performances for 4GRH 1:6. This may be due to the extensive leaching of alumina from the activated kaolin. These results also agreed with the finding that the alumina contents in the activated kaolins influence their bleaching properties. Similar results have been reported for smectites by many authors (Yang et al., 2006; Kheok and Lim, 1982; among them), who described the acid treatments opening the edges of the clay platelets and causing a charge deficiency in the activated samples, which consequently enhanced their bleaching performances corresponding to the partial dissolution of alumina from the samples. They, however, also reported that sorption properties decreased at high acid concentrations along with the extensive leaching of alumina from the clay corresponding to the collapse of clay structure.

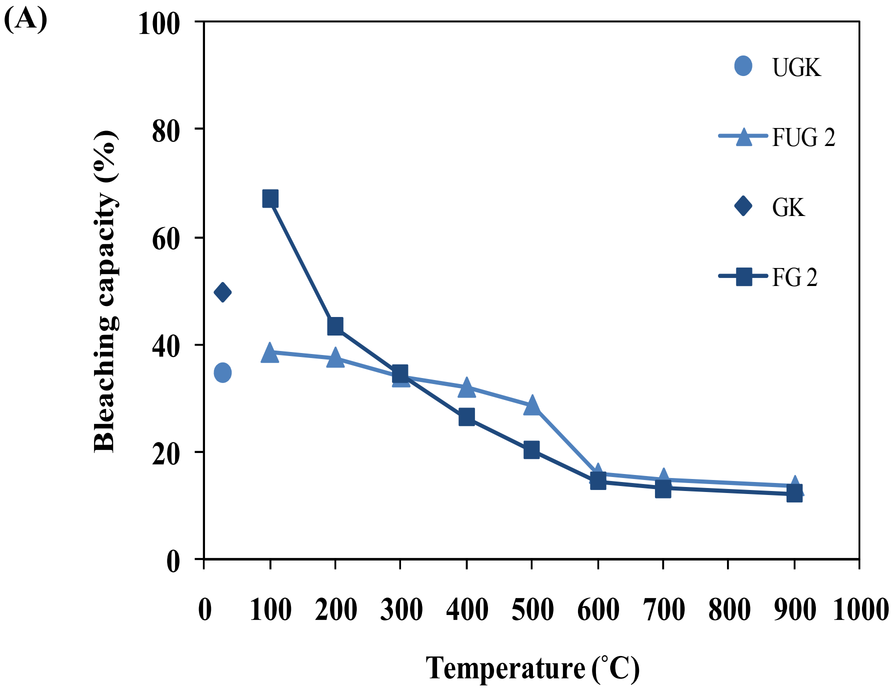

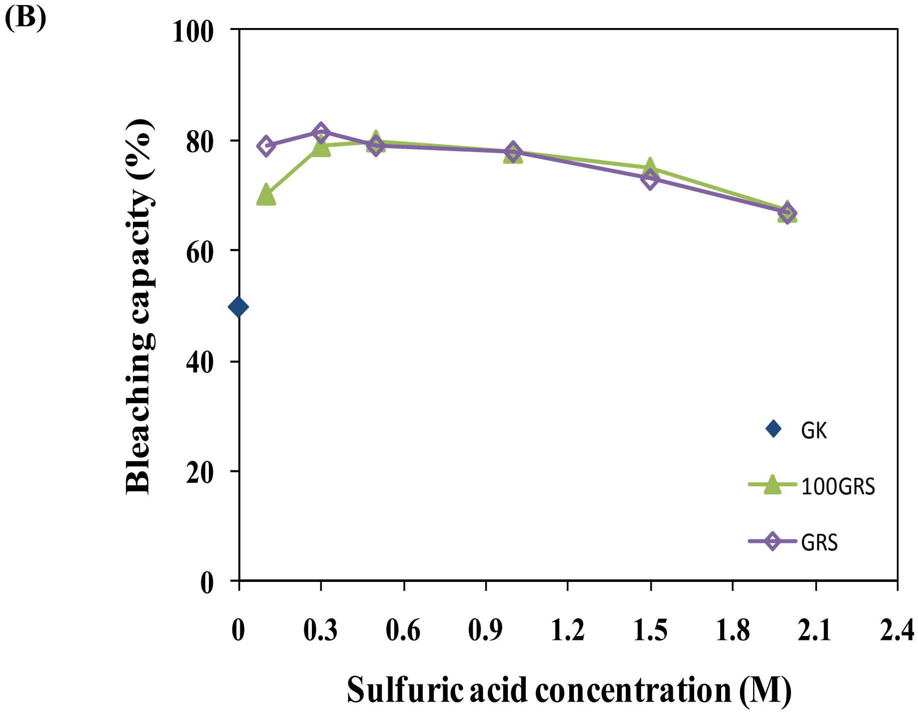

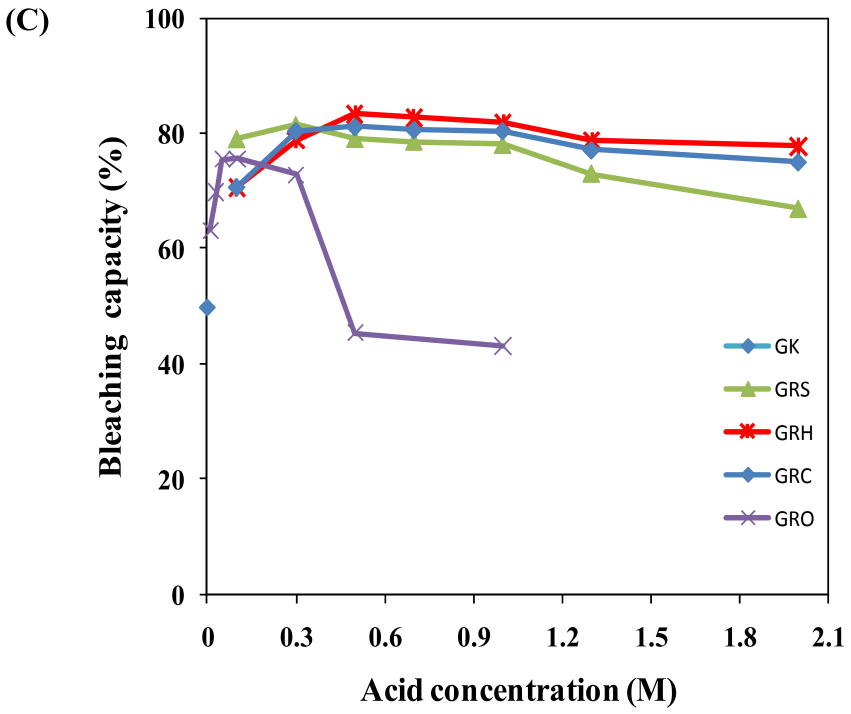

Figure 4.29 Effect of various parameters on the bleaching capacities of activated kaolins. (A) Effect of the drying temperature used prior to the activation of unground and ground samples in 2 M sulfuric acid. (B) Effect of the sulfuric acid concentration used for refluxing ground samples heating at 100˚C or 80˚C. (C) Effect of the different acid concentration using sulfuric acid, hydrochloric acid, citric acid and oxalic acid with clay/acid ratio of 1:50 on the ground kaolin (GRS, GRH, GRC and GRO samples).

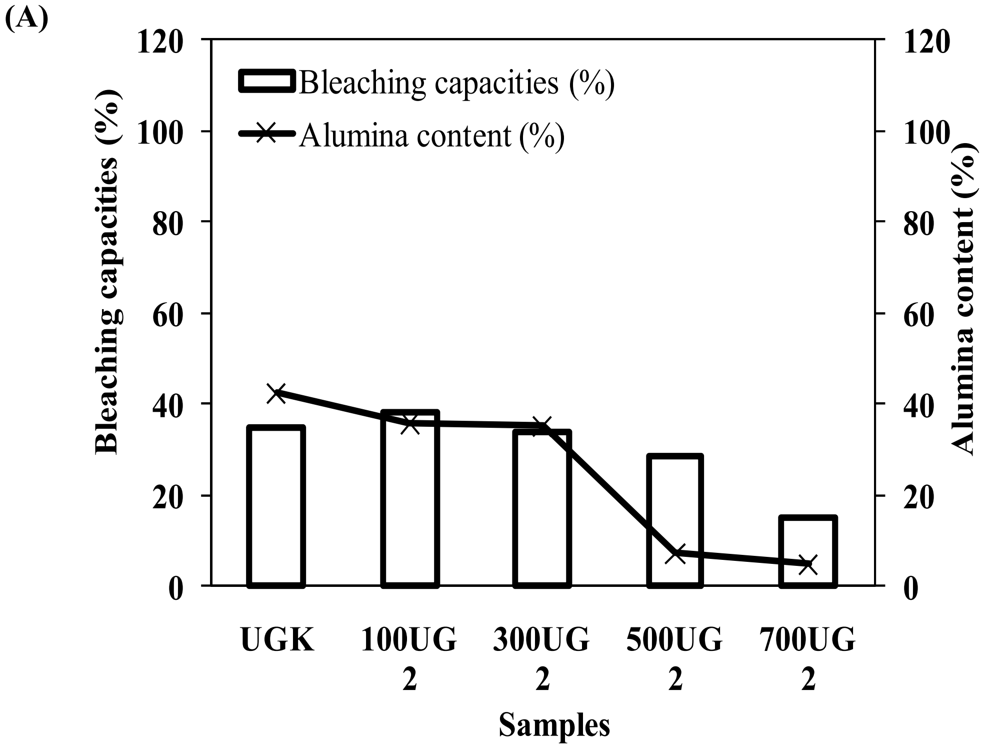
(A)
Bleaching capacities (%)
Alumina content (%)
120
100
80
60
40
20
0
UGK
100UG 2
300UG 2
500UG 2
700UG 2
Samples

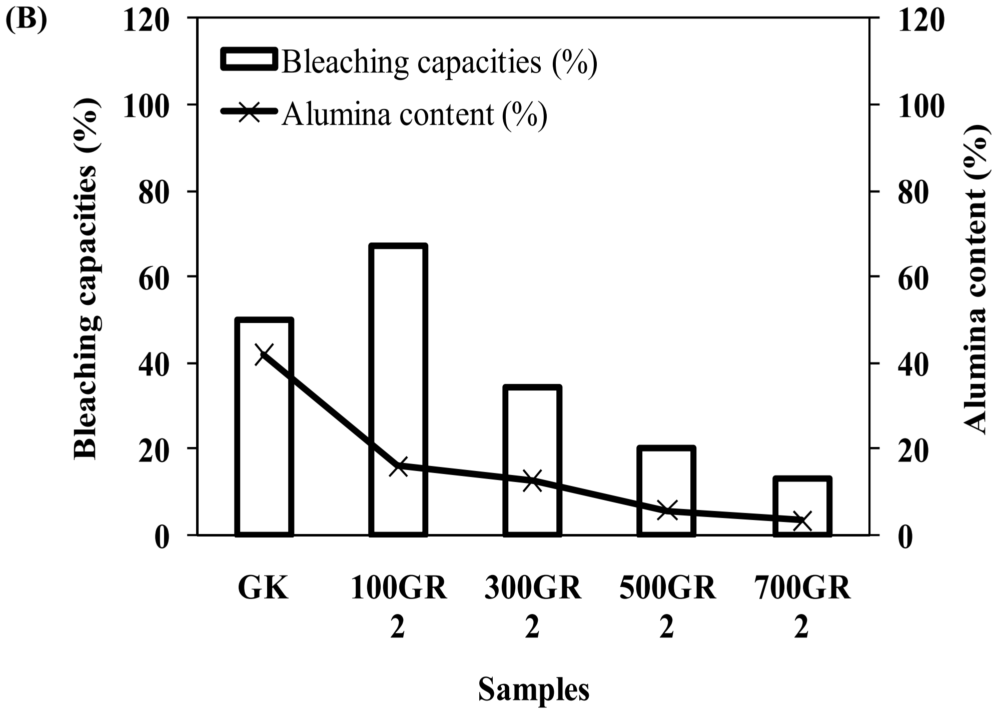
(B)
Bleaching capacities (%)
Alumina content (%)
120
100
80
60
40
20
0
GK
100GR 2
300GR 2
500GR 2
700GR 2
Samples

(C)

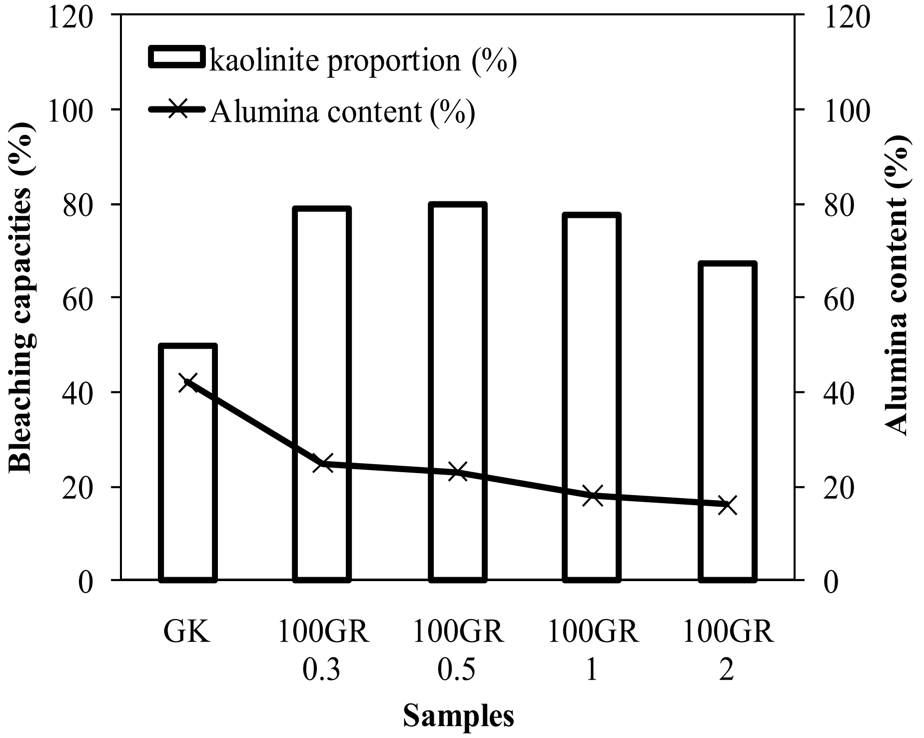
kaolinite proportion (%)
Alumina content (%)
Bleaching capacities (%)
Alumina content (%)
0
20
40
60
80
100
120
GK
100GR 0.3
100GR 0.5
100GR 1
100GR 2
Samples

(D)

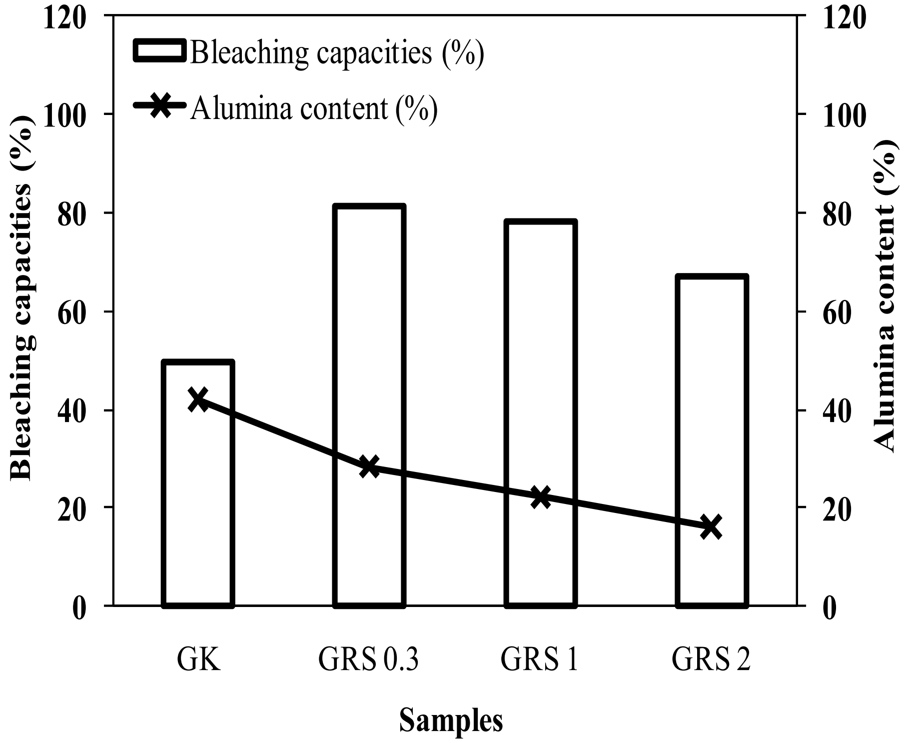
Bleaching capacities (%)
Alumina content (%)
Bleaching capacities (%)
Alumina content (%)
0
20
40
60
80
100
120
GK
GRS 0.3
GRS 1
GRS 2
Samples

(E)

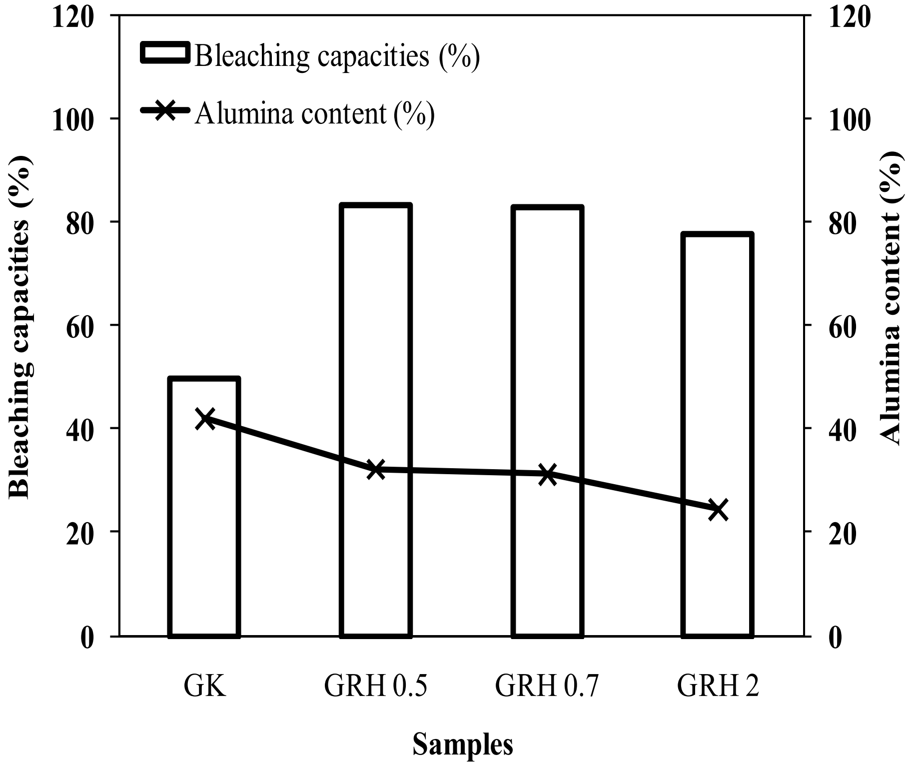
Bleaching capacities (%)
Alumina content (%)
120
100
80
60
40
20
0
Bleaching capacities (%)
Alumina content (%)
GK
GRH 0.5
GRH 0.7
GRH 2
Samples

(F)

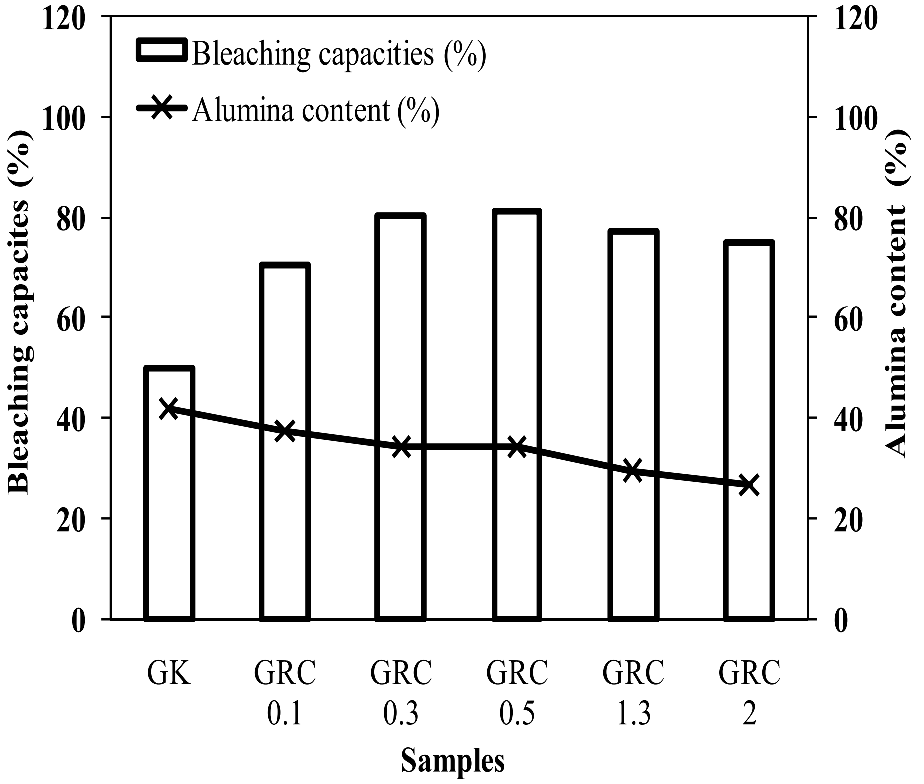
Bleaching capacities (%)
Alumina content (%)
120
100
80
60
40
20
0
Bleaching capacites (%)
Alumina content (%)
GK
GRC 0.1
GRC 0.3
GRC 0.5
GRC 1.3
GRC 2
Samples

(G)

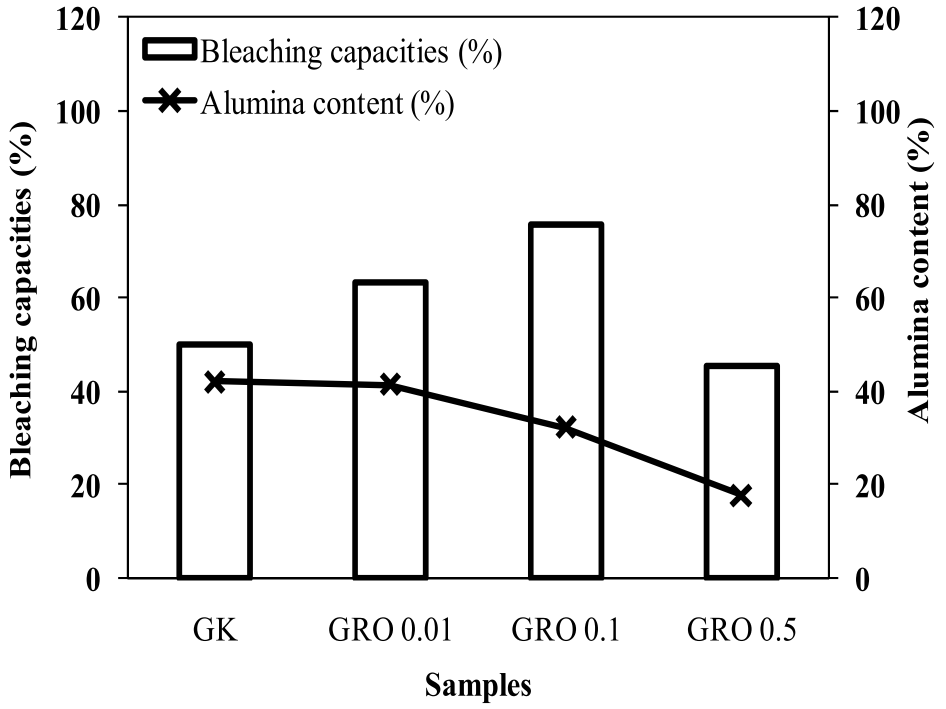
Bleaching capacities (%)
Alumina content (%)
Bleaching capacities (%)
Alumina content (%)
0
20
40
60
80
100
120
GK
GRO 0.01
GRO 0.1
GRO 0.5
Samples

(H)

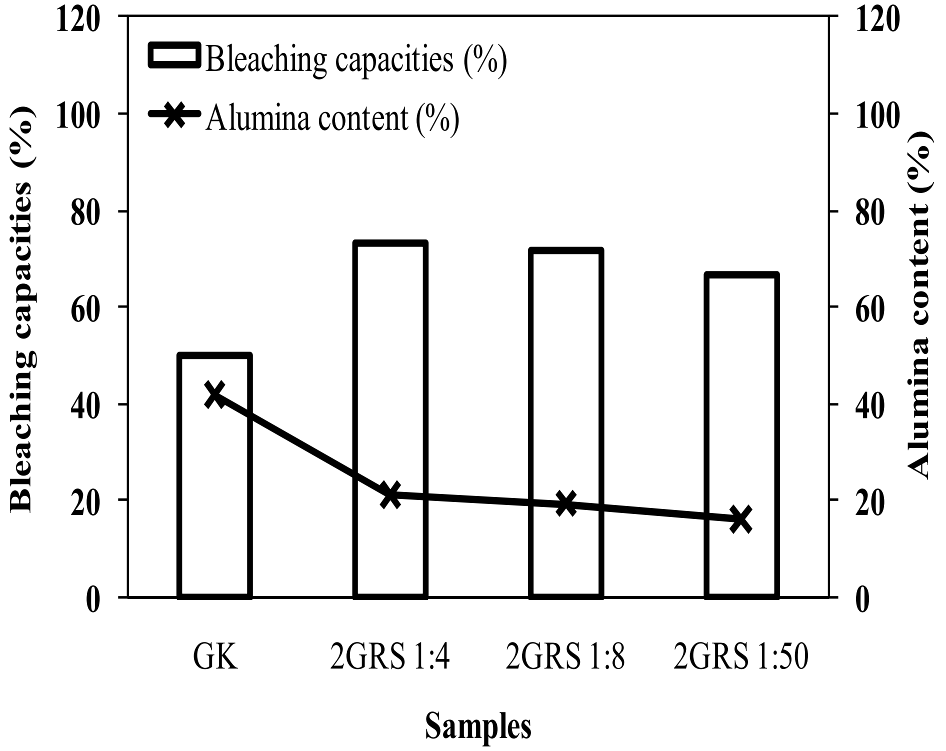
Bleaching capacities (%)
Alumina content (%)
Bleaching capacities (%)
Alumina content (%)
0
20
40
60
80
100
120
GK
2GRS 1:4
2GRS 1:8
2GRS 1:50
Samples

(I)

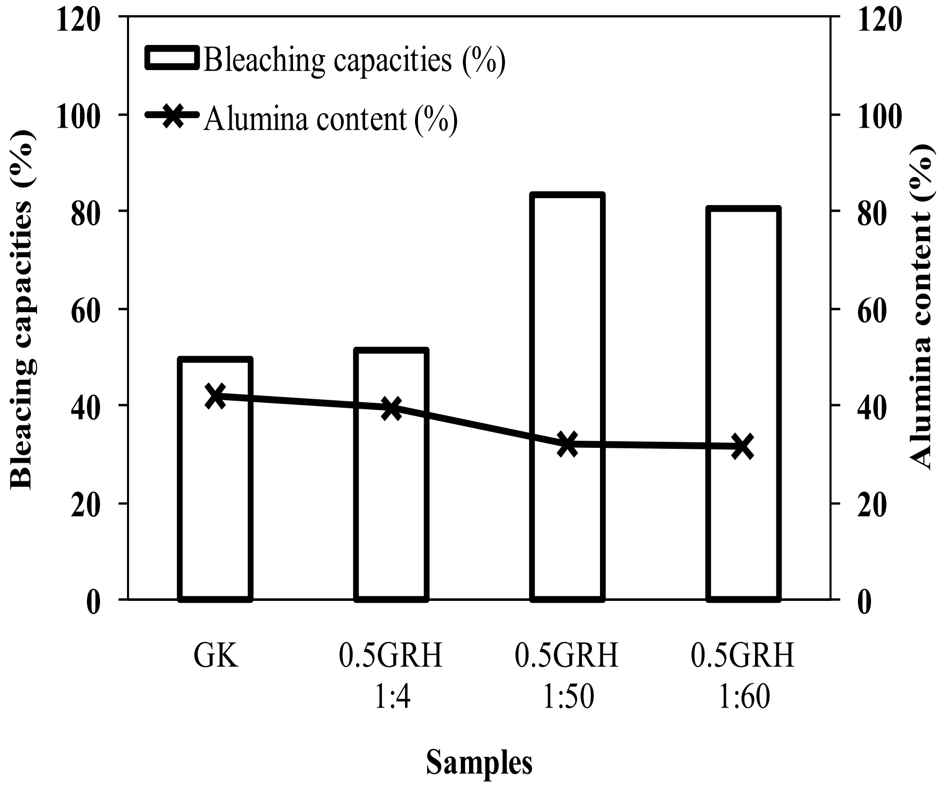
120
100
80
60
40
20
0
Bleacing capacities (%)
Bleaching capacities (%)
Alumina content (%)
Alumina content (%)
GK
0.5GRH 1:4
0.5GRH 1:50
0.5GRH 1:60
Samples

(J)

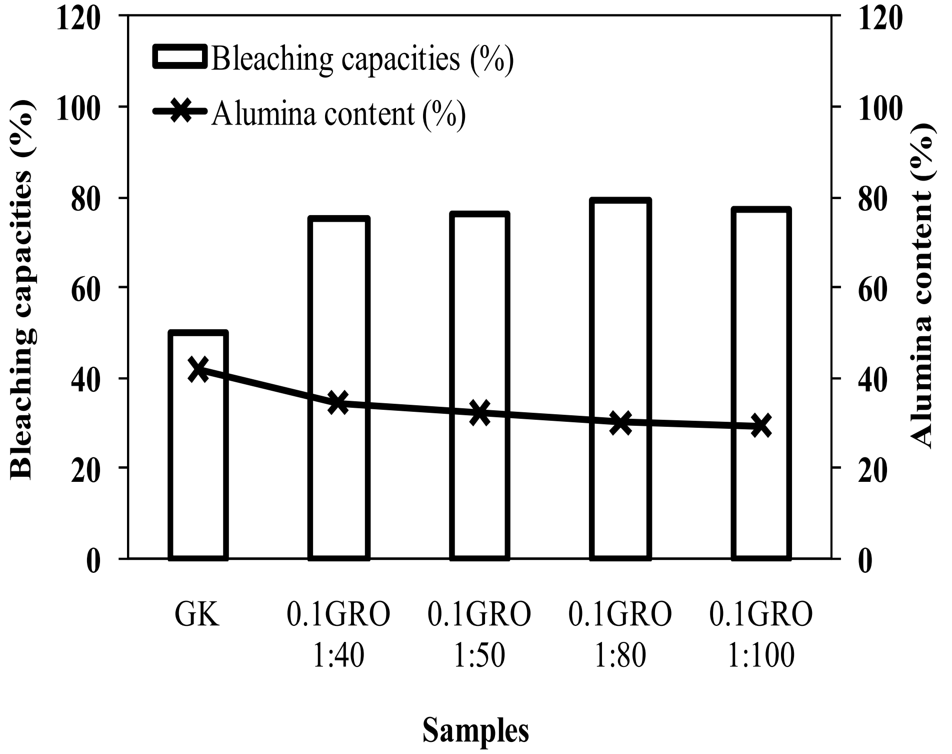
120
100
80
60
40
20
0
Bleaching capacities (%)
Bleaching capacities (%)
Alumina content (%)
Alumina content (%)
GK
0.1GRO 1:40
0.1GRO 1:50
0.1GRO 1:80
0.1GRO 1:100
Samples

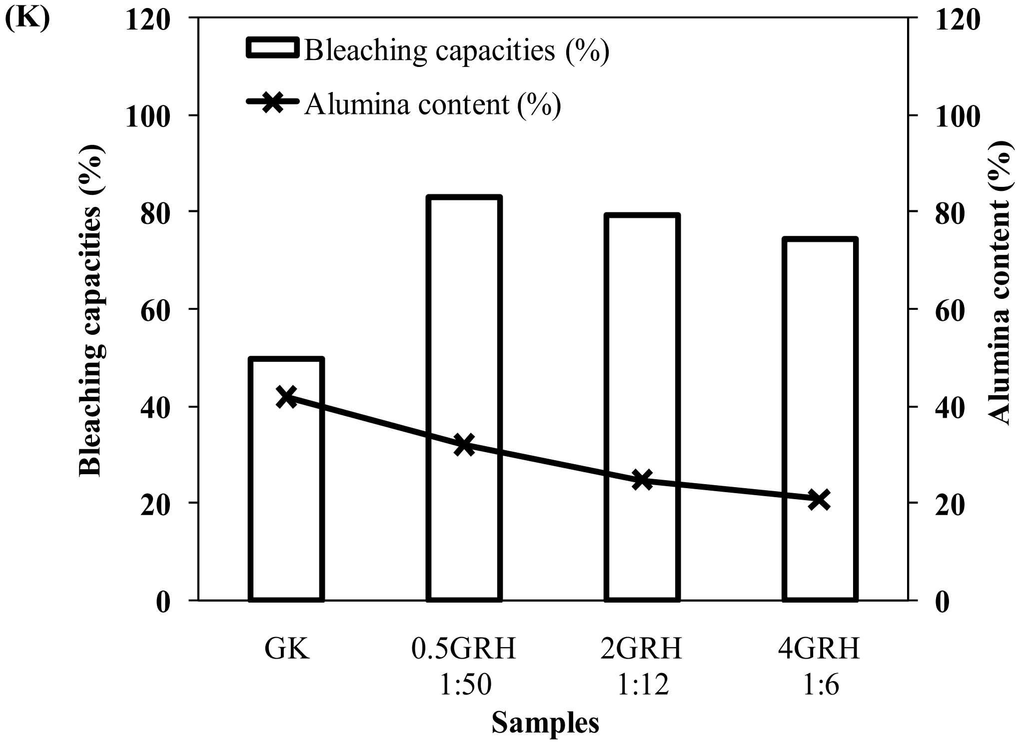

Figure 4.30 Comparison of bleaching capacities and alumina contents present in the activated kaolins (GRS, GRH, GRC and GRO samples) (A to K).
*The names of each sample are defined in the materials and methods (see **Section 3.1.4**).

4.1.6 Interaction of pigment on activated kaolin

To study the adsorption mechanism of pigment on modified kaolins, after adsorption experiment GRH 0.5 sample is washed with hexane several times and left overnight in order to extract any rice bran oil retaining in the clay. It is observed that the adsorption of pigment on the clays changes the adsorbent color from white to greenish-brown (Figure 4.31). As chlorophyll is soluble in hexane and in the oil, this indicates that the chlorophyll-a molecule is strongly attached to the GRH 0.5 sample and cannot be desorbed easily. This result is in agreement with Worasith et al. (2011a) who reported that it is due to the adsorption of chlorophyll or its derivative pheophytin on the clay which are the main pigments of rice bran oil. Nguetnkam et al. (2008) also studied the clay-pigment interaction between carotene molecule from palm oil and Cameroonian clay. They found that there is a strong interaction between carotene molecule and the clay, and the carotene cannot be desorbed using cyclohexane. Although chlorophyll-a is less polar than carotene molecule, it also had a strong interaction to the kaolin.

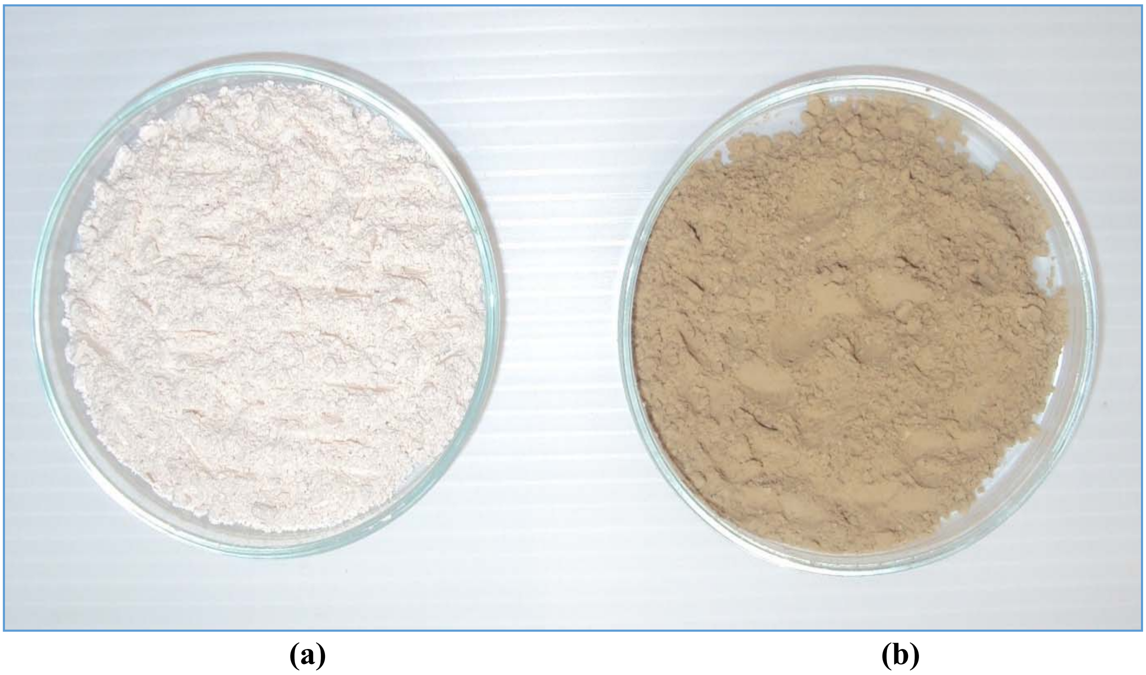
(a) **(b)**

Figure 4.31 Photos of initial activated GRH 0.5 sample (before adsorption experiment) (a) and hexane-washed GRH 0.5 sample (after adsorption experiment) (b).

For further studies of the clay-pigment interaction, the initial activated kaolins (before adsorption experiments) and hexane-washed kaolin samples (after adsorption experiments) are analyzed by diffuse reflection Fourier Transform Infrared (DRIFT). The spectra of crude rice bran oil and some activated kaolins, viz., GRS 0.3, GRH 0.5, GRC 0.5 and GRO 0.1, before and after adsorption experiments are illustrated in figure 4.32 to figure 4.35, respectively. When the spectra of hexane-washed kaolin compared to the initial one, the new peak appears in all hexane-washed samples. For GRS 0.3 sample, the new bands at 2935 cm^{-1}, 2869 cm^{-1} and 1461 cm^{-1} (Figure 4.32). These bands correspond to the vibration of -CH_3 and -CH_2 groups of hydrocarbon chains. Such hydrocarbon chains are due to the contribution of the branch of the chlorophyll-a molecule. Crude rice bran oil shows a peak at ~1744 cm^{-1} (in the C=O region). This peak is slightly shift to 1735 cm^{-1} in GRS 0.3 sample (after adsorption). This suggests that chlorophyll-a molecule is attached to the adsorbent acidic sites through its ring and consequently that the chlorophyll-a adsorption on kaolin is a chemical process. This result is in agreement with that of Worasith et al. (2011a) who also concluded that the chlorophyll-a adsorption include chemisorption. They also mentioned that a phytol of chlorophyll-a molecule (pheophytin), shows a sharp C-H stretching band at ~2935 cm^{-1} and the ester carbonyl groups of chlorophyll gives a band at ~1744 cm^{-1} (Weigl and Livingston, 1953, Holt and Jacobs,1955, Worasith et.al., 2011a). Comparison between the spectra of activated kaolins, viz., GRH 0.5, GRC 0.5 and GRO 0.1 (before and adsorption experiments) also show the similar results as that of GRS 0.3 (see Figure 4.33 to Figure 4.35).

Desorption study is carried out with hexane-washed GRH 0.5 sample by eluting it with absolute ethanol and 0.1M NaOH. Ethanol showed the low desorption value of ~52% whereas 0.1M NaOH of ~95%. It shows that the pigment-clay interaction is more extensively affected by 0.1M NaOH solution than by the ethanol. The polar solvent ethanol also has a week affect on the clay-pigment interactions indicating that the clay-pigment adsorption is both electrostatic interaction and chemisorptions. This behavior is in agreement with the trends reported previously by Worasith et al. (2011a).

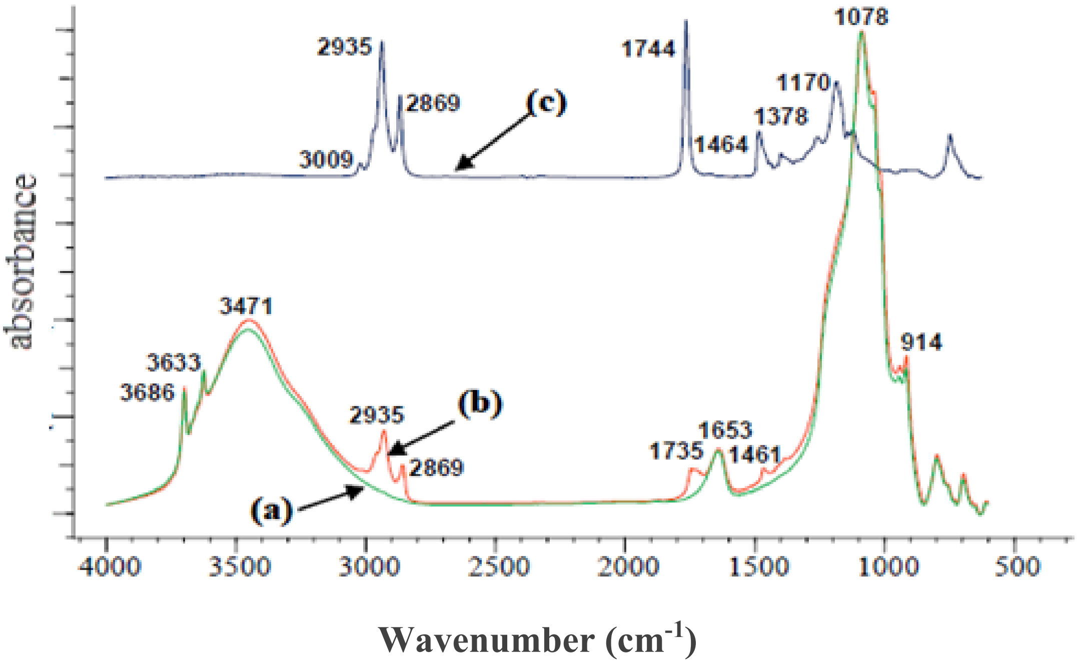

Figure 4.32 DRIFT spectra of GRS 0.3 (clay/acid ratio of 1:50) sample before (a), after (b) adsorption experiments, and crude rice bran oil (c).

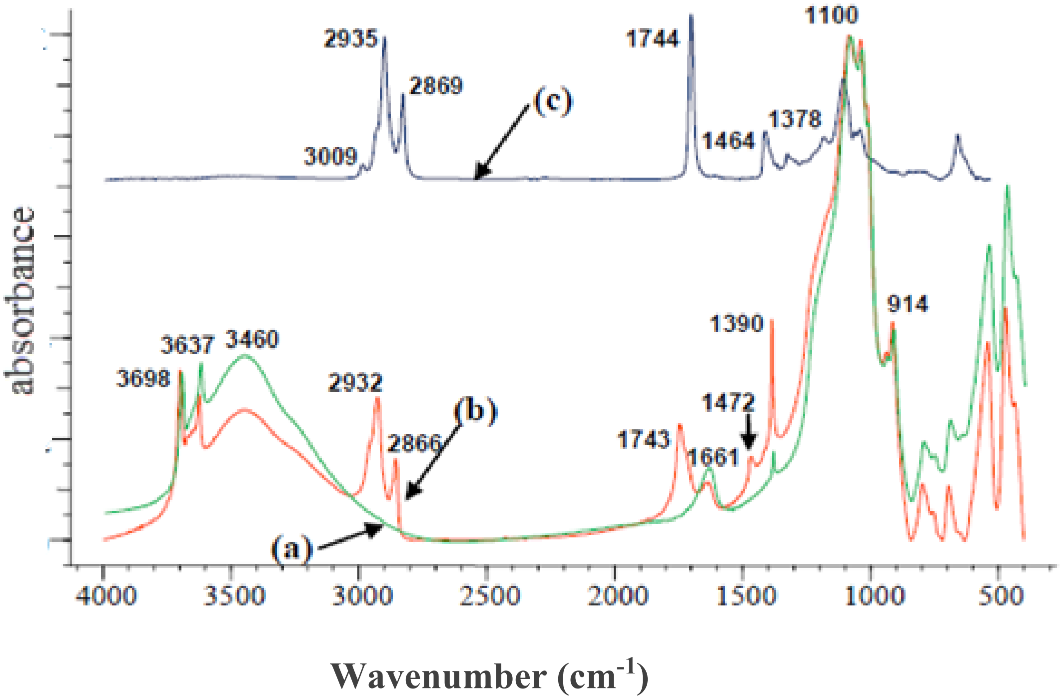

Figure 4.33 DRIFT spectra of GRH 0.5 (clay/acid ratio of 1:50) sample before (a), after (b) adsorption experiments, and crude rice bran oil (c).

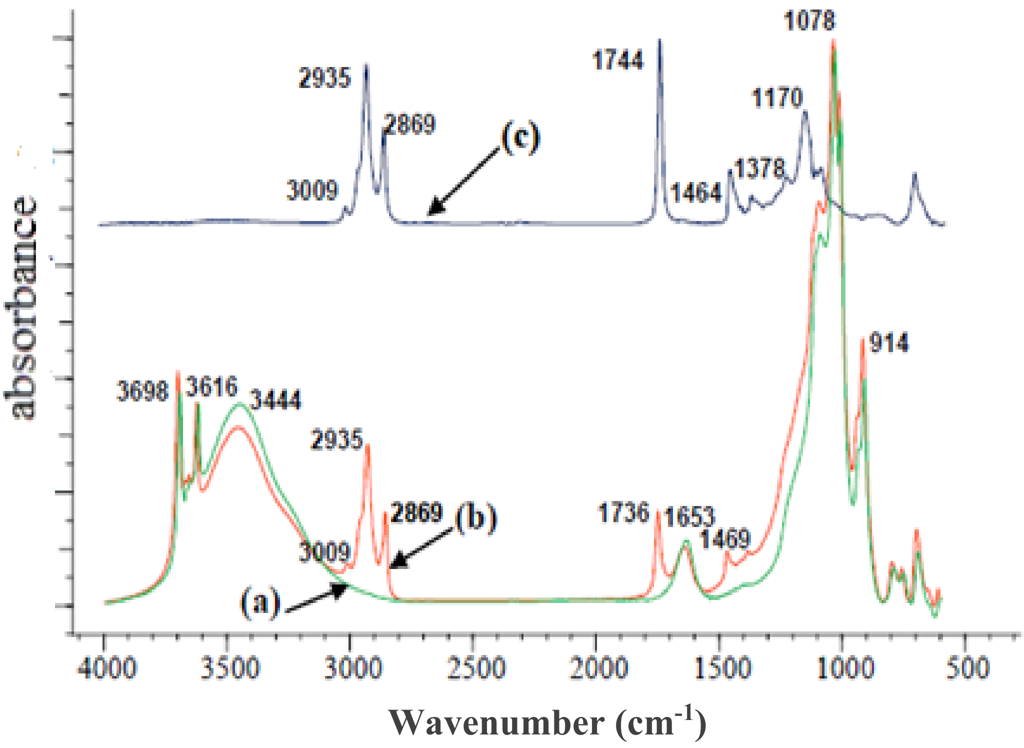

Figure 4.34 DRIFT spectra of GRC 0.5 (clay/acid ratio of 1:50) sample before (a), after (b) adsorption experiments, and crude rice bran oil (c).

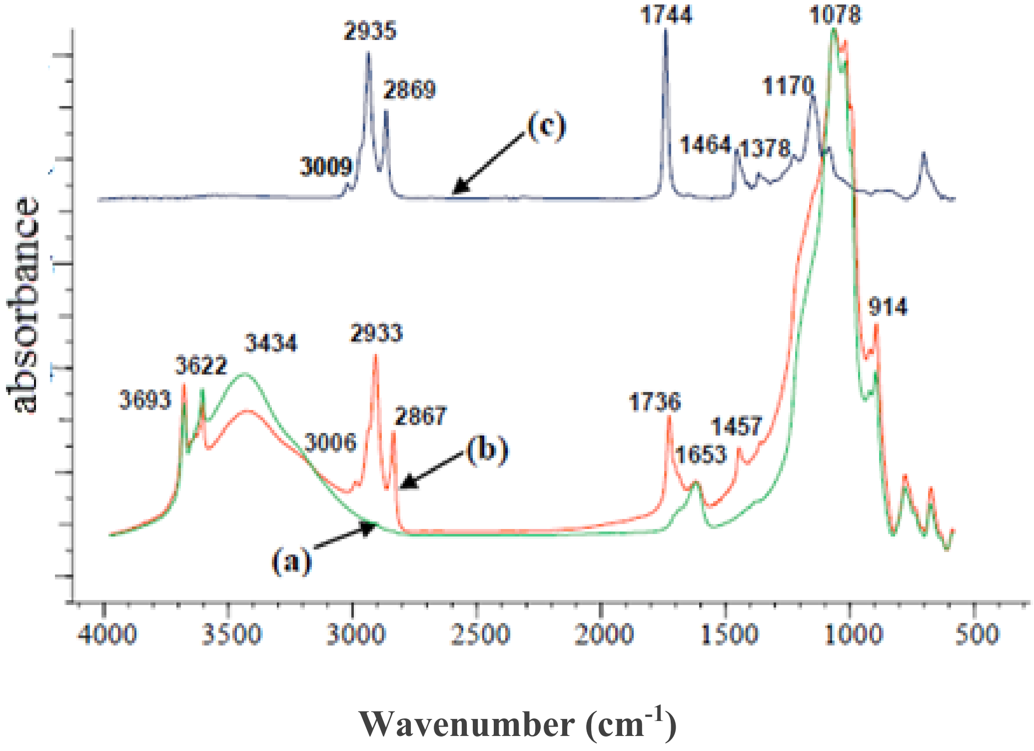

Figure 4.35 DRIFT spectra of GRO 0.1 sample (clay/acid ratio of 1:80) before (a), after (b) adsorption experiments, and crude rice bran oil (c).

4.1.7 Large scale bleaching of rice bran oil

Lab-scale bleaching of rice bran oil shows that the maximum bleaching capacity is obtained for GRS 0.3, GRH 0.5 and GRC 0.5 among each series of bleaching rice bran oil when the ground kaolin is treated with 0.5 M hydrochloric acid, 0.3 M sulfuric acid and 0.5 M citric acid, respectively. As compared with that of commercial bleaching clay, GRH 0.5 and GRH 0.7 give the better bleaching capacity during lab-scale experiment. Thus, the large-scale bleaching experiments are made to ascertain the optimum conditions of kaolin for bleaching rice bran oil. For this study, GRH 0.5 and GRC 0.5 are further analyzed their adsorption capacities by scaling up from lab- scale bleaching to large-scale bleaching. When performing the large-scale bleaching experiments (see section 3.1.5), the bleaching capacities of these activated kaolins are slightly inferior to that of commercial clay as shown in Table 4.18. However, these values are quite similar as those from laboratory-scale bleaching (Tables 4.17 and 4.18). This means ground kaolin treated with low acid concentrations can be prepared as adsorbent for vegetable oil bleaching.

Table 4.18 Bleaching capacities of activated kaolins (GRC 0.5 and GRH 0.5), and commercial bleaching clay

Sample (1:50 clay/acid ratio, 2% w/w)	Bleaching capacity (%)
Ground, dried at 80˚C and refluxed with 0.5M citric acid	
GRC	81.77 ± 0.02
Commercial clay	82.63 ± 0.03
Ground, dried at 80˚C and refluxed with 0.5M hydrochloric acid	
GRH 0.5	82.33 ± 0.02
Commercial clay	82.41 ± 0.01

The chemical properties of degummed and refined rice bran oil, and bleached rice bran oil using modified kaolins such as GRH 0.5 and GRC 0.5 are summarized in Table 4.19. The peroxide values of bleached rice bran oil are decreased where as the acid values are slightly increased after bleaching the degummend and refined rice bran oil. Upon bleaching, the free fatty acid value of oil is slightly increased from ~0.3 to ~0.4 (% oleic acid). The increase of free fatty acid in the bleached oil may be possible attribution of using acid-activated kaolin. Peroxide value is sharply decreased from 16 meq/kg to 8 meq/kg for GRH 0.5, and 10 meq/kg for GRC 0.5 due to the removal of oxidizing pigments such as pheophytin. Color reduction in activated ground kaolin (GRH 0.5 and GRC 0.5) also indicates that the color pigments from rice bran oil were removed after adsorption experiments.

Table 4.19 Chemical properties of initial degummed and refined rice bran oil, and bleached rice bran oil

Parameter	Degummed and refined rice bran oil	Bleached rice bran oil	
		GRH 0.5	GRC 0.5
Free fatty acid (% oleic acid)	0.28	0.39	0.39
Peroxide value (meq/kg)	16	8	10
Color (5¼”)			
Red	3.5	2.9	3.2
yellow	65	36	36

4.2 Part II: Correlation between the morphology of synthetic kaolinites on their sorption properties

4.2.1 Characterization of the synthetic kaolinites

1. X-ray diffraction analysis

XRD powder patterns of the Starting Material (SM) and synthetic kaolinites are shown in Figure 4.36. For samples prepared in acidic conditions ($0.8 \leq pH_F \leq 5.1$), narrow and intense peaks, corresponding to d_{001} and d_{020} reflections (~7.16 and ~3.57Å respectively) of kaolinites, are observed (Figure 4.36). This suggests that such kaolinites are well-crystallized and contain low defect. These peaks become weak and broad with increasing pH_F. For $pH_F \geq 7.4$, less crystallization is occurred. Pseudo-boehmite peaks are identified at 14 and 28° (2θ) for samples synthesized under both acidic and basic conditions (from pH_F 0.8 to pH_F 8.3) and a supplementary broad peak occurred at 6-9 °(2θ) for the samples synthesized under the most basic conditions (pH_F 7.9 and pH_F 8.3) (see Figure 4.36). Boehmite is a chemical precursor of kaolinite (Tsuzuki, 1976) and kaolinite is favorably formed from the starting material containing soluble alumina and silica due to the high rate of solution with respect to amorphous alumina and subsequent supersaturation with respect to boehmite at lower temperature (Carr and Dioxan, 1967). Fialips et al., 2000 also observed the same pseudo-boehmite broad peak at 6-7 °(2θ) in the kaolinite synthesized at final pH 8.4, and concluded that it is associated with a synthetic form of paragonite.

A general positive relationship between synthesis pH and the amount of defects is observed (see Figure 4.37A). HI value is almost constant in acidic pH ($0.8 < pH_F < 5.1$) and decreases for $pH_F > 5.1$. Miyawaki et al. (1991) and Fialips et al. (2000) reported that HI is directly proportional to the kaolinite yield. This means that the crystallization percentage of SM in the synthetic products is higher when final pH of crystallization is acid than when it is basic, as it was observed by Fialips et al. 2000. The R_2 parameter decreases with an increase of the final pH (Figure 4.37B) revealing that samples synthesized in basic conditions have a more monoclinic character than samples obtained in acid conditions.

The pH of the synthesis has a strong effect too on the apparent CSDs both along the c*axis and b axis (Figure 4.38). Note that the effect is globally twice stronger along the c*axis. However, for pH up to 5, the CSD_{001} which is assimilated to the particle thickness does not vary. This is in agreement with Fialips et al. (2000) who observed that CS_{001} did not change significantly up to pH_F 5.5 while this parameter decreased slightly when the final pH of synthesis was above 5.5.

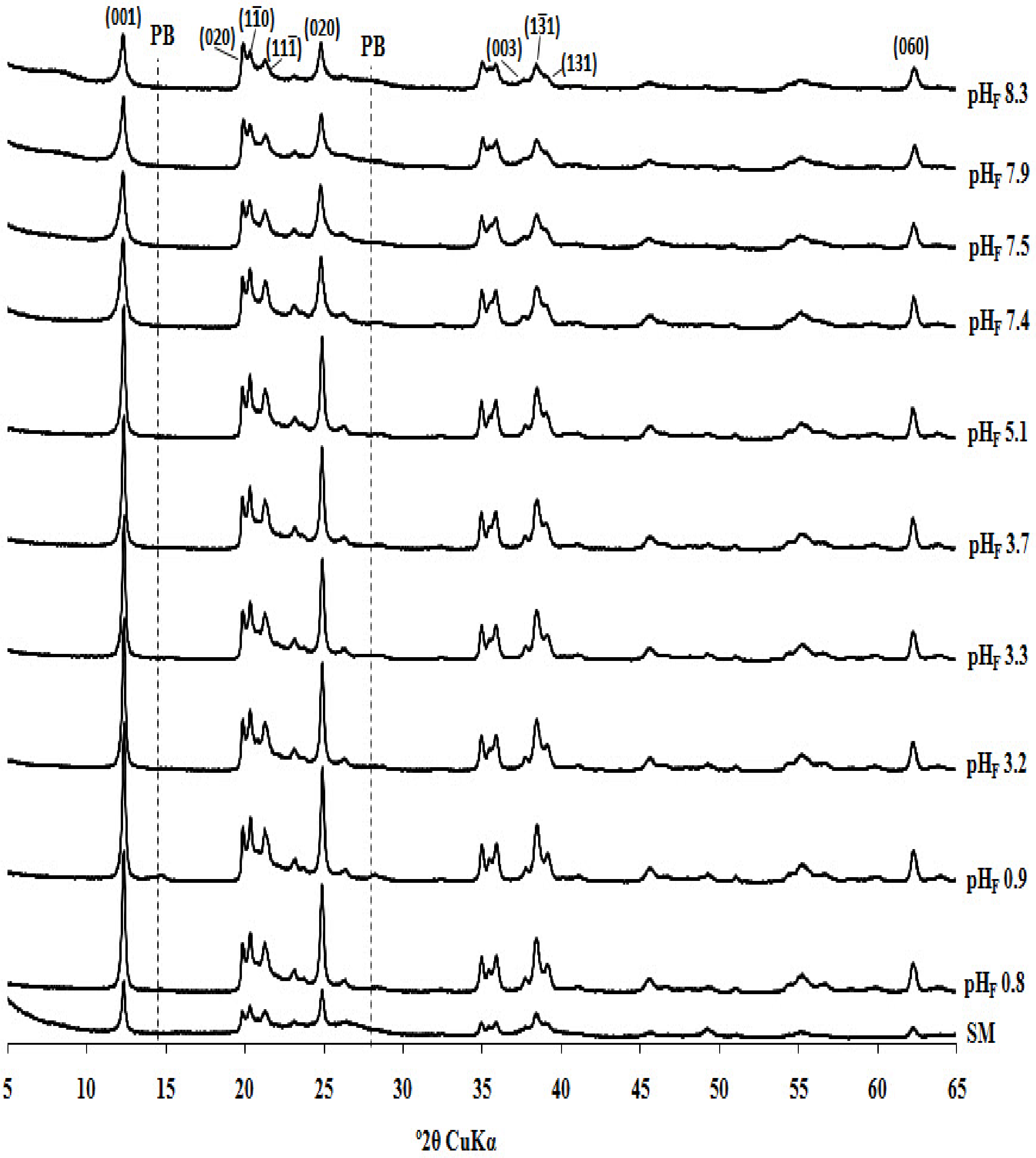

Figure 4.36 XRD patterns (bulk powder) of Starting Material (SM) and the synthesized kaolinites (pH_F: pH measured at the end of synthesis)

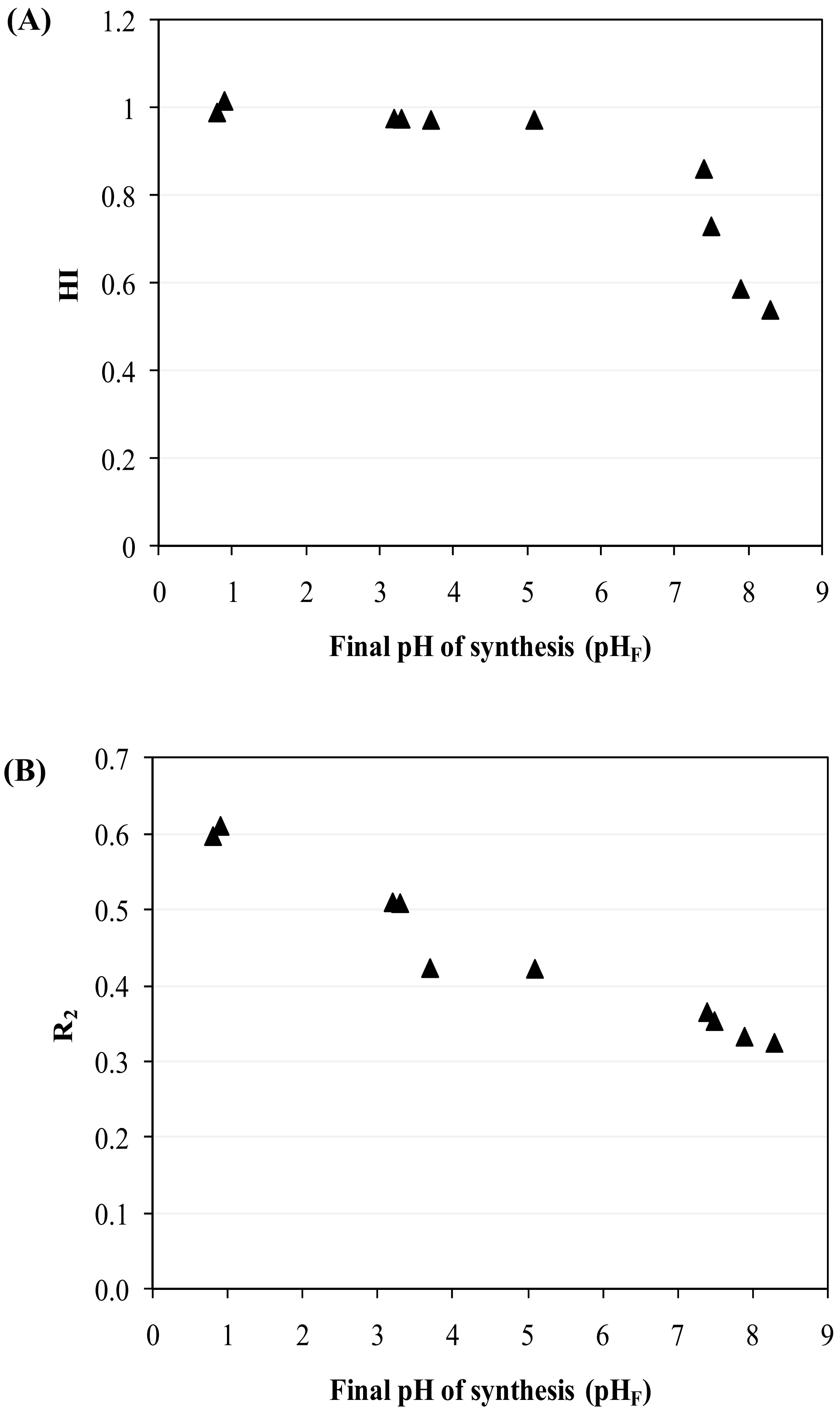

Figure 4.37 Relation between crystallinity indices, Hinckley index (HI) (A) and R_2 of the synthetic kaolinites (B) with their final pH of synthesis

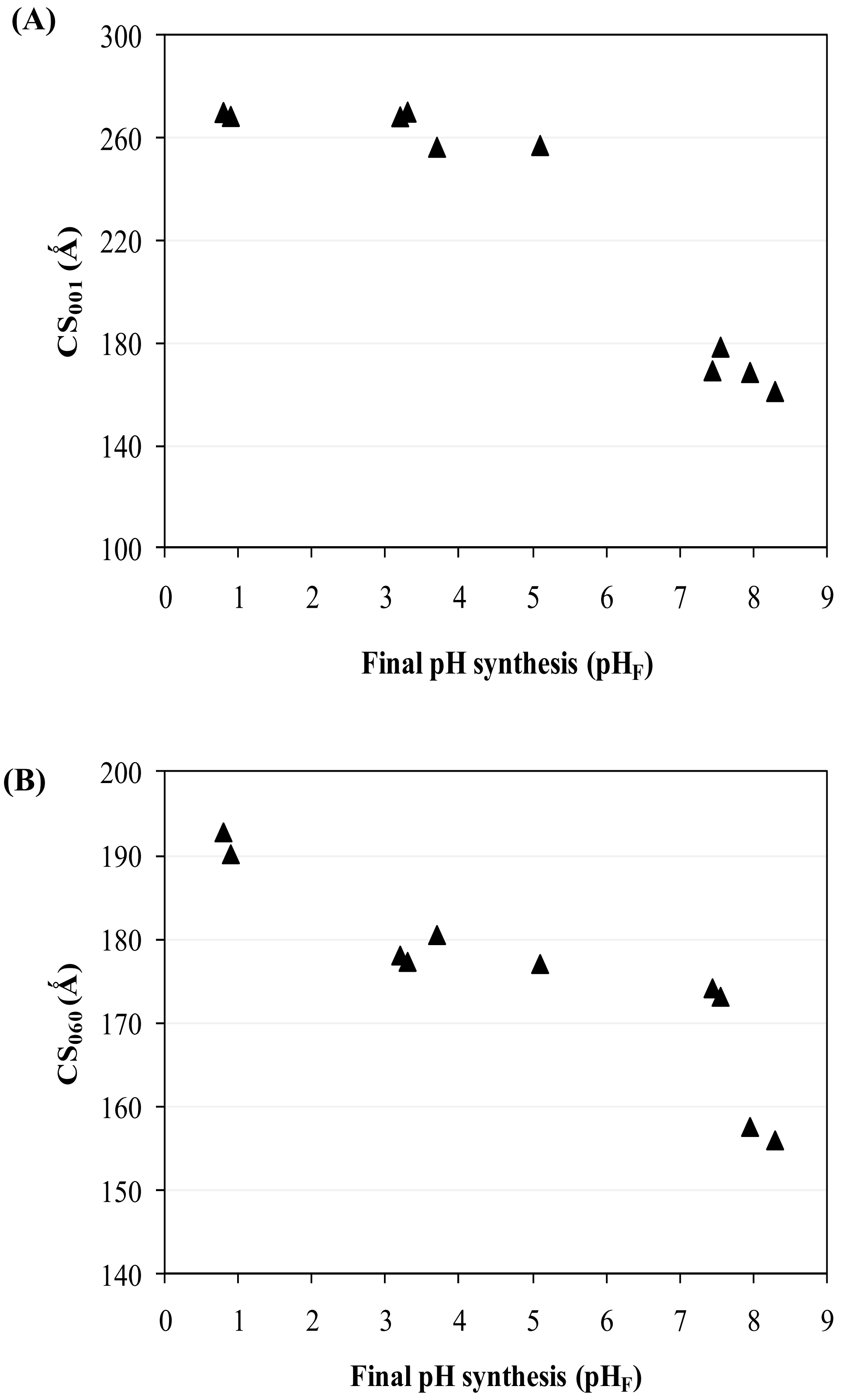

Figure 4.38 Size of the coherent domain of the synthetic kaolinites plotted as a function of the final pH of synthesis. Data are calculated with d_{001} (A) and d_{060} reflections (B) obtained from XRD patterns recorded for bulk samples.

2. Fourier Transform Infrared Spectroscopy (FTIR)

The FTIR spectra of kaolinites synthesized at different final pH are shown in figure 4.39. For most of the samples, the four typical hydroxyl bands of kaolinite can be observed at 3693, 3668, 3651 and 3620 cm^{-1} (Van der Marel and Krohmer, 1969). Bands are more intense and well-resolved for samples prepared in acidic conditions ($0.8<pH_F<5.1$). This suggests that these samples are well-ordered (Fialips et al., 2000). In contrast, peaks intensities decrease and the 3668 and 3651 cm^{-1} bands merge into a broad band for samples prepared at higher pH_F. Concomitantly, a shoulder appears at around 3600 cm^{-1} which could be due to the intrinsic disorder nature of the kaolinite synthesized at $pH_F>5$. In the 400-1400 cm^{-1} range, the observed bands correspond to kaolinite (Farmer and Russel, 1964; Russell, J.D., 1987; Petit, 2006), and no other compound can be observed, except for the SM in which part of unreacted product and boehmite may be identified by the band at around 500 cm^{-1} (Fialips et al., 2000).

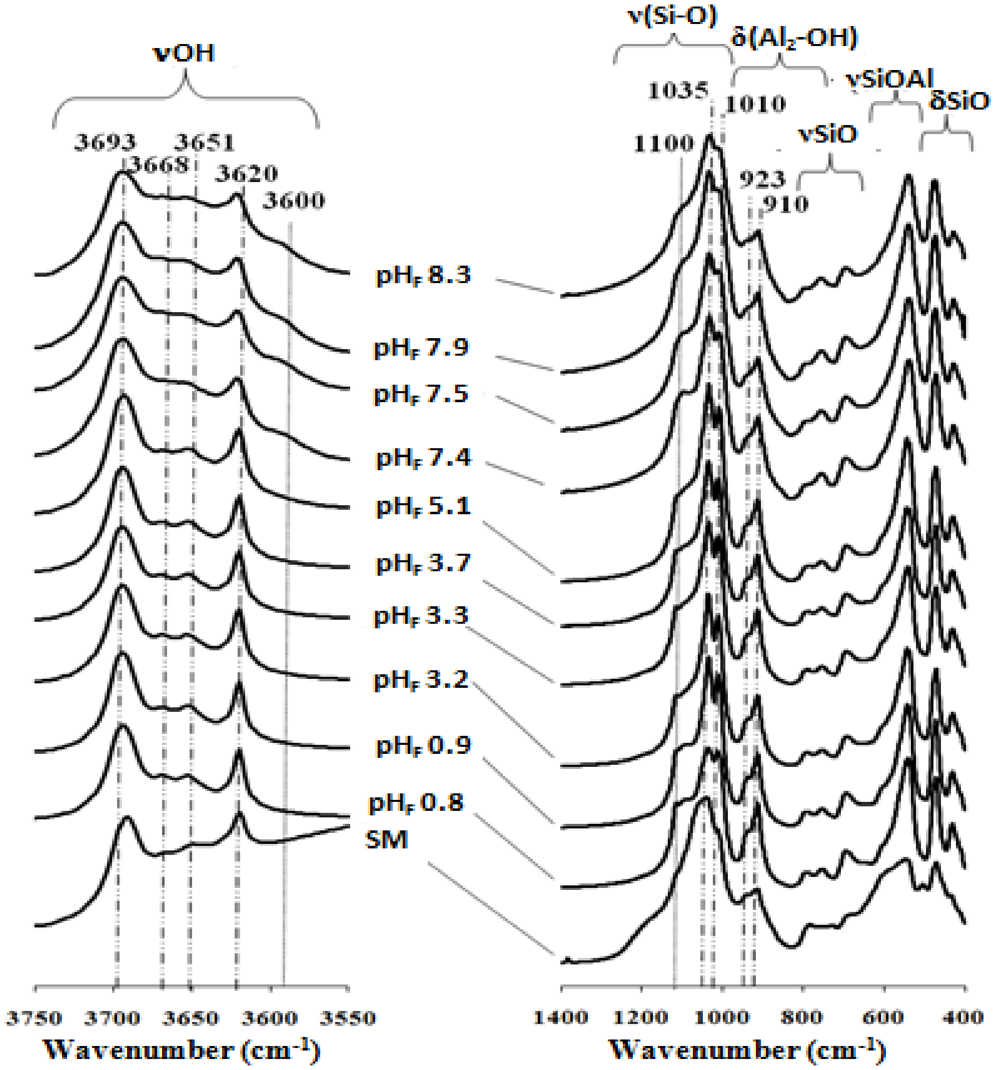

Figure 4.39 FTIR spectra of Starting Material (SM) and synthetic kaolinites as a function of final synthesis pH.

3. Transmission Electron Microscopy

Transmission electron micrographs of kaolinites synthesized at pH_F 0.8, 3.3, 5.1, 7.4, 7.9 and 8.3 exhibit hexagonal shape with an increase of the anisotropy when pH increases (Figure 4.40) leading to lath-shaped kaolinites for $pH_F \geq 7.4$. Fialips et al., 2000 hypothesized that the elongation of particle is promoted by the sorption of sodium on kaolinite lateral surfaces. The lath morphology is not common for natural kaolinite. KGa--1b as well-crystallized kaolinite showed a platy hexagonal morphology (not shown) (Pruett and Webb, 1993).

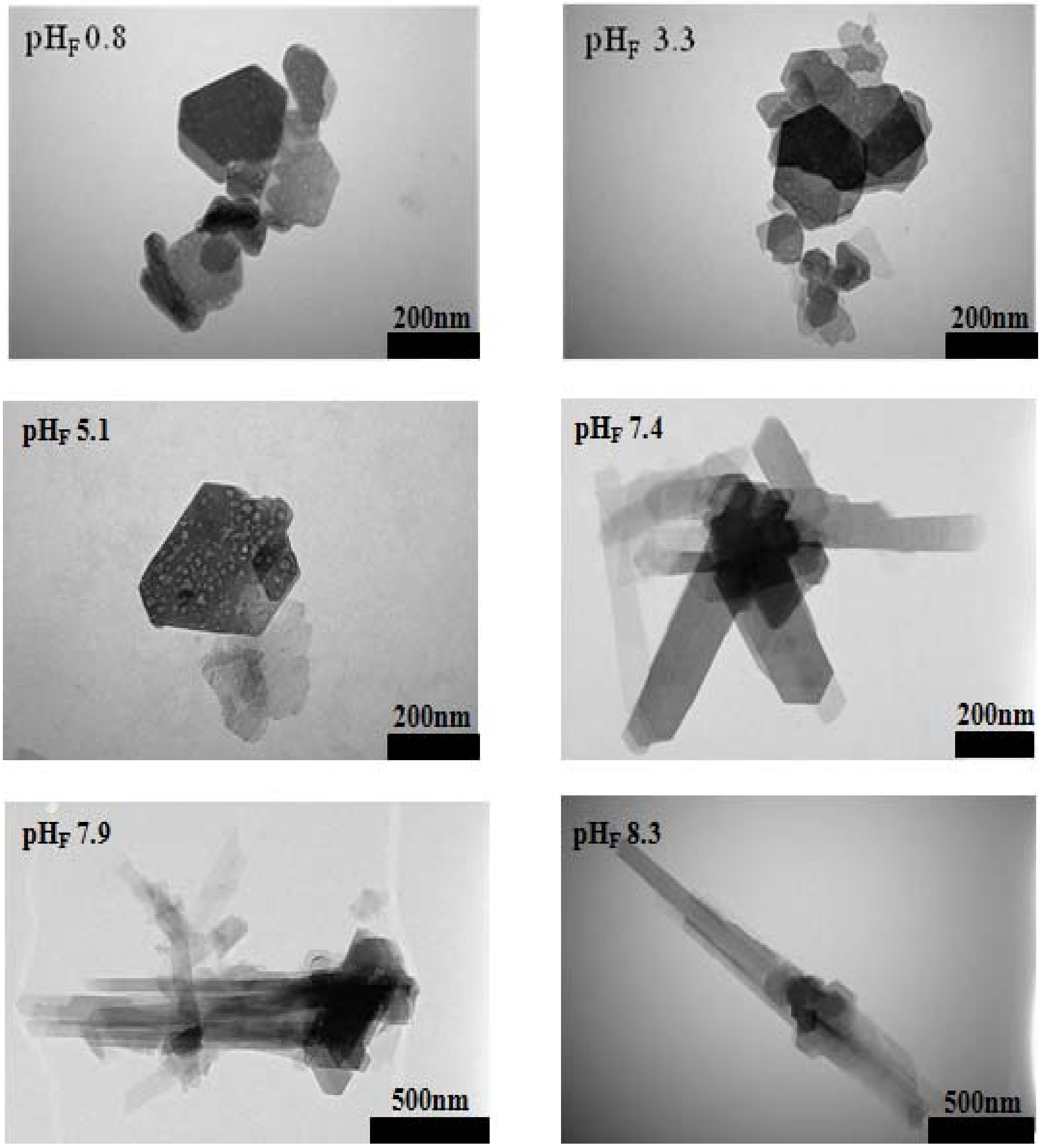

Figure 4.40 Transmission electron micrographs of some synthetic kaolinites synthesized at pH_F 0.8, pH_F 3.3, pH_F 5.1, pH_F 7.4, pH_F 7.9 and pH_F 8.3.

4.2.2 Brunauer-Emmet-Teller (BET) method and morphological parameters

The specific surfaces areas of both lateral and basal surfaces, and BET surface area of some synthetic kaolinites are shown in Table 4.20. The average specific surfaces for lateral and basal surfaces of the acidic samples (for pH$_F$ 0.8 and pH$_F$ 3.3) are 6.6 m^2/g and 28.3 m^2/g, respectively. The total surface obtained by geometric considerations is 34.9 m^2/g which is slightly higher than the BET surface area of those samples (23.1 and 24.1 m^2/g). Similar results was also found by Macht et al. (2011) who reported that AFM images calculation gave a higher surface area than the mean BET surface for illite particles. They assumed that the preparation of their clay suspension in NaOH solution, following by a sonication of their suspension before AFM analysis resulted in delamination of the clay particles, which in turn induced a higher specific surface than the one obtained with BET measurement with a dried sample. In this study, the kaolinite samples were gently crushed with mortar and dispersed in distilled water with sonification before TEM analysis. Then, this treatment may slightly increase the surface area deduced from TEM images as compared with that obtained with BET analysis. For kaolinite synthesized at high pH$_F$, the SSA obtained from geometric consideration are ~54 m^2/g for sample synthesized at pH$_F$ 7.4, and 55 m^2/g for sample synthesized at pH$_F$ 8.3. Note that these values are in good agreement with values derived from BET analysis (54 m^2/g), proposing that the obtained lateral surface is robust. The lateral specific surfaces expressed in percentage of the total surface area 19% for samples synthesized in acidic conditions (pH$_F$ 0.8 and pH$_F$ 3.3), and around 14% for samples synthesized in neutral conditions (pH$_F$ 7.4 and pH$_F$ 8.3). These values are in well agreement with percentage values proposed in literature for most of the well crystallized or not kaolinites (Cases et al., 1986). Well-crystallized kaolinite KGa--1b has a BET surface area of 11.6 m^2/g and the edge area represents from 20 to 30% of the total surface area (Wan and Tokunaga, 2002). Although the kaolinites prepared in acidic conditions (pH$_F$ 0.8 and pH$_F$ 3.3) in this study have higher BET surface area than KGa--1b, their percentage of edge surface is slightly inferior to that of KGa--1b. This confirms that the synthetic kaolinites prepared in acidic conditions are well-crystallized as proven above by XRD, FTIR and TEM analysis (see Figures 4.36, 4.39 and 4.40).

Table 4.20 Specific surfaces obtained from geometrical considerations for both lateral and basal surfaces, and BET surface area measured for synthetic kaolinites.

Samples	average basal surface (nm^2)	Full-Width Half-Maximum at d$_{001}$ peak [FWHM (°2θ)]	average thickness (nm)	average lateral surface (nm^2)	average specific surface for lateral surfaces (m^2/g)	average specific surface for basal surfaces (m^2/g)	total surface obtained considering geometric considerations (m^2/g)	BET surface (m^2/g)
pH$_F$ 0.8	34640	0.296	27	16200	6.6	28.3	34.9	23.1
pH$_F$ 3.3	51961	0.296	27	24300	6.6	28.3	34.9	24.1
pH$_F$ 7.4	65550	0.475	16.7	23046	8	45.7	53.7	54
pH$_F$ 8.3	91500	0.499	16.1	29463	7.6	47.4	55	54

4.2.3 Cation exchange capacity (CEC) and relation with mineralogy

Cation exchange capacity of synthetic kaolinites measured at pH=9 are shown in figure 4.41 as a function of the final pH of synthesis. CEC of kaolinites are highly variable. Indeed, CEC measured for samples synthesized in acid conditions ($0.8<pH_F<5.1$) are close to 1 $cmol_c$/kg whereas CEC increases dramatically to 33 $cmol_c$/kg for samples prepared in basic conditions ($pH_F=8.3$). Low CEC measured for samples prepared in acid conditions demonstrates that the permanent charge of synthetic kaolinites is equal to 0. This contrasts with natural kaolinites, such as KGa--1b, for which CEC due to permanent charge is around 0.6 $cmol_c$/kg according to Wan and Tokunaga (2002) whereas the total CEC (due to both permanent and variable charge) of the same material is around 2 $cmol_c$/kg in neutral pH conditions (Van Olphen and Fripiat, 1979). For the samples synthesized in acid conditions ($pH_F<5.1$), CEC value is then only due to the contribution of edge sites (silanol and aluminol). However, the values reported are minimal due to the fact that all edges are not necessary deprotonated and then available for Na^+ cations at the pH used during the measurement (pH=9). Indeed, the CEC of mineral depends on the pH of the solution (Tournassat et al., 2004a; Tournassat et al., 2004b; Itami and Fujitani, 2005). Sharp increase of CEC for sample prepared in basic pH may be due to the increase of surface area or to the presence of secondary phases in the synthetic products. As demonstrated in the section devoted to XRD and FTIR results, no secondary phases were detected other than pseudo-boehmite for sample prepared at $pH_F=7.4$. This was detected around 14 and 28°(2θ) (see Figure 4.36). However, this phase was also detected at this angular region for samples synthesized at lower pH and for which CEC are very low (1 $cmol_c$/kg). Such behavior proposed that the relative high CEC measured for sample synthesized at $pH_F=7.4$ is not due to mineralogical impurities, as pseudo-boehimite, but to a different morphology for this sample compared to samples prepared in acidic conditions (lath *vs* hexagon). Note however, that the very high CEC values (>20 $cmol_c$/kg) for samples prepared at $pH_F>7.4$ may be due to swelling pseudo-boehmite, since this phase have been revealed by XRD pattern recorded for orientated preparations (Figure 4.42).

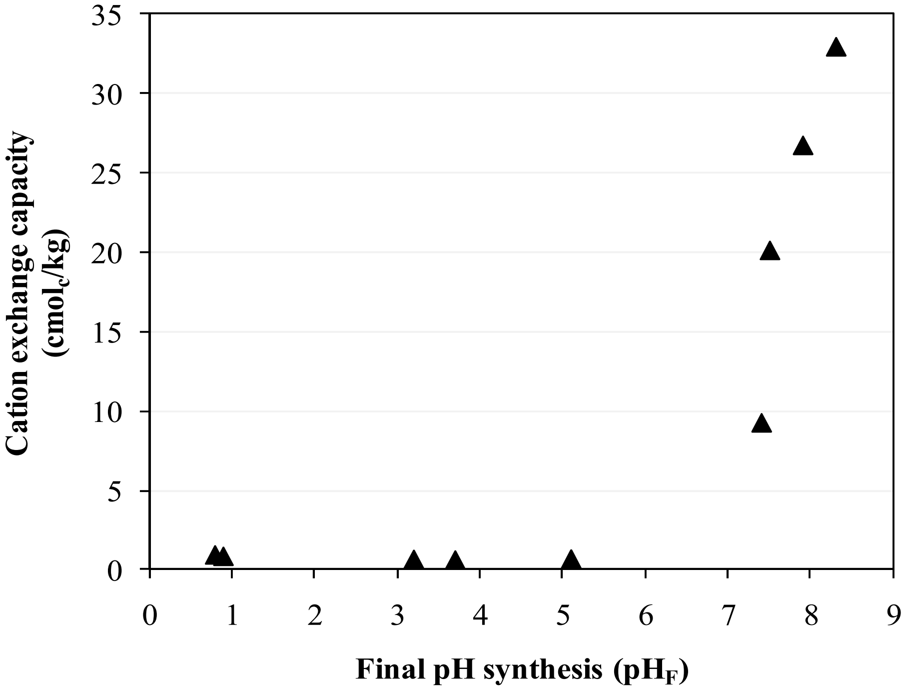

Figure 4.41 Cation-exchange capacities of kaolinites measured at pH=9 as a function of the synthesized final pH of the kaolinite.

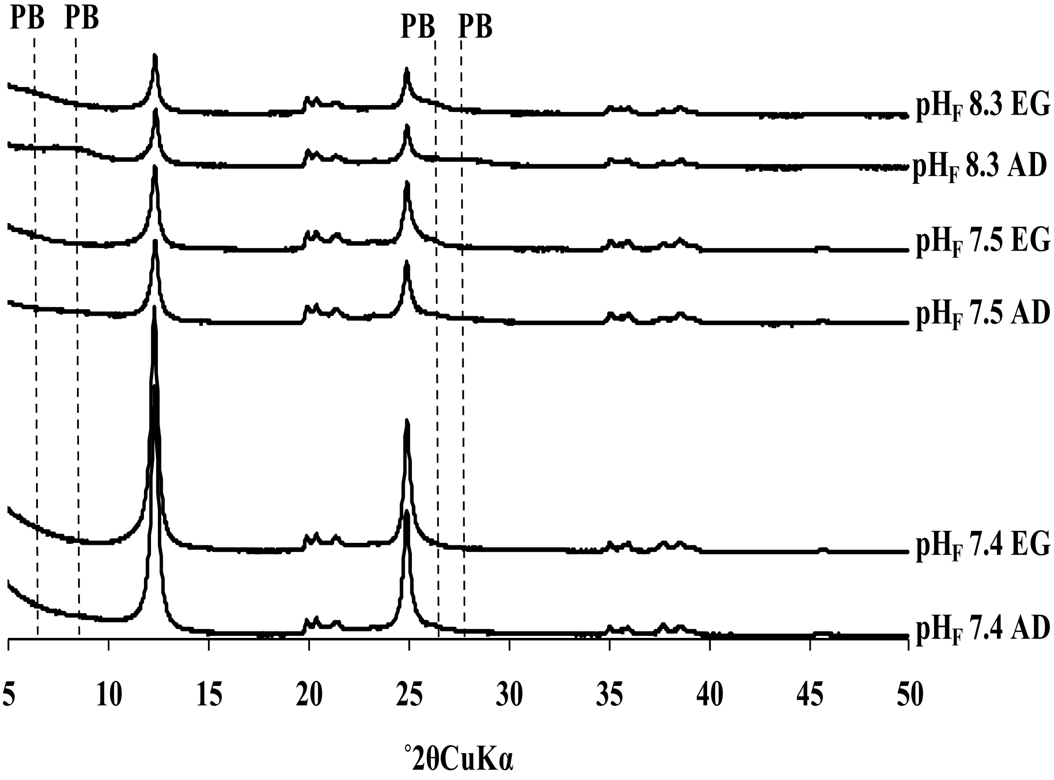

Figure 4.42 XRD patterns (oriented preparations) of kaolinites synthesized at pH$_F$ 7.4, 7.5 and 8.3 after heating at 120°C; AD= samples prepared with Air-Dried treatment and EG= samples prepared with Ethylene-Glycol treatment.

4.2.4 Na^+/H^+ sorption isotherms

Figure 4.43A shows the number of mol of Na^+ sorbed on kaolinites synthesized at pH_F 0.8, 3.3, 7.4, and 8.3, and on low-defect Georgia kaolinite KGa--1b, as a function of pH. This figure shows that sorption of Na^+ strongly increases with increasing pH. This is in agreement with previous studies dealing with exchange between Na^+ and H^+ cation on clay surfaces (Nolin, 1997; Tournassat et al., 2004a; Tertre et al., 2013) and is directly related to sorption of Na^+ onto the deprotonated edges. At pH=3 and 4 a relative high sorption of Na^+ is observed for Georgia kaolinite KGa--1b compared to values obtained at higher pH (Figure 4.43B). After washing with a saline, acid solution (NaCl/HCl) to remove the possible organic compounds, the Na^+ sorption of KGa--1b at pH=3 and 4 decreased to 0 (not shown). This indicates that the high sorption of Na^+ in KGa--1b at pH 3 and 4 is due to the presence of organic impurities. The permanent charge and edge site density proposed in literature for KGa--1b were equal to 0.6 and 0.8 $cmol_c$/kg, respectively (Schroth and Sposito, 1997) (see Figure 4.43C). The sum of the two charges is then equal to 1.4 $cmol_c$/kg. CEC measured at pH=9 in the present study for this sample is 0.78 $cmol_c$/kg. This value is higher than the permanent charge but lower than the sum of the permanent charge and the edge charge proposed by Schroth and Sposito, 1997. The total deprotonation of the aluminol and silanol sites at the edges of kaolinite occurs at very high pH (pKa2 of >aluminol and >silanol, respectively equal to ~9.38 (Tertre et al., 2006; Martinez et al., 2010) and ~9.5 (Helling et al., 1964). Then, at pH=9, the pH value used for CEC measurements, all edges were not deprotonated. The measured CEC value (0.78 $cmol_c$/kg) is in agreement with values proposed by Schroth and Sposito (1997). Such results obtained with KGa--1b fully validate this approach and proposing that this experimental method can be used with good confidence to assess a possible effect of the morphology of the particles on kaolinite sorption properties.

For synthetic kaolinites prepared at acidic pH (for pH_F 0.8 and pH_F 3.3), very low sorption of Na^+ occurs at pH<7, and sorption increases dramatically in basic conditions due to the sorption on silanol and aluminol groups located at the edges of the particles (see Figure 4.43B). In contrast to KGa--1b, there is no sorption of Na^+ until the pH reached 7. This indicates that there is no permanent charge in these synthetic kaolinites and the high Na^+ sorption in basic pH is only due to the contribution of edge charges (Ganor et al., 2003). Smilar results are obtained with the kaolinite synthesized at pH_F=7.4. The amount of Na^+ sorbed on pH_F 7.4 is approximately zero at low pH until it reaches pH=6 indicating that this sample has no permanent charge. However, at above pH~8, the sorption sharply increases to 12 $cmol_c$/kg at pH~10 (Figure 4.43A). For sample synthesized at pH=8.3, the amount of Na^+ sorbed on the sample is very low until pH =5, while sorption dramatically increases for basic pH conditions. The high sorption of Na^+ in neutral conditions (pH~6.5) on sample prepared at pH_F 8.3 is in relation to a significant Na^+ sorption on the swelling pseudo-boehmite; phase detected in the XRD pattern recorded for orientated preparation (Figure 4.42). This significant contribution is also related to the poor crystallinity and high surface area already mentioned for this sample.

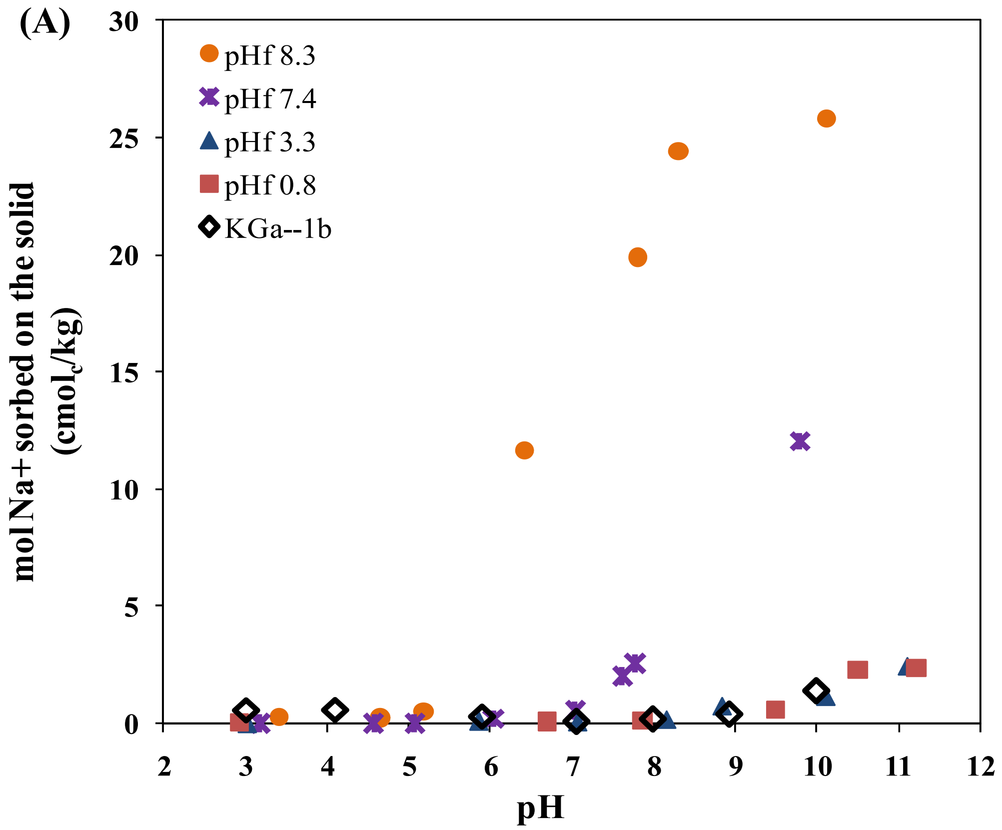
(A)
pHf 8.3
pHf 7.4
pHf 3.3
pHf 0.8
KGa--1b
mol Na+ sorbed on the solid
($cmol_c$/kg)
0
5
10
15
20
25
30
pH
2
3
4
5
6
7
8
9
10
11
12

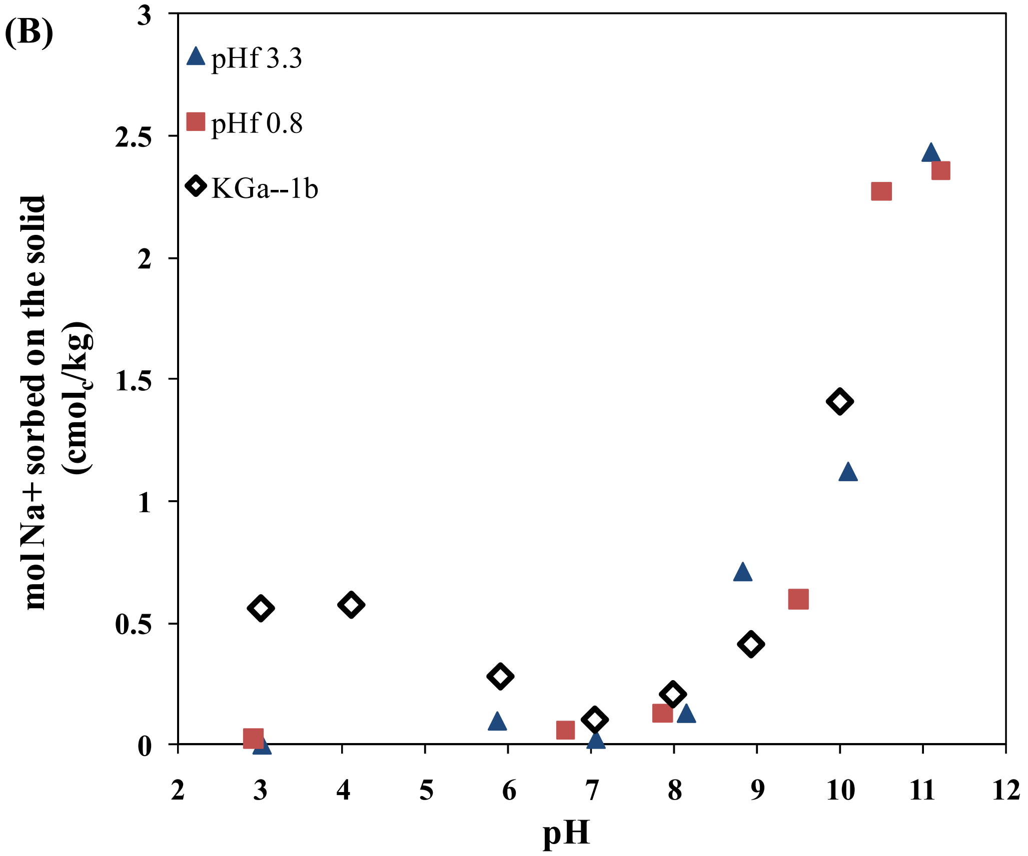
(B)
pHf 3.3
pHf 0.8
KGa--1b
mol Na+ sorbed on the solid
($cmol_c$/kg)
0
0.5
1
1.5
2
2.5
3
pH
2
3
4
5
6
7
8
9
10
11
12

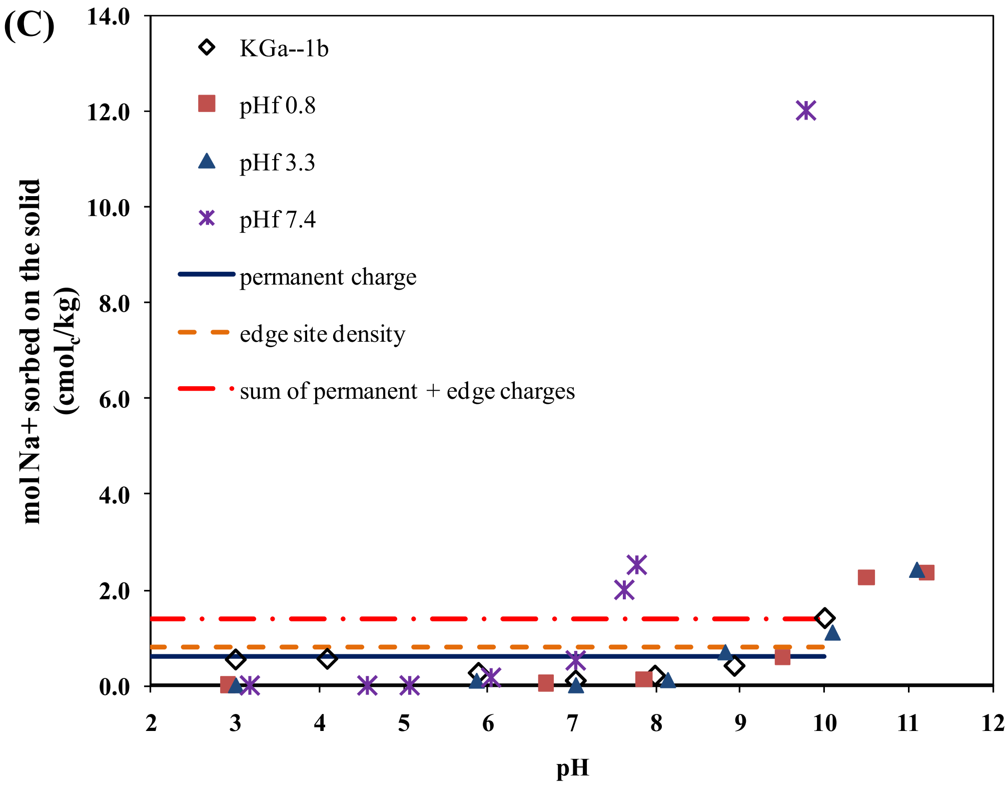

Figure 4.43 (A) Comparison of whole Na^+/H^+ sorption isotherms obtained with synthetic kaolinite synthesized at pHF 0.8, 3.3, 7.4, and 8.3 and low defect Georgia kaolinite KGa--1b. (B) Zoom of the isotherms obtained with low defect Georgia kaolinite KGa--1b and synthetic kaolinites synthesized at pHF 0.8 and 3.3, (C) Comparison of Na^+/H^+ sorption isotherms obtained with KGa--1b and synthetic kaolinites. The contributions due to permanent charge and edge site for KGa--1b are reported and issued from Schroth and Sposito (1997).

In order to assess the stability of the kaolinite surface during Na^+/H^+ isotherm (constant edge site density), dissolution was followed. Data are reported in figure 4.44, in term of massic percentages of solid dissolved during experiments, and percentages of edges dissolved, versus pH. Assuming that the edge site density can be considered constant (no significant dissolution) if the percentage of edge site dissolved during experiments is <10 %. In this context, Na^+/H^+ isotherms can be interpreted with a constant sorption site density (no dissolution) when pH is between 4 and 10 whatever the particle size and morphology (except for isotherm performed with sample synthesized at pHF 8.3).

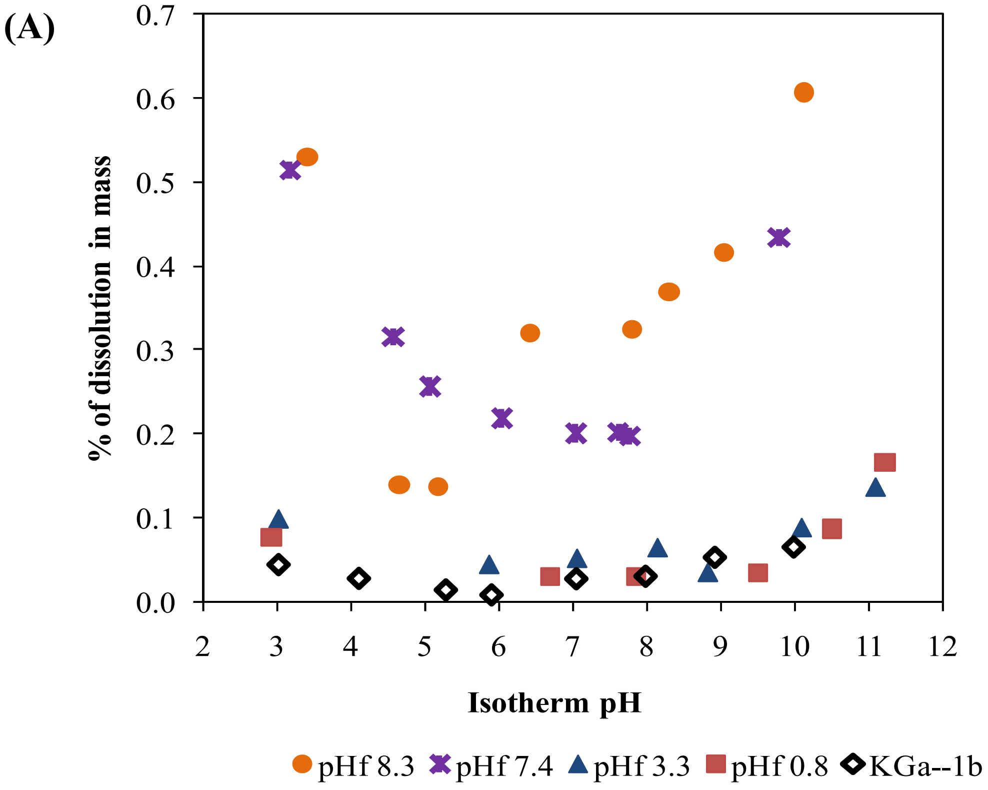

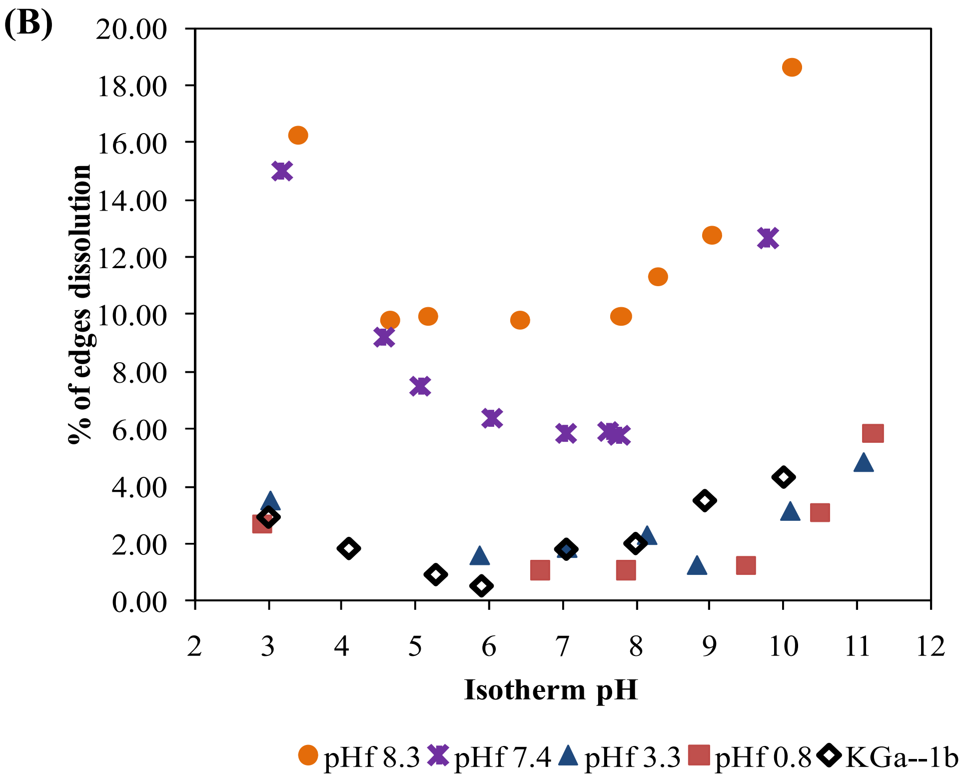

Figure 4.44 Dissolution data plotted as a function of the equilibrium pH measured all along the Na^+/H^+ isotherms and obtained from measurements of silica aqueous concentrations. (A) Representation using massic percentages of solid dissolved during experiments. (B) Representation using percentages of edges dissolved during

experiments. Data are relative to experiments carried out with kaolinite synthesized at pH_F 0.8, 3.3, 7.4 and 8.3, and Na-Georgia Kaolinite (KGa--1b) (see text for the details of the calculations).

4.2.5 Thermodynamic Modeling: effect of hexagonal/lath-shaped morphology on selectivity coefficient values

The isotherms obtained for samples synthesized at pH_F 0.8 and pH_F 3.3 are rigorously superimposed demonstrating that both kaolinites have exactly the same sorption properties (Figure 4.43). Moreover, both solids have the same morphologies and specific surfaces of both basal and lateral sites (Table 4.20 and Figure 4.40). Then, the two experiments data sets for these two samples were merged, and the edge site densities as well as selectivity coefficients between H^+ and Na^+ are assumed to be the same for these two solids. In contrast, isotherms obtained for kaolinites synthesized at pH_F 7.4 and pH_F 8.3 are not superimposed, although both solids have the same lath morphology (see Figure 4.40); this behavior is probably due to a significant proportion of secondary phase (pseudo-boehmite) as shown in XRD patterns (figures 4.36 and 4.42) for sample synthesized at pH_F 8.3. Then, selectivity coefficient between Na^+ and H^+ cations for sample prepared at $pH_F=8.3$ is not given since this sample does not correspond to a pure kaolinite sample. Finally, selectivity coefficients between Na^+ and H^+ cations on pure kaolinite synthesized at pH_F 0.8 and pH_F 7.4 differing only by morphology (hexagonal-shaped *vs* lath-shaped) are calculated using a surface complexation model without electrostatic term.

Considering that Na^+ and H^+ cations were sorbed on the lateral edge sites of the kaolinites only since the samples have not permanent charge. For hexagonal particles, we supposed that there is the same contribution of the three faces: (010), (110) and ($1\bar{1}0$), whereas only one type of face is supposed for lath particles: (010) face. According to edge site densities proposed by Koretsky et al. (1998) for each of these faces (in sites/nm^2) and the specific surface of lateral sites estimated in this study for both morphology particles (in m^2/g), total edge site densities are calculated to be equal to 11.7 and 20 mmol/100g for hexagonal and lath shaped particles, respectively. Protonation and deprotonation constants for edge sites are fixed whatever the particle shape, and are common values proposed in literature for aluminol/silanol sites onto the edges of kaolinite. The protonation of the silanol sites is assumed to be unreactive in this study (see Tertre et al., 2005) and the value considered for deprotonation of the aluminol site is that proposed by Brady et al. (1996). Furthermore, deprotonation constant for the whole silanol/aluminol edge site corresponds to an average value reported in literature for both silanol and aluminol sites (Brady et al., 1996 and Tertre et al., 2005). Moreover, the reactivity of the aluminol sites located in the gibbsite sheet was not considered, due to the coordination of the Al atoms, which leads to no reactivity of such sites in the [3, 11] pH range (see discussions in Huertas et al. (1998) and Tertre et al. (2006)). When the kaolinite was hexagonal-shaped, log $Kc(Na^+/H^+)$ of -5.5 was required to interpret experimental data, whereas for lath-shaped particles, log $Kc(Na^+/H^+)$ of -4.7 was needed. These results show that the Na^+/H^+ selectivity coefficient depend on the kaolinite's size/morphology. Comparison between experimental and predicted data is reported in Figure 4.45, while the model is described in Table 4.21.

Table 4.21 Selectivity coefficients proposed in this study with a surface complexation model to interpret Na^+/H^+ isotherms obtained for hexagonal and lath particles of pure kaolinites. Associated edge site densities assessed from surface area of lateral sites and crystallography data are 11.7 and 20 mmol/100g for hexagonal and lath shaped particles, respectively (see text for explanations).

Ion-exchange reaction	log K (25°C)	Observations
$>H^+ + XaOH = XaOH_2^+$	2.33	The value is given for aluminol site by Brady et al. (1996).
$>XaOH = XaO^- + H^+$	-7	An average value between the deprotonation value for both aluminol and silanol sites (Brady et al., 1996 and Tertre et al., 2005)
$>XaOH + Na^+ = XaONa + H^+$	-5.5	hexagonal-shaped
	-4.7	lath-shaped

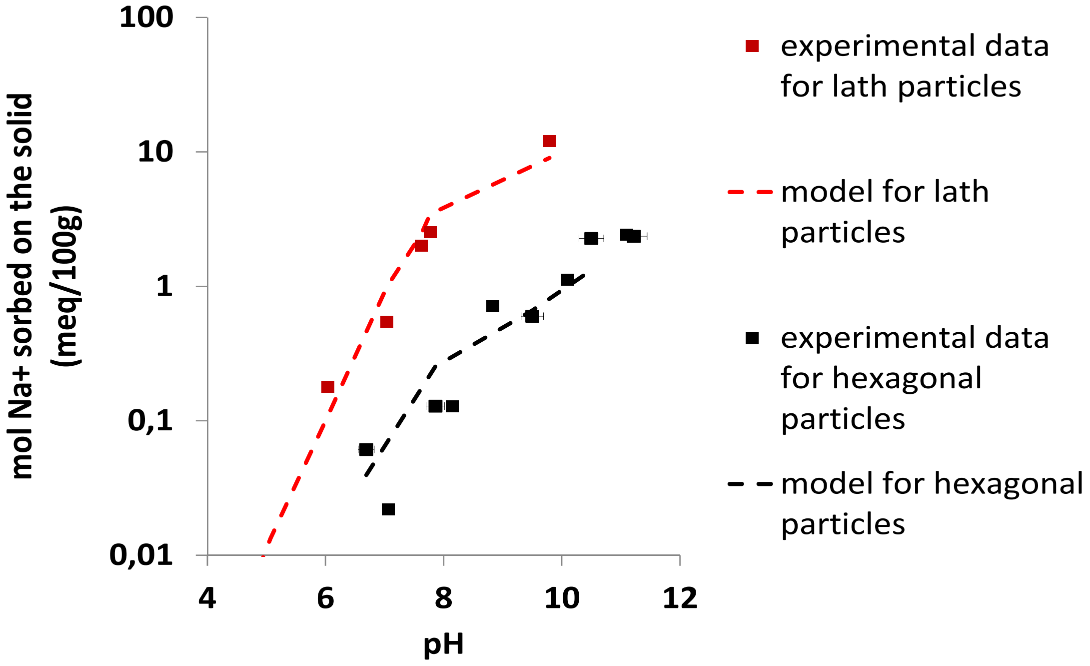

Figure 4.45 Comparison between experimental data and fitted ones using a surface complexation model, without electrostatic term, for Na^+/H^+ sorption isotherms obtained from hexagonal and lath particles. The predicted curves are obtained by calculating edge site densities from morphology particles (specific surfaces of lateral sites) and crystallography data for (010), (110) and $(1\bar{1}0)$ faces from Korestsky et al. (1998).

For testing the sensibility of the model, the value describing sorption on hexagonal particles (log $Kc(Na^+/H^+)$ of -5.5) is used to predict the sorption on lath particles. The prediction of sorption on lath with constant fitting data of hexagonal particles is shown as green curve (Figure 4.46). The result showed that green curve cannot interpret correctly sorption on lath particles.

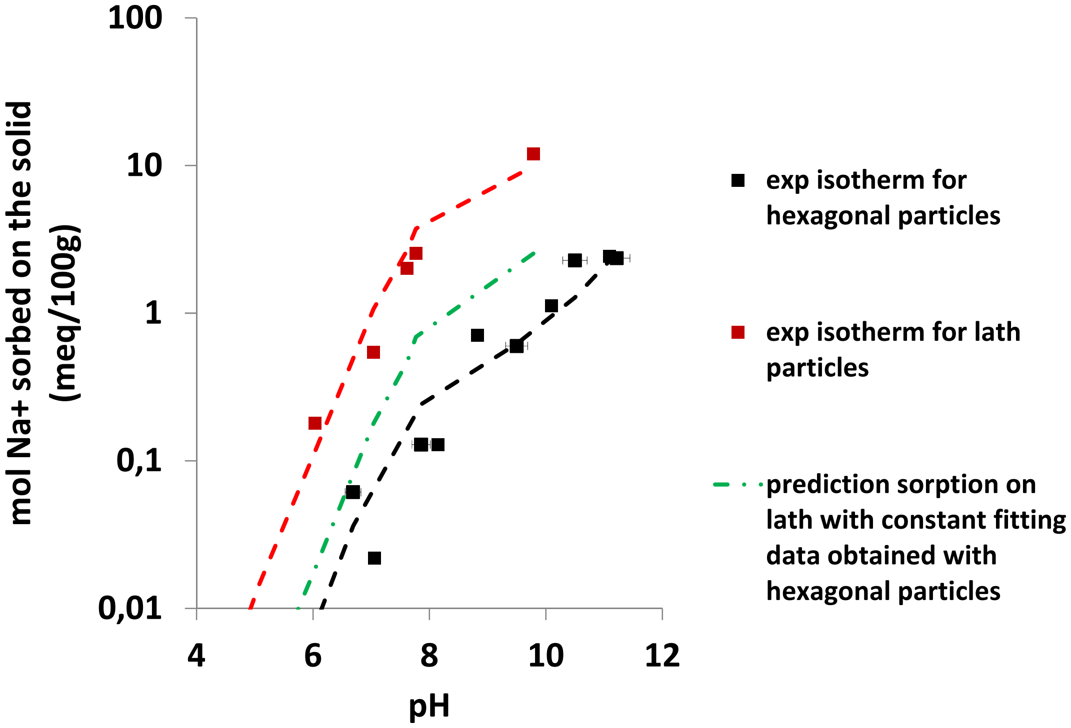

Figure 4.46 Comparison between experimental data and fitted data for both hexagonal and lath particles, and prediction sorption on lath with constant fitting data obtained with hexagonal particles.

CHAPTER 5 CONCLUSIONS

5.1 Conclusions

Unground kaolin had lower bleaching capacities than the ground kaolin. The bleaching capacities of ground kaolin enhanced upon acid activation. Using low acid treatments (<1 M) allow to obtain good bleaching capacities in relation to the high surface area of the samples, while too high acid concentrations (>1 M) lead to low bleaching capacities although surface area are still increasing. Acid activation of ground kaolin using 0.3 M sulfuric acid, 0.5 M hydrochloric acid and 0.5 M citric acid allow to obtain maximum bleaching capacities of ~82%, ~83% and ~81% respectively. Such values are very close to that of commercial bleaching clay (montmorillonite) (~82%). Preheating of kaolins at very high temperatures (>100˚C) and/or using acid at very high concentrations for the reflux step (2 M) yielded activated samples with high specific surface areas and pore volumes. However, further increased in temperature and acid concentrations decreased the bleaching performance of the adsorbents. This may be due to the partial or complete destruction of the kaolinite structure of the samples during the preparation. Study of the effect of the same hydrochloric acid strength using different acid concentrations and different clay/acid ratios on kaolin's bleaching performance also confirmed that the maximum bleaching value was not necessarily related to higher specific surface area. Kaolin treated with high temperature or acid concentrations lead to the formation of large amounts of silica and small amounts of alumina in the activated samples, which causes poor affinity for the chlorophyll-a presence in the rice bran oil.

Diluted acids, such as 0.3 M or 0.5 M concentration, can be economically used to enhance the bleaching performance of ground kaolin by creating the active acid centers on the kaolin samples along with the partial preservation of kaolinite structure, which is related to the alumina contents in the samples. Thus, the preservation of the kaolinite structure is a key parameter for obtaining a good bleaching capacity of Ranong kaolin and is directly related to the preservation of the aluminol sites present at the kaolinite surface. These sites are likely involved in the sorption of chlorophyll-a molecules present in the crude rice bran oil, which are largely responsible for the undesired color of edible oil. For a given temperature of pre-heating prior to reflux, the optimum bleaching capacity is not necessarily obtained with the highest acid concentration due to the formation of a Si-amorphous phase during dissolution, which is not favorable for good bleaching.

Another aspect of this dissertation research was to observe the sorption properties of kaolinite by exchanging Na^+ and H^+ cations from lateral surfaces of synthetic particles, differing by morphology (hexagonal shape *vs* lath shape). For that, kaolinites were hydrothermally synthesized using partially crystallized kaolinite as a starting material at different final pH. The acidic conditions enhance the formation of well-ordered, low-defect kaolinites with hexagonal-shaped particles whereas the basic conditions promote high-defect, poorly crystallized lath particles. Poor crystallinities of kaolinite are believed to cause a high CEC and large specific surface in lath particles.

Results showed that there was no sorption of Na^+ on all synthetic kaolinites until pH ~7 (except for the one synthesized at pH_F 8.3) suggesting that there was no permanent charge in these samples. Then, dramatic increase of the sorption of Na^+ was observed for pH>7 whatever the morphology of the kaolinite particles, due to sorption onto the edge sites.

Assuming that if percentage of edge sites dissolved during Na^+/H^+ isotherm is <10%, a constant sorption site density can be considered to obtain selectivity coefficient between Na^+ and H^+ cations for both hexagonal and lath morphology. This criteria was obtained for a [4-10] pH range. In this context and with edge site densities calculated from both specific surface of lateral sites and crystallographic data for (010), (110) and ( ) faces, selectivity coefficient interpreting Na^+/H^+ isotherms, and obtained with a surface complexation model, were given. Results show that selectivity coefficient between Na^+ and H^+ cations is strongly dependent on the morphology of the kaolinite particle. Then, morphology of the particles is a key parameter to take into account in all geochemical models devoted to predict the sorption of cations onto clay minerals, in particular on kaolinites.

5.2 Suggestions

For industrial applications, Ranong kaolin can be used as an effective adsorbent to bleach crude rice bran oil. Low concentrations of sulfuric acid, such as 0.3 or 0.5 M, as well as a low pre-heating temperature (less than or equal to 100˚C) prior to reflux are sufficient to activate kaolin and obtain the best bleaching capacity. In addition, grinding should be done prior to acidic reflux which also enhances the bleaching capacity of the entire material by increasing the number of small particles and increasing the specific surface area compared to the unground sample. Since the different morphologies of kaolinite influence their sorption properties, the effect of particle size and surface charge on kaolin's bleaching capacity should be studied. Among the chemical reaction between the adsorbate and adsorbent such as ion-exchange reaction, the surface charge density of different clay faces viz. the silica face, the alumina face and the edge face will also be play a vital role in clay-pigment interaction.

REFERENCES

Adams, F., 1984, “**Soil Acidity and Liming”**, 2nd ed., Agronomy Monograph 12, American Society of Agronomy, Inc., Crop Science Society of America, Inc., Soil Science Society of America, Inc. Madison, Wisconsin.

Aglietti, E.F., Porto Lopez, J.M., and Pereira, E., 1986, “Mechanochemical effects in kaolinite grinding**”, International Journal of Mineral**, Vol. 16, pp. 125-133.

Al-Harahsheh, M., Shawabkeh, R., Al-Harahsheh, A., Tarawneh, K. and Batiha, M.M., 2009, “Surface modification and characterization of Jordanian kaolinite: Application for lead removal from aqueous solutions”, **Applied Surface Science**, Vol. 255, pp. 8098-8103.

Alther, G.R., 1986, "The effect of the exchangeable cations on the physico-chemical properties of Wyoming bentonites", **Applied Clay Science**, Vol. 1, pp. 273-284.

American Oil Chemists’s Society. 2004, **Official Methods and Recommended Practices of the AOCS**, 5th ed.,_AOCS Press, Champaign, Illinois, p. Cc 13e-92, Cd 3d-63, Cd 8-53.

Barrett, E.P., Joyner, L.G. and Halenda, P.H., 1951, “Determination of pore volumes and area distributions in porous substances. I. Computation from nitrogen isotherms”, **Journal of American Chemical Society**, Vol. 73, pp. 373–380.

Barrios, J., Planҫon, A., Cruz, M.I. and Tchoubar, C., 1977, "Qualitative and quantitative study of stacking faults in a hydrazine treated kaolinite-relationship with the infrared spectra", **Clays and Clay Minerals**, Vol. 25, pp. 422-429.

Bergaya, F. and Lagaly, G., 2006, “General introduction: Clays, clay minerals, and clay science”, In: **Handbook of Clay Science**, Bergaya, F., Theng, B.K.G. and Lagaly, G., (ed.), Development in Clay Science, EMU books in mineralogy, Vol. 1, pp. 1-18.

Bhattacharyya, A.C., and Bhattacharyya, D.K., 1985, “Refining of high FFA rice bran oil by mixed solvent-alkali neutralization process” **Journal of Oil Technologist Association of India**, Vol. 17, pp. 31-32.

Bhattacharyya, K.G. and Gupta, S.S., 2008, "Influence of acid activation on adsorption of Ni(II) and Cu(II) on kaolinite and montmorillonite: Kinetic and thermodynamic study", **Chemical Engineering Journal,** Vol. 136, pp. 1-13.

Bickmore, B.R., Bosbach, D., Hochella, M.F. Jr., Charlet, L., and Rufe, E., 2001, "In situ atomic force microscopy study of hectorite and nontronite dissolution: Implications for phyllosilicate edge surface structures and dissolution mechanisms", **American Mineralogist**, Vol. 86, pp. 411-423.

Birks, L.S., 1969, "X-Ray Spectrochemical Analysis", **Chemical Analysis**, Vol. 11, 2nd ed., Wiley-Interscience, Wiley, New York, p. 143.

Boki, K., Kubo, M., Wada, T. and Tamura, T., 1992, "Bleaching of alkali-refined vegetable oils with clay minerals", **Journal of the American Oil Chemists' Society** Vol. 69, 232-236.

Boyd, S.A. and Jaynes, W.F., 1994, "Role of layer charge in organic contaminant sorption by organo-clays", In: Mermut, A.R. (Ed.), **Layer Charge Characteristics of 2:1 Silicate Clay Minerals,** CMS workshop lectures, Vol. 6, pp. 47-77.

Brady, P.V., Cygan, R.T. and Nagy, K.L., 1996, "Molecular controls on kaolinite surface charge", **Journal of Colloid and Interface Science,** Vol. 183, pp. 356-364.

Breeuwsma, A. and Lyklema, J., 1973," Physical and chemical adsorption of ions in the electrical double layer", **Journal of Colloid and Interface Science**, Vol. 43, pp. 437-448.

Brigatti, M.F., Galan, E. and Theng, B.K.G., 2006, "Structures and mineralogy of clay minerals", In: **Handbook of Clay Science**, Bergaya, F., Theng, B.K.G. and Lagaly, G., (ed.), Development in Clay Science, EMU books in minerlogy, Vol. 1, pp. 19-86.

Brindley, G.W. and Brown, G., 1980, "Crystal structures of clay minerals and their X-ray identification", **Mineralogical Society Monograph No. 5. Mineralogical Society**, London, p. 495.

Brouwer, P., 2010, "**Theory of XRF: Getting Acquainted With the Principles**", 3rd ed., PANalytical BV, The Netherlands.

Brunauer, S., Emmett, P.H. and Teller, E.J., 1938. "Adsorption of gases in multimolecular layers", **Journal of American Chemical Society**, Vol. 60, pp. 309-318.

Buttle, J.M. and Labadia, C.F., 1999, "Deicing salt accumulation and loss in highway snowbanks", **Journal of Environmental Quality**, Vol. 28, pp. 155-164.

Caglayan, M.O. and Yigit, S.K.N., 2005, "Al-Pillared clay for cottonseed oil bleaching: An optimization study", **Journal of the American Oil Chemists' Society**, Vol. 82, pp. 599-602.

Carr, R.M. and Dioxan, J.B., 1967, "Synthesis of some aluminium silicates", **Australian Journal of Chemistry**, Vol. 20, pp. 2767-2769.

Carrado, K.A., Decraaeau, A., Petit, S., Bergaya, F. and Lagaly, G., 2006, "Synthetic clay minerals and purification of natural clays": In **Handbook of Clay Science**, Bergaya, F., Theng, B.K.G. and Lagaly, G., (ed.), Development in Clay Science, EMU books in mineralogy, Vol. 1., pp. 115-139.

Cases, J. M., Cunin, P., Grillet, Y., Poinsigon, C. and Yvon, J., 1986, "Methods of analyzing morphology of kaolinites: Relations between crystallographic and morphological properties", **Clay Minerals,** Vol. 21, pp. 55-68.

Cases, J.M., Liétard, O., Yvon, J., and Delon, J.F., 1982, "Etude des propriétés cristallographiques, morphologiques et superficielles de kaolinites désordonnées", **Bulletin de Minéralogie**, Vol. 105, pp. 439-457.

Cheng, H., Yang, J., Liu, Q., He, J. and Frost, R.L., 2010, “Thermogravimetric analysis-mass spectrometry (TG-MS) of selected Chinese kaolinites", **Thermochimica Acta**, Vol. 507, pp. 106-114.

Christidis, G.E., Scott, P.W. and Dungam, A.C., 1997, "Acid activation and bleaching capacity of bentonites from the islands of Milos and Chios, Aegean, Greece", **Applied Clay Science**, Vol. 12, pp. 329-347.

Cleary, R.W., 1978, "Pollution of groundwater: In water problems of urbanizing areas”, **Proceedings of the research conference**, New England College, Henniker, New Hampshire, July 16-21. The American Society of Civil Engineers, New York. pp. 134-142.

Cullity, B.D., 1956, “**Elements of X-ray diffraction”**, Addison-Wesley Company, Inc. Reading, Massachusetts, 514p.

Didi, M.A., Makhoukhi, B., Azzouz, A. and Villemin, D., 2009, "Colza oil bleaching through optimized acid activation of bentonite: A comparative study", **Applied Clay Science**, Vol. 42, pp. 336–344.

Diosady, L.L., 2005, "Chlorophyll Removal from Edible Oils", **International Journal of Applied Science and Engineering,** Vol. 3, pp. 81-88.

Drits, V., Srodon, J. and Eberl, D.D., 1997, XRD measurement of mean crystallite thickness of illite and illite/smectite: Reappraisal of the kubler index and the scherrer equation, **Clays and Clay Minerals**, Vol. 45, pp. 461-475.

Dudkin, B.N., Loukhina, I.V., Isupov, V.P. and Avvakumov, E.G., 2005, "Mechanical activation of kaolinite in the presence of concentrated sulfuric acid", **Russian Journal of Applied Chemistry**, Vol. 78, pp. 33-37.

Dunford. N.T., 2005. “Germ Oils from Different Sources” In: **Bailey’s Industrial Oil and Fat Products**, 6th ed., John Wiley and Sons, New Jersey. Vol. 3, “Edible Oil and Fat Products: Specialty Oils and Oil Products”, Ch. 8, pp. 195-231.

Ekkose, G.I., 2005, " Fourier Transform infrared spectrophotometry and X-ray powder diffractometry as complementary techniques in characterizing caly size fraction of kaolin", **Journal of Applied Science and Environmental Management**, Vol. 9, pp. 43-48.

Elsass, F., 2006, “Transmission electron microscopy”, In: **Handbook of Clay Science**, Bergaya, F., Theng, B.K.G. and Lagaly, G., (ed.), Development in Clay Science, EMU books in mineralogy, Vol. 1, pp. 934-969.

Falaras, P., Kovanis, I., Lezou, F. and Seiragaskis, G., 1999, "Cottonseed oil bleaching by acid-activated montmorillonite", **Clay Minerals**, Vol. 34, pp. 221-232.

Farmer V.C., 1974, “The Layer silicates”, In: **the Infrared Spectra of Minerals**, Farmer, V.C., (ed.), Monograph 4, Mineralogical Society, London, pp. 331-365.

Farmer, V.C. and Russell, J.D., 1964, "The infrared spectra of layered silicates", **Spectrochimica Acta**, Vol. 20, pp. 1149-1173.

FEI, 2010, "**An introduction to electron microscopy**", FEI Company, p. 36.

Fernandez, R., Martirena, F. and Scrivener, K.L., 2011, "The origin of the pozzolanic activity of calcined clay minerals: A comparison between kaolinite, illite and montmorillonite", **Cement and Concrete Research**, Vol. 41, pp. 113-122.

Ferris, A.P., and Jepson, W.B., 1975, "The exchange capacities of kaolinite and the preparation of homoionic clays", **Journal of Colloid and Interface Science**, Vol. 51, pp. 245–259.

Fialips, C.I., Petit, S., Decarreau, A. and Beaufort, D., 2000, "Influence of synthesis pH on the kaolinite crystallinity and surface properties", **Clays and Clays Minerals**, Vol. 48, pp. 173-184.

Fijal, J., Klapyta, Z., Kwieciuska, B., Zietkiewitcz, J. and Zyla, M., 1975, "On the mechanism of acid activation of montmorillonite. II. Changes in the morphology and porosity in the light of electron microscopic and adsorption investigations", **Mineralogical Society of Poland**, Vol. 6, pp. 49-57.

Firestone, D., 2006, “**Physical and chemical characteristics of oils, fats and waxes”**, 2nd ed. , American Oil Chemist Society Press, Washington, D.C.

Foletto, E.L., Volzone, C. and Porto, L.M., 2006, "Clarification of cottonseed oil: How structural properties of treated bentonites by acid affect bleaching efficiency", **Latin American Applied Research**, Vol. 36, pp. 37-40.

Foo, C.T., Mahmooda, C.S. and Sallehb, M.A.M., 2011, "The study of aluminum loss and consequent phase transformation in heat-treated acid-leached kaolin", **Materials Characterization**, Vol. 62, pp. 373-377.

Francisco, R. and Santos, S., 2001, "Studies on the acid activation of Brazilian smectitic clays", **Quimica Nova**, Vol. 24, pp. 345-353.

Ganor, J., Cama, J. and Metz, V., 2003, "Surface protonation data of kaolinite-reevaluation based on dissolution experiments", **Journal of Colloid and Interface Science**, Vol. 264, pp. 67-75.

Grim, R.E., 1962, "**Applied Clay Mineralogy**", McGraw-Hill, New York, p. 422.

Gu, X. and Evans, L.J., 2008, "Surface complexation modeling of Cd(II), Cu(II), Ni(II), Pb(II) and Zn(II) adsorption onto kaolinite", **Geochimica et Cosmochimica Acta**, Vol. 72, pp. 267-276.

Hechi, E., Amor, O.B., Srasra, E. and Zargouni. F., 2009, "Physico-chemical characterization of acid-activated clay: Its industrial application in the clarification of vegetable oils", **Surface Engineering and Applied Electrochemistry**, Vol. 45, pp. 140-144.

Helling, C. S., Chesters, G. and Corey, R.B., 1964, "Contribution of organic matter and clay to soil cation exchange capacity as affected by pH of the saturating solution", **Processing of Soil Science Society of America**, Vol. 28, pp. 517-520.

Hinckley, D.N., 1963, "Variability in crystallinity values among the kaolin deposits of the coastal plain of Georgia and South Carolina", **Clays and Clay Minerals**, Vol. 11, pp. 229-235.

Holt, A.S., Jacobs, E.E., 1955, "Infrared absorption spectra of chlorophylls and derivatives". **Plant Physiology**, Vol. 30, pp. 553-559.

Huertas, J.F., Chou, L. and Wollast, R., 1998. "Mechanism of kaolinite dissolution temperature and pressure: Part 1. Surface speciation", **Geochimica et Cosmochimica Acta**, Vol. 62, pp. 417−431.

Hui, Y.H., 1996, "Industrial and consumer nonedible products from fats and oils", In: **Bailey's industrial oil and fat products**, Wiley-Interscience publication, New York.

Hussein, M.Z., Kuang, D., Zainal, Z. and Teck, T.K., 2001, "Kaolin-carbon adsorbents for carotene removal of red palm oil", **Journal of Colloid and Interface Science**, Vol. 235, pp. 93-100.

Ilic, B.R., Mitrovic, A.A. and Milicic, L.R., 2010, **"**Thermal treatment of kaolin clay to obtain metakaolin**"**, **Hemijska Industrija**, Vol. 64, pp. 351-356.

Itami, K. and Fujitani, H., 2005, "Charge characteristics and related dispersion/flocculation behavior of soil colloids as the cause of turbidity", **Colloids and Surfaces A- Physicochemical and Engineering Aspects**, Vol. 265, pp. 55-63.

James, O.O., Mesubi, M.A., Adekola, F.A., Odebunmi, E.O., Adekeye, J.I.D. and Bale, R.B., 2008, "Bleaching performance of a Nigerian (Yola) bentonite", **Latin American Applied Research**, Vol. 38, pp. 45-49.

James, S.R., 1995, "**Principles of Ceramics Processing**", John Wiley & Sons, New York, p. 492.

Jenkins, R., 1999, "**X-Ray Fluorescence Spectrometry**", 2nd ed., Wiley, Chichester.

Johnston, C.T. and Tombácz, E., 2002, "Surface chemistry of soil minerals", In: **Soil mineralogy with environmental applications**, Dixon, J.B. and Schulze, D.G. (ed.), Soil Science Society of America, Madison, Wisconsin, USA, pp. 37–67.

Joussein, E., Petit, S., Churchman, J., Theng, B., Righi, D. and Delvaux, B., 2005, "Halloysite clay minerals - A review", **Clay Minerals**, Vol. 40, pp. 383-426.

Junmao, T., Zhansheng, W.U., Xifang, S.U.N. and Xiaolin, X.U., 2008, "Adsorption kinetics of β-carotene and chlorophyll onto acid-activated bentonite in model oil", **Chinese Journal of Chemical Engineering**, Vol. 16, pp. 270-276.

Kahlon, T.S., Saunders, R.M., Sayre, R.N., Chow, F.I., Chiu, M.M. and Betschart, A.A., 1992, "Cholesterol-lowering effects of rice bran and rice bran oil fractions in hypercholesterolemic hamsters", **Cereal Chemistry**, Vol. 69, pp. 485-489.

Kakali, G., Perraki, T., Tsivilis, S. and Badogiannis, E., 2001, “Thermal treatment of kaolin: the effect of mineralogy on the pozzolanic activity”, **Applied Clay Science**, Vol. 20, pp. 73-80.

Kaviratna, H. and Pinnavaia, T., 1994, "Acid hydrolysis of octahedral Mg^{2+} sites in 2:1 layered silicates: An assessment of edge attack and gallery access mechanisms", **Clays and Clay Minerals**, Vol. 42, pp. 717-723.

Kheok, S.C. and Lim, E.E., 1982. "Mechanism of palm oil bleaching by montmorillonite clay activated at various acid concentrations", **Journal of the American Oil Chemists’ Society**, Vol. 59, pp. 129-131.

Khoo, L.E., Morsingh, F. and Liew, K.Y., 1979, "The adsorption of β-carotene I. by bleaching earths", **Journal of the American Oil Chemists’ Society**, Vol. 56, pp. 672-675.

Kirschenbauer, H.G., 1960, “**Fats and Oils, An outline of their chemistry and technology**”, 2nd ed., Van Nostrand Reinhold, New York.

Kolta, G.A., Novak, I., Samir, Z.E.T. and Kamilia, A.E.B, 1975, "Evaluation of bleaching capacity of acid-leached Egyptian bentonites", **Journal of Applied Chemistry and Biotechnology**, Vol. 26, pp. 355-360.

Koretsky, C.M., Sverjensky, D.A. and Sahai, N., 1998, "A model of surface site types on oxide and silicate minerals based on crystal chemistry: Implications for site types and densities, multi-site adsorption, surface infrared spectroscopy, and dissolution kinetics", **American Journal of Science**, Vol. 298, pp. 349-438.

Kristóf, E., Juhász, A.Z. and Vassányi, I., 1993,"The Effect of Mechanical Treatment of the crystal structure and thermal behavior of kaolinite", **Clays and Clay Minerals**, Vol. 41, pp. 608-612.

Langford, J.I. and Wilson, A.J.C., 1978, "Scherrer after sixty years. A survey and some new results in the determination of crystallite size", **Journal of Applied Crystallography**, Vol. 11, pp. 102-113.

Leddy, N., 2010, "**Material characterisation for surface area and porosity utilising gas sorption**", CMA Postgraduate Analytical Workshop.

Ledoux, R.L. and White, J.L., 1964, "Infrared study of selective deuteration of kaolinite and halloysite at room temperature", **Science**, Vol. 145, pp. 47-49.

Liétard, O., 1977, "Contribution á l'étude des propriétés physicochimiques, cristallographiques et morphologiques des kaolins", **PhD thesis**, University of Nancy, Nancy, France, p. 322.

Liu, X., Chen, G. and Su, C., 2011, "Effects of material properties on sedimentation and aggregation of titanium dioxide nanoparticles of anatase and rutile in the aqueous phase", **Journal of Colloid and Interface Science**, Vol. 363, pp. 84-91.

Lloyd, M.K. and Robert, F.C., 1970, "Adsorption studies on kaolinites", **Clays and Clay Minerals**, Vol. 18, pp. 37-46.

Lyklema, J., and Keizer, A., 1995, "**Solid-Liquid Interfaces**", Vol. 2, Academic Press.

Ma, C. and Eggleton, R.A., 1999, "Cation exchange capacity of kaolinite", **Clays and Clay Minerals**, Vol. 47, pp. 174–180.

Macht, F., Eusterhues, K., Pronk, G.J. and Totsche, K.U., 2011, "Specific surface area of clay minerals: Comparison between atomic force microscopy measurements and bulk-gas (N_2) and -liquid (EGME) adsorption methods", **Applied Clay Science**, Vol. 53, pp. 20–26.

Madejová, J., Kečkéš, J., Pálková, H. and Komadel, P., 2002, "Identification of components in smectite/kaolinite mixtures", **Clay Minerals**, Vol. 37, pp. 377–388.

Martin, R.T., Bailey, S.W., Eberl, D.D., Fanning, D.S., Guggenheim, S., Kodama, H., Pevear, D.R., Środoń, J. and Wicks, F.J., 1991, "Report of the Clay Minerals Society Nomenclature Committee: Revised Classification of Clay Materials", **Clays and Clay Minerals**, Vol. 39, pp. 333-335.

Martinez, R.E., Sharma, P. and Kappler, A., 2010, "Surface binding site analysis of Ca^{2+}-homoionized clay–humic acid complexes", **Journal of Colloid and Interface Science**, Vol. 352, 526–534.

Mason, C.F., Norton, S.A., Fernandez, I.J. and Katz, L.E., 1999, "Deconstruction of the chemical effects of road salt on stream water chemistry", **Journal of Environmental Quality**, Vol. 28, pp. 82-91.

Mills, G.A., Holmes, J. and Cornelius, E.B., 1950, "Acid activation of some bentonite clays", **Journal of Physical and Colloid Chemistry**, Vol. 54, pp. 1170-1185.

Miranda-Trevino, J.C. and Coles, C.A., 2003, "Kaolinite properties, structure and influence of metal retention on pH", **Applied Clay Science**, Vol. 23, pp. 133– 139.

Miyawaki, R., Tomura, S., Samejima, S., Okazaki, M., izuta, H., Muruyama, S.I., and Shibasaki, Y., 1991, "Effects of solution chemistry on the hydrothermal synthesis of kaolinite", **Clays and Clay minerals**, Vol. 39, pp. 498-508.

Mokaya, R., Jones, W., Davies, M.E. and Whittle, M.E., 1993, "Chlorophyll adsorption by alumina-pillared acid-activated clays", **Journal of the American Oil Chemists' Society**, Vol. 70, No.3, pp. 241-244.

Molinard, A., Peeters, K.K., Maes, N. and Vansant, E.F., 1994,"Restoring the cation exchange capacity of alumina pillared montmorillonite through modification with ammonium", In: **Separation Technology**, Vansant, E.F. (ed.), Proceeding of 3rd International Symposium on Separation Technology, Elsevier Science, Amsterdam, pp. 445-454.

Moore, D. M. and Reynolds, R.C., 1997, "**X-Ray Diffraction and the Identification and Analysis of Clay Minerals**", 2nd ed., Oxford University Press, Inc.: New York. Vol. 1-5, 378 p.

Morgan, D.A., Shaw, D.B., Sidebottom, M.J., Soon, J.C. and Taylor, R.S., 1985, "The function of bleaching earths in the process of palm, palm kernel and coconut oils", **Journal of the American Oil Chemists' Society**, Vol. 62, pp. 292-298.

Nandi, B.K., Goswami, A. and Purkait, M.K., 2009, "Adsorption characteristics of brilliant green dye on kaolin", **Journal of Hazardous Materials**, Vol. 161, pp. 387-395.

Nguetnkam, J.P., Kamga, R., Villiéras, F., Ekodeck, G.E., Razafitia-namaharavo, A.,Yvon, J., 2005." Assessment of the surface areas of silica and clay in acid leached clay materials using concepts of adsorption on heterogeneous surfaces", **Journal of Colloid and Interface Science**, Vol. 298, pp. 104–115.

Nguetnkam, J.P., Kamga, R., Villiéras, F., Ekodeck, G.E. and Yvon, J., 2008, "Assessing the bleaching capacity of some Cameroonian clays on vegetable oils", **Applied Clay Science**, Vol. 39, pp. 113–121.

Nolin, D., 1997, " **Rétention de radioéléments à vie longue par des matériaux argileux. Influence d'anions contenus dans les eaux naturelles**", PhD Thesis, University of Paris, p.6.

Novak, I. and Gregor, M., 1969, "Surface area and decolorizing ability of some acid-treated montmorillonites", **Proceeding of International Clay Conference**, Tokyo, pp. 851-857.

Noyan, H., Onal, M. and Sankaya, Y., 2007, "The Effect of Sulphuric Acid Activation on the Crystallinity, Surface Area, Porosity, Surface Acidity, and Bleaching Power of a Bentonite", **Food Chemistry**, Vol. 105, pp. 156-163.

Nuntiya, A. and Prasanphan, S., 2006, "The rheological behavior of kaolin suspensions", **Chiang Mai Journal of Science**, Vol. 33, pp. 271-281.

Odom, I.E., 1984, "Smectite clay minerals: Properties and uses", **Philosophical Transactions of the Royal Society of London**, Series A, Vol. 311, pp. 391-409.

Okada, K., Shimai, A., Takei, T., Hayashi, S., Yausmori, A. and MacKenzie, K.J.D., 1998, "Preparation of Microporous Silica from Metakaolinite by Selective Leaching Method", **Microporous and Mesoporous Materials**, Vol. 21, pp. 289-296.

Olphen, H.V., 1963, "**An Introduction to Clay Colloid Chemistry: For Clay Technologists, Geologists and Soil Scientists**", Interscience, New York.

Orthoefer, F.T., 1996, “Rice bran oil: Health lipid source”, **Food Technology**, Vol.50, pp. 62-64.

Orthoefer, F.T., 2005, “Rice Bran Oil”: In **Bailey's Industrial Oil and Fat Products**, Vol. 2, Shahidi, F. (ed.), John Wiley & Sons, Inc., New York, pp. 465-489.

Panda, A. K., Mishra, B.G., Mishra, D.K. and Singh, R.K., 2010, "Effect of sulphuric acid treatment on the physico-chemical characteristics of kaolin clay", **Colloids and Surfaces A: Physicochemical and Engineering Aspects**, Vol. 363, pp. 98-104.

Palm Oil Research Institute of Malaysia, 1993, “**Selected readings on palm oil and its uses**”, Palm Oil Research Institute of Malaysia, Ministry of Primary Industries, Malaysia.

Petit, S., 2006., “Fourier transform infrared spectroscopy”, In: **Handbook of Clay Science**, Vol. 1, Bergaya, F., Theng, B.K.G. and Lagaly, G., (ed.), Development in Clay Science, EMU books in minerlogy, pp. 909-918.

Petit, S., Madejova, J., Decarreau, A. and Martin, F., 1999, “Characterization of octahedral substitutions in kaolinites using near infrared spectroscopy”, **Clays and Clay Minerals**, Vol. 47, pp.103-108.

Pruett, R.J. and Webb, H.L., 1993, "Sampling and analysis of KGa-1B well-crystallized kaolin source clay", **Clays and Clay Minerals**, Vol. 41, pp. 514-519.

Rhodes, C.N. and Brown, D.R., 1992, " Structural characterization and optimization of acid-treated montmorillonite and high-porosity silica supports for $ZnC1_2$ alkylation catalysts", **Journal of the Chemical Society, Faraday Transactions**, Vol. 88, pp. 2269-2274.

Rider, M., 1996, “**Geological Interpretation of Well Logs**”, Caithness, Whittles Publication, p.280.

Rouxhet, P.G., Samudacheata, N., Jacogs, H. and Anton, O., 1977, "Attribution of the OH stretching bands of kaolinite", **Clay Minerals**, Vol. 12, pp. 171-179.

Rupert, J.P., Granquist, W.T. and Pinnavaia, T.J., 1987, "Catalytic properties of clay minerals”, In: **Chemistry of clays and clay minerals**. Newman, A.C.D. (ed.), Mineralogical Society, London, pp. 275-318.

Russell, J.D., 1987, "Infrared method”, In: **A Handbook of Determinative Methods in Clay Mineralogy**, M.J. Wilson (ed.), Chapman and Hall, New York, pp. 133-173.

Sabah, E. and Çelik, M.S., 2005, "Sepiolite: an effective bleaching adsorbent for the physical refining of degummed rapeseed oil", **Journal of the American Oil Chemists’ Society**, Vol. 82, pp. 911-916.

Sabir, B.B., Wild, S. and Bai, J., 2001, “Metakaolin and calcined clays as pozzolans for concrete: a review”, **Cement and Concrete Composites**, Vol. 23, pp. 441-454.

Salawudeen, T.O., Dada, E.O. and Alagbe, S.O., 2007, "Performance evaluation of acid treated clays for palm oil bleaching", **Journal of Engineering Applied Science**, Vol. 2, pp. 1677-1680.

Sánchez, R.M.T., Basaldella, E.I. and Marco, J.F., 1999, "The effect of thermal and mechanical treatments on kaolinite: characterization by XPS and IEP measurements", **Journal of Colloid and Interface Science**, Vol. 215, pp. 339-344.

Sánchez-Soto, P.J., Carmen Jiménez de Haro, M., Pérez-Maqueda, L.A., Varona I. and Pérez-Rodrígueq, J.L., 2000, "Effects of dry grinding on the structural changes of kaolinite powders", **Journal of the American Ceramic Society**, Vol. 83, pp. 1649-1657.

Schoonheydt, R.A. and Johnston, C.T., 2006, “Surface and interface chemistry of clay minerals”: In **Handbook of Clay Science**, Bergaya, F., Theng, B.K.G. and Lagaly, G., (ed.), Development in Clay Science, EMU books in mineralogy, Vol. 1., pp. 87-113.

Schroth, B.K. and Sposito, G., 1997, "Surface charge properties of kaolinite", **Clays and Clay Minerals**, Vol. 45, pp. 85–91.

Schwitzer, M.K., 1956, **“Margarine and other food fats, their history, production and uses”**, Leonard Hill (Books) Ltd., London, p. 365.

Shirsath, S.R., Patil, A.P., Patil, R., Naik, J.B., Gogate, P.R. and Sonawane, S.H., 2013, "Removal of Brilliant Green from wastewater using conventional and ultrasonically prepared poly (acrylic acid) hydrogel loaded with kaolin clay: A comparative study", **Ultrasonics Sonochemistry**, Vol. 20, pp. 914-923.

Siddiqui, M.K.H., 1968, "**Bleaching earths**", Pergamon Press, Oxford, p. 63.

Sposito, G., 1989, "**The Chemistry of Soils**", Oxford University Press, Inc., New York, p. 277.

Srasra, E., Bergaya, F., Van Damme, H. and Arguib, N.K., 1989, "Surface properties of an activated bentonite. Decolorization of rape-seed oil", **Applied Clay Science**, Vol. 4, pp. 411-421.

Srodon J. (2006). “Identification and quantitative analysis of clay minerals”, In: **Handbook of Clay Science, Developments in Clay Science,** Vol.1, Bergaya, F., Theng, B.K.G. and Lagaly, G. (ed.), Elsevier, Amsterdam, pp. 765–786.

Stout, L.E., Donald, F., Chamberlain, D.F. and McKelvey, J.M., 1949, "Factors influencing vegetable oil bleaching by adsorption", **Journal of the American Oil Chemists’ Society**, Vol. 26, pp. 120-126.

Stuart, B.H., 2004, "**Infrared Spectroscopy: Fundamental and Applications**", John Wiley and Sons, England, p. 219.

Sugiyama, K., Filio, J.M., Saito, F. and Waseda, Y., 1994, "Structural Change of Kaolinite and Pyrophyllite Induced by Grinding", **Mineralogical Journal**, Vol. 17, pp. 28-41.

Suraj, G., Iyer, C.S.P. and Lalithambikca, M., 1998, "Adsorption of cadmium and copper by modified kaolinites", **Applied Clay Science**, Vol. 13, pp. 293-306.

Tang, A., Su, L., Li, C. and Wei, W., 2010, "Effect of mechanical activation on acid-leaching of kaolin residue", **Applied Clay Science**, Vol. 48, pp. 296-299.

Taylor, D.R., 2005, “Bleaching” In: **Bailey's Industrial Oil and Fat Products**”, Wiley-Interscience publication, New York.

Temuujin, J., Burmaa, G. and Amgalan, J., 2001, "Preparation of porous silica from mechanically activated kaolinite", **Journal of Porous Material**, Vol. 8, pp. 233-238.

Temuujin, J., Jadambaa, T., Burmaa, G., Erdenechimeg, S., Amarsanaa, J. and MacKenzie, K.J.D., 2004, "Characterisation of acid activated montmorillonite clay from Tuulant (Mongolia)", **Ceramics International**, Vol. 30, pp. 251-255.

Temuujin, J., Senna, M., Jadambaa, T., Burmaa, D., Erdenechimeg, Sh. and MacDenzid, K.J.D. 2006, "Characterization and bleaching properties of acid-leached montmorillonite", **Journal of Chemical Technology and Biotechnology**, Vol. 81, pp. 688-693.

Tertian, R and Claisse, F. 1982, "**Principles of Quantitative X-Ray Fluorescence Analysis**", Heyden, p. 385.

Tertre, E., Berger, G., Castet, S., Loubet, M. and Giffaut, E., 2005, “Experimental study of adsorption of Ni^{2+}, Cs^{+} and Ln^{3+}onto Na-montmorillonite up to 150°C", **Geochimica et Cosmochimica Acta**, Vol. 69, pp. 4937- 4948.

Tertre, E., Castet, S., Berger, G., Loubet, M. and Giffaut, E., 2006, "Surface Chemistry of Kaolinite and Na-montmorillonite in Aqueous Electrolyte Solutions at 25 and 60°C: Experimental and Modeling Study", **Geochimica et Cosmochimica Acta**, Vol. 70, pp. 4579-4599.

Tertre, E., Ferrage, E., Bihannic, I., Michot, L.J. and Prêt, D., 2011, "Influence of the ionic strength and solid/solution ratio on Ca(II)-for-Na^{+} exchange on montmorillonite. Part 2: Understanding the effect of the m/V ratio. Implications for pore water composition and element transport in natural media", **Journal of Colloid and Interface Science**, Vol. 363, pp. 334–347.

Tertre, E., Hubert, F., Bruzac, S., Pacreau, M., Ferrage, E. and Pret, D., 2013, "Ion-exchange reactions on clay minerals coupled with advection/dispersion processes. Application to Na^{+}/Ca^{2+} exchange on vermiculite: Reactive-transport modeling, batch and mix-flow reactor experiments", **Geochimica et Cosmochimica Acta**, Vol. 112, pp. 1-19.

Tkac, I., Komadel, P. and Miiller, D., 1994, "Acid treated montmorillonites: A study by 29Si and 27A1 MAS-NMR", **Clay Minerals**, Vol. 29, pp. 11-19.

Tsuzuki, Y., 1976, "Solubility diagrams for explaining zone sequences in bauxite, kaolin and pyrophyllite-diaspore deposits", **Clays and Clay Minerals**, Vol. 24, pp. 297-302.

Tooley, P., 1971, "**Fats, Oils and Waxes (Chemistry in Industry)**", 2nd ed., John Murray (Publishers) Ltd, London, p. 176.

Tournassat, C., Ferrage, E., Poinsignon, C.and Charlet, L., 2004a, "The titration of clay minerals II. Structure-based model and implications for clay minerals", **Journal of Colloid and Interface Science**, Vol. 273, pp. 234-246.

Tournassat, C., Greneche, J. M., Tisserand, D. and Charlet, L., 2004b, "The titration of clay minerals I. Discontinuous back titration technique combined with CEC measurements", **Journal of Colloid and Interface Science**, Vol. 273, pp. 224-233.

Uğurlu, M. and Kula, I., 2007, "The removal of color, carotene and acidity from crude olive oil by using sepiolite", **Intetnational Journal of Food Science and Technology**, Vol. 42, pp. 359-365.

Van der Marel, H.W. and Krohmer, P., 1969, "O-H stretching vibrations in kaolinite and related minerals", **Contributions to Mineralogy and Petrology**, Vol. 22, pp. 73-82.

Van Olphen, H. and Fripiat, J.J., 1979, "**Data Handbook for Clay Materials and Other Non-metallic Minerals**", Pergamon Press, Oxford, p. 347.

Velde, B. 1995, "**Origin and Mineralogy of Clays**", Springer-Verlag, Berlin.

Vesely, V. and Pekárek, V., 1972, "Synthetic inorganic ion-exchangers I. Hydrous oxides and acidic salts of multivalent metals", **Talanta**, Vol. 19, pp. 219-262.

Wan, J. and Tokunaga, T.K., 2002, "Partitioning of clay colloids at air-water interfaces", **Journal of Colloid and Interface Science**, Vol. 247, pp. 54-61.

Weider Mann, L.H., 1981, "Degumming, refining and bleaching soybean oil", **Journal of American Oil Chemist Society**, USA.

Weigl, J.W., Livingston, R., 1953, "Infrared spectra of chlorophyll and related compounds 1". **Journal of the American Chemical Society**, Vol. 75, pp. 2173-2176.

Wells, O.C., Boyde, A., Lifshin, E. and Rezanowich, A., 1974, "**Scanning Electron Microscopy**", McGraw-Hill, p. 421.

White, R.E., 1987, "**Introduction to the Principles and Practice of Soil Science**", 2nd ed., Blackwell, Boston, p. 244.

Wilson, M.J., 1987, "**A Handbook of Determinative Methods in Clay Mineralogy**", Blackie, Glasgow, p. 308.

Worasith, N., Goodman, B.A., Jeyashoke, N. and Thiravetyan, P., 2011a, "Decolorization of Rice Bran Oil using Modified kaolin", **Journal of the American Oil Chemists' Society**, Vol. 88, pp. 2005-2014.

Worasith, N., Goodman, B.A., Neampan, J., Jeyashoke, N. and Thiravetyan, P., 2011b, "Characterisation of modified kaolin from the Ranong deposit Thailand by XRD, XRF, SEM, FTIR, and EPR techniques", **Clay Minerals**, Vol. 46, pp. 539-559.

Wypych. F., 2004, "**Clay surfaces: fundamentals and applications**", Wypych. F. and Satyanarayana, K.G. (ed.), Vol. 1, Academic Press, UK, p. 553.

Yang, T., Wen, X.D, Li, J. and Yang, L., 2006, "Theoretical and experimental investigations on the structures of purified clay and acid-activated clay", **Applied Surface Science,** Vol. 252, pp. 6154–6161.

Yue-hua, HU, Wei, S., Xiao-wen, L. and Diarr-zuo, W., 2003, "Cleavage nature, electrokienetics, aggregation and dispersion of kaolinite", **Transactions of Nonferrous Metals Society of China**, Vol. 13, pp. 1430-1435.

Zaki, I., Abdel-Khalik, M. and Habashi, G.M., 1986, "Acid leaching and consequent pore structure and bleaching capacity modifications of Egyptian clays", **Colloids and Surfaces**, Vol. 17, pp. 241-249.

Zhabrova, G.M. and Egorov, E.V., 1961, "Sorption and ion exchange on amophoteric oxides and hydroxides", **Russian Chemical Reviews**, Vol. 30, pp. 338-346.

APPENDIXES

Appendix A Experimental data of part I

Table A-1 Alumina and silica ratio of the initial and activated kaolins

Samples	SiO_2 (%)	Si (%)	Al_2O_3 (%)	Al (%)	Al:Si
UGK	53.90	25.15	42.40	22.45	0.89
GK	54.10	25.24	42.00	22.24	0.88
Samples heated at different temperatures and refluxed with 2 M sulfuric acid (FUG 2 samples)					
100UG 2	60.50	28.23	35.80	18.95	0.67
300UG 2	61.50	28.70	35.2	18.64	0.65
500UG 2	89.20	41.63	7.31	3.87	0.09
700UG 2	92.70	43.26	4.90	2.59	0.06
Samples heated at different temperatures from 100˚C to 700˚C prior to ground and reflux with 2 M sulfuric acid (FG2 samples)					
100GR 2	80.20	37.42	16.60	8.79	0.23
300GR 2	84.40	39.39	12.70	6.72	0.17
500GR 2	91.40	42.65	5.68	3.01	0.07
700GR 2	94.40	44.05	3.48	1.84	0.04
Samples heated at 100˚C, ground, and refluxed with different concentrations of sulfuric acid equal to 0.3 to 2 M (100GRS samples)					
100GR 0.3	71.12	33.19	24.87	13.17	0.40
100GR 0.5	73.69	34.39	23.10	12.23	0.36
100GR 1	79.14	36.93	17.79	9.42	0.26
100GR 2	80.20	37.43	16.60	8.79	0.23
Samples ground and heated at 80˚C prior to reflux with different concentrations of sulfuric acid equal to 0.3, 1, and 2 M using clay/acid ratio of 1:50					
GRS 0. 3	68.00	31.74	28.30	14.98	0.47
GRS 1	74.5	34.77	22.20	11.75	0.34
GRS 2	80.7	37.66	16.20	8.58	0.23
Samples ground and heated at 80˚C prior to reflux with 2M sulphuric acid with different clay/acid ratio of 1:4, 1:8 and 1:50					
2GRS 1:4	75.20	35.09	21.30	11.28	0.32
2GRS 1:8	77.33	36.08	19.30	10.22	0.28
2GRS 1:50	80.70	37.66	16.20	8.58	0.23

Table A-1 Cont.

Samples	**SiO_2 (%)**	**Si (%)**	**Al_2O_3 (%)**	**Al (%)**	**Al:Si**
Samples ground and heated at 80˚C prior to reflux with different concentrations of hydrochloric acid equal to 0.5, 0.7, and 2 M using clay/acid ratio of 1:50					
GRH 0.5	64.40	30.05	32.1	16.99	0.57
GRH 0.7	65.10	30.38	31.2	16.52	0.54
GRH 2	72.70	33.93	24.4	12.92	0.38
Samples ground and heated at 80˚C prior to reflux with 0.5M hydrochloric acid with different clay/acid ratio of 1:4, 1:50 and 1:60					
0.5GRH 1:4	54.80	25.57	39.60	20.96	0.82
0.5GRH 1:50	64.40	30.05	32.10	16.99	0.57
0.5GRH 1:60	65.00	30.33	31.70	16.78	0.55
Samples ground and heated at 80˚C prior to reflux with different hydrochloric acid concentrations with different clay/acid ratio					
*0.5GRH 1:50	64.40	30.05	32.10	16.99	0.57
*2GRH 1:12	72.20	33.69	24.80	13.13	0.39
*4GRH 1:6	76.30	35.61	20.90	11.06	0.31
Samples ground and heated at 80˚C prior to reflux with different concentrations of citric acid equal to 0.1, 0.3, 0.5, 1.3 and 2 M using clay/acid ratio of 1:50					
GRC 0.1	58.27	27.19	37.30	19.74	0.73
GRC 0.3	62.30	29.07	34.20	18.11	0.62
GRC 0.5	62.40	29.12	34.20	18.11	0.62
GRC 1.3	67.40	31.45	29.50	15.62	0.50
GRC 2.0	69.93	32.63	26.77	14.17	0.43
Samples ground and heated at 80˚C prior to reflux with different concentrations of oxalic acid equal to 0.01, 0.1, and 0.5 M using clay/acid ratio of 1:50					
GRO 0.01	53.90	25.15	41.40	21.92	0.87
GRO 0.1	64.50	30.10	32.30	17.10	0.57
GRO 0.5	79.00	36.87	17.70	9.37	0.25
Samples ground and heated at 80˚C prior to reflux with 0.1M oxalic acid with different clay/acid ratio of 1:40, 1:50, 1:80 and 1:100					
0.1GRO 1:40	62.20	29.03	34.6	18.32	0.63
0.1GRO 1:50	64.50	30.10	32.3	17.10	0.57
0.1GRO 1:80	66.20	30.89	30.2	15.99	0.52
0.1GRO 1:100	67.40	31.45	29.4	15.56	0.49

*Assuming the atomatic weight of Si is equal to 0.46667 in SiO_2 compound and the atomatic weight of Al is equal to 0.5294 in Al_2O_3 compound.

Appendix B Experimental data of part II

Table B-1 Percentage of silica dissolution (in mass) in pH$_F$ 0.8 sample during Na$^+$/H$^+$ isotherm

supernatent (pH)	sample (g)	$n_{Kaolinite}$ (in sample) mol	n_{Si} (in sample) mol	Si (in supernatant) (ppm)	Si (in supernatant) (mol/l)	n_{Si} (in supernatent) mol
2.92	0.0483	1.87E-04	3.74E-04	1.60	5.70E-05	2.85E-07
6.69	0.0512	1.98E-04	3.97E-04	0.67	2.39E-05	1.19E-07
7.86	0.0512	1.98E-04	3.97E-04	0.68	2.42E-05	1.21E-07
9.50	0.0500	1.94E-04	3.88E-04	0.75	2.68E-05	1.34E-07
10.50	0.0470	1.82E-04	3.64E-04	1.77	6.32E-05	3.16E-07
11.22	0.0483	1.87E-04	3.74E-04	3.47	1.24E-04	6.20E-07

Table B-2 Percentage of silica dissolution (in mass) in pH$_F$ 3.3 sample during Na$^+$/H$^+$ isotherm

supernatent (pH)	sample (g)	$n_{Kaolinite}$ (in sample) mol	n_{Si} (in sample) mol	Si (in supernatant) (ppm)	Si (in supernatant) (mol/l)	n_{Si} (in supernatent) mol
3.02	0.0510	1.98E-04	3.95E-04	2.19	7.82E-05	3.91E-07
5.87	0.0506	1.96E-04	3.92E-04	0.99	3.55E-05	1.77E-07
7.06	0.0507	1.97E-04	3.93E-04	1.15	4.12E-05	2.06E-07
8.15	0.0511	1.98E-04	3.96E-04	1.44	5.14E-05	2.57E-07
8.83	0.0504	1.95E-04	3.91E-04	0.78	2.79E-05	1.40E-07
10.10	0.0510	1.98E-04	3.95E-04	1.96	7.01E-05	3.50E-07
11.10	0.0505	1.96E-04	3.91E-04	2.99	1.07E-04	5.34E-07

Table B-3 Percentage of silica dissolution (in mass) in pH$_F$ 7.4 sample during Na$^+$/H$^+$ isotherm

supernatent (pH)	sample (g)	$n_{Kaolinite}$ (in sample) mol	n_{Si} (in sample) mol	Si (in supernatant) (ppm)	Si (in supernatant) (mol/l)	n_{Si} (in supernatent) mol
3.18	0.015	5.81E-05	1.16E-04	3.35	1.20E-04	5.98E-07
4.57	0.011	4.26E-05	8.53E-05	1.51	5.39E-05	2.69E-07
5.07	0.0143	5.54E-05	1.11E-04	1.59	5.68E-05	2.84E-07
6.04	0.0138	5.35E-05	1.07E-04	1.31	4.67E-05	2.34E-07
7.04	0.0147	5.70E-05	1.14E-04	1.28	4.57E-05	2.28E-07
7.62	0.0143	5.54E-05	1.11E-04	1.26	4.49E-05	2.24E-07
7.77	0.0145	5.62E-05	1.12E-04	1.24	4.44E-05	2.22E-07
9.79	0.015	5.81E-05	1.16E-04	2.83	1.01E-04	5.05E-07

Table B-4 Percentage of silica dissolution (in mass) in pH_F 8.3 sample during Na^+/H^+ isotherm

supernatent (pH)	sample (g)	$n_{Kaolinite}$ (in sample) mol	n_{Si} (in sample) mol	Si (in supernatant) (ppm)	Si (in supernatant) (mol/l)	n_{Si} (in supernatent) mol
3.41	0.0148	5.74E-05	1.15E-04	3.40	1.22E-04	6.08E-07
4.65	0.0153	5.93E-05	1.19E-04	0.93	3.31E-05	1.65E-07
5.18	0.0147	5.70E-05	1.14E-04	0.88	3.13E-05	1.57E-07
6.42	0.0149	5.78E-05	1.16E-04	2.07	7.38E-05	3.69E-07
7.80	0.0155	6.01E-05	1.20E-04	2.18	7.79E-05	3.89E-07
8.30	0.0149	5.78E-05	1.16E-04	2.39	8.53E-05	4.26E-07
9.04	0.0148	5.74E-05	1.15E-04	2.67	9.53E-05	4.77E-07
10.12	0.0148	5.74E-05	1.15E-04	3.90	1.39E-04	6.96E-07

Table B-5 Percentage of silica dissolution (in mass) in KGa--1b sample during Na^+/H^+ isotherm

supernatent (pH)	sample (g)	$n_{Kaolinite}$ (in sample) mol	n_{Si} (in sample) mol	Si (in supernatant) (ppm)	Si (in supernatant) (mol/l)	n_{Si} (in supernatent) mol
3.01	0.0404	1.57E-04	3.13E-04	0.77	2.73E-05	1.37E-07
4.10	0.0407	1.58E-04	3.16E-04	0.48	1.73E-05	8.65E-08
5.28	0.0407	1.58E-04	3.16E-04	0.25	8.76E-06	4.38E-08
5.90	0.0409	1.59E-04	3.17E-04	0.14	5.09E-06	2.55E-08
7.05	0.0404	1.57E-04	3.13E-04	0.47	1.69E-05	8.46E-08
7.99	0.0406	1.57E-04	3.15E-04	0.53	1.89E-05	9.44E-08
8.93	0.0406	1.57E-04	3.15E-04	0.92	3.29E-05	1.64E-07
10.00	0.0406	1.57E-04	3.15E-04	1.13	4.05E-05	2.03E-07

Table B-6 Percentage of edge dissolution in pH$_F$ 0.8 sample during Na$^+$/H$^+$ isotherm

supernatent (pH)	sample (g)	m^2	sites	mol
2.92	0.0483	0.32	6.37E+18	1.06E-05
6.69	0.0512	0.34	6.75E+18	1.12E-05
7.86	0.0512	0.34	6.75E+18	1.12E-05
9.50	0.0500	0.33	6.60E+18	1.10E-05
10.50	0.0470	0.31	6.20E+18	1.03E-05
11.22	0.0483	0.32	6.37E+18	1.06E-05

*Assuming S$_{kaolinite}$ = 6.6 m^2/g, theoretical site density of kaolinite = 20 sites/nm^2 (Koretsky, 1998).

Table B-7 Percentage of edge dissolution in pH$_F$ 3.3 sample during Na$^+$/H$^+$ isotherm

supernatent (pH)	sample (g)	m^2	sites	mol
3.02	0.0510	0.34	6.73E+18	1.12E-05
5.87	0.0506	0.33	6.67E+18	1.11E-05
7.06	0.0507	0.33	6.69E+18	1.11E-05
8.15	0.0511	0.34	6.74E+18	1.12E-05
8.83	0.0504	0.33	6.65E+18	1.11E-05
10.10	0.0510	0.34	6.73E+18	1.12E-05
11.10	0.0505	0.33	6.66E+18	1.11E-05

*Assuming S$_{kaolinite}$ = 6.6 m^2/g, theoretical site density of kaolinite = 20 sites/nm^2 (Koretsky, 1998).

Table B-8 Percentage of edge dissolution in pH$_F$ 7.4 sample during Na$^+$/H$^+$ isotherm

supernatent (pH)	sample (g)	m^2	sites	mol
3.18	0.0150	0.12	2.40E+18	3.99E-06
4.57	0.0110	0.09	1.76E+18	2.92E-06
5.07	0.0143	0.11	2.28E+18	3.80E-06
6.04	0.0138	0.11	2.20E+18	3.67E-06
7.04	0.0147	0.12	2.35E+18	3.91E-06
7.62	0.0143	0.11	2.28E+18	3.80E-06
7.77	0.0145	0.12	2.32E+18	3.85E-06
9.79	0.0150	0.12	2.40E+18	3.99E-06

*Assuming S$_{kaolinite}$ = 8 m^2/g, theoretical site density of kaolinite = 20 sites/nm^2 (Koretsky, 1998).

Table B-9 Percentage of edge dissolution in pH$_F$ 8.3 sample during Na$^+$/H$^+$ isotherm

supernatent (pH)	sample (g)	m^2	sites	mol
3.41	0.0148	0.11	2.24E+18	3.74E-06
4.65	0.0153	0.12	2.32E+18	3.86E-06
5.18	0.0147	0.11	2.23E+18	3.71E-06
6.42	0.0149	0.11	2.26E+18	3.76E-06
7.80	0.0155	0.12	2.35E+18	3.91E-06
8.30	0.0149	0.11	2.26E+18	3.76E-06
9.04	0.0148	0.11	2.24E+18	3.74E-06
10.12	0.0148	0.11	2.24E+18	3.74E-06

*Assuming S$_{kaolinite}$ = 7.6 m^2/g, theoretical site density of kaolinite = 20 sites/nm^2 (Koretsky, 1998).

Table B-10 Percentage of edge dissolution in KGa--1b sample during Na^+/H^+ isotherm

supernatent (pH)	sample (g)	m^2	sites	mol
3.01	0.0404	0.14	2.81E+18	4.67E-06
4.10	0.0407	0.14	2.83E+18	4.71E-06
5.28	0.0407	0.14	2.83E+18	4.71E-06
5.90	0.0409	0.14	2.84E+18	4.73E-06
7.05	0.0404	0.14	2.81E+18	4.67E-06
7.99	0.0406	0.14	2.82E+18	4.69E-06
8.93	0.0406	0.14	2.82E+18	4.69E-06
10.00	0.0406	0.14	2.82E+18	4.69E-06

*Assuming $S_{kaolinite}$ of KGa--1b = 3.48 m^2/g (Wan and Tokunaga, 2002), theoretical site density of kaolinite = 20 sites/nm^2 (Koretsky, 1998).

CURRICULUM VITAE

NAME	Miss Lei Lei Aung
DATE OF BIRTH	11 January 1978
EDUCATIONAL RECORD	
HIGH SCHOOL	Basic Education High School No.5, Botataung, Yangon, Myanmar, 1995
BACHELOR'S DEGREE	Bachelor of Science (Honours) (Industrial Chemistry) University of Yangon, Yangon, Myanmar, 2004
MASTER'S DEGREE	Master of Science (Industrial Chemistry) University of Yangon, Yangon, Myanmar, 2006 Master of Research (Industrial Chemistry) University of Yangon, Yangon, Myanmar, 2007
DOCTORAL DEGREE	Doctor of Philosophy (double badged degree) Doctor of Philosophy (Biotechnology) King Mongkut's University of Technology Thonburi, Bangkok, Thailand, (2015) and Doctor of Philosophy (Earth Science) University of Poitiers, Poitiers, France (2014)
SCHOLARSHIP/ RESEARCH GRANT	The Thailand Research Fund, Thailand International Cooperation Agency and The French Embassy in Indonesia through the Royal Golden Jubilee Ph.D. Program (Grant No. PHD/0123/2552)
EMPLOYMENT RECORD	Demonstrator, Industrial Chemistry Department, University of Yangon, Yangon, Myanmar. (2005-2011) Demonstrator, Industrial Chemistry Department, Yadanabon University, Amarapura, Myanmar. (2011-2013)

Assistant Lecturer, Industrial Chemistry Department, Yadanabon University, Amarapura, Myanmar. (2013-present)

PUBLICATION

Lei Lei Aung, Myint Pe and Pansy Kyaw Hla, 2009, “Palm Oil Fractionation Process”, **Jouranl of Myanmar Academy of Arts and Science**, Vol. 7, pp. 435-446.

Lei Lei Aung, Emmanuel Tertre, Niramon Worasith, Parinda Suksabye, and Paitip Thiravetyan, 2014, “The Capacity of Activated Kaolins to Remove Colour Pigments from Rice Bran Oil: The Effects of Acid Concentration and Pre-heating Prior to Activation”, **Clay Minerals** 49, pp. 513-526.

Lei Lei Aung, Emmanuel Tertre, Sabine Petit, 2015, “Effect of the Morphology of Synthetic Kaolinites on their Sorption Properties”, **Journal of Colloid and Interface Science** 443, pp. 177-186.

Lei Lei Aung, Emmanuel Tertre, Parinda Suksabye, Niramon Worasith and Paitip Thiravetyan, “Effect of Alumina Content and Surface Area of Acid-Activated Kaolin on Bleaching of Rice Bran Oil”, **Journal of American Oil Chemist’ Society** 92, pp. 295-304. (DOI 10.1007/s11746-014-2583-2).

Lei Lei Aung, Parinda Suksabye, Niramon Worasith and Paitip Thiravetyan, 2013, “Characterization of activated kaolins and their bleaching of rice bran oil”, **The 2nd International conference on Clays, Clay Minerals and Layered Materials-CMLM2013**, Saint Petersburg, Russia. September 11-15. (Oral presentation)

Lei Lei Aung, Niramon Worasith, Parinda Suksabye and Paitip Thiravetyan, 2013, “Removal of Color from Rice Bran Oil using Acid-activated Kaolin”, **TSB 2013-The 25th annual meeting of Thai Society for Biotechnology and International Conference,** Agro-Industrial Biotechnology for Global Sustainable Prosperity, Bangkok, Thailand. October 16-19. (Oral presentation & Conference paper proceeding)

Lei Lei Aung, Parinda Suksabye, Niramon Worasith and Paitip Thiravetyan, 2014, "Acid Activation of Kaolin for Bleaching of Rice Bran Oil", **RGJ-Ph.D. Congress XV,** Jomtien Palm Beach Resort, Chonburi, Thailand. May 27-29. (Oral presentation)

Lei Lei Aung, Parinda Suksabye, Niramon Worasith and Paitip Thiravetyan, 2014, "Modification of Kaolin Using Oxalic Acid Treatment: Focus on the Correlation between its Structural Changes and Bleaching Capacities", **The Fifth International conference on Science and Engineering (ICSE 2014)**, Yangon, Myanmar. December 29-30. (Oral presentation & Conference paper proceeding)